

AFML-TR-70-213

PART II

**NDE**

82763

**INVESTIGATION OF THE PROPERTIES OF  
CARBON-CARBON COMPOSITES  
AND THEIR RELATIONSHIP TO  
NONDESTRUCTIVE TEST MEASUREMENTS**

*J. S. EVANGELIDES*

*R. A. MEYER*

*J. E. ZIMMER*

*McDONNELL DOUGLAS ASTRONAUTICS COMPANY*

*SANTA MONICA, CALIFORNIA 90406*

TECHNICAL REPORT AFML-TR-70-213, PART II

AUGUST, 1971

Approved for public release; distribution unlimited.

AIR FORCE MATERIALS LABORATORY  
AIR FORCE SYSTEMS COMMAND  
WRIGHT-PATTERSON AIR FORCE BASE, OHIO

## NOTICE

When Government drawings, specifications, or other data are used for any purpose other than in connection with a definitely related Government procurement operation, the United States Government thereby incurs no responsibility nor any obligation whatsoever; the fact that the government may have formulated, furnished, or in any way supplied the said drawings, specifications, or other data, is not to be regarded by implication or otherwise as in any manner licensing the holder or any other person or corporation, or conveying any rights or permission to manufacture, use, or sell any patented invention that may in any way be related thereto.

Copies of this report should not be returned unless return is required by security considerations, contractual obligations, or notice on a specific document.

AIR FORCE: 15-3-72/700

**AFML-TR-70-213**

**PART II**

**INVESTIGATION OF THE PROPERTIES OF  
CARBON-CARBON COMPOSITES  
AND THEIR RELATIONSHIP TO  
NONDESTRUCTIVE TEST MEASUREMENTS**

*J. S. EVANGELIDES*

*R. A. MEYER*

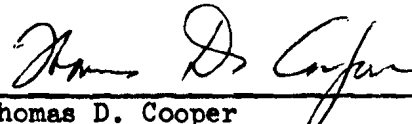
*J. E. ZIMMER*

Approved for public release; distribution unlimited.

## FOREWORD

This final report is prepared for the United States Air Force Materials Laboratory (AFML), Wright Patterson AFB, Ohio. The work was performed under contract F33615-69-C-1640, initiated on Project Number 7351 Metallic Materials, Task Number 735109, "Nondestructive Methods". Mr. William L. Shelton, AFML/LLN is the AFML Project Engineer. This report documents the activities of the McDonnell Douglas Astronautics Company-West (MDAC) for the two year period, 1 June 1969 through 1 June 1971, on the Investigation of the Properties of Carbon-Carbon Composites and Their Relationship to Nondestructive Test Measurements. Dr. H. W. Babel was program manager and Dr. R. A. Meyer was principal investigator. The authors of the report, Mr. J. S. Evangelides (NDT task leader), Dr. R. A. Meyer, and Mr. J. E. Zimmer are indebted to Mr. D. Eitman (material processing), and Mr. J. Jortner (mechanical behavior) for their contributions to the work. The authors wish to express their particular thanks to Mr. B. V. Whiteson for valuable assistance and discussions during the course of this program. The efforts involved in this contract were directly related to the entire carbon-carbon materials development program at MDAC and as such some of the tasks reported were accomplished under a parallel Independent Research and Development Program.

This technical report has been reviewed and is approved.



---

Thomas D. Cooper  
Chief, Processing and Nondestructive  
Testing Branch  
Metals and Ceramics Division

## ABSTRACT

*Begin*  
Material variations and discrete discontinuities can be encountered in carbon-carbon composites. The object of this program was to identify and evaluate those factors that affect the quality and performance of carbon-carbon composites by nondestructive and destructive test methods. In addition, it was to be determined what correlations existed between the nondestructive test response data and the physical and mechanical property measurements. The general approach was to characterize the precursor materials, apply the non-destructive test techniques to the composites on an in-process basis, determine mechanical and physical properties and determine what relationships may exist between the NDT and property measurements. A number of different types of defects were intentionally introduced during the processing steps to aid in this evaluation.

The characterization of the VYB 70 1/2 yarn has indicated that considerable weight losses and shrinkages occur upon heating. The Thornel 50 and Modmor II graphite fibers did not undergo any significant weight loss under similar conditions. By selected binder pretreatments, coke values of some coal tar pitch components were increased.

The combination of the X-ray radiography and attenuation and velocity techniques detected the intentional defects introduced into the unidirectional and multidirectional composites. The use of an X-ray absorbing doping agent provided additional defect information on Thornel 50 - pitch unidirectional composites. The pulse echo technique was only useful in evaluating fine weave-high density composites. The ultrasonic attenuation increased while the longitudinal velocity decreased with increasing porosity of the composites.

Different mechanical properties were obtained depending on the type of yarn and binder used, the material condition and the type of intentional defect present. The porosity present in the composites had a significant and different effect on each of the mechanical properties. An optimum porosity level appears to exist for the tensile properties of the composites, implying that the highest density does not always result in the highest tensile strength. The nondestructive test measurements were correlated to the porosity and mechanical properties of the carbon-carbon composites. The test data suggested that in-process prediction of final composite properties is possible.

It was concluded that monitoring material nonuniformities, detecting discrete discontinuities and predicting material properties in unidirectional and multidirectional carbon-carbon composites on an in-process basis can be successfully accomplished.

## TABLE OF CONTENTS

<u>Section</u>	<u>Page</u>
I. INTRODUCTION . . . . .	1
II. SUMMARY. . . . .	5
III. RESULTS AND DISCUSSION . . . . .	9
1.0 Material Selection. . . . .	9
2.0 Characterization of Precursor Materials . . . . .	9
3.0 Processing . . . . .	14
4.0 Composite Characterization. . . . .	19
5.0 Nondestructive Analysis . . . . .	42
6.0 Mechanical Testing . . . . .	114
IV. CONCLUSIONS AND RECOMMENDATIONS . . . . .	209

## APPENDICES

### Appendix

I. Nondestructive Characterization Measurements on Unidirectional and Multidirectional Composites . . . . .	211
II. Mechanical Test Results on Unidirectional and Multidirectional Composites. . . . .	221
III. Nondestructive Test Data on Unidirectional Mechanical Test Specimen . . . . .	232
REFERENCES . . . . .	241

# ILLUSTRATIONS

<u>Figure</u>		<u>Page</u>
1	Program Flow Chart . . . . .	2
2	DACLOCK 120 Weave Pattern. . . . .	11
3	Photograph of Top Surface and Positive Print of X-Ray Radiographic Negative of One-Inch Thick Orthogonal Woven Panel . . . . .	13
4	Unidirectional Winding Apparatus . . . . .	15
5	Bulk Density of VYB 70 1/2-SC1008 Composites . . . . .	20
6	Bulk Density of VYB 70 1/2-Pitch Composites. . . . .	21
7	Bulk Density of Modmor II-Pitch Composites . . . . .	22
8	Pore Diameter Versus Pore Volume Occupied by Mercury of VYB 70 1/2-SC1008 Composites . . . . .	25
9	Pore Diameter Versus Pore Volume Occupied by Mercury for VYB 70 1/2-Pitch Composites. . . . .	26
10	Pore Diameter Versus Pore Volume Occupied by Mercury for Modmor II-Pitch Composites . . . . .	27
11	Bulk Density Versus Total Porosity of Unidirectional Composites. . . . .	31
12	Photomicrograph of Graphitized VYB 70 1/2- Pitch Composite in Transverse Direction under Polarized Light (76°). . . . .	33
13	Photomicrograph of Pyrolyzed Modmor II-Pitch No-Intentional-Defect Composite Specimen in Transverse Direction Under Polarized Light (80°) . . . . .	34
14	Photomicrograph of Graphitized Modmor II-Pitch No-Intentional-Defect Composite Specimen in Transverse Direction Under Bright Field. . . . .	34
15	Photomicrograph of Pyrolyzed VYB 70 1/2-Pitch Unidirectional Composite, 475X with Polarized Light (90°). .	35

# ILLUSTRATIONS (Cont'd)

<u>Figure</u>		<u>Page</u>
16	Graph of Relative X-Ray Intensity Versus Scattering Angle for ATJ Graphite and VYB 70 1/2-SC1008 and VYB 70 1/2-Pitch Graphitized Unidirectional Composites. . . .	37
17	Bulk Density of Multidirectional Composite. . . . .	37
18	Pore Diameter Versus Pore Volume Occupied by Mercury for Multidirectional DACLOCK 120 Composite. . . . .	39
19	Total Porosity Versus Bulk Density of DACLOCK 120 Multidirectional Composite. . . . .	41
20	Photomicrograph of Multidirectional Composite After Two Impregnations and Pyrolysis - Graphitization - Three Impregnations. . . . .	43
21	X-Ray Radiographic Standard for Pyrolyzed VYB 70 1/2-Pitch Composites . . . . .	43
22	Nondestructive Test Maps for Pyrolyzed VYB 70 1/2-SC1008 Composite Specimen 14D Containing no Intentional Defects (Good). . . . .	47
23	Nondestructive Test Maps for Pyrolyzed VYB 70 1/2-SC1008 Composite Specimen 28C Containing Large Voids. . . . .	48
24	Positive Print of X-Ray Radiograph and Through Transmission Map of Pyrolyzed VYB 70 1/2-SC1008 Specimen 15D Containing Weave Irregularities. . . . .	49
25	Schematic Diagram of Through-Transmission Velocity Measurement Techniques . . . . .	50
26	Longitudinal Velocity of VYB 70 1/2-SC1008 Composite. . . . .	52
27	Bulk Density Versus Ultrasonic Longitudinal Velocity for Unidirectional Composites . . . . .	54
28	Graph of Ultrasonic Longitudinal Velocity of Fused Quartz Standard as a Function of Frequency (Time delay as average of three initial cycles) . . . . .	55



# ILLUSTRATIONS (Cont'd)

<u>Figure</u>		<u>Page</u>
29	Graph of Ultrasonic Longitudinal Velocity of Pyrolyzed and Graphitized VYB 70 1/2-SC1008 Composites as a Function of Frequency . . . . .	56
30	Apparatus for Through-Transmission Attenuation Measurement . . . . .	58
31	Sound Beam Profile of Flat Transmitter-Flat Receiver Combination. . . . .	60
32	Sound Beam Profile of Focus Transmitter Collimated Flat Receiver Combination at 3-Inch Water Path. . . . .	61
33	Ultrasonic Attenuation of VYB 70 1/2-SC1008 Composites. . .	63
34	Nondestructive Test Maps for Pyrolyzed VYB 70 1/2-SC1008 Composite Specimen 18C Containing Crack . . . . .	65
35	Ultrasonic Attenuation Versus Apparent Porosity of VYB 70 1/2-SC1008 Composite. . . . .	66
36	Attenuation of Pyrolyzed Composite Versus the Apparent Porosity of Graphitized VYB 70 1/2- SC1008 Composite. . . . .	66
37	Pulse-Echo Equipment Arrangement. . . . .	67
38	Comparison of Pulse-Echo Responses for Focused and Flat Transducers. . . . .	68
39	Ultrasonic Pulse-Echo and Through-Transmission Attenuation C-Scan Maps of Graphitized VYB 70 1/2- SC1008 Composite Containing a Delamination Defect . . . . .	70
40	Positive Prints of X-Ray Radiograph of As-Impregnated and Pyrolyzed VYB 70 1/2-Coal Tar Pitch Composite . . . . .	71
41	Longitudinal Velocity of VYB 70 1/2-Pitch Composite . . . .	76

# ILLUSTRATIONS (Cont'd)

<u>Figure</u>		<u>Page</u>
42	Ultrasonic Longitudinal Velocity Versus Frequency for Pyrolyzed and Graphitized VYB 70 1/2-Pitch Composite . . . . .	77
43	Ultrasonic Attenuation of Pyrolyzed and Graphitized VYB 70 1/2-Pitch Unidirectional Composites. . . . .	80
44	Total Porosity Versus Attenuation of VYB 70 1/2- Pitch Composites Processed Under the Same Conditions. . . .	81
45	Comparison of Half-Tone and Regular Attenuation C-Scan Maps . . . . .	83
46	X-Ray Radiographs and Attenuation C-Scan Maps of Graphitized VYB 70 1/2-Pitch Composite Specimen 1A3 After Flexure Test. . . . .	84
47	Photomicrographs of Graphitized VYB 70 1/2-Pitch Composite Specimen 1A3 After Flexure Test . . . . .	85
48	Longitudinal Velocity of Modmor II-Pitch Composite. . . . .	87
49	Ultrasonic Longitudinal Velocity Versus Frequency for Pyrolyzed and Graphitized Modmor II-Pitch Composites. . . . .	89
50	Ultrasonic Attenuation of Pyrolyzed and Graphitized Modmor II-Pitch Composites. . . . .	90
51	Polarized Shear Wave Velocity of Modmor II- Pitch Composite . . . . .	93
52	Polarized Shear Wave Velocity of VYB 70 1/2- SC1008 and VYB 70 1/2-Pitch Composites. . . . .	94
53	Photomicrograph and X-Ray Radiograph of DACLOCK 120 As-Woven Fabric . . . . .	98
54	Positive Prints of X-Ray Radiographs of Specimen 98-7 Multidirectional DACLOCK 120 Before and After Three Impregnations and Pyrolysis (Dark areas represent higher density) . . . . .	99

# ILLUSTRATIONS (Cont'd)

<u>Figure</u>		<u>Page</u>
55	Ultrasonic Longitudinal Velocity of Pyrolyzed and Graphitized DACLOCK 120 Multidirectional Composite . . . . .	101
56	Ultrasonic Longitudinal Velocity Versus Bulk Density of DACLOCK 120 Multidirectional Composite . . . . .	101
57	Frequency Dependence of Longitudinal Velocity for Pyrolyzed DACLOCK 120 Multidirectional Composite. . . . .	102
58	Through Transmission C-Scan Map at 0.5 MHz of Multidirectional DACLOCK 120 Specimen 98-7 After Three Impregnations and Pyrolysis . . . . .	104
59	Attenuation Versus Total Porosity for DACLOCK 120 Composite . . . . .	105
60	Sketch of Attenuation C-Scan Maps of Orthogonal Composite . . . . .	108
61	Ultrasonic Through Transmission Attenuation C-Scan Map of 1.00 Inch Thick Orthogonally Woven Multidirectional Composite with Intentional Defects Present (Dark areas more attenuating) . . . . .	109
62	Positive Print of X-Ray Radiograph of AVCO Mod III Billet 715 . . . . .	111
63	Ultrasonic Through-Transmission Attenuation Map of Billet 709 Through View B (Recording level 65 db or 16 db/in). . . . .	112
64	Positive Print of Pulse-Echo C-Scan Map of Billet 715 . . . . .	113
65	Pulse-Echo Test Standard ATJ-S Graphite C-Scan Map and A-Scan of 1/16" Flat Bottom Hole. . . . .	115
66	Graph of Ultrasonic Longitudinal Velocity Versus Frequency for AVCO Mod III Multidirectional Carbon-Carbon Composite . . . . .	116
67	Stress Directions for Mechanical Testing of Unidirectional Composites . . . . .	117

# ILLUSTRATIONS (Cont'd)

<u>Figure</u>		<u>Page</u>
68	Dogbone Specimen Configuration . . . . .	119
69	Specially Designed Assembly Fixture for the Bonding of Test Specimens and Doublers . . . . .	120
70	Photomicrographs of Pyrolyzed VYB 70 1/2-Coal Tar Pitch Composite Specimens After Tensile Testing (2X) . . . . .	123
71	Posttest Photographs of Strip Tension Specimens of Unidirectional Composite. . . . .	124
72	Current Tension Specimen Design. . . . .	127
73	Failed Tensile Specimens of Pyrolyzed VYB 70 1/2- SC1008 Composite Using Current Specimen Design . . . . .	128
74	Double Shear Fixture Schematic . . . . .	129
75	Uniaxial Tensile Test Results on Pyrolyzed VYB 70 1/2-SC1008 Composite. . . . .	133
76	Shear Strength of Pyrolyzed VYB 70 1/2- SC1008 Composite . . . . .	134
77	Uniaxial Tensile Test Results for Graphitized VYB 70 1/2-SC1008 Composite. . . . .	135
78	Uniaxial Tensile Test Results on Pyrolyzed and Graphitized VYB 70 1/2-Pitch Composites. . . . .	137
79	Effect of Binder on the Tensile Properties of the VYB 70 1/2 Composites. . . . .	138
80	Model of No-Intentional-Defect Composite . . . . .	140
81	Model for Small Void Composite . . . . .	141
82	Tensile Test Results for Pyrolyzed and Graphitized Modmor II-Pitch Composites . . . . .	143

# ILLUSTRATIONS (Cont'd)

<u>Figure</u>		<u>Page</u>
83	Effect of Yarn on the Tensile Properties of the Pitch Binder Composites . . . . .	144
84	Average Shear Strength of Unidirectional Composites . . . . .	146
85	Average Tensile Strength and Modulus of VYB 70 1/2-SC1008 Composite System. . . . .	148
86	Average Tensile Strength Versus Total Porosity. . . . .	149
87	Graph of Average Shear Strength Versus Average Porosity of Pyrolyzed and Graphitized VYB 70 1/2- SC1008 Composite. . . . .	150
88	Total Porosity Versus Shear Strengths of VYB 70 1/2- Pitch, Modmor II-Pitch Composites . . . . .	151
89	Prediction of Tensile Strength and Modulus of Graphitized VYB 70 1/2-SC1008 Composite from Average Porosity of Pyrolyzed Composite . . . . .	152
90	Prediction of Tensile Strength of Graphitized VYB 70 1/2-Pitch Composite from the Porosity of Pyrolyzed Composite. . . . .	153
91	Shear Strength of Graphitized Composite Versus Total Porosity of Pyrolyzed Composite . . . . .	155
92	Electron Fractographs of Graphitized VYB 70 1/2- SC1008 Tensile Specimen 14A3. . . . .	156
93	Electron Fractographs of Graphitized VYB 70 1/2- SC1008 Tensile Specimen 10A5. . . . .	157
94	Scanning Electron Micrographs of Graphitized VYB 70 1/2-SC1008 Tensile Specimen 14A3 . . . . .	158
95	Scanning Electron Micrographs of Graphitized VYB 70 1/2-SC1008 Tensile Specimen 10A5 . . . . .	159

# ILLUSTRATIONS (Cont'd)

<u>Figure</u>		<u>Page</u>
96	Electron Fractographs of Graphitized VYB 70 1/2-SC1008 Tensile Specimens 10A5 and 14A3. . . . .	160
97	Positive Print of X-Ray Radiograph of Graphitized VYB 70 1/2-SC1008 Tensile Specimens . . . . .	161
98	Scanning Electron Micrographs of Graphitized VYB 70 1/2-Pitch Tensile Specimen . . . . .	163
99	Scanning Electron Micrographs of Graphitized VYB 70 1/2-Pitch Tensile Specimen . . . . .	164
100	Scanning Electron Micrographs of Graphitized VYB 70 1/2-Pitch Tensile Specimen . . . . .	165
101	Electron Fractographs of Graphitized VYB 70 1/2-Pitch Tensile Specimen. . . . .	166
102	Electron Fractograph of Graphitized VYB 70 1/2-Pitch Tensile Specimen. . . . .	167
103	Photograph of Ultrasonic Longitudinal Velocity and Attenuation Measurement Apparatus by Dry Coupling Methods . . . . .	169
104	Bar Graph of Nondestructive Test Measurements on Pyrolyzed VYB 70 1/2-SC1008 Tensile Specimens . . . . .	170
105	Bar Graph of Nondestructive Test Measurements on Pyrolyzed VYB 70 1/2-SC1008 Shear Test Specimens. . . . .	171
106	Bar Graph of Nondestructive Test Measurements of Graphitized VYB 70 1/2-SC1008 Tensile Specimens . . . . .	172
107	Bar Graph of Nondestructive Test Measurements on Graphitized VYB 70 1/2-SC1008 Shear Specimens . . . . .	173
108	Nondestructive Test Measurements on Pyrolyzed VYB 70 1/2-Pitch Tensile Specimens. . . . .	174
109	Nondestructive Test Data on Graphitized VYB 70 1/2-Pitch Tensile Specimens . . . . .	175

# ILLUSTRATIONS (Cont'd)

<u>Figure</u>		<u>Page</u>
110	Nondestructive Test Measurements on Pyrolyzed VYB 70 1/2-Pitch Shear Specimens . . . . .	176
111	Nondestructive Test Data on Graphitized VYB 70 1/2-Pitch Shear Specimens . . . . .	177
112	Nondestructive Test Data on Pyrolyzed Modmor II- Pitch Tensile Specimens. . . . .	178
113	Nondestructive Test Data on Graphitized Modmor II- Pitch Tensile Specimens. . . . .	179
114	Nondestructive Test Data on Pyrolyzed Modmor II- Pitch Shear Specimens. . . . .	180
115	Nondestructive Test Data on Graphitized Modmor II- Pitch Shear Specimens. . . . .	181
116	Electrical Resistivity of Pyrolyzed VYB 70 1/2- SC1008 Composite Tensile Specimens . . . . .	182
117	Electrical Resistivity of Graphitized SC1008-VYB 70 1/2 Tensile Specimens . . . . .	183
118	Attenuation Versus Composite Strengths . . . . .	184
119	Attenuation of Pyrolyzed Composite Versus Strength of Graphitized Composite. . . . .	185
120	Ultrasonic Longitudinal Velocity Versus Shear Strength for the VYB 70 1/2-SC1008 and Modmor II- Pitch Composites . . . . .	187
121	Dynamic Modulus Versus Tensile Modulus of VYB 70 1/2-SC1008 and Modmor II-Pitch Composites . . . . .	189
122	Dynamic Modulus of Pyrolyzed Composite Versus Tensile Modulus of Graphitized VYB 70 1/2-SC1008 and VYB 70 1/2-Pitch Composites. . . . .	190
123	X-Ray Radiographic Enhancement Evaluation. . . . .	192

# ILLUSTRATIONS (Cont'd)

<u>Figure</u>		<u>Page</u>
124	Tension Test Specimen Design for Multidirectional Composite . . . . .	195
125	Compressive Stress-Strain Curves for VYB 70 1/2-Pitch Multidirectional Composite. . . . .	196
126	Compressive Strength Versus Strain-to-Failure for Multidirectional Composite. . . . .	199
127	Tension Stress-Strain Curves for VYB 70 1/2-Pitch Multidirectional Composite. . . . .	203
128	Average Ultimate Compression Strengths Versus Total Porosity of DACLOCK 120 Multidirectional Composite . . . . .	204
129	Ultimate Tensile Strength Versus Total Porosity of DACLOCK 120 Multidirectional Composite . . . . .	204
130	Longitudinal Velocity Versus Ultimate Tensile Strength of DACLOCK 120 Composite . . . . .	206
131	Attenuation Versus Ultimate Tensile Strength of DACLOCK 120 Multidirectional Composite . . . . .	206
132	Longitudinal Velocity Versus Ultimate Compressive Strength of DACLOCK 120 Composite . . . . .	207
133	Attenuation Versus Ultimate Compressive Strength of DACLOCK 120 Composite. . . . .	207



# LIST OF TABLES

<u>Table</u>		<u>Page</u>
I	Composite Materials . . . . .	9
II	Typical CX 70 1/2 Yarn Properties . . . . .	10
III	Methods of Fabricating Specific Defects in SC1008 Unidirectional Composites . . . . .	16
IV	Porosimetry Measurements for Unidirectional Composites . . .	23
V	Estimated Yarn Pitch Matrix Densities . . . . .	28
VI	Closed Pore Porosity Estimates . . . . .	30
VII	Optically Measured Pore Diameters . . . . .	32
VIII	Porosimetry Data on DACLOCK 120 Multidirectional Composite .	38
IX	Closed Pore Porosity Estimates . . . . .	40
X	NDT Standards for Helium Chamber X-Ray Radiography . . . . .	45
XI	Applicability of Nondestructive Test Techniques to VYB 70 1/2-SC1008 . . . . .	46
XII	Ultrasonic Attenuation of VYB 70 1/2-SC1008 Composites . . .	62
XIII	Summary of Applicable Nondestructive Test Techniques for the VYB 70 1/2-Pitch Composite System . . . . .	73
XIV	Ultrasonic Attenuation and Porosity of VYB 70 1/2-Pitch Composite Specimens . . . . .	81
XV	Summary of Applicable Nondestructive Test Techniques for the Modmor II-Pitch Composite System . . . . .	86
XVI	Shear Wave Velocity Measurements . . . . .	92
XVII	Percentage Change in Velocity Measurements . . . . .	95
XVIII	Applicability of Nondestructive Test Techniques for DACLOCK 120 Pyrolyzed Multidirectional Composite . . . . .	96
XIX	Attenuation of DACLOCK 120 Multidirectional Composites . . .	103

# LIST OF TABLES (Cont'd)

<u>Table</u>		<u>Page</u>
XX	Transducer Combination for Through-Transmission Attenuation Evaluation . . . . .	106
XXI	Tension Test Results of POCO AXF-5Q Graphite Bonded-Doubler Specimens . . . . .	121
XXII	Mechanical Test Results of Unidirectional VYB 70 1/2-Pitch Composite, Batch No. 8 . . . . .	122
XXIII	Mechanical Test Results for Pyrolyzed VYB 70 1/2-SC1008 Composite . . . . .	122
XXIV	Summary of Average Mechanical Properties . . . . .	130
XXV	Mechanical Test Data on Thornel 50-Pitch Composite No Intentional Defect Specimens after Graphitization . . . . .	132
XXVI	Percentage Change in Average Electrical Resistivity Values for Pyrolyzed and Graphitized VYB 70 1/2-SC1008 Composite . . . . .	186
XXVII	Average Mechanical Properties of Multidirectional DACLOCK 120 Composite . . . . .	194
XXVIII	Summary of Process Characterization Data for Multidirectional Composite . . . . .	197
XXIX	Nondestructive Test Data on Multidirectional Test Specimens . . . . .	200

## I. INTRODUCTION

The current aerospace industry interest in carbon-carbon composites as a high temperature structural material is based on their ablation resistance and strength in hyperthermal environments. These properties have made this material a candidate for nose tips, leading edges, and heat shields for reentry vehicles, high-speed, aerodynamically-controlled vehicles, and nozzle inserts for rocket engines. Progress with new high-modulus, high-strength carbonaceous reinforcement materials, new techniques for making multidimensionally-reinforced structures, and oxidation protection by inhibitors and coatings have added significant potential to the future use of carbon composites as a high-temperature structural material.

The methods of fabricating carbon-carbon composites are very complex and the mechanisms that control critical properties are not well understood. It is extremely difficult at present to repeatably or uniformly produce composites which are free of inhomogenieties or variations. Those variations that affect the quality and performance of the carbon-carbon composites must be identified and characterized.

Due to the significant differences that can exist in precursor materials and the methods used to process the composites, many types of defects, material variations, and discrete discontinuities can be encountered. These types of defects will also vary with the type of reinforcement and matrix employed. It becomes desirable to obtain information on the material uniformity and properties during the processing sequences which will allow the evaluation of specific processing steps. This information can then be used for the rapid development of new and improved carbon-carbon composites. The next question that arises is whether the material defects or anomalies that affect composite properties can be identified and characterized early in the process cycle to allow for corrective action to insure composite integrity. Therefore, it is necessary both to know the effect of specific defects on the composite properties and to possess the means of identifying or detecting them within the carbon-carbon composite.

The object of this program was to identify and evaluate the factors that affect the quality and performance of carbon-carbon composites by nondestructive and destructive test methods. In addition, it was to be determined what correlations existed between the nondestructive test response data and the physical and mechanical property measurements. The general approach was to characterize the precursor materials, apply the nondestructive test techniques to the composites on an in-process basis, determine mechanical and physical properties and determine what relationship may exist between the NDT and property measurements. A general program flow chart is shown in Figure 1.

A number of different types of defects were introduced during the processing steps. This material provided a means for evaluating the effect of a specific defect on the composite properties and of the detectability of this defect within the composite. It was also the intent of this study to determine whether the application of nondestructive test techniques after various processing steps could aid in establishing when defects arise in the processing

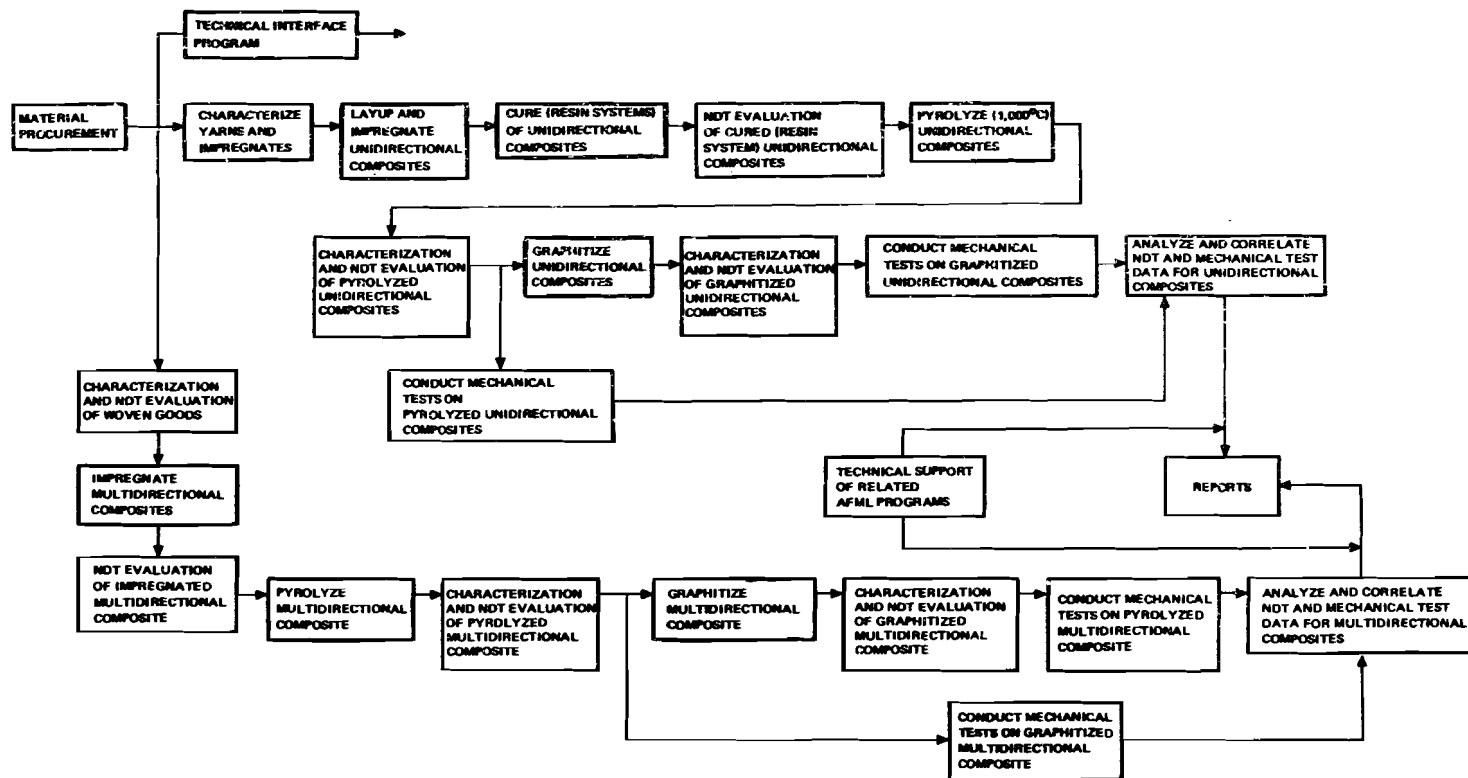


Figure 1. Program Flow Chart

cycle and how they were altered during subsequent processing. Critical and specific fabrication steps may be related to the following quality problems:

- o Inadequate reproducibility and uniformity
- o Lack of fiber-to-matrix bond and fiber bundle penetration
- o Voids, cracks (micro- and macrocracks), broken yarns or irregular weaving, and other process flaws
- o Scale-up from laboratory to production hardware

The possible advantages of an in-process investigation are: (1) to eliminate the time and expense caused by processing faulty material, (2) to provide information that may lead to improved production methods, and (3) to help assure that the material in the final form will contain no significant defects.

Both unidirectional and multidirectional specimens were fabricated for this study. The unidirectional composites provided an easy geometry for introducing defects into the composite and interpreting their effect on the physical properties. The introduction of defects into the multidirectional composite was considered to be more difficult as was the interpretation of the effect of specific defects on properties. Due to a rapidly growing composite technology, a variety of precursor materials (yarns and impregnates) existed from which the composite materials could be fabricated. In order to utilize state-of-the-art materials and as broad a material geometry spectrum as possible, three unidirectional and one multidirectional composites were studied for this program.

Since slight differences in the precursor materials and processing steps can cause significant changes in the properties of the composite, the precursor materials were characterized by physical measurements and visual observations to: (1) determine initial properties, and (2) determine if any pretreatment or conditioning is necessary prior to impregnation.

Various nondestructive test techniques were evaluated as to their ability to detect the intentionally-introduced processing defects and holes and cracks in artificial standards. The results of this investigation aided in establishing the limits of detectability, repeatability and sensitivity, the requirements for possible refinement of existing NDT methods, and the need to develop new techniques. The application of the nondestructive analysis techniques to these carbon-carbon composites will provide information that will be valuable in the evaluation of other composite materials.

Control specimens and those containing intentionally-introduced defects were evaluated to determine what relationships existed between nondestructive test response data and room temperature mechanical properties. The effect of these defects on the mechanical properties of the composite system were evaluated. The program was designed to evaluate the interrelationship between the yarns and binders in the unidirectional composites by employing uniaxial tension and shear tests. Uniaxial tension and compression tests were performed on the multidirectional composite.

## II. SUMMARY

The application of nondestructive testing techniques to unidirectional and multidirectional carbon-carbon composites for the detection and characterization of material discontinuities and variability has provided insights into the relationships among these materials, processing procedures, and material properties. Mechanical testing of the composites containing intentional defects has significantly contributed to the understanding of the factors affecting the mechanical properties. The characterization of precursor materials and the processed composites has aided in understanding the effect of processing conditions on composite properties.

Characterization of the precursor materials, yarns, woven fabric, and binders, included Differential Thermogravimetric Analysis, determination of thermal expansion and breaking load, and chemical analyses. A preheat treatment of the VYB 70 1/2 yarn was necessary to minimize the weight loss and shrinkage of the yarn during pyrolysis. The weight loss was typically 20 to 25 percent. Irreversible shrinkages of the VYB 70 1/2 yarn were observed to increase with increasing oxygen concentration in a helium atmosphere at 975°C. The characterization of the Thornel 50 and Modmor II yarns indicated that these yarns did not undergo any significant weight losses (approximately 1 percent at 1000°C). The sizing material added during the weaving of the multidirectional fabric was removed, a required step prior to processing. This was accomplished by washing with a polar solvent. The breaking load of the carbon yarn was not appreciably reduced by preheat treatment or handling of the yarn during the weaving process.

The thermal degradation behavior of the coal tar pitch was determined as a function of composition by a Differential Thermogravimetric Analysis technique. Groups of related species or components have been isolated by both progressive heat treatment (vacuum fractionation) and solvent extraction procedures. By selected treatments, coke values of some components were increased greatly. The viscosity for the pitch fraction heated to 475°C had a pronounced increase after a given time which was attributed to a loss of volatiles and/or thermal decomposition of the pitch.

The processed composite panels were characterized by porosimetry and microstructural analyses after the pyrolysis and graphitization steps to provide information on composite uniformity. Upon graphitization, the apparent density and porosity increased from the pyrolyzed values. Both closed and open pores were found to increase. The intentional-defect specimens consistently had a higher porosity than the no-intentional-defect specimens.

The nondestructive analysis techniques were applied to the carbon-carbon composites after each major processing step (weave, cure, pyrolysis, and graphitization). The techniques employed for the evaluation included X-ray and neutron radiography, ultrasonic attenuation and pulse-echo C-scan mapping, and ultrasonic longitudinal and transverse velocity measurements. The combination of the X-ray radiography and attenuation and velocity techniques detected the intentional defects introduced into the unidirectional and multidirectional composites. Monitoring of material uniformity and detecting discrete discontinuities was successful. The techniques were sensitive to the concentration and magnitude of defects present. The techniques were also sensitive to the composite processing conditions.

X-ray radiography, applied on an in-process basis, was useful in aiding the composite material development. The X-ray technique was capable of detecting areas of nonuniformities in the 0.10-inch thick unidirectional composites and in the 0.5- to 4.0-inch thick multidirectional composites. The sensitivity of the X-ray radiographic technique was affected by material thickness and weave geometry. The selected X-ray parameters provided a sensitivity of 0.5 percent for the unidirectional, 0.8 percent for the 0.5-inch thick DACLOCK 120 multidirectional, and 2.0 percent for the 1.0-inch thick orthogonal multidirectional composites. The use of an X-ray absorbing doping agent, tetrabromoethane, and an image enhancement technique provided additional defect information on Thornel 50 - pitch unidirectional composites. The largest increases in sensitivity were obtained with samples impregnated with the doping agent. The application of neutron radiography to the unidirectional composites was not as successful as X-ray radiography and it did not supply any additional information.

The ultrasonic through-transmission attenuation technique was sensitive to material nonuniformity, discrete discontinuities, and processing conditions. The measured attenuation of the intentional defect specimens was higher than the attenuation of the no-intentional-defect specimens. The attenuation also increased upon graphitization. The sensitivity and resolution of the technique was determined with the use of a standard containing artificial defects. The material thickness and weave geometry were found to have a pronounced effect on defect sensitivity. For the 0.10-inch thick unidirectional composites, the sensitivity (size of defect) was approximately a .060-inch diameter flat-bottom hole penetrating 50 percent of the thickness with a resolution (distance between adjacent defects) of 0.20 inches. For the multidirectional composites, the sensitivities were a 0.20-inch diameter hole for the 0.50-inch thick DACLOCK 120 and a 0.39-inch diameter hole for the 1.0 inch thick orthogonal composite. Evaluation of the attenuation technique showed that a collimated receiver increased the sensitivity and resolution of the technique. It was found that a narrow sound beam profile was best for defect detection. The attenuation technique was successfully employed in evaluating the 4.0-inch thick multidirectional composites.

The measured ultrasonic attenuation was related to the porosity of the composites. The trends indicated that higher attenuation corresponded to higher porosity. In addition, trends were found to exist between attenuation measurements made on the pyrolyzed composites and porosity measurements made on the graphitized composites. This suggests the value of using the attenuation technique on an in-process basis.

The attenuation technique provided better results than the pulse-echo technique for in-process and final inspection of the unidirectional and coarse weave (DACLOCK 120) multidirectional composites. The degree of scattering and attenuation present within the composites greatly limited the pulse-echo technique. However, the pulse-echo technique was useful in evaluating the fine weave, high density, AVCO MOD II 4-inch thick multidirectional composite.

The ultrasonic longitudinal and transverse velocity measurements made on the composites indicated a lower velocity for the defect specimens as compared to the no-intentional-defect specimens. The transverse velocity measurements did not appear to offer any advantage over the longitudinal velocity measurements for defect detection. The longitudinal velocity of the pyrolyzed composites was greater than the velocity of the graphitized composites. The velocity was related to the density of the pyrolyzed and graphitized composites with the trends indicating higher velocity corresponding to higher density. These trends in velocity were attributed to the increase in porosity. This suggested that the screening of low density composites could be accomplished by the velocity measurements.

The longitudinal velocity of the unidirectional and multidirectional carbon-carbon composites was frequency dependent. This dependence was different for each of the composite systems evaluated. The velocity-frequency results have shown that defect detection can be enhanced by selection of the proper frequency.

Mechanical tests were performed at room temperature on the unidirectional and multidirectional composites to determine the effect of the intentional defects, to establish correlations with porosity and the NDT data and to determine the effect of different yarn-binder combinations. The mechanical testing included uniaxial tension and shear tests for the unidirectional composites and uniaxial tension and compression tests for the multidirectional composites. Different mechanical properties were obtained depending on the type of yarn and binder used and their compatibility. The material condition, pyrolyzed or graphitized, played an important role in the mechanical properties.

In general, the tension and shear properties of the unidirectional composites and the compressive properties of the multidirectional composites were reduced by the presence of intentional defects. However, the tensile strength of the VYB 70 1/2 - pitch unidirectional and DACLOCK 120 multidirectional composites were actually increased by the presence of small voids and lack of wetting. After graphitization, the shear strengths of the unidirectional and compressive strengths of the multidirectional composites decreased while the tensile properties of both composite systems increased. For the graphitized multidirectional composites, the compressive strengths were one-half the pyrolyzed composite strengths and the compressive strains were twice the pyrolyzed composite strains.



A bilinear stress-strain curve was observed for the unidirectional VYB 70 1/2 composites with the final tangent modulus being higher than the initial Young's modulus. This was particularly true for the pitch composites which had an initial modulus of  $6.0 \times 10^6$  psi and a final of  $12.0 \times 10^6$  psi. The final modulus of the graphitized VYB 70 1/2 - SC1008 and VYB 70 1/2 - pitch composites was greater than the modulus of the VYB 70 1/2 yarn itself. The less graphitic matrix (SC1008) appeared to be more sensitive to defects. The VYB 70 1/2 - and Modmor II - pitch composites gave similar composite tensile strengths while the Thornel 50 - pitch composite had at least double the Modmor II - pitch composite strengths. This suggested that sufficient differences in yarn surface conditions provided better wetting and bonding of the matrix to the yarn and therefore, better utilization of the Thornel 50 yarn strength than of the Modmor II yarn strength.

The porosity present in the composites had a significant and different effect on each of the mechanical properties. The VYB 70 1/2 - SC1008 unidirectional composites had a porosity range of 16 to 30 percent. Over this range, tensile and shear strengths decreased with increasing porosity. The VYB 70 1/2 - pitch unidirectional and multidirectional composites had a porosity range of 5 to 15 percent. At low porosities in this range, the tensile strength appeared to increase with increasing porosity to a maximum value and then to decrease with further increase in porosity. The compressive strength (multidirectional VYB 70 1/2 - pitch) decreased monotonically with increasing porosity. The Modmor II - pitch unidirectional composites had a similar range of porosity as the VYB 70 1/2 - pitch. The tensile strength showed a similar trend to that of the VYB 70 1/2 - pitch data and the shear strengths decreased monotonically with increasing porosity. The apparent existence of an optimum porosity level for maximizing tensile strength shows that maximizing composite density does not always result in optimum composite properties.

The porosity of the pyrolyzed unidirectional composites was correlated to the strengths of the graphitized unidirectional composites. This suggests that in-process measurements can provide information on final composite properties.

The nondestructive test data which was obtained on the mechanical test specimen was correlated to their mechanical properties. The trends indicated lower attenuation and higher velocity corresponded to higher shear and compressive strengths. The attenuation of the pyrolyzed composites was indicative of the strength of the graphitized composites. No trends were found to exist between the velocity in the thickness direction and the strengths in the fiber direction of the unidirectional composites.

The dynamic modulus,  $\rho v_{11}^2$  (velocity in thickness direction), was related to the measured modulus in the yarn direction of the unidirectional composites. The dynamic modulus on the pyrolyzed composite correlated to the modulus of the graphitized composite, suggesting the use of an in-process nondestructive analysis for evaluating composite properties.

### III. RESULTS AND DISCUSSION

#### 1.0 Material Selection

The primary criterion used for the selection of precursor materials was that the carbon-carbon composites be fabricated from current state-of-the-art materials. A combination of unidirectional and multidirectional-woven composites were chosen for evaluation. Both carbon and graphite yarns together with a pitch binder and a synthetic resin binder were evaluated. The composite systems evaluated are listed in Table I. The rationale for selection of these materials is presented in Reference 1.

Another unidirectional composite, Thornel 50 - coal tar pitch, had a limited evaluation involving characterization and mechanical testing. Two multidirectional composites, a 1.0-inch thick orthogonally woven CX 70 1/2 - coal tar pitch composite and AVCO MOD III carbon-carbon billets, were evaluated to determine what limitations existed in the nondestructive test techniques developed for the angle-interlocked composite due to thickness and reinforcement construction.

#### 2.0 Characterization of Precursor Materials

The characterization of the precursor materials (binders and fibers) is important in a materials development program since slight differences in the precursor materials or processing steps may cause significant changes in the physical and mechanical properties of the final product. In addition, this characterization study was a starting point from which to investigate alterations of these materials during processing. A brief summary of the characterization test results for the VYB 70 1/2, Thornel 60, and Modmor II yarns, SC1008 and pitch binders, and DACLOCK 120 multidirectional fabric, which were presented in detail in Reference 1, is made in the following subsections. The main emphasis of the discussion is placed on the characterization of the CX 70 1/2 yarn, pitch binder, and orthogonal multidirectional fabric.

Table I

#### COMPOSITE MATERIALS

<u>Composite Geometry</u>	<u>Yarn - Binder System</u>
Unidirectional	VYB 70 1/2 - SC1008 phenolic VYB 70 1/2 - Coal tar pitch Modmor II - Coal tar pitch
Multidirectional Angle-Interlocked (DACLOCK 120)	VYB 70 1/2 - Coal tar pitch

## 2.1 Yarns

The VYB 70 1/2, Thornel 50, and Modmor II yarns were characterized as to carbon assay, ash analysis, emission spectral analysis, and weight loss as a function of temperature. Analysis and tests showed that a preheat treatment of VYB 70 1/2 yarn was necessary to minimize the weight loss and shrinkage of the yarn during pyrolysis (Reference 1). In characterizing the VYB carbon yarn, the volatiles obtained from the yarn upon heating were resolved into its component parts, moisture, coating, sorbed oxygen, and other elements such as phosphorus, by Differential Thermogravimetric Analysis (DTA). The weight loss was typically 20 to 25 percent. The oxygen is lost in the form of carbon dioxide or monoxide. The thermal expansion of the VYB 70 1/2 carbon yarn was evaluated as a function of temperature and oxygen concentration in a helium atmosphere. Irreversible shrinkages were observed to increase with increasing oxygen concentration at 975°C. The characterization of the Thornel 50 and Modmor II graphite fibers indicated that these fibers do not undergo any significant weight losses (approximately 1 percent at 1000°C).

The carbon yarn used in the weaving of the one-inch thick orthogonally woven multidirectional composite was Fiber Technology CX 70 1/2 yarn sized with polyvinyl alcohol. A single ply of this yarn consists of 720 filaments. Typical filament properties as supplied by the manufacturer are summarized in Table II.

## 2.2 Woven Goods

The 0.5-inch thick DACLOCK 120 multidirectional fabric construction (Figure 2) consisted of fibers in the X-(length) and Y-(width) directions being layed up at 90° to each other in layers with the fiber for the third direction being angled at approximately 38° through the thickness.

Table II

### TYPICAL CX 70 1/2 YARN PROPERTIES

Tensile Strength	150 - 180 ksi
Modulus of Elasticity	3 - 8 x 10 <sup>6</sup> psi
Density	1.45 g/cc
Carbon Assay	90 - 99%
Specific Heat	0.16 Btu/lb°F
Total Ash	0.5%
Chemical Analysis	
Sodium	1500 ppm
Potassium	150 ppm
Lithium	1 ppm
Calcium	100 ppm
Magnesium	10 ppm

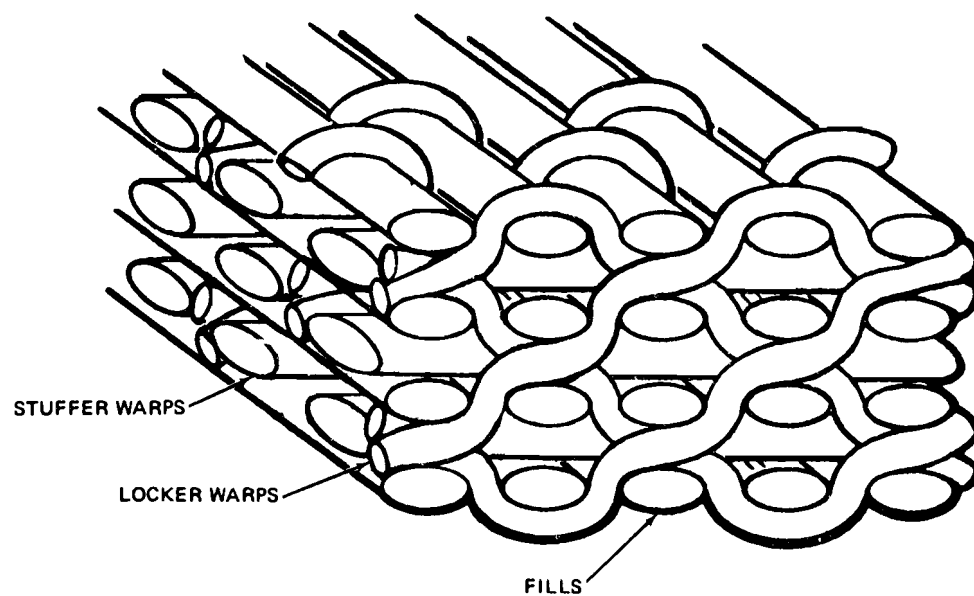


Figure 2. DACLOCK 120 Weave Pattern

It was found the sizing material added during the weaving process of the yarn for the multidirectional fabric can be removed by washing with polar solvents, including water, which was required before processing. The breaking strength of the carbon yarn was not appreciably reduced by preheat treatment or handling of yarn during the weaving process (Reference 1).

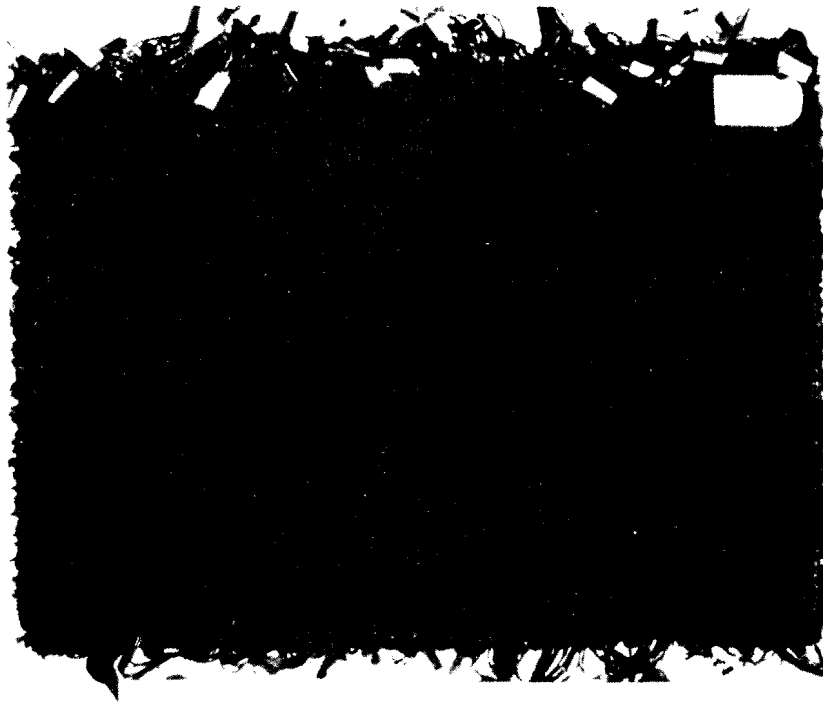
The characterization of the as-woven 1.0-inch thick orthogonal multidirectional composite consisted of measuring fabric thickness, density and yarn count, photographing the top and bottom surfaces, and X-ray radiographing the fabric panel. This fabric is constructed such that the fibers in the three directions are at 90° to each other. The longitudinal fibers are on 0.125-inch centers while the radial and circumferential fibers are on 0.050-inch centers. The fabric thickness ranged from 1.000- to 1.120-inches thick with the average being 1.101 inches. The fabric density was determined to be 0.776 g/cc by bulk measurements. The volume fraction of yarn was approximately 52 percent based on a yarn density of 1.5 g/cc. Approximately 50 square inches of this fabric were obtained from Fiber Materials, Inc.

The X-ray radiographic analysis was conducted on the fabric to determine the weave uniformity. The X-ray radiographic parameters were selected by conducting a series of radiographic film exposures and then qualitatively comparing the image definition obtained for the weave pattern. The exposure parameters selected were voltage - 28 kv, current - 10 ma, film to focal point distance - 29 in., film-Kodak Type M, and screen - .004-inch polyethylene.

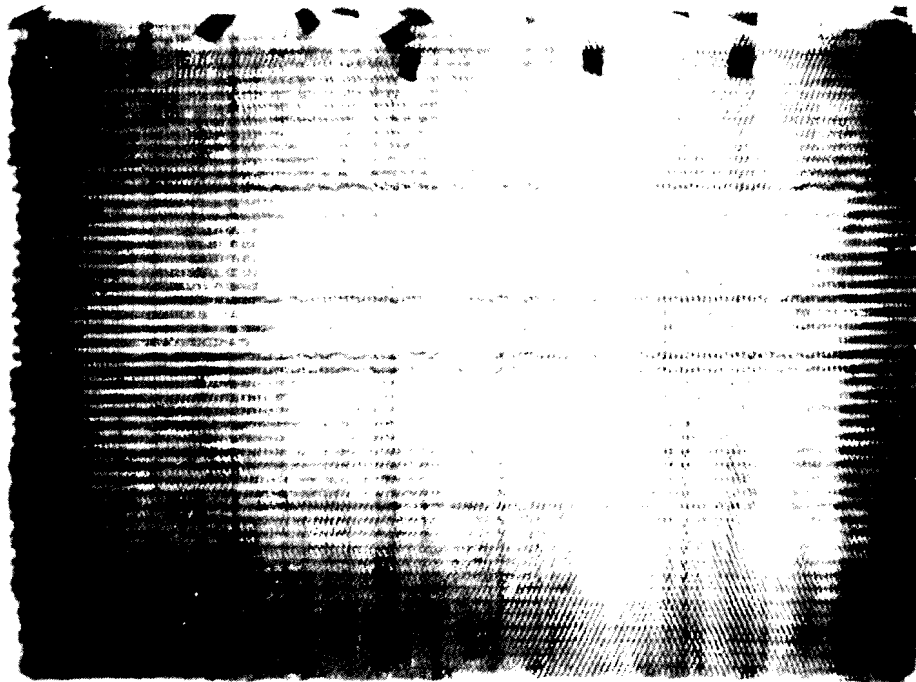
The photograph of the top surface and the positive print of the X-ray radiograph are shown in Figure 3. The positive prints of the X-ray radiograph, which were taken with the top surface facing the X-ray source, revealed weaving irregularities that were present within the woven fabric. By comparing the photograph of the surface of the fabric, some weave irregularities are visible on the surface of the fabric. However, surface inspection can be misleading as to the extent of an irregularity because of a relatively subtle surface manifestation (or none at all) can mask large-scale yarn turbulence beneath the surface. The application of the X-ray radiographic technique to the as-woven multidirectional fabric has shown that the X-ray indications can be directly related to weaving irregularities present within the fabric (Reference 1).

### 2.3 Impregnants

Analysis of the thermal degradation behavior of the coal tar pitch as a function of composition was determined by a Differential Thermogravimetric Analysis technique (Reference 1). Groups of related species of components were isolated by both progressive heat treatment (vacuum fractionation) and solvent extraction procedures. By selected treatments, coke values of some components were increased greatly. The viscosity for the pitch fraction heated to 475°C had a pronounced increase after a given time which was attributed to a loss of volatiles and/or thermal decomposition of the pitch.



Photograph of Top Surface



Positive Print of X-Ray Negative

Figure 3. Photograph of Top Surface and Positive Print of X-Ray Radiographic Negative of One-Inch Thick Orthogonally Woven Panel

### 3.0 Processing

A number of processing methods were evaluated for the fabrication of the unidirectional and multidirectional carbon-carbon composites. Microstructural analyses, porosimetry, measurements, and mechanical tests were conducted to evaluate each processing procedure. Based upon the results of these tests (Reference 1), the optimum processing methods for each unidirectional and multidirectional composite system were selected and are described herein.

A laboratory evaluation was conducted to develop the methods for producing the specific intentional defects in the composites. The intentional defects which were examined include (1) matrix porosity or low density, (2) lack of wetting and bonding at the reinforcement-binder interface, (3) broken yarns and misaligned or irregular weaving, and (4) delaminations and cracks (unidirectional system only). The fabrication of intentional defects in the unidirectional composites was accomplished by changing or disrupting the fabrication procedure so that a particular type of defect was produced. This aided the determination of the effect of the particular defect on the composite properties.

#### 3.1 Unidirectional Fabrication

Conventional unidirectional winding techniques were employed in an argon atmosphere to prepare the composite test specimens. The unidirectional winding apparatus (Figure 4) included a yarn heating assembly to permit the heating, impregnation, and winding of the yarn under argon without intermittent transfers. This minimized contamination of the yarn due to excessive handling and exposure to the atmosphere. The VYB 70 1/2, Thornel 50 and Modmor II yarns were heat treated by internal resistance to between 1100°C and 1300°C for approximately two seconds prior to the yarn passing through the pan containing the impregnant. In the case of the VYB 70 1/2 yarn, which was found to absorb moisture and air (Reference 1), an outgassing at approximately 110°C under vacuum for 24 hours was performed prior to the winding procedure.

The unidirectional VYB 70 1/2 composite fabricated with the SC1008 resin underwent three processing procedures; cure, pyrolysis, and graphitization. The cure procedure consisted of vacuum bagging and heating to 150°F for 8 hours, pressing to 160 psi for 4 hours at 180°F and pressing to 160 psi for 4 hours at 325°F. A 30-hour pyrolysis cycle to 1000°C was selected for all the SC1008 composites so that a minimum number of pores would be produced in the composite. The specimens were then graphitized to 2800°C with a one-hour hold at temperature. The methods of fabricating the controlled defects in this material system (Reference 1) are summarized in Table III. Composite specimens with all of these defects were fabricated for the VYB 70 1/2 - SC1008 system. The number of types of defects was reduced for the VYB 70 1/2 - pitch and Modmor II - pitch composites due to a change of scope during the program. The term weave defect here describes broken, misaligned, or misplaced yarns produced manually.

The pitch composites, VYB 70 1/2, Thornel 50, and Modmor II, underwent the same winding operation as in the SC1008 system. The pitch extraction (Reference 1) used for impregnation was heated under an argon atmosphere at approximately 300°C for 4 hours to remove excess benzene. During the winding operation the pitch was maintained at approximately 150°C.

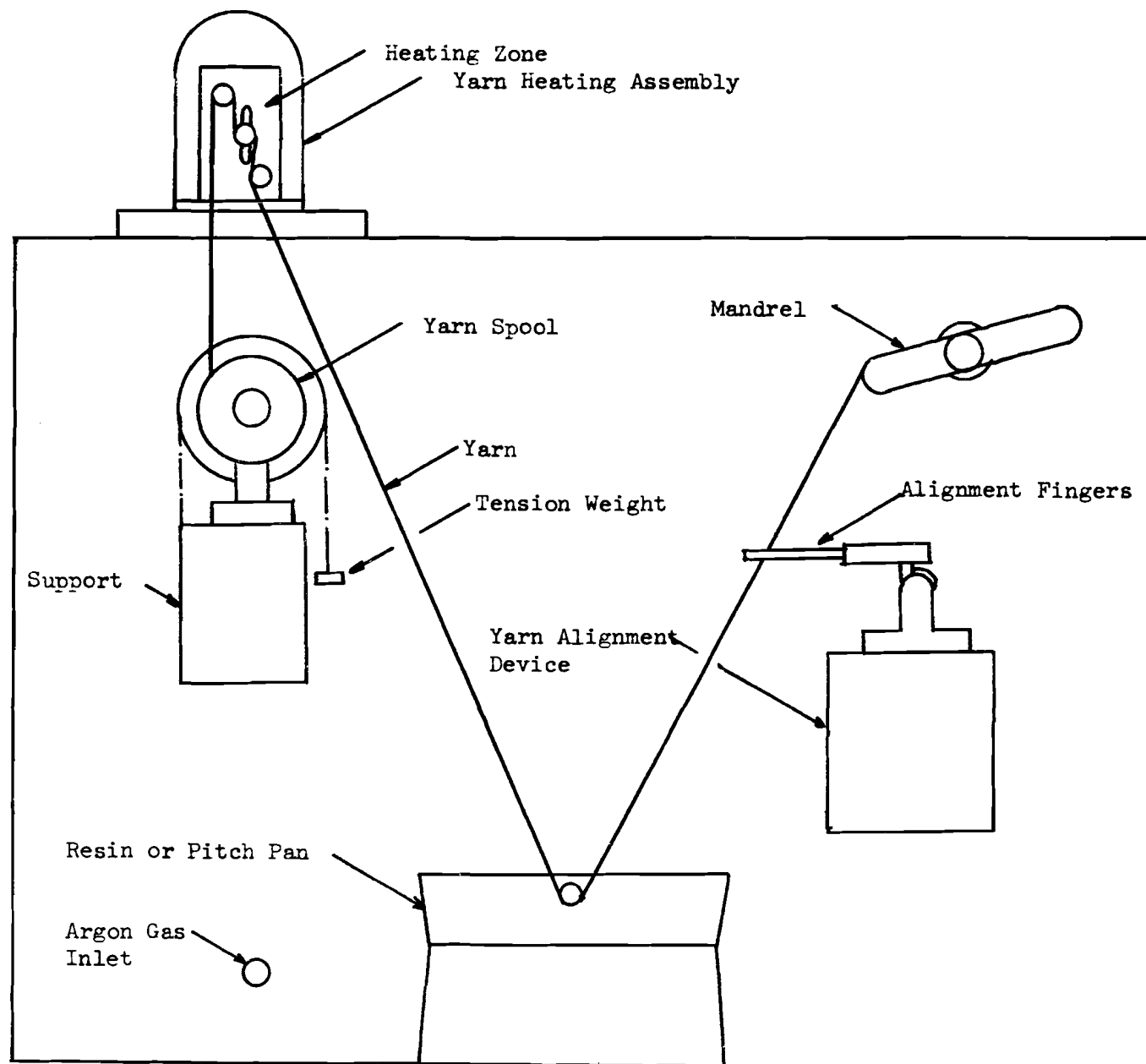


Figure 4. Unidirectional Winding Apparatus



Table III

METHODS OF FABRICATING SPECIFIC DEFECTS IN SC1008  
UNIDIRECTIONAL COMPOSITES

Defect Type	Method of Fabrication	Amount
Small voids	Sugar - 0.00696 to 0.00586-in. dia. (added during winding operations)	12-1/2% by volume
Weave	Disrupting winding operation	----
Cracks in binder	Proper selection of specimens for the SC1008 system	----
Delamination	Mylar - 0.0005 or 0.00015-in. thick (added during winding operations)	one layer
Lack of wetting	Colloidal graphite spray prior to yarn entering pan	all yarn
Large voids	Sugar - 0.0232 to 0.0197-in. dia. (added during winding operations)	12-1/2% by volume
Poor fiber bundle	Prepreg yarn with camphor - ethyl alcohol mixture prior to impreg- nating with binder	all yarn
Noncarbonaceous impurities	Addition of silica spheres	12-1/2% by volume

The processing procedure for the majority of the VYB 70 1/2 and all the Thornel 50 and Modmor II specimens consisted of a low temperature press to obtain the desired fiber packing and thickness (approximately 0.150 inches) and contained a pyrolysis cycle to 500°C. The specimens were then pyrolyzed to 1000°C followed by a contained (autoclave) pyrolysis reimpregnation sequence. The specimens then underwent another pyrolysis sequence to 1000°C and a graphitization to 2800°C with a one-hour hold at temperature.

Eight of the VYB 70 1/2 - pitch no-intentional-defect specimens underwent a slightly different processing procedure. The specimens were pressed at 170°F to a thickness of 0.25 inches. The specimen then underwent a pressure pyrolysis cycle at a predetermined schedule to 1000°C followed by the graphitization procedure described above. This pressure pyrolysis was conducted to investigate the effect of pressure on the pore structure and mechanical properties of these composites.

Intentional defects were introduced into the VYB 70 1/2 - and Modmor II - pitch composite systems by utilizing similar methods as used in the SC1008 system. One exception to this was the fabrication of small voids and lack of wetting defects. In this case, the second impregnation and contained pyrolysis sequence were eliminated. The intentional defects introduced into the VYB 70 1/2 - and Modmor II - pitch were of less severity than those introduced into the VYB 70 1/2 - SC1008 composites. This provided the opportunity to evaluate the NDT technique's sensitivity to small defects. In addition, the effect of smaller defects on the mechanical properties could be assessed.

### 3.2 Multidirectional Fabrication

The general objective in the fabrication of the multidirectional composites, DACLOCK 120 - angle interlocked, and orthogonally woven fabrics, was to impregnate and fill the voids between and within yarns with a matrix which has a high density and a minimum number of flaws. Experience with the specially processed coal tar pitch has shown that after impregnation the yarns are readily filled as are the voids between yarns. The major problem was to retain the impregnant during the early stages of the pyrolysis cycle.

The as-received DACLOCK 120 fabric was coated with a water-glycerin mixture to minimize yarn breakage during weaving. The yarn was also sized with polyvinyl alcohol (PVA). To remove these contaminants which jeopardize good wetting and bonding and produce an excessively large amount of volatiles during pyrolysis, the fabric was washed in boiling water for 60 minutes to remove the glycerin and then heat treated to 1000°C in an inert atmosphere (argon) to remove the PVA and any absorbed gases. The orthogonally woven fabric underwent only the heat cleaning cycle since the yarns were coated only with a PVA sizing.

After impregnation, there was excellent retention of the impregnant within the yarns because of the surface tension effects between the filaments and the impregnant, provided the yarns are properly cleaned. The small spaces between the filaments greatly assist this process. However, the spacing between the yarns, which are hundreds of times greater than those between the filaments, is of such an extent that surface tension forces are insufficient. Gases evolved from volatile components of the pitch tend to build up pressure in

these spaces and this pressure is relieved by forcing the impregnant out of the fabric which leaves voids. Thus, processing becomes a question of extracting sufficient gaseous components prior to impregnation to minimize expulsion of the impregnant between yarns during pyrolysis while having sufficient viscosity of the impregnant to be able to force it into and between yarns. The approach was to adjust the pyrolysis time to be of sufficient length so that the amount of gas produced was a minimum and the gas can have time to diffuse out of the matrix without forming excessively large voids. A number of pyrolysis rates were investigated between room temperature and 1000°C. The rate selected was between 4 and 12°C per hour.

The pitch fraction used in this multidirectional processing consisted of a thermally-treated coal tar pitch with the higher volatiles removed and with a minimum of quinoline insolubles present. This was different from that used in the unidirectional case where a benzene extract was first made prior to thermal treatment and the quinolene insolubles were removed. Thermally-treated pitch was used because it had a reduced amount of volatiles and an increased carbon yield.

Reimpregnation of the composite material was required because of the loss of weight of the impregnant during pyrolysis which led to the creation of voids. Another means of creating voids was contraction of the impregnant in the temperature range of 600 to 1000°C. This effect led to defects such as cracking or delamination between yarn and matrix. The number of cycles for reimpregnation depended on the carbon yield during pyrolysis and the stability of the woven material during its processing. Five impregnation cycles were utilized for the DACLOCK 120 and orthogonal fabrics. A graphitization step to 2800°C was conducted after the second impregnation. This step caused further contractions of the matrix permitting additional binder to be impregnated into the composite. The graphitization cycle was not considered critical from a rate point of view. The normal rate employed was about 1000°C per hour after the sample had been heated to 1000°C. This graphitization step was conducted in an inert atmosphere at slightly below one atmosphere pressure in order to minimize sublimation effects.

The effect of the different processing sequences on the composite was evaluated. The tests employed to evaluate these processing conditions were room temperature compression tests for ultimate strength, strain to failure, and modulus, mercury porosimetry for density and porosity, thermal stress disc tests, and microstructural analysis. A detailed discussion of these results has been presented in Reference 1. Briefly, these results showed that the maximum density was obtained for composites graphitized after the second impregnation and pyrolysis followed by one additional impregnation. Graphitization during the multiple impregnation process increased both compressive strength and strain-to-failure as compared to graphitization after the multiple impregnations. The microstructural analysis showed that the voids created by graphitization were filled by the subsequent impregnations.

The small void or low density defect was fabricated by simply eliminating the final impregnation sequence. The lack of yarn wetting by the binder defect was accomplished by leaving the PVA and water glycerin sizing mixture on the yarn bundles to inhibit yarn-binder bonding. In addition, the panels were

not processed through the last impregnation sequence. Two of the initially woven panels had sufficient occurrence of weave defects such that a number of defect specimens were excised.

#### 4.0 Composite Characterization

The characterization tests of the three unidirectional systems (VYB 70 1/2 - SC1008, VYB 70 1/2 - pitch and Modmor II - pitch) and the one multidirectional system (DACLOCK 120 - pitch) were conducted after pyrolysis and graphitization. These tests included bulk density and mercury porosimetry measurements and microstructural analyses. Chemical analyses (discussed in Reference 1) and electrical resistivity measurements (Section 6.0) were also made on the VYB 70 1/2 - SC1008 system. X-ray diffraction was used to examine the degree of graphitic structure of the graphitized composites with both the pitch and SC1008 binders. The characterization tests were conducted to provide information on composite uniformity. This information was used to aid in the interpretation and analysis of the NDT and mechanical test data.

#### 4.1 Unidirectional Composites

##### Density and Porosity

The bulk density measurements were made by water immersion with the composite panels coated with a thin film of polyvinyl chloride (PVC). The effect of the PVC coating, which was used to prevent water absorption by the specimen, on the measured densities was found to be very small (1/2 percent) and was neglected. The densities are summarized in Appendix I and Figures 5 to 7. The bulk densities of the specimens containing the intentional defects were generally slightly lower.

Mercury porosimetry measurements were used to measure the amount of apparent porosity present in the samples and to determine the apparent and bulk densities (Reference 2). The bulk density includes both open and closed porosity, whereas the apparent density includes only closed porosity. A summary of the data for the three unidirectional composite systems is shown in Table IV. The porosimetry values for the defect-containing specimens were larger than the no-intentional-defect specimens for the three unidirectional systems. The concentration of void and lack of wetting defects was considerably less in the VYB 70 1/2 - pitch and Modmor II - pitch composites. Generally the apparent density of the composites increases upon graphitization. However, the porosity of the samples also increased upon graphitization. The composites fabricated with the pitch binder (VYB 70 1/2 and Modmor II) had between 2 and 5 times lower porosity in the pyrolyzed condition and 1 to 3 times lower in the graphitized condition than the SC1008 composite system. The density of the VYB 70 1/2 - pitch and Modmor II composites was also significantly larger than the VYB 70 1/2 - SC1008 system. The Modmor II composites had the highest apparent density of the three systems, 1.86 and 2.06 g/cc in the pyrolyzed and graphitized condition.

The no-intentional-defect specimens of the VYB 70 1/2 - pitch system, which had lower porosity values, were processed under a pressure pyrolysis cycle while the remaining specimens, including the small void specimens which had

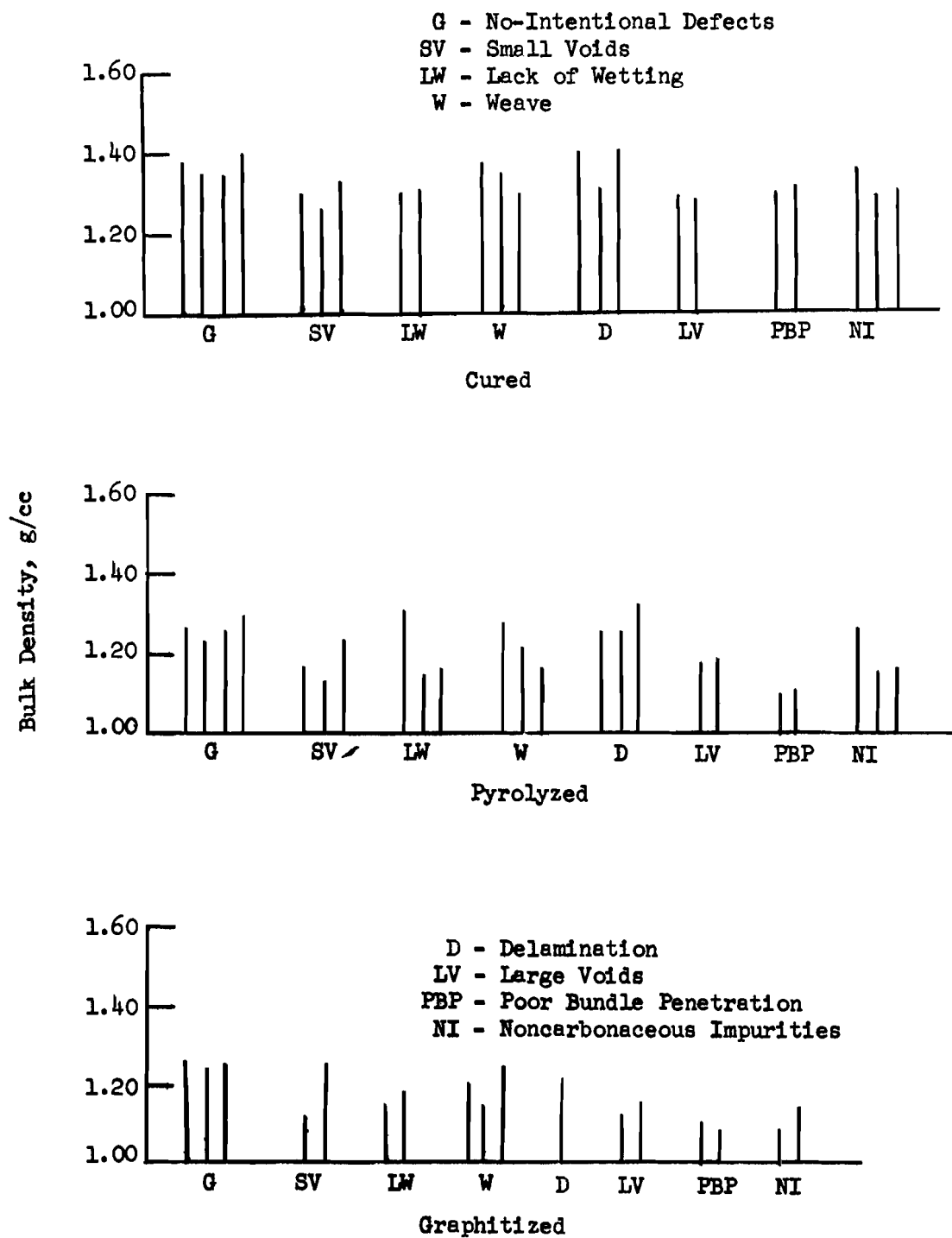


Figure 5. Bulk Density of VYB 70 1/2 - SC1008 Composites

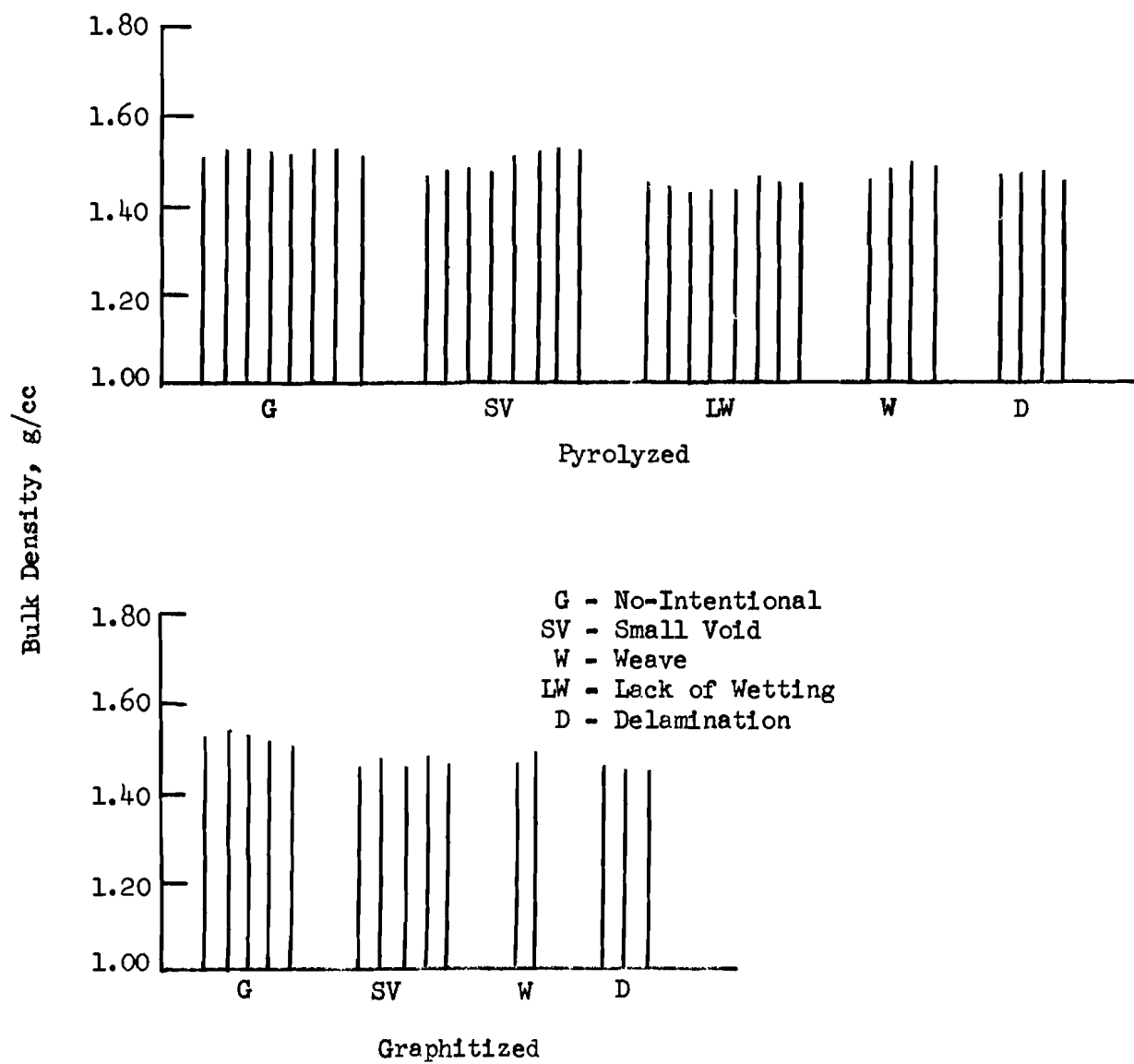


Figure 6. Bulk Density of VYB 70 1/2 - Pitch Composites

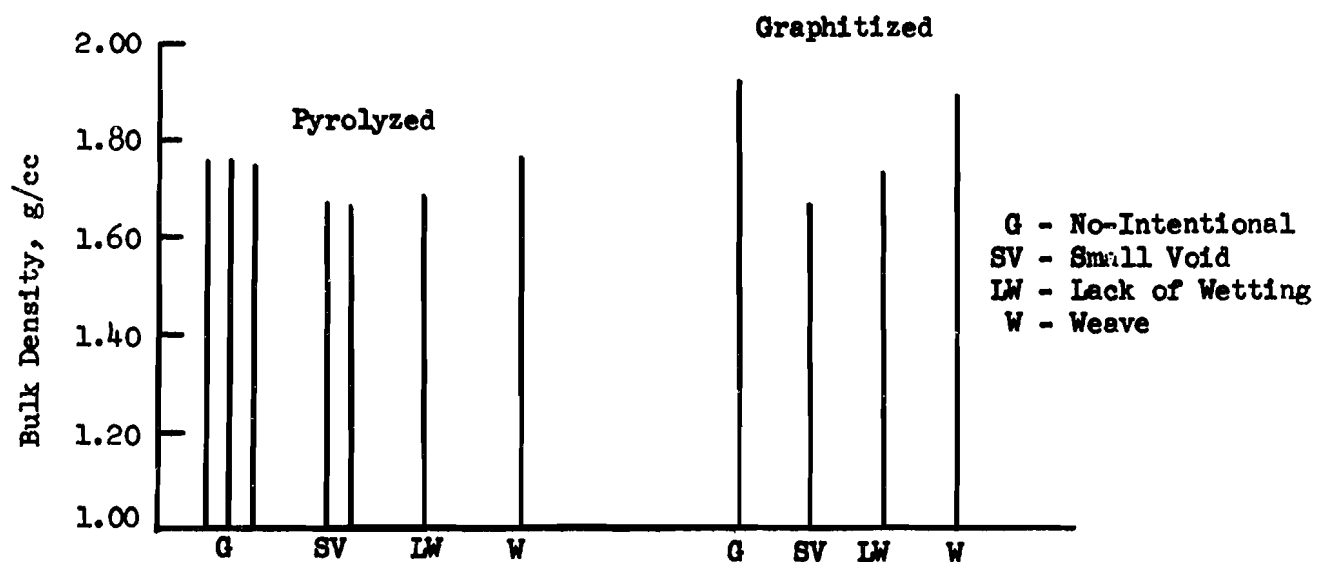


Figure 7. Bulk Density of Modmor II - Pitch Composites

Table IV

## POROSIMETRY MEASUREMENTS FOR UNIDIRECTIONAL COMPOSITES

Specimen	Composite System	Material Condition	Defect	Bulk Density, (g/cc)	Apparent Density, (g/cc)	Apparent Porosity, (%)
14D	VYB 70 1/2 - SC1008	P <sup>(1)</sup>	No-Intentional	1.21	1.43	15.2
14A	VYB 70 1/2 - SC1008	G	No-Intentional	1.23	1.51	19.1
26D	VYB 70 1/2 - SC1008	P	Small Voids	1.15	1.48	22.1
26C	VYB 70 1/2 - SC1008	G	Small Voids	1.22	1.61	24.8
22A	VYB 70 1/2 - SC1008	P	Lack Wetting	1.13	1.45	22.0
22C	VYB 70 1/2 - SC1008	G	Lack Wetting	1.19	1.63	30.3
27A	VYB 70 1/2 - SC1008	P	Large Voids	1.15	1.42	19.1
28C	VYB 70 1/2 - SC1008	G	Large Voids	1.12	1.52	26.3
30C	VYB 70 1/2 - SC1008	P	Poor Bundle Penetration	1.14	1.42	19.8
30D	VYB 70 1/2 - SC1008	G	Poor Bundle Penetration	1.11	1.59	26.9
20C	VYB 70 1/2 - SC1008	G	Noncarbonaceous Impurities	1.07	1.57	31.4
13B	VYB 70 1/2 - Pitch	P	No-Intentional	1.57	1.62	2.9
13A	VYB 70 1/2 - Pitch	G	No-Intentional	1.50	1.60	6.0
21B	VYB 70 1/2 - Pitch	P	Small Voids	1.48	1.63	9.2
22D	VYB 70 1/2 - Pitch	G	Small Voids	1.46	1.66	12.3
6B	VYB 70 1/2 - Pitch	P	Lack Wetting	1.43	1.64	12.7
5A	VYB 70 1/2 - Pitch	G	Lack Wetting	1.39	1.62	14.1
3-8	Modmor II - Pitch	P	No-Intentional	1.73	1.86	6.9
2-5	Modmor II - Pitch	G	No-Intentional	1.79	2.06	13.4
14A	Modmor II - Pitch	P	Small Void	1.61	1.77	9.5
14B	Modmor II - Pitch	G	Small Void	1.62	1.93	16.0
13C	Modmor II - Pitch	P	Lack Wetting	1.62	1.74	6.8
13B	Modmor II - Pitch	G	Lack Wetting	1.66	1.91	13.3

(1) P - Pyrolyzed      G - Graphitized



the higher porosity values, underwent a hydrostatic processing procedure. This difference in processing procedure became important in the analysis of the NDT and mechanical properties.

The analysis of the porosimetry data included relating the pore volume occupied by mercury to the pore diameter. To determine the pore volume occupied by mercury, the following equation was used:

$$M = \frac{V-C}{W}$$

where

M = pore volume occupied by mercury  
V = volume of mercury intruding the pores as a function of pressure  
C = correction constant for compressibility of mercury  
W = weight of sample.

This pore volume was plotted as a function of pressure, and therefore, pore size. From previous work with graphitic materials, the porosity data were evaluated only up to 2000 psi. This was based on the fact that crushing of the graphites appears to occur at higher pressures. This is based on comparing mercury porosimetry data to nitrogen permeability studies (Reference 3).

Graphs of pore volume versus pore size from the porisimeter data for the various unidirectional material systems are shown in Figures 8 to 10. Figure 8 graphically shows the higher porosity (total pore volume occupied by mercury at 2000 psi) of the defect specimens as compared to the porosity of the no-intentional-defect specimens. The pore size distributions (shape of the curves) of the VYB 70 1/2 - SC1008 composite samples changed after the graphitization step from that which was present in the pyrolyzed condition, indicating that a larger number of smaller pore sizes were present.

The pore size variations for the two pitch binder systems (Figures 9 and 10) were not as pronounced as in the SC1008 system. The amount of smaller pores was appreciably reduced in the pitch systems which led to the lower total pore volume occupied by mercury. The VYB 70 1/2 - pitch no-intentional-defect-specimens, which were processed under the pressure pyrolysis cycle, had a uniform distribution of pore sizes. The remaining VYB 70 1/2 - pitch composites, which were processed under the autoclave cycle, had an increase in the number of pore sizes less than 4 microns. The Modmor II - pitch composite specimens also had a uniform distribution of pore sizes.

The pitch systems, as in the SC1008 system, had an increase in the apparent porosity after graphitization. However, this increase was much less than that observed in the SC1008 systems (Figures 9 and 10). The apparent porosity differences which existed between the defect specimens and the no-intentional-defect specimens in the pitch systems were less than in the SC1008 system. This is particularly true for the Modmor II - pitch system where some defect specimens were not significantly different from the no-intentional-defect-specimens (Table IV).

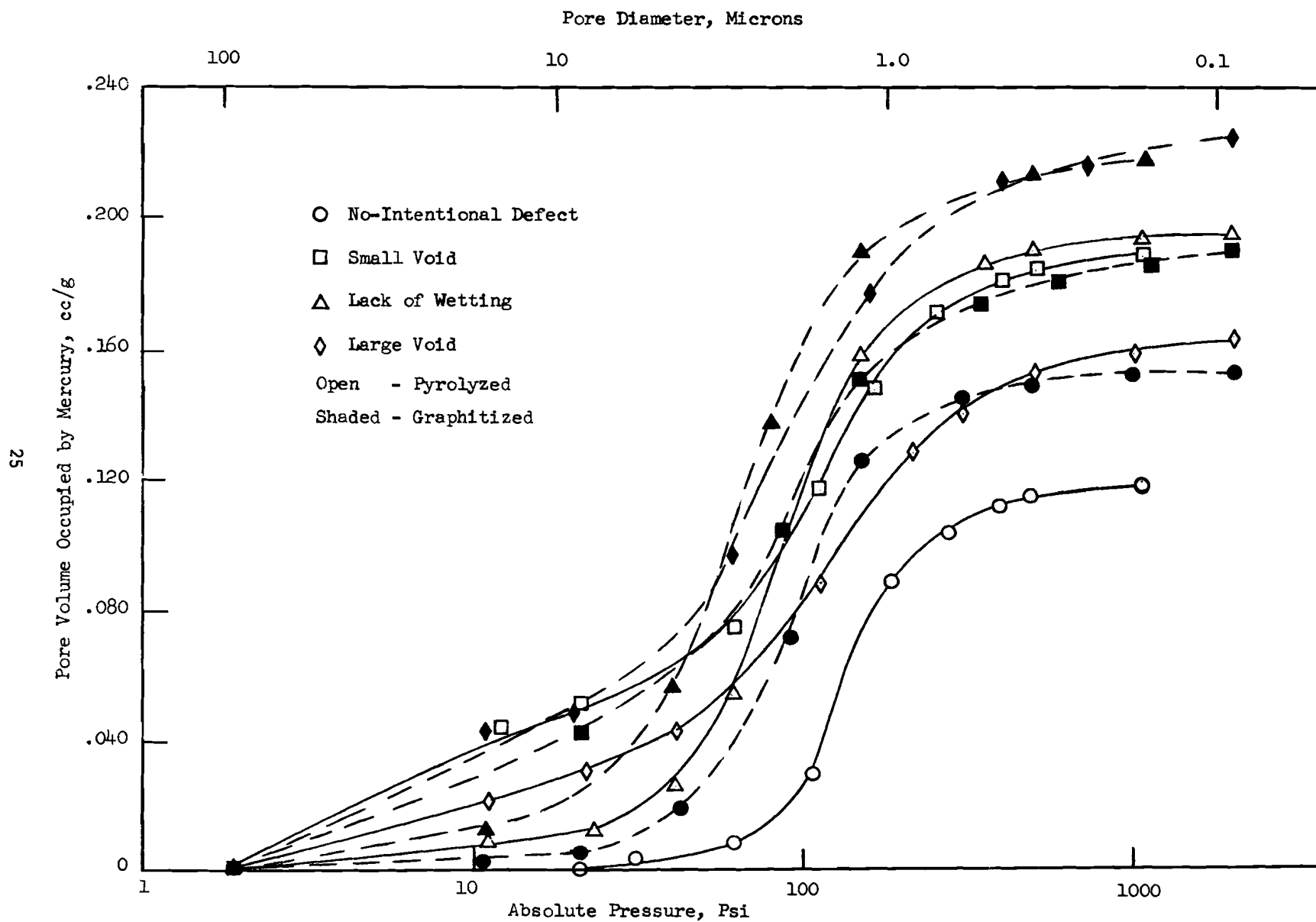


Figure 8. Pore Diameter Versus Pore Volume Occupied by Mercury of VYB 70 1/2 - SC1008 Composites

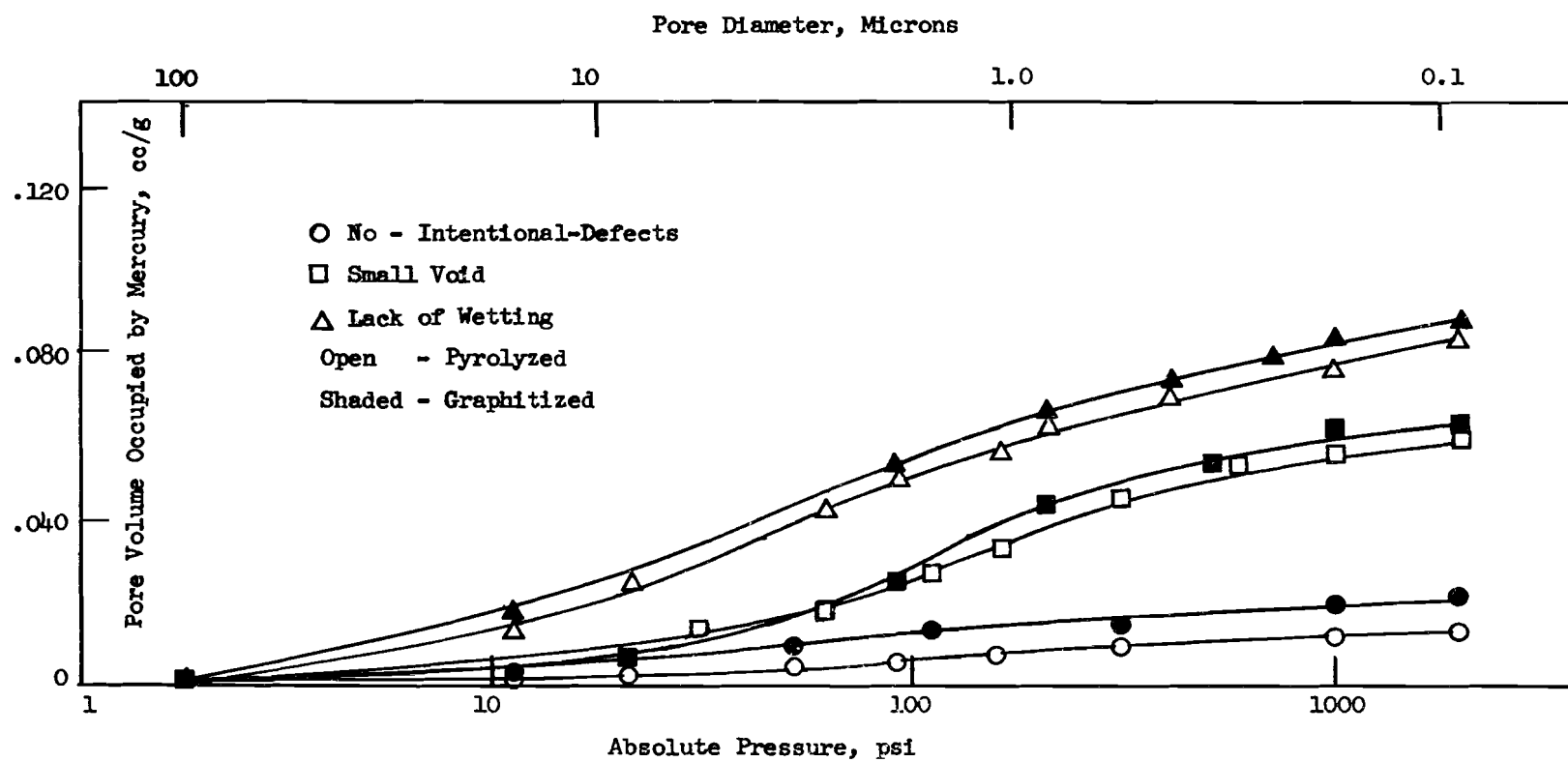


Figure 9. Pore Diameter Versus Pore Volume Occupied By Mercury For VYB 70 1/2 - Pitch Composites

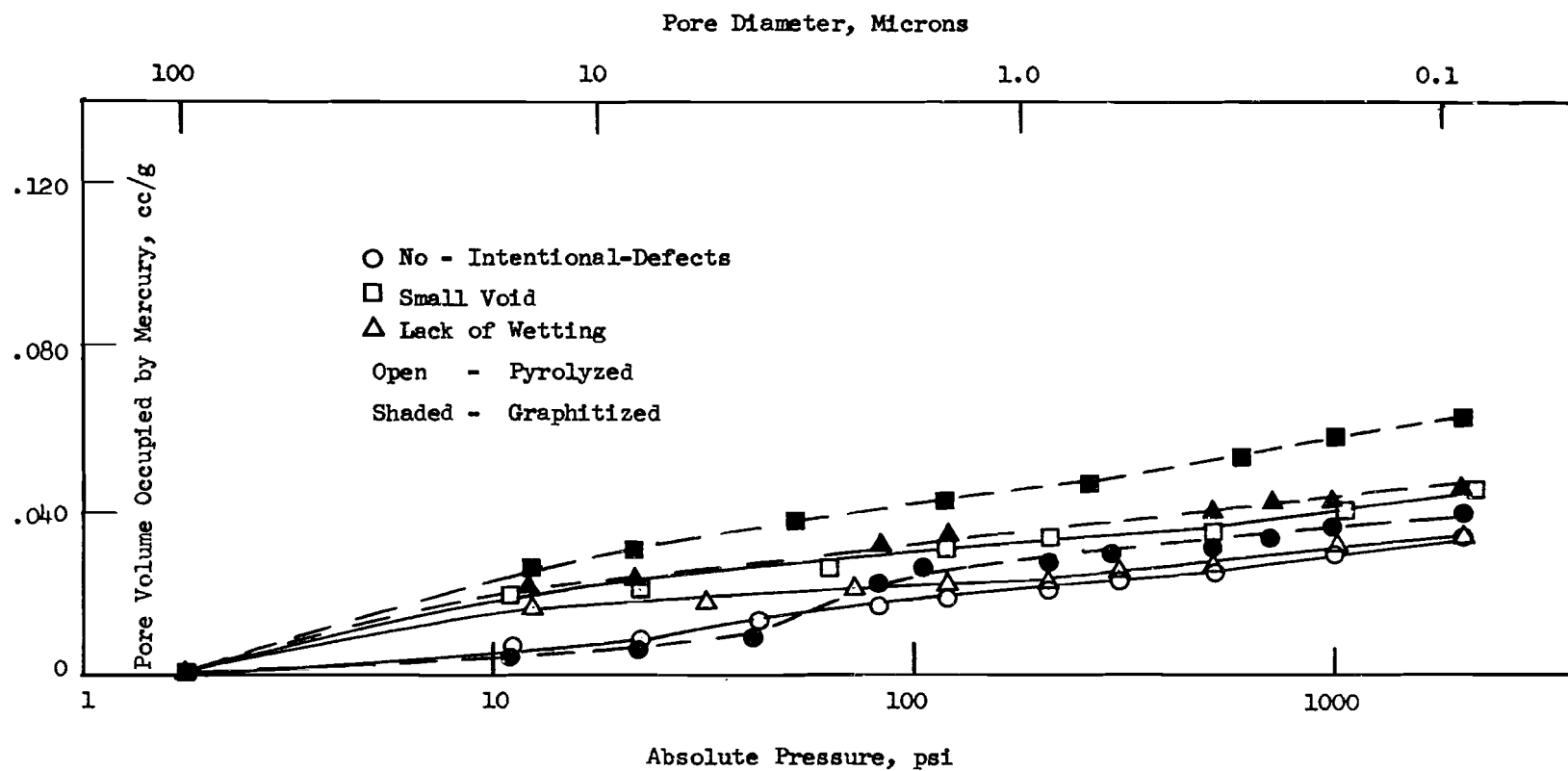


Figure 10. Pore Diameter Versus Pore Volume Occupied By Mercury For Modmor II - Pitch Composites

An estimate of the theoretical density of the pitch composites can be made by using the estimated densities for the yarn and pitch matrix (Table 5) and the following relationship:

$$\begin{aligned}\rho_c &= x_y \rho_y + x_m \rho_m \\ &= x_y \rho_y + (1 - x_y) \rho_m\end{aligned}$$

where

$\rho_c$  = composite density

$\rho_y$  = yarn density

$\rho_m$  = matrix density

$x_m$  = matrix volume percent

$x_y$  = yarn volume percent.

The volume percent of yarn for the VYB 70 1/2 and Modmor II composites was estimated to be 60 percent and 50 percent, respectively. The estimated theoretical composite density for the pyrolyzed and graphitized pitch composites changed by only 5 percent over the limits of the yarn volume percent. The estimated theoretical densities for the VYB 70 1/2 - pitch composites are

$\rho_c$  = 1.68 g/cc      pyrolyzed

$\rho_c$  = 1.72 g/cc      graphitized

Table V  
ESTIMATED YARN AND PITCH MATRIX DENSITIES

Material	Condition	Density, g/cc
Pitch Matrix	Pyrolyzed	1.90
	Graphitized	2.20
VYB 70 1/2	Pyrolyzed	1.54*
	Graphitized	1.40
Modmor II	Pyrolyzed	1.74*
	Graphitized	1.90

\*Manufacturer's data

and for the Modmor II - pitch composites

$$\begin{aligned}\rho_c &= 1.82 \text{ g/cc} && \text{pyrolyzed} \\ \rho_c &= 2.05 \text{ g/cc} && \text{graphitized.}\end{aligned}$$

An estimate of the closed-pore porosity present in the composites can be made using

$$\rho_a = \rho_y x_y + \rho_m (x_m - c_1)$$

where  $\rho_a$  is the measured apparent density and  $c_1$  is the volume percent closed pores, with the assumption that the volume percent of porosity in the yarn is small. The closed porosity estimates for the two pitch composite systems are given in Table VI. The total porosity, closed plus open pores, of the no-intentional-defect-specimens for each of the three unidirectional systems was lower than the total porosity of the defect specimens for both the pyrolyzed and graphitized condition.

The tabulation of the closed porosity estimates for the pitch composites indicates an increase in the amount of closed-pore porosity upon graphitization. Also, the pitch systems had a larger increase in the open pore porosity (Table VI). An increase in open pore porosity was also evident in the SC1008 system (Table IV). The opening of porosity during the graphitization sequence suggests its possible use during the reimpregnation sequences. Reimpregnation after a graphitization sequence will permit an additional and a more thorough flow of impregnate into the composite. This fact will be demonstrated in the following section on multidirectional composite characterization.

The graph of total porosity versus bulk density of the unidirectional composites is shown in Figure 11. The three composite systems had similar trends (lower total porosity - higher density) approximating the general relationship,  $P = 1 - \rho/\rho_c$ . The VYB 70 1/2 - pitch system had the same relationship for both the pyrolyzed and graphitized conditions while the Modmor II - pitch and VYB 70 1/2 - SC1008 systems had different ranges of values for each condition. Total porosity was used in this graph in lieu of the apparent (open) porosity since the closed porosity does significantly effect the results (particularly the graphitized Modmor II - pitch system).

#### Microstructural Analysis

The microstructural analysis was conducted on the pyrolyzed and graphitized VYB 70 1/2 - pitch and Modmor II - pitch unidirectional composites. The approximate pore sizes of the various composite defect groups are summarized in Table VII. The photomicrographs of typical VYB 70 1/2 - pitch and Modmor II-pitch composite specimens in the transverse direction are shown in Figure 12 through 14. The difference in the geometric shape of the Modmor II, round, and VYB 70 1/2, crenulated irregular, yarns is apparent on comparison of Figures 13 and 15. It is apparent that tighter packing of filaments is achieved with regular cross sections.

Table VI  
CLOSED PORE POROSITY ESTIMATES

Composite System	Condition	Defect	Approximate Closed Porosity, (%)	Measured Open <sup>(1)</sup> Porosity, (%)	Total Porosity, (%)	Bulk Density, (%)	Apparent <sup>(2)</sup> Density, (g/cc)
VYB 70 1/2-Pitch	Pyrolyzed Graphitized	No-Intentional	3.2	2.9	6.1	1.57	1.62
			5.5	6.0	11.5	1.50	1.60
	Pyrolyzed Graphitized	Small Void	2.6	9.2	11.8	1.48	1.63
			2.8	12.3	15.1	1.46	1.66
	Pyrolyzed Graphitized	Lack Wetting	2.1	12.7	14.8	1.43	1.64
			4.5	14.1	18.6	1.39	1.62
Modmor II-Pitch	Pyrolyzed Graphitized	No-Intentional	0+	6.9	6.9	1.73	1.86
			0+	13.4	13.4	1.79	2.06
	Pyrolyzed Graphitized	Small Void	2.6	9.5	12.1	1.61	1.77
			5.5	16.0	21.5	1.62	1.93
	Pyrolyzed Graphitized	Lack Wetting	4.2	6.8	11.0	1.62	1.74
			6.4	13.3	19.7	1.66	1.91

(1) Measured apparent porosity by mercury porosimetry

(2) Measured density by mercury porosimetry

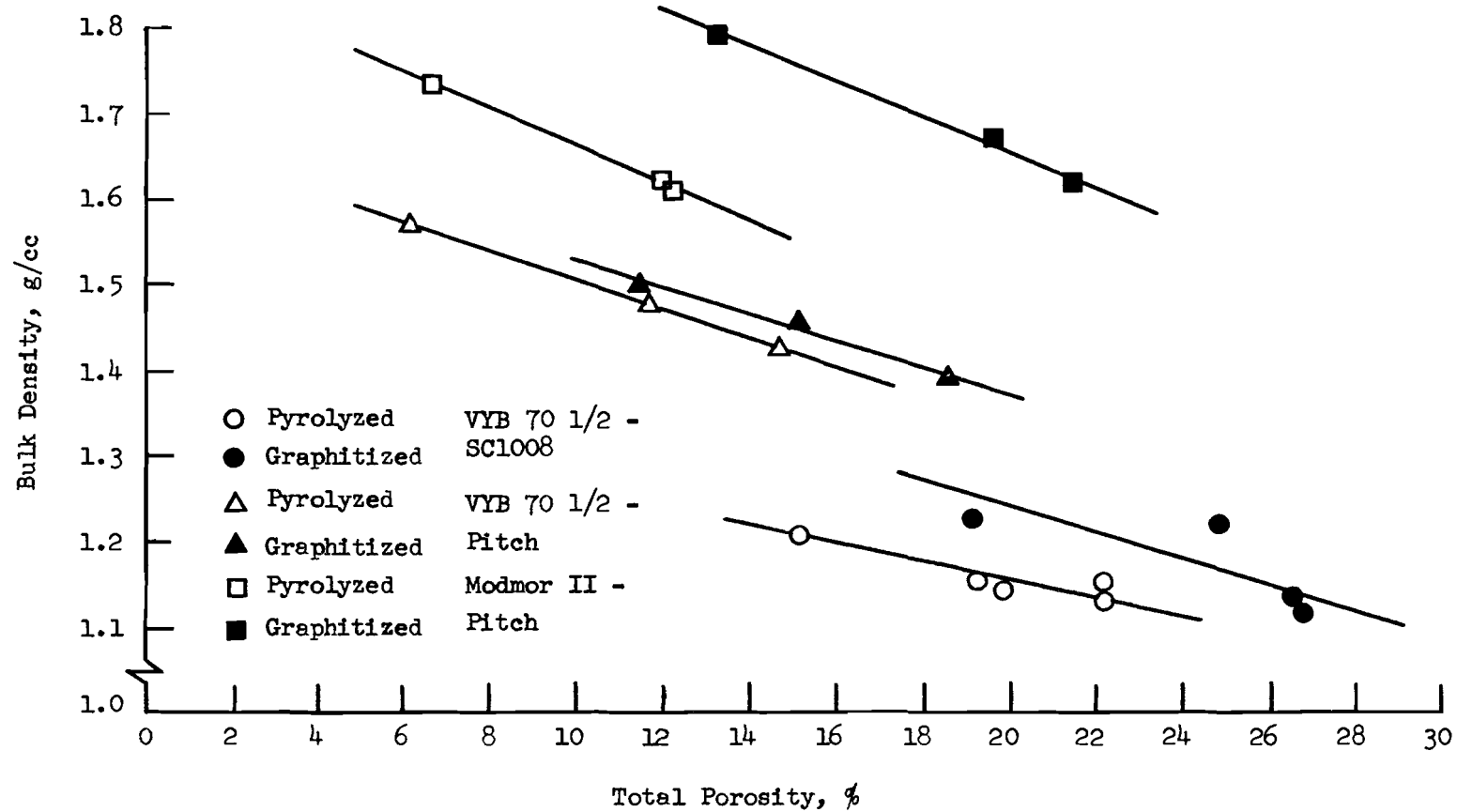
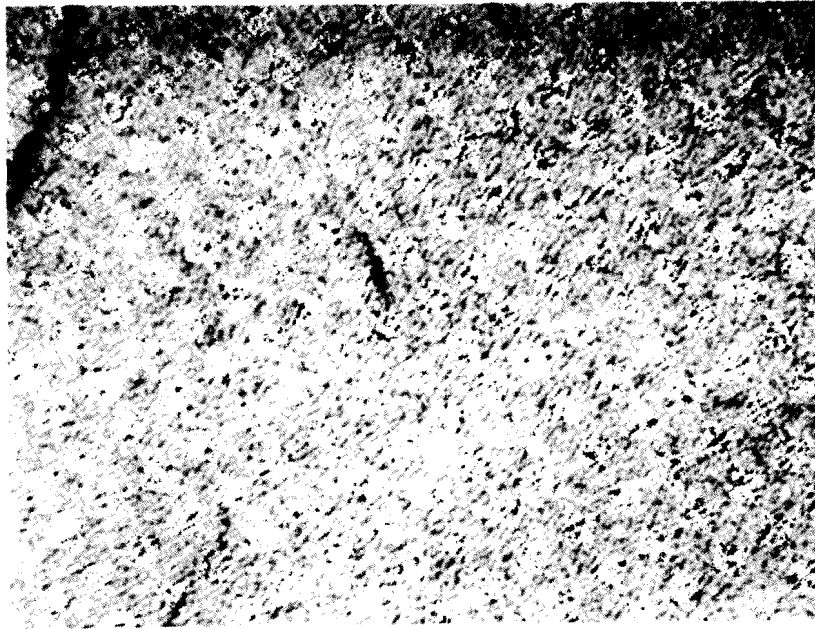


Figure 11. Bulk Density Versus Total Porosity of Unidirectional Composites

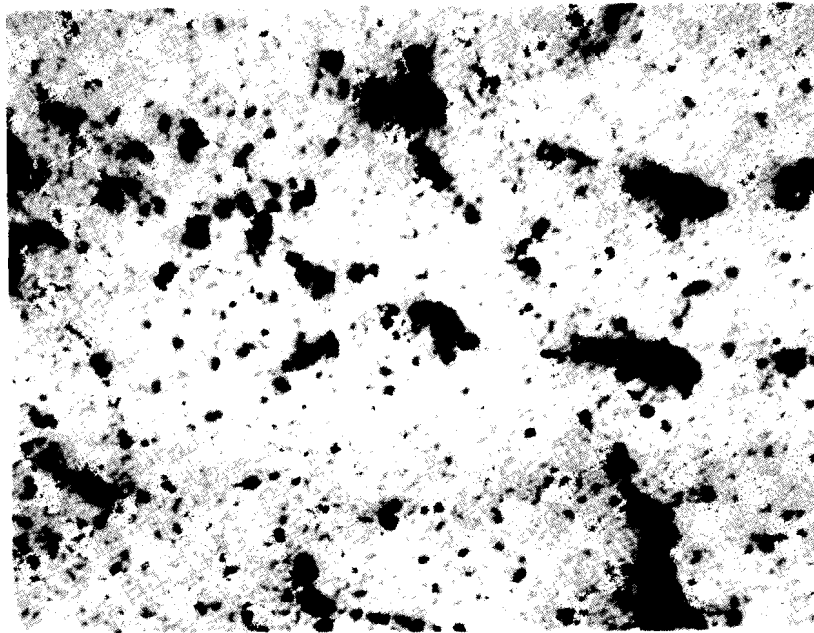


Table VII  
OPTICALLY MEASURED PORE DIAMETERS

System	Defect	Condition	Approximate Pore Diameter, ( $10^{-3}$ in.)	(Microns)
VYB 70 1/2 - Pitch	No-Intentional	Pyrolyzed	0.2 - 0.5	(5-15)
		Graphitized	.05 - 0.3	(1-8)
	Small Void	Pyrolyzed	0.6 - 2.3	(15 - 58)
		Graphitized	0.3 - 3.0	( 8 - 76)
	Lack Wetting	Pyrolyzed	0.5 - 2.0	(15 - 51)
Modmor II - Pitch	No-Intentional	Pyrolyzed	0.2 - 1.5	(5 - 38)
		Graphitized	0.3 - 1.0	(8 - 25)
	Small Void	Pyrolyzed	0.5 - 3.5	(15 - 89)
	Lack Wetting	Pyrolyzed	0.3 - 3.0	( 8 - 76)

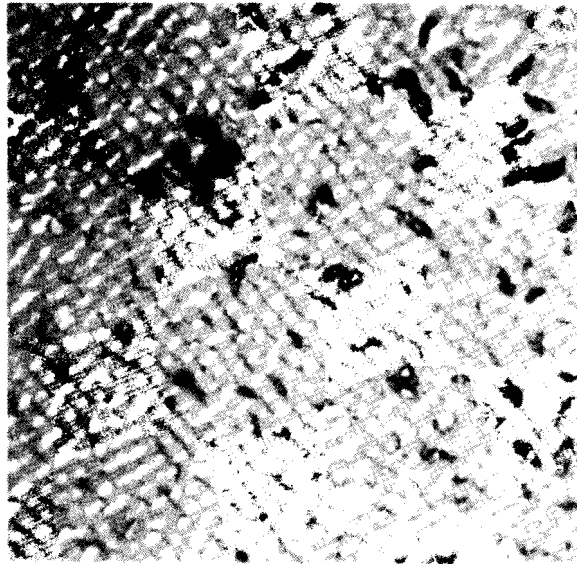


Specimen 12C No-Intentional-Defects 100X



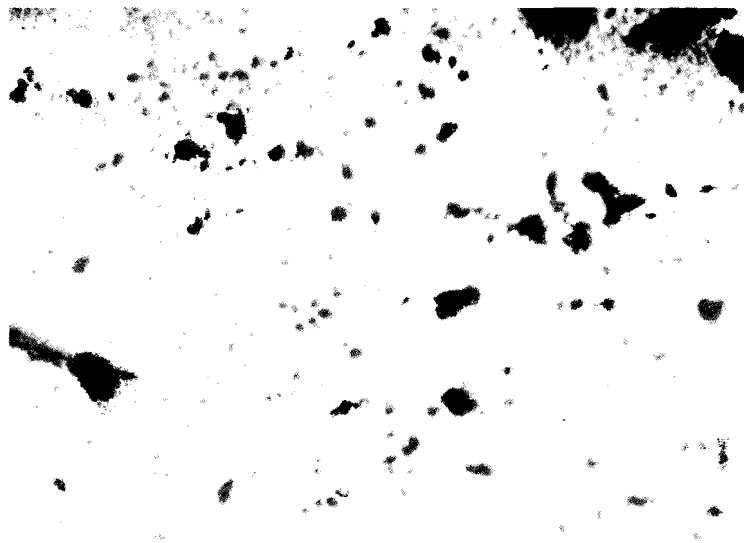
Specimen 22C Small Voids 100X

Figure 12. Photomicrograph of Graphitized VYB 70 1/2 - Pitch Composite in Transverse Direction Under Polarized Light ( $76^{\circ}$ )



300X

Figure 13. Photomicrograph of Pyrolyzed Modmor II - Pitch No-Intentional-Defect Composite Specimen in Transverse Direction Under Polarized Light ( $80^\circ$ )



100X

Figure 14. Photomicrograph of Graphitized Modmor II - Pitch No-Intentional-Defect Composite Specimen in Transverse Direction Under Bright Field

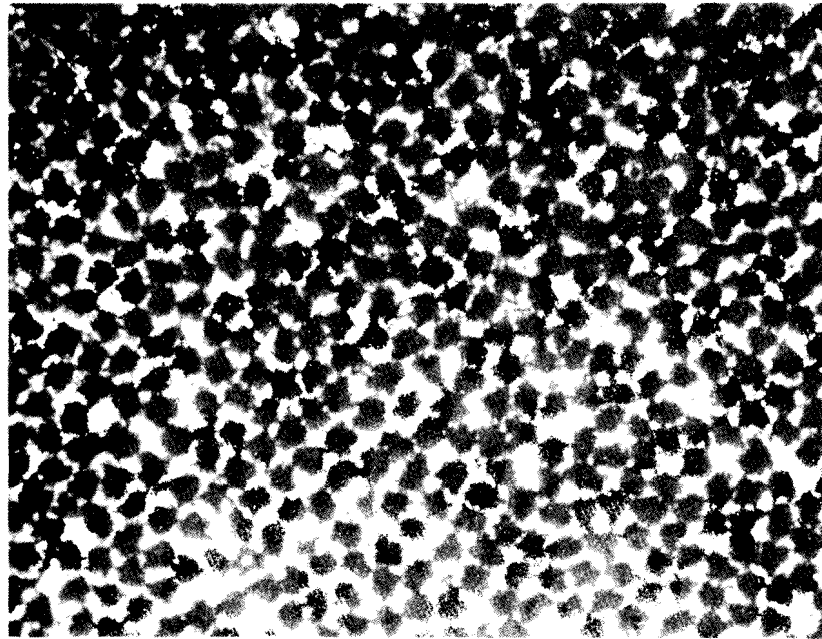


Figure 15. Photomicrograph of Pyrolyzed VYB 70 1/2-Pitch Unidirectional Composite, 475X with Polarized Light (90°)

### Degree of Graphitization

The degree of graphitization of the pyrolyzed and graphitized composites was noted qualitatively based on X-ray diffraction analysis techniques. The X-ray analysis was conducted using copper  $K_{\alpha}$  radiation, wavelength of  $1.54\text{\AA}$ , at 30 kva and 20 ma. A nickel filter was used with  $1^{\circ}$  angle slits. For graphite a d-spacing of  $3.37\text{\AA}$  for the 0002 plane corresponds to a Bragg angle of  $26.4^{\circ}$ . In order to provide a basis for assessing the degree of graphitization, a sample of ATJ graphite was also examined. Figure 16 shows the relative intensity traces of the graphitized VYB 70 1/2 - pitch and VYB 70 1/2 - SC1008 unidirectional composites and the ATJ sample. The graphitized SC1008 and pitch composites did graphitize to some degree as indicated by the peak at  $26.4^{\circ}$ . However, the amount of graphitized material was much less for the composites, with the pitch composites having a larger amount than the SC1008, as indicated by the differences in the relative intensity.

### 4.2 Multidirectional Composites

#### Density and Porosity

The bulk density measurements of the pyrolyzed and graphitized composites were made by water immersion (Figure 17). A complete tabulation of characterization data is made in Appendix I. The pyrolyzed and graphitized DACLOCK 120 composites had a bulk density of 1.66 and 1.60 g/cc, respectively. The pyrolyzed defect containing specimens, small void, weave and lack of wetting, were approximately 10, 5, and 9 percent lower in density, respectively.

The mercury porosimetry measurements were made to determine apparent porosity and density and they are summarized in Table VIII. As in the unidirectional composites, the apparent porosity increased upon graphitization. The small void and lack of wetting defects were approximately 60 percent higher in porosity than the no-intentional-defect specimens. The graph of pore volume versus pore size for the various specimens is shown in Figure 18. The pore distributions, which were fairly uniform, were very similar to those obtained previously on DACLOCK 120 multidirectional composites (Reference 1). There is very little change of the pore spectrums between pyrolyzed and graphitized condition. This is because the composite has been multiply reimpregnated and pyrolyzed.

An estimate of the theoretical density of the multidirectional composite was obtained by using the same approximate densities for the yarn and matrix as in the unidirectional case. Using a volume percent of yarn for the fabric of 34 percent, and estimated theoretical density for the pyrolyzed composite was 1.78 g/cc and 1.93 g/cc for the graphitized composite.

An estimate of the closed pore porosity was made for the composite panels using the same approach as in the unidirectional case (Table IX). The amount of closed pore porosity increased with decreasing apparent density. A graph of total porosity versus bulk density is shown in Figure 19. The closed-pore porosity estimates suggested an increase in the amount of closed pores upon graphitization as in the unidirectional composites.

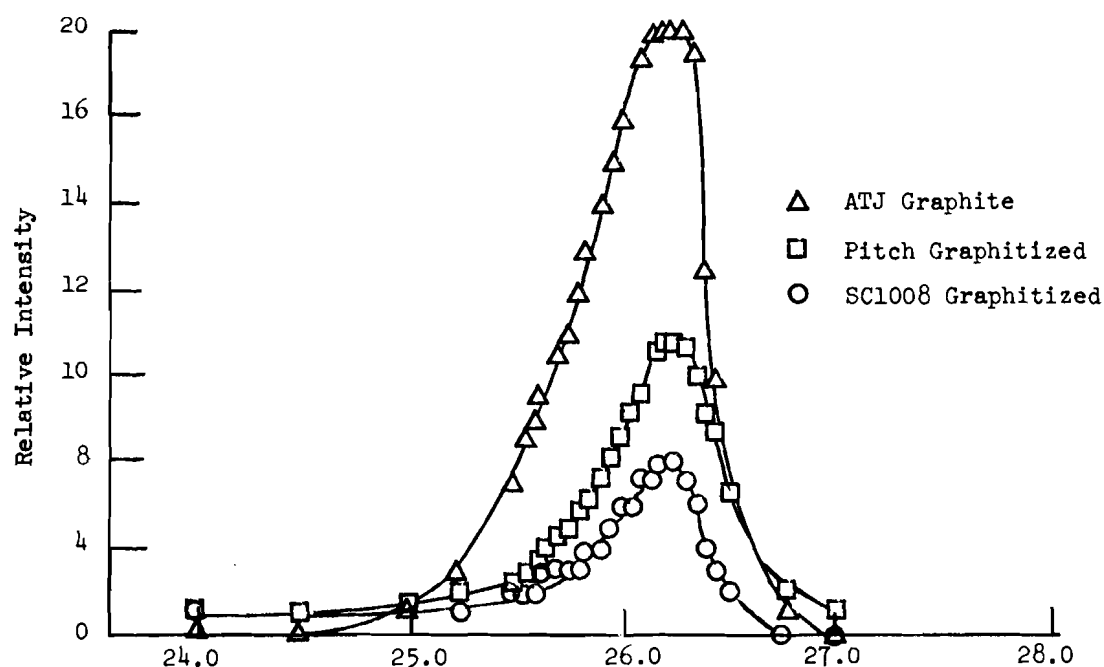


Figure 16. Graph of Relative X-ray Intensity versus Scattering Angle for ATJ Graphite and VYB 70 1/2 - SC1008 and VYB 70 1/2 - Pitch Graphitized Unidirectional Composites

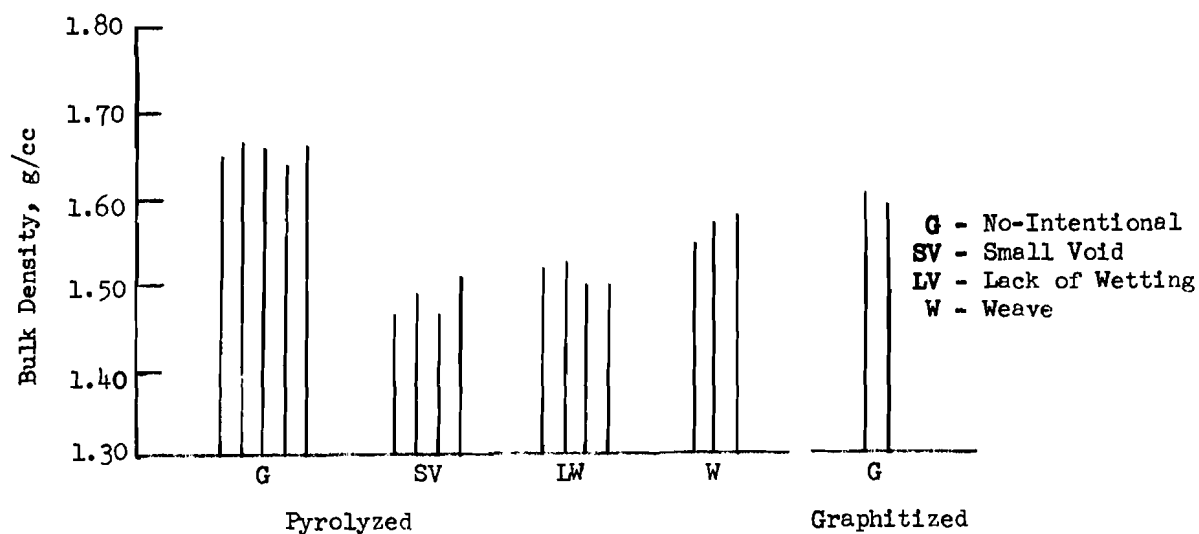


Figure 17. Bulk Density of Multidirectional Composite

Table VIII

POROSIMETRY DATA ON DACLOCK 120  
MULTIDIRECTIONAL COMPOSITE

Specimen	Defect	Condition	Bulk Density, (g/cc)	Apparent Density, (g/cc)	Apparent Porosity, (%)
3D71	No-Intentional	Pyrolyzed	1.69	1.78	5.5
3D65	Small Void	Pyrolyzed	1.57	1.71	8.6
3D61	Lack Wetting	Pyrolyzed	1.60	1.77	9.6
3D75	No-Intentional	Graphitized	1.65	1.79	7.7

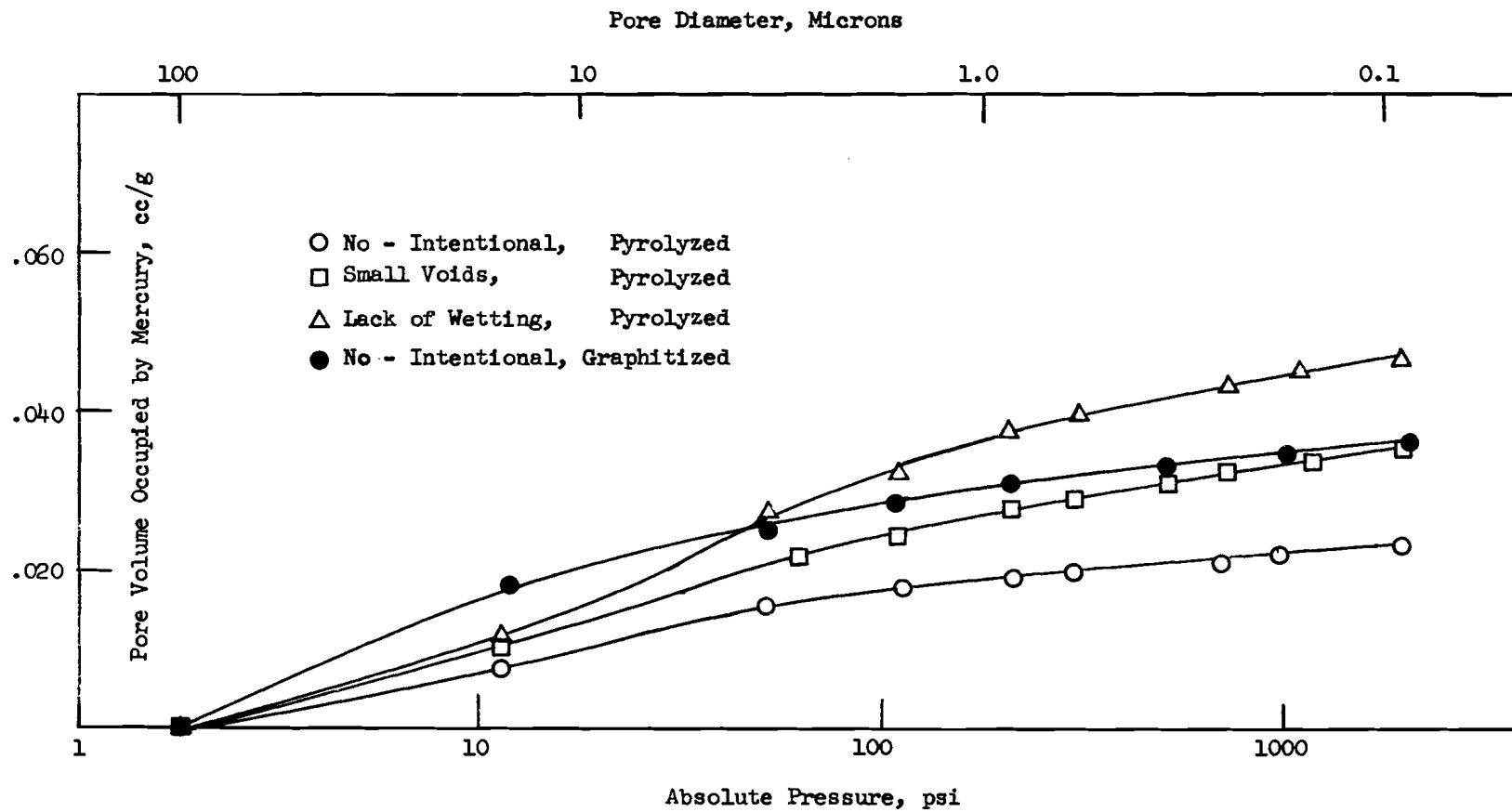


Figure 18. Pore Diameter Versus Pore Volume Occupied By Mercury for Multidirectional DACLOCK 120 Composite



Table IX  
CLOSED PORE POROSITY ESTIMATES

of

Defect Group	Condition	Approximate Closed Porosity, (%)	Measured Open <sup>(1)</sup> Porosity, (%)	Total Porosity, (%)	Bulk <sup>(2)</sup> Density, (g/cc)	Apparent <sup>(1)</sup> Density, (g/cc)
No-Intentional	Pyrolyzed	0+	5.5	5.5	1.69	1.78
	Graphitized	6.0	7.7	13.7	1.65	1.79
Small Void	Pyrolyzed	4.0	8.6	12.6	1.57	1.71
Lack of Wetting	Pyrolyzed	1.0	9.6	10.6	1.60	1.77

(1) Mercury porosimetry

(2) Water immersion

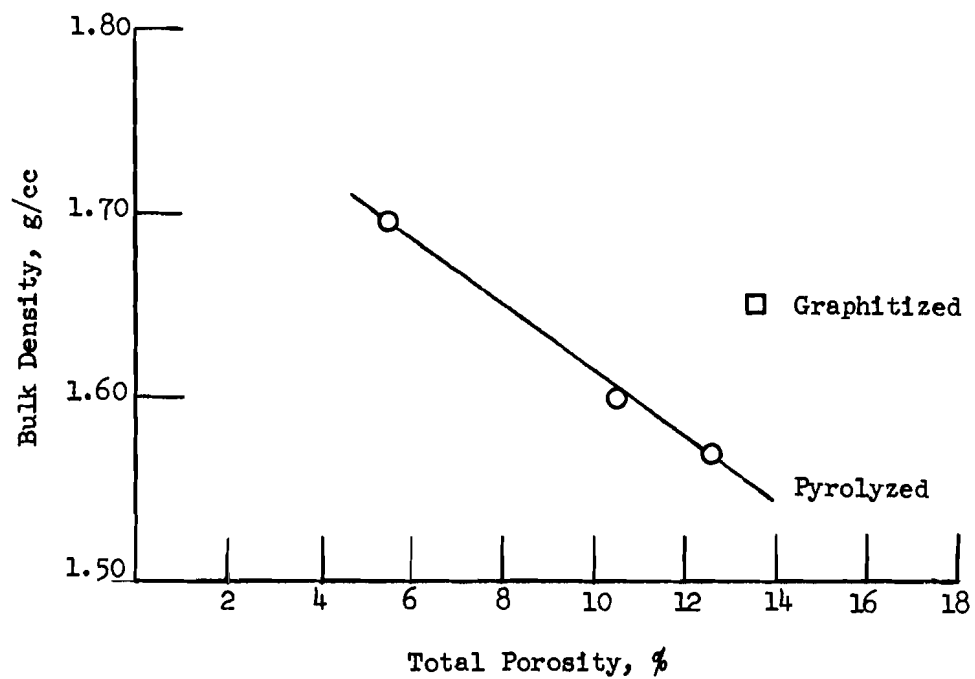


Figure 19. Total Porosity Versus Bulk Density of DACLOCK 120 Multidirectional Composite

## Microstructural Evaluation

Microstructural analysis were conducted on the pyrolyzed and graphitized DACLOCK 120 multidirectional composites containing small voids, lack of wetting, and no-intentional defects. The microstructural analysis was particularly useful in demonstrating the success of the reimpregnation procedure. Figure 20 shows an area of matrix composed of graphitized pitch which was from the initial two impregnations and of pyrolyzed pitch from the last three impregnation cycles which were performed after the graphitization step. The ability of the pitch binder to impregnate into the open porosity of the matrix (which was enhanced by the graphitization sequence) is quite apparent. It can be seen from this micrograph that pores of less than one micron in diameter are being filled.

## 5.0 Nondestructive Analysis

Nondestructive analysis techniques were applied to the unidirectional and multidirectional composites after specific processing steps to obtain in-process data which was correlated to changes in the composite properties. The nondestructive analysis techniques included penetrating radiation (X-ray and neutron radiography), ultrasonic techniques (velocity measurements and attenuation and pulse-echo C-scan mapping), and visual inspection. In addition to the unidirectional and DACLOCK 120 and orthogonal multidirectional composites, a carbon-carbon orthogonally woven cylinder and an AVCO MOD III composite were evaluated. A number of nondestructive test methods and parameters were evaluated for each technique to determine their effect on defect sensitivity.

### 5.1 Unidirectional Composites

The unidirectional composites were evaluated after the cure (SC1008 only), pyrolysis, and graphitization steps. The analysis of the nondestructive test techniques included an evaluation of a helium chamber to reduce air scatter in X-ray radiography, half-tone recording methods for the through-transmission attenuation technique-and the selection of an operating frequency for the ultrasonic techniques. In addition to the longitudinal velocity, ultrasonic transverse wave measurements were made on selected control samples from the three unidirectional systems. The combination of nondestructive analysis techniques were generally able to detect the discontinuities which were intentionally introduced into the composites. The relationship and applicability of the various NDT techniques to the intentional defects of the unidirectional composites in the pyrolyzed and graphitized condition are discussed below.

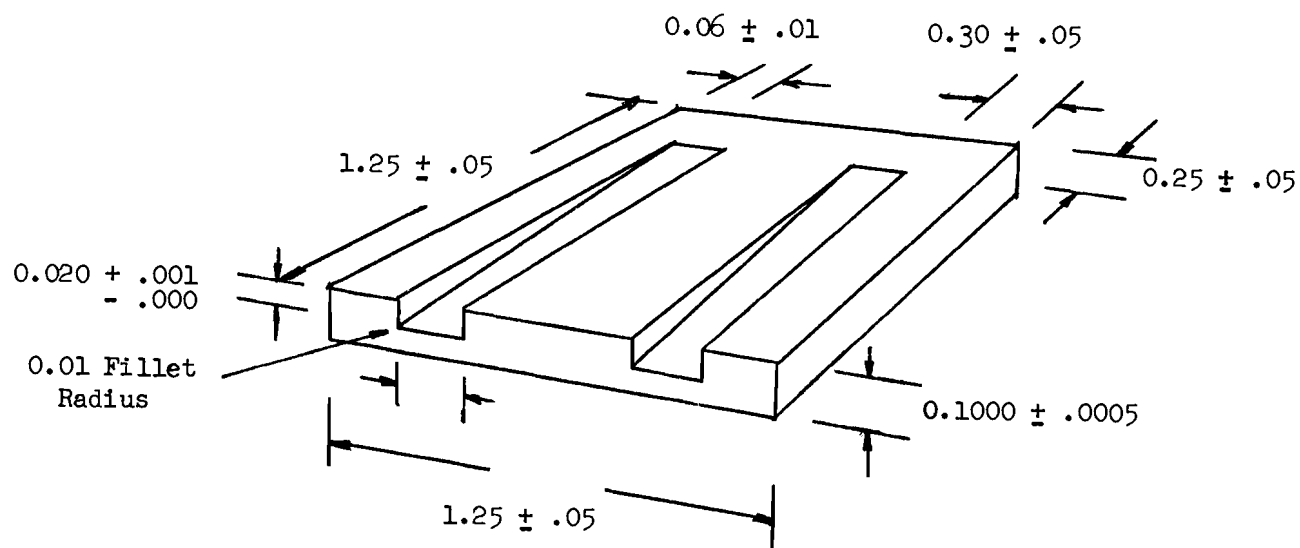
#### 5.1.1 VYB 70 1/2 - SC1008

##### X-Ray Radiography

The X-ray radiographic parameters, voltage, time and distance, were examined to obtain high sensitivity using a Penetrex 50 kV unit. The beam voltage was varied over the range of 14 to 26 kilovolts, and the film-to-focal spot distance from 18 to 34 inches. All exposures were made using Eastman Type M film in ready pack and the beam current was 10 ma throughout. To determine the optimum X-ray radiographic parameters, a machined, tapered slot standard (Figure 21) was examined. A sensitivity of 0.5 percent for the pyrolyzed and



Figure 20. Photomicrograph of Multidirectional Composite After Two Impregnations and Pyrolysis - Graphitization - Three Impregnations



All Dimensions in Inches

Figure 21. X-ray Radiographic Standard for Pyrolyzed VYB 70 1/2 - Pitch Composites

graphitized VYB 70 1/2 - SC1008 composites was obtained with an exposure of 18 kV at 190 sec with a 29-inch film-to-focal spot distance for the pyrolyzed composite and 16 kV at 180 sec with a 29-inch film-to-focal spot distance for the graphitized composite. The optimized parameters included the use of a 0.004-inch screen of polyethylene between the part and the X-ray source to absorb the low-energy, air-scattered X-rays. The use of other radiographic films (Type R or AA) either produced marginal improvement (Type R) or resulted in inferior quality image definition (Type AA) (Reference 1). This evaluation was performed by conducting a series of radiographic film exposures on the DACLOCK 120 multidirectional fabric and then qualitatively comparing the image definition obtained for a number of identifiable weave irregularities in the woven goods test panel.

The use of a helium chamber for the X-ray radiography of the unidirectional VYB 70 1/2 - SC1008 composites to reduce the effect of low-energy, air-scattered X-rays was evaluated. The analysis was conducted using four pyrolyzed and four graphitized composite standards containing known intentional defects (Table X). The sensitivity of this radiographic technique using a helium chamber was 0.5 percent for both the pyrolyzed and graphitized conditions. Therefore, the helium chamber offered very little additional information on the material.

To analyze the specific defects by X-ray radiography standards containing particular defects were machined (surfaces parallel to within 0.0005 inches) from the pyrolyzed and graphitized VYB 70 1/2 - SC1008 composites. Using the optimized radiographic conditions for the examination, the X-ray radiographic technique detected the majority of the intentional defects which were introduced into the composites (Table XI). This was accomplished after the three major processing steps of cure, pyrolysis, and graphitization. An X-ray radiograph of a specimen free of intentional defects is shown in Figure 22.

A typical X-ray radiograph of a pyrolyzed specimen containing large voids is shown in Figure 23. The radiograph also shows a number of line defects which are oriented in the thickness direction. These line defects were identified as cracks having an irregular path through the composite (Reference 1). The weave-defect was detected by X-ray radiography in all processed conditions. Figure 24 shows the clarity with which X-ray radiography was capable of showing this defect. As expected, X-ray radiography was not capable of detecting the delamination since the X-ray technique is least sensitive to laminar or flat which lie perpendicular to the incident beam.

The poor fiber bundle penetration and lack of yarn wetting defects went undetected by X-ray radiography. This was due to a uniform distribution of the defect throughout the composite. The detection of a material anomaly or defect by X-ray radiography usually requires that it possess a different absorptance than the surrounding bulk material.

#### Ultrasonic Velocity

The ultrasonic longitudinal velocity of the unidirectional composite panels was measured through the thickness direction by a through-transmission technique. This technique, shown schematically in Figure 25, employs two transducers in direct contact with the specimen using glycerin as the couplant

Table X

## NDT STANDARDS FOR HELIUM CHAMBER X-RAY RADIOGRAPHY

Specimen	Condition	Defect Group
14D	Pyrolyzed	No-intentional-defects (machined taper slot)
26A		Small Voids
27C		Large Voids
17C		Delamination
14A		No-intentional-defects (machined taper slot)
19B2	Graphitized	Delamination
26C		Small Voids
27B		Large Voids

Table XI

APPLICABILITY OF NONDESTRUCTIVE TEST TECHNIQUES  
TO VYB 70 1/2 - SC1008 COMPOSITES

Defect	Condition	X-Ray	Pulse - Echo	Attenuation	Velocity
Small voids	C	Yes	No (2)	Yes	No
	P	Yes	No (3) (4)	Yes (3)	Yes
	G	Yes	*	Yes	(6)
Large voids	C	Yes	No (2)	Yes	No
	P	Yes	No (3)	Yes	Yes
	G	Yes	No	Yes	No
Poor bundle penetration	C	No	No	Yes (5)	No
	P	No	No (3)	Yes (5)	Yes
	G	No	*	Yes (5)	(6)
Lack of wetting	C	No	No (3)	No	No
	P	No	No (3)	Yes (5)	Yes
	G	No	*	Yes (5)	(6)
Noncarbonaceous Impurities	C	Yes	No	No	No
	P	Yes	No (3)	Yes	No
	G	Yes (1)	*	Yes (1)	(1)(6)
Delamination	C	No	No	No	No
	P	No	Yes	Yes	No
	G	No	No (3)	Yes	No
Weave	C	Yes	No (3)	Yes	No
	P	Yes	No (3)	Yes	Yes
	G	Yes	No (3)	Yes	Yes
Cracks	C	Yes	No (3)	Yes (4)	No
	P	Yes	No (3)	Yes (4)	No
	G	Yes	No (3)	Yes (4)	No

(1) However porosity was formed upon graphitization.

(2) In two cases it was detected.

(3) Distinct discontinuity indications were obtained for the composite specimens but not definitely related to the introduced defect.

(4) Cracks oriented at an angle to ultrasonic beam provided reflecting surface.

(5) Defect detected throughout panel as an increase in attenuation over a good specimen.

(6) Material attenuation prohibited measurements.

\*Technique not applied.

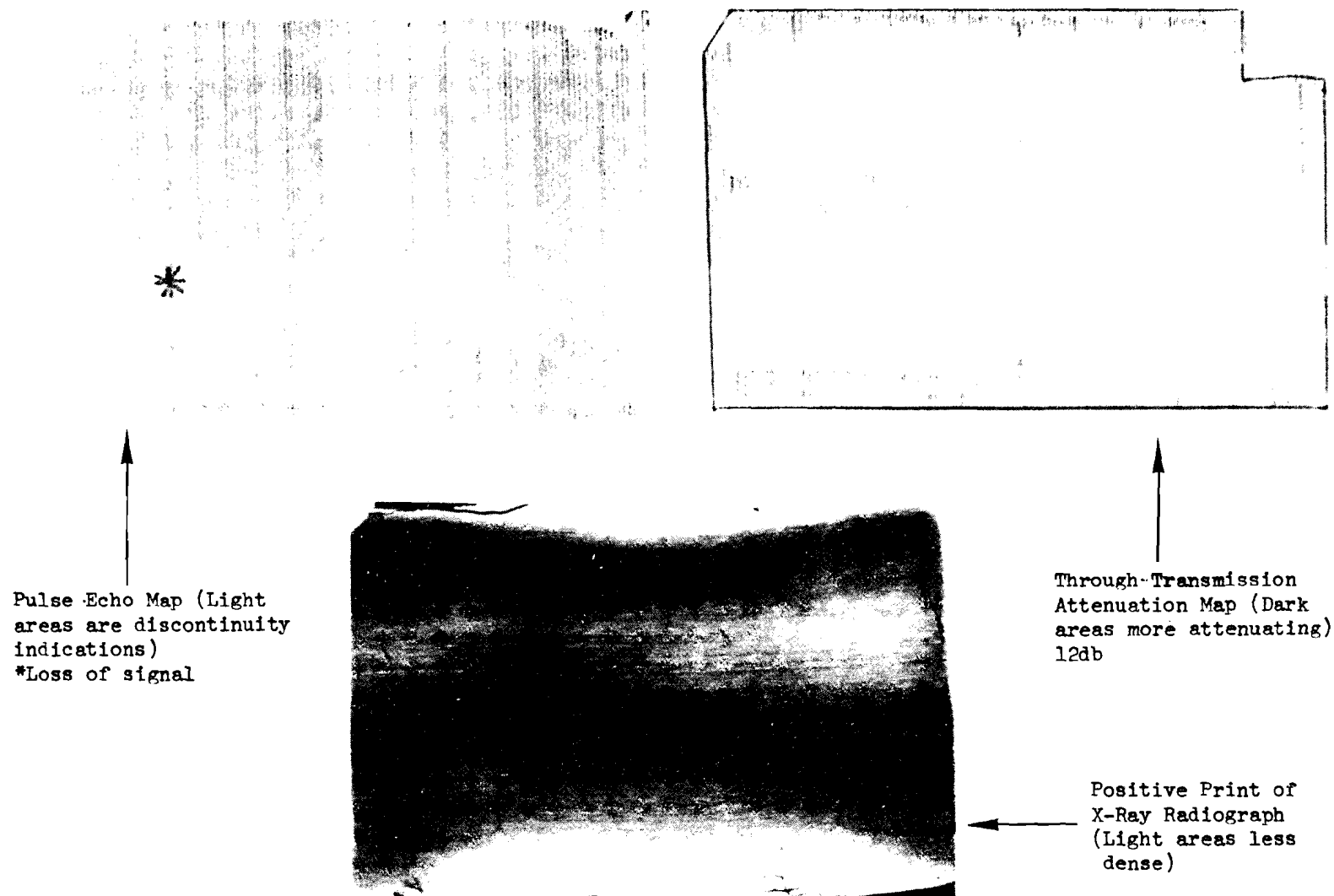
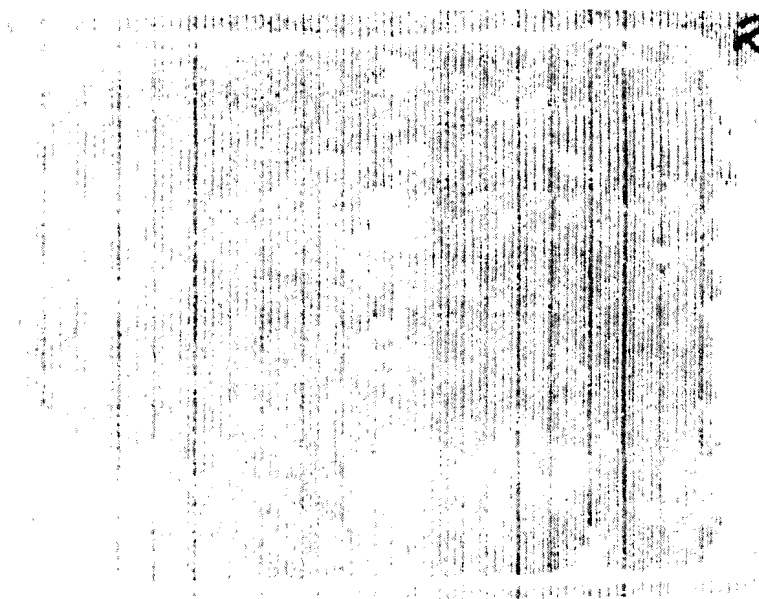
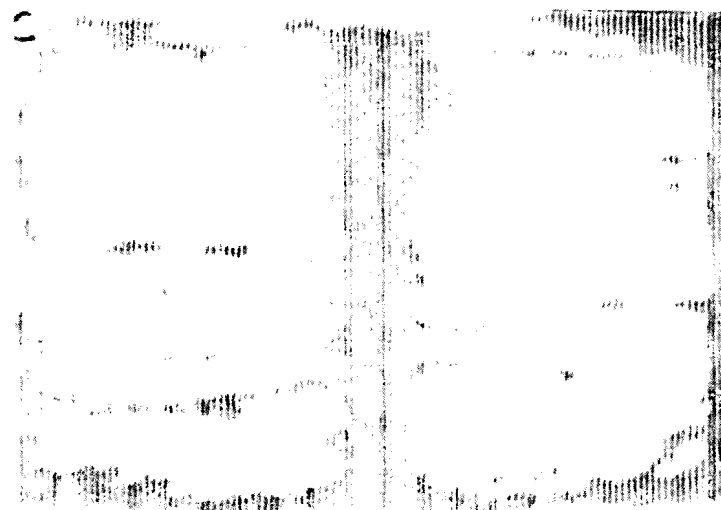


Figure 22. Nondestructive Test Maps for Pyrolyzed VYB 70 1/2-SC1008 Composite Specimen 14D Containing No Intentional Defects (Good)





Pulse-Echo Map  
(Light areas are  
Defect Indications)

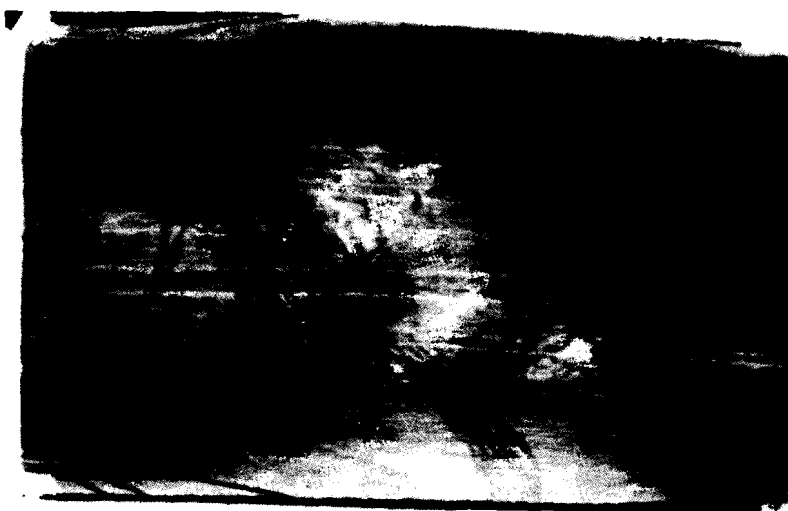


Through-Transmission  
Attenuation Map (Dark  
Areas More Attenuating) 15db

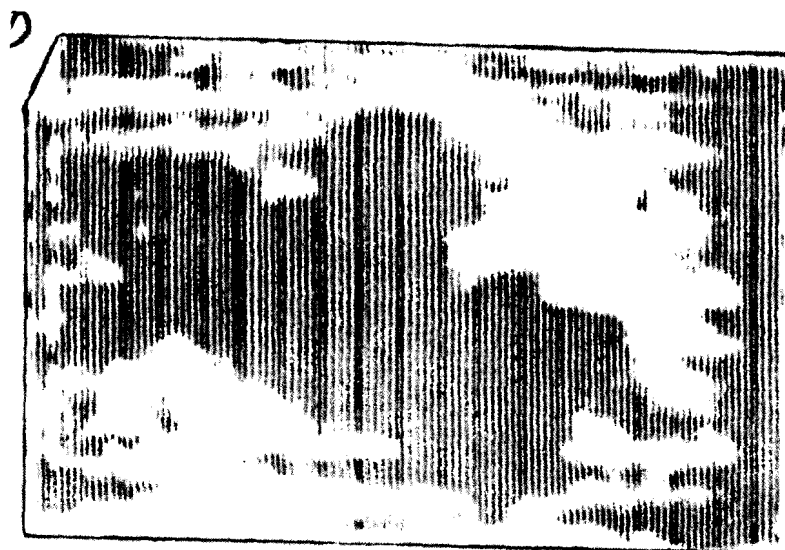


Positive Print of  
X-ray Radiograph  
(Light areas lower  
density)

Figure 23. Nondestructive Test Maps for Pyrolyzed VYB 70 1/2-SC1008 Composite Specimen 28C Containing Large Voids.



a) Positive Print of X-ray Radiograph  
(Light areas are less dense)



b) Through-Transmission Attenuation Map  
(Dark areas are more attenuating) 18db

Figure 24. Positive Print of X-ray Radiograph and Through Transmission Map of Pyrolyzed VYB 70 1/2-SC1008 Specimen 15D Containing Weave Irregularities

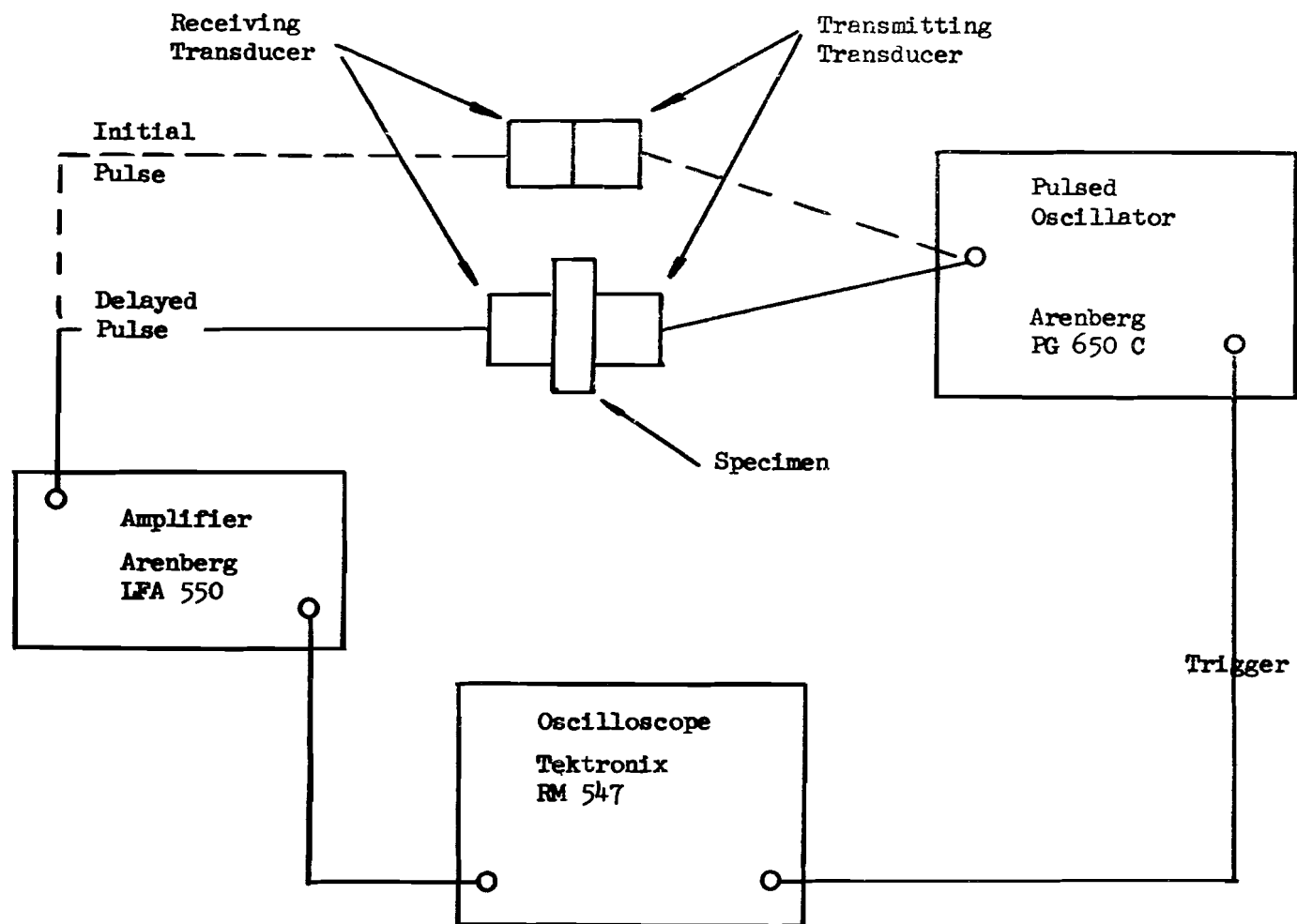


Figure 25. Schematic Diagram of Through-Transmission Velocity Measurement Technique

(Reference 1). A strippable vinyl coating was applied to all specimens to prevent absorption of the couplant. In measuring the time delay, corresponding cycles of the initial and delayed ultrasonic pulses were selected. The first cycle of the pulse was used to eliminate any error resulting from a frequency shift in the frequency content of the pulse. The shift to lower frequencies was due to preferential attenuation of the higher frequency components (Reference 4). The accuracy of the technique was within one percent as determined by comparing the experimental value of the ultrasonic longitudinal velocity of a fused quartz standard to literature values (Reference 5).

The ultrasonic longitudinal velocity measurements for VYB 70 1/2 - SC1008 unidirectional composite is summarized in Figure 26. A detailed tabulation of the measurements is contained in Appendix I. The velocity measurements on the pyrolyzed and graphitized composites generally enabled a differentiation of defective from nondefective material. However, some fluctuation in the measurements from panel to panel within a particular group did exist. The velocity measurements did show a significant difference for each composite processing condition (cured, pyrolyzed, or graphitized).

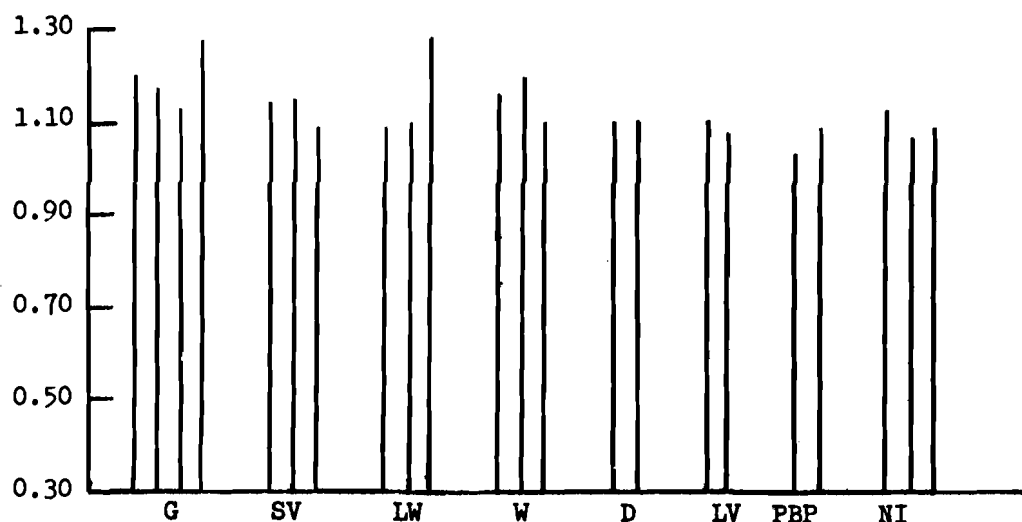
For the cured VYB 70 1/2 - SC1008 composite, it was difficult to differentiate the defect material. In the pyrolyzed composite, most of the defective material had a velocity less than the no-intentional-defect material. In the graphitized condition, the defect specimens were difficult to differentiate. This was attributed to the selected operating frequency for the measurements and the high attenuation of the specimens. The velocity measurements were made at 2.5 MHz for the pyrolyzed and graphitized composite. It will be shown below that at other frequencies, the difference in velocity between the no-intentional-defect and defective specimens is more pronounced due to the frequency dependence of velocity.

The VYB 70 1/2 - SC1008 composite panels were processed in groups of specimens which allowed the monitoring of batch-to-batch uniformities. Several specimens which were pyrolyzed in one batch were very resin lean after pyrolysis and some oxidation had taken place. The ultrasonic velocity showed a difference between these batches and within each defect group (Reference 1). The velocity at a point on one specimen which had signs of oxidation had a 20 percent lower velocity than that on an area which had no signs of oxidation. These anomalous specimens compared very well with the other batches in the cured condition prior to pyrolysis. After graphitization, the longitudinal velocity could not be measured on the anomalous batch specimens due to the high attenuation present.

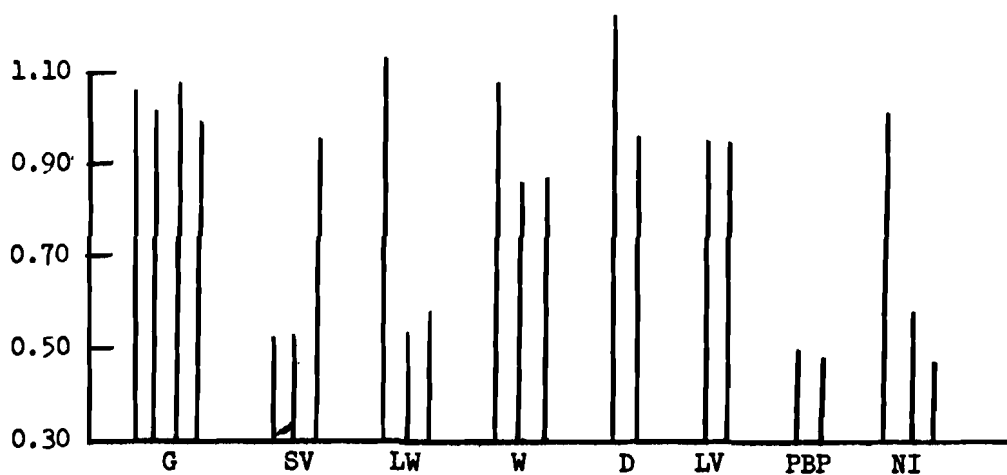
The ultrasonic longitudinal velocity measurements on the no-intentional-defect SC1008 composites were typically 1.20, 1.03, and  $0.70 \times 10^5$  in/sec for the cured, pyrolyzed, and graphitized conditions, respectively. The decrease in velocity after pyrolysis ranged from 4 to 15 percent of the cured condition value and after graphitization from 28 to 38 percent of the pyrolyzed condition value. From these data it was apparent that the velocity measurements can be used to monitor the processing condition.

The evaluation of the intentionally-introduced defects indicated that this velocity technique was sensitive to the concentration or degree of the defects

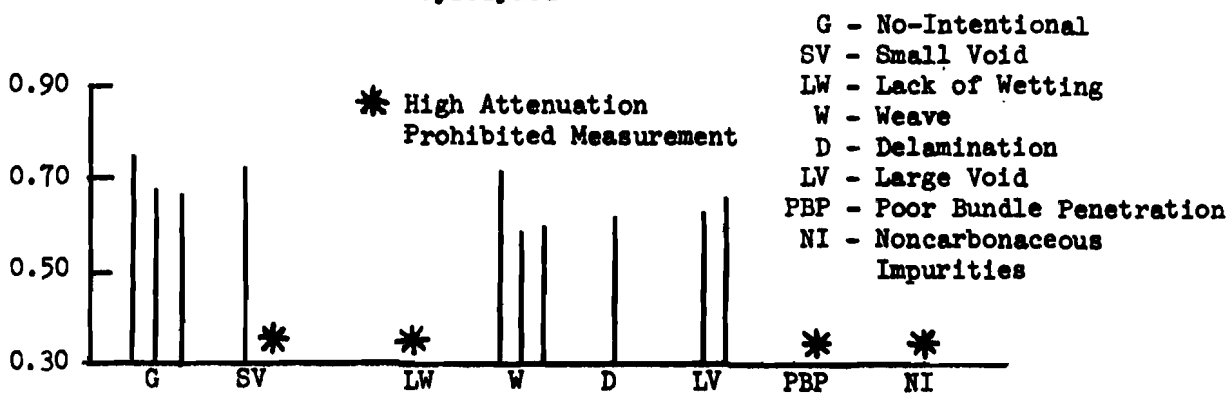
Longitudinal Velocity,  $10^5 \text{ in/sec}$



Cured



Pyrolyzed



Graphitized

Figure 26. Longitudinal Velocity of VYB 70 1/2 - SC1008 Composite

present. A number of SC1008 defect specimens contained a particular defect to a much lesser or greater degree (concentration) than the other specimens in the group as determined from microscopic evaluation and X-ray radiography (Reference 1). The specimens with a smaller concentration of a defect had a much higher velocity in both the pyrolyzed and graphitized condition.

The bulk density, as measured by water immersion, was related to the measured ultrasonic longitudinal velocity for the three unidirectional systems (Figure 27). The trends indicate a higher velocity corresponding to higher density. The decrease in velocity with decreasing density can be attributed to an increase in the porosity of the composites. Analytically, the square of the velocity (perpendicular to the fiber direction) is directly proportional to an elastic constant in that direction and inversely proportional to density. The elastic constant, or modulus, of a heterogeneous material is directly related to the material porosity (Reference 6). For a given change in composite porosity (density), the change in modulus is more pronounced than the change in density, verifying the experimental velocity - density relationship. The composite density varied over a range of approximately 9 percent which corresponded to a 20 percent range in velocity. This dependence of velocity on density suggests its use in the screening of low density carbon-carbon composites.

The ultrasonic longitudinal velocity was measured as a function of frequency for the pyrolyzed and graphitized SC1008 composites. Five specimens were selected for this evaluation: a good specimen (14C) which did not contain any intentional defects, a small void specimen (26C), a large void specimen (27C), a fused quartz standard, and the same fused quartz standard coated with a 0.005-inch film of polyvinyl chloride (PVC). This test standard was used to determine the effect of PVC on the velocity measurements. The frequency was varied from 1 MHz to approximately 10 MHz. The lowest frequency used was that which had a wavelength no longer than the thickness of the specimen being examined.

The time delays for the five specimens were measured for three successive cycles starting with the initial cycle. The time delay was found to increase for each successive cycle of the pulse for the pyrolyzed SC1008 composite specimens. This was believed to be partly due to the preferential attenuation of the higher frequency components of the pulse which causes a gradual shifting of the pulse frequency and therefore a shift in the time delay (Reference 4).

The graph of velocity as a function of frequency for the quartz standard with and without PVC coating (Figure 28) shows that there was a dependence of velocity on frequency below approximately 3 MHz. The time delay measurements for the three cycles of the pulse did not show the same increasing shift as the composite specimens. The PVC-coated quartz had a 3 to 8 percent lower velocity at the particular frequencies, but the same trend of velocity to frequency existed. Since the velocity values were only being used for comparison, no further corrections for the vinyl coating were made.

The frequency dependence of the velocities for the no-intentional-defect, small void, and large void specimens of the pyrolyzed and graphitized composites are significantly different as shown in Figure 29. Due to the high attenuation of the defective SC1008 specimens, the maximum frequency used

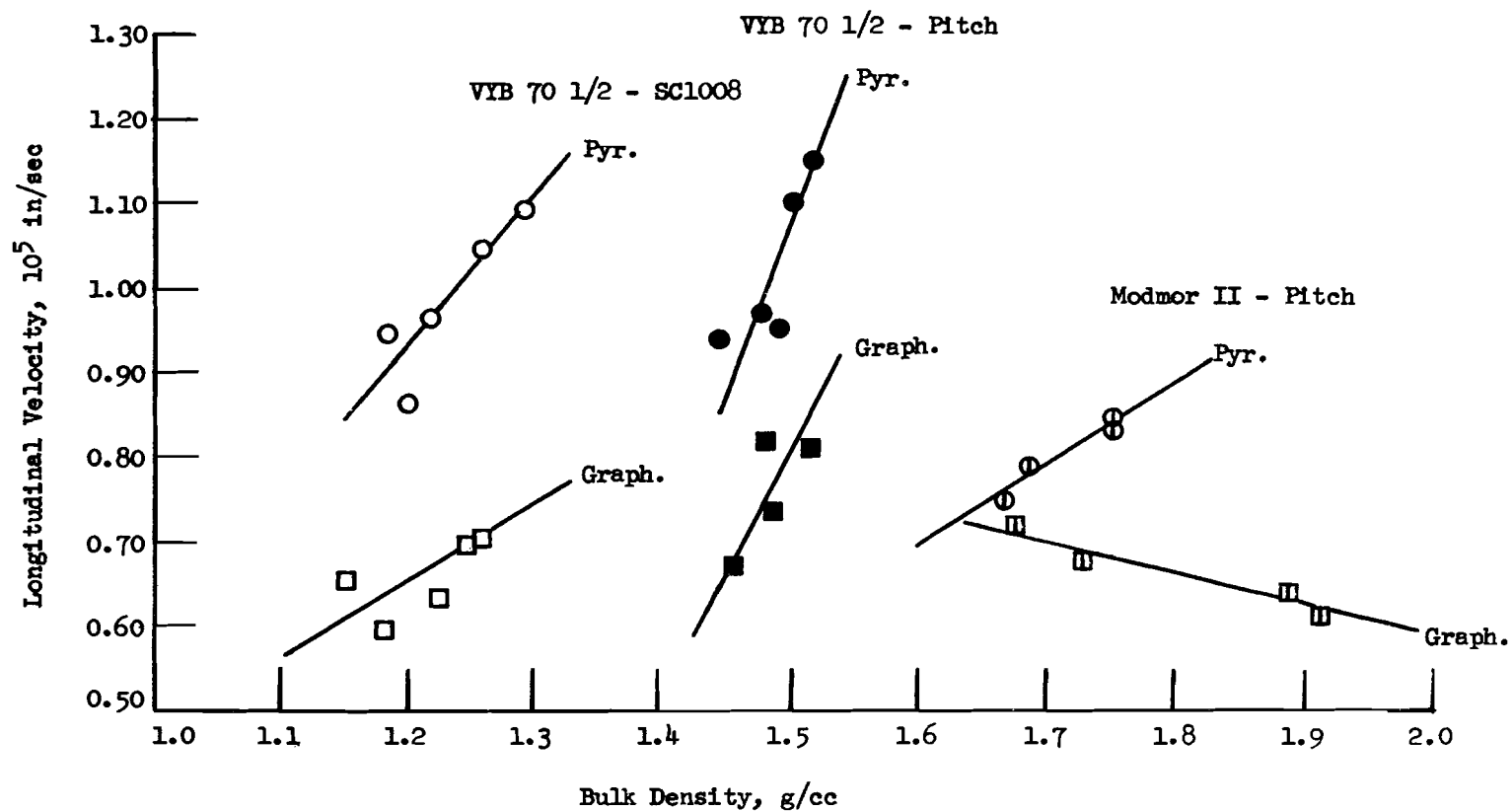


Figure 27. Bulk Density Versus Ultrasonic Longitudinal Velocity For Unidirectional Composites

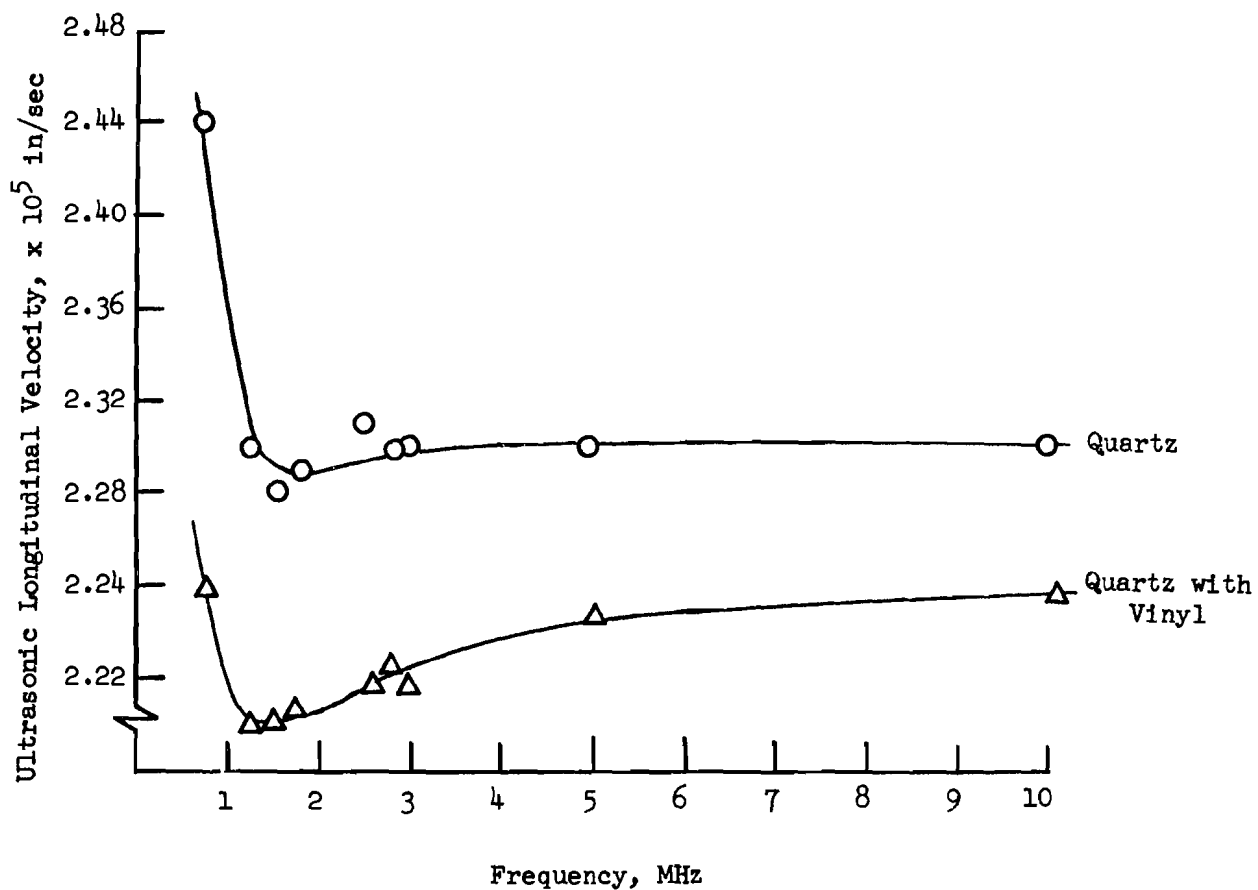


Figure 28. Graph of Ultrasonic Longitudinal Velocity of Fused Quartz Standard as a Function of Frequency (Time delay as average of three initial cycles)



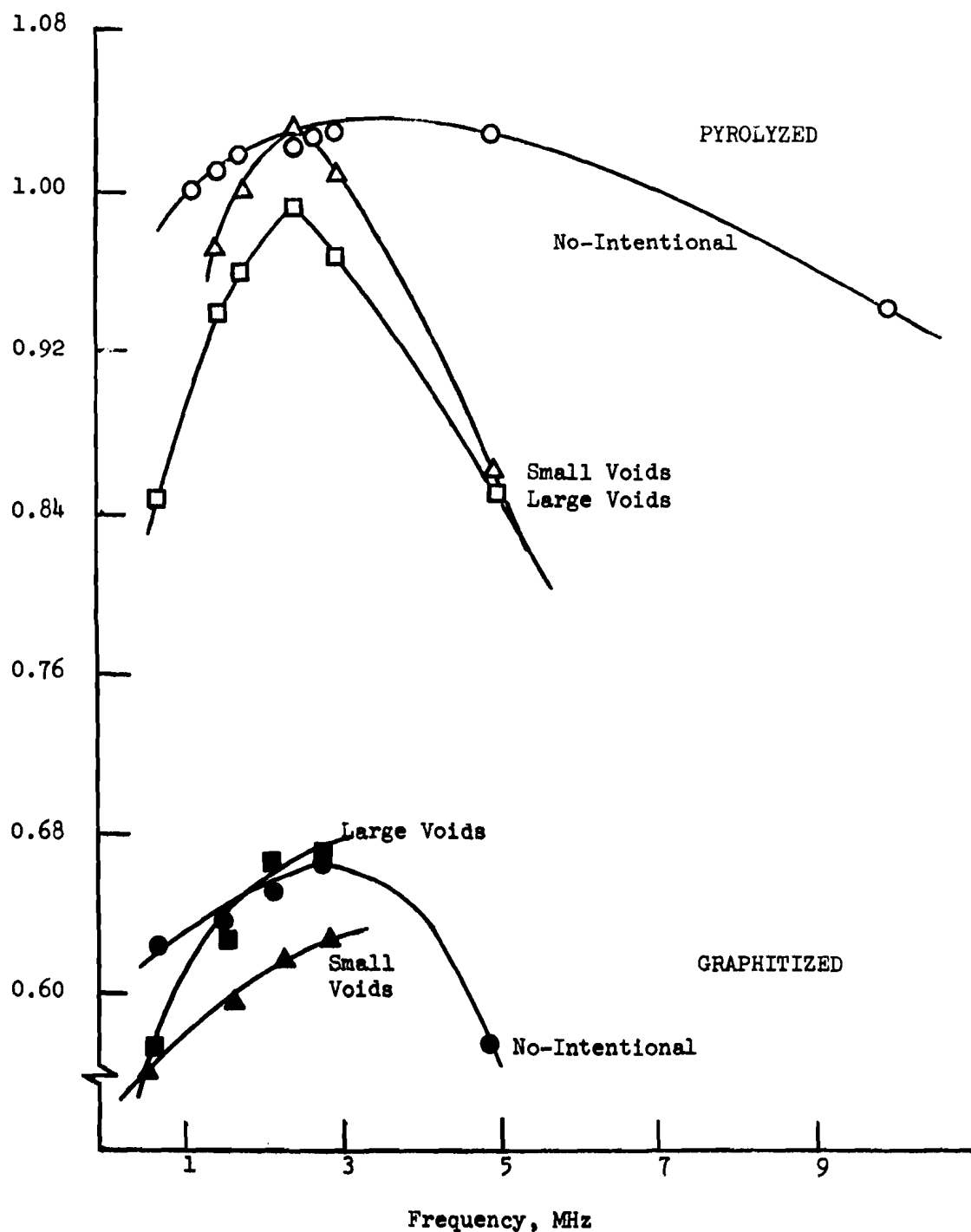


Figure 29. Graph of Ultrasonic Longitudinal Velocity of Pyrolozed and Graphitized VYB 70 1/2 - SC1008 Composites as a Function of Frequency

for the measurements was 5 MHz for the pyrolyzed composites and 3.0 MHz for the graphitized composites. It was found that a frequency dependence of velocity existed for both process conditions although the absolute values were different. This frequency dependence is probably due to geometric dispersion, interference of the ultrasonic wave caused by the heterogeneous material. The difference in the frequency dependence between the specimens thus may be related to the differences in the pore size and fiber bundle size present. As was discussed previously, the large voids are approximately 0.021 inch, small voids 0.003 inch, and the no-intentional-defect-specimen pores 0.001 inch in diameter. The other fact which must be taken into account is the size of the fiber bundle which, after pyrolysis, is between 0.020 and 0.030 inches. Therefore, a combination of dispersion effects due to the yarn bundles and the size and amount of pores present may account for the differences in the frequency-velocity curves.

### Ultrasonic Attenuation

The ultrasonic attenuation, absorption of acoustic energy by a material, was measured by an immersed, through-transmission technique (Reference 1). The measurement of the ultrasonic attenuation was used to detect defects and monitor material variability. These anomalies in the composite cause the material to be a discontinuous medium which inhibits the transmittance of ultrasonic waves. The through-transmission technique is an immersed two-transducer method which measures attenuation by comparing the attenuation of a specimen to a specimen-free water path. The apparatus used to measure and record ultrasonic attenuation is shown in Figure 30. Since the coupling medium is water, a strippable vinyl coating was used to protect the specimens. An increase or decrease in the attenuation of the energy passing through the specimen was indicated by a change in the amplitude of the received signal. By use of the variable decibel attenuation, specific levels of attenuation were recorded, with the writing current of the recorder being switched on or off by a change in the signal amplitude. C-scan maps were made with the use of an X-Y scanning bridge. The attenuation of the water path was very small (0.002 db/cm) and may be neglected. It should be noted that this technique measures relative attenuation, not an absolute value. Reflections at the specimen-water interface and scattering of the ultrasonic wave by the specimen surface prohibited the measurement of the absolute attenuation by this technique. Many factors must be taken into account if more absolute values are wanted. Some of these factors include impedance mismatches between the different mediums, interface losses, lack of parallelism of surfaces, surface roughness effects, and ultrasonic beam characteristics. Since the measurements used in this study were for comparison, only relative values are adequate as long as the general surface conditions are similar. The vinyl coat can increase the attenuation of the composite specimens. This effect was measured on the quartz standard where the attenuation increased by 15 percent with the application of a 0.005-inch vinyl coat.

A number of transducer combinations and operating conditions for the through-transmission technique were evaluated to select the parameters for maximum sensitivity. The different transmitter-receiver transducer combinations evaluated included flat-flat, focused-flat, focused-focused, and focused-collimated flat. The detection limit was determined by using a 0.10-inch thick ultrasonic test standard containing various size holes of various orientations

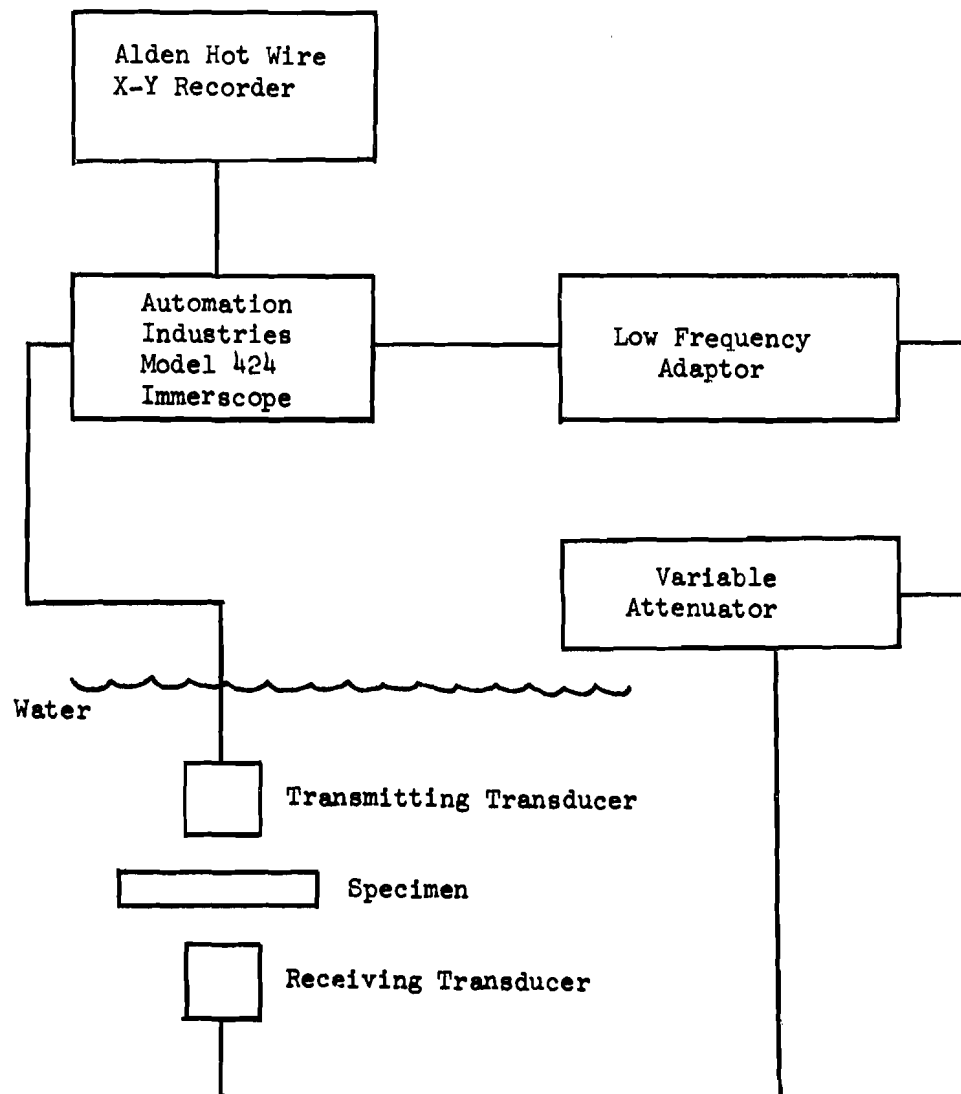


Figure 30. Apparatus for Through-Transmission Attenuation Measurement

fabricated from a pyrolyzed VYB 70 1/2 - SC1008 composite. The most accurate and sensitive through-transmission C-scan maps were obtained with the focused transmitter-collimated flat receiver combination (Reference 1). The minimum detectable defect was a 0.032-inch round bottom hole.

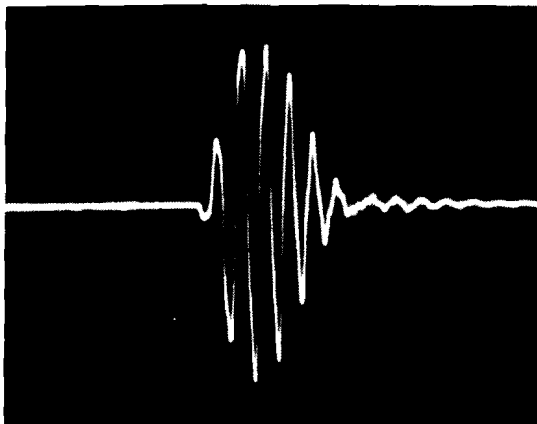
The transducer combinations which were used in the through-transmission study were characterized by the sound beam profiling technique (Reference 1). Since these transducers were used in conjunction with one another, the analysis was conducted in the through-transmission mode by scanning the transmitting transducer with the receiver. A comparison of the sound beam profiles for two transducer - receiver combinations is shown in Figures 31 and 32. The beam width, measured at one-half amplitude, is much less for the focused transmitter-collimated receiver combination, providing a narrower beam for better defect detection. This transducer combination also had a more symmetric sound beam profile. These figures shown that the sound beam profiling technique was an important factor in evaluating and applying ultrasonic transducers for defect detection (Reference 1).

The ultrasonic attenuation of the pyrolyzed and graphitized VYB 70 1/2 - SC1008 composites were considerably greater for the defective material as compared to no-intentional-defect material (Table XII and Figure 33). The difference in attenuation for the cured composites was not as great as in the pyrolyzed and graphitized conditions. The estimates of the attenuation of the composites were made by examining a number of maps made at several different attenuation levels and selecting the level at which the C-scan maps did not indicate areas of higher attenuation. Generally, the defects which were easily detectable in the cured condition were large and small voids and weave irregularities. Although the attenuation maps were not always taken to the characteristic attenuation (value at which ultrasonic energy will get through specimen) of the specimens, the attenuation maps were taken to a high enough decibel level to ascertain that the defect specimens had a significant attenuation above that of the no-intentional-defect specimens.

As mentioned in a previous section, certain specimens contained defects which were either significantly greater or less than the other specimens within a particular defect group. The very high attenuation of one delamination specimen, compared with other specimens in that group, was due to the thickness of the delamination. It was found that even in the cured condition the attenuation of the delamination area was extremely high.

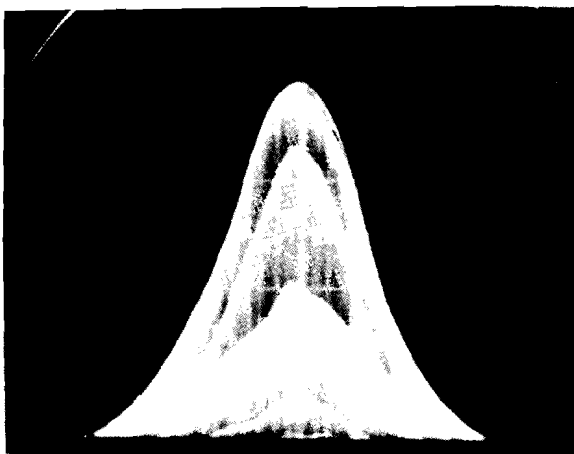
The attenuation technique was successful in detecting most of the intentional discontinuities of interest (Table XI). In cases where the X-ray technique did not detect the existence of a particular defect, as with the lack of wetting and poor fiber bundle penetration, the attenuation technique did. This indicates the usefulness of employing both these NDT techniques for the evaluation of these composite materials.

Typical attenuation C-scan maps which were obtained for two of the intentional defects specimens were shown in Figures 23 and 24. The weave defect was detected as a higher attenuating area. This weave defect also caused an area of porosity or delamination to exist around the defect which allowed the ultrasonic attenuation method to detect its presence. This was verified by sectioning and visually examining the defect area.



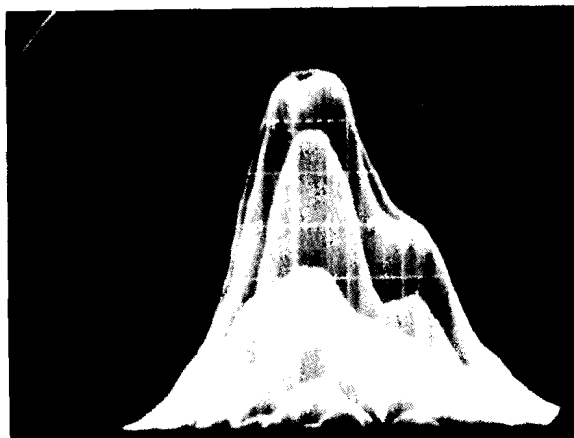
Transmitter: Nortec, Flat 2.25 MHZ  
 3/4 inch diameter J-Z-12-0  
 Receiver: Nortec, Flat 2.25 MHZ  
 3/8 inch diameter A-Z-6-0

Measured Frequency: 2.28 MHZ  
 Damping Factor: 3.0  
 Pulse Duration: High 9.75  
 Sensitivity: 1.0  
 Scope Sensitivity: 1v/div  
 Sweep: 10μ sec/div  
 Water Path: 5.5 inches



A

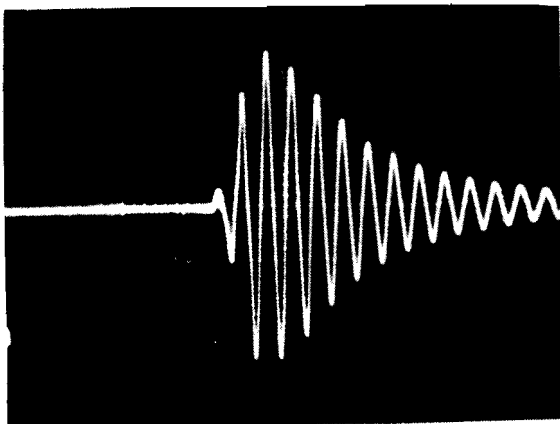
Sound Beam Profile  
 1 div = 1.90 inches  
 Beam Width at 6 db: .531 inches



B

Sound Beam Profile  
 1 div = .185 inches  
 Beam Width at 6 db: .691 inches

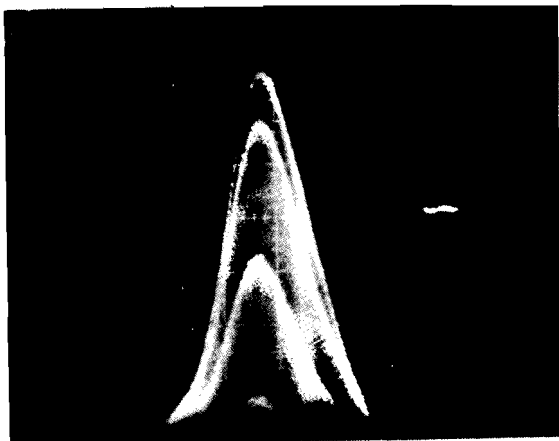
Figure 31. Sound Beam Profile of Flat Transmitter-  
 Flat Receiver Combination



Transmitter: Nortec, Focused Dish  
Crystal (no lens), 2.25 MHZ  
PZT 5, Air Backed, 1 inch diameter

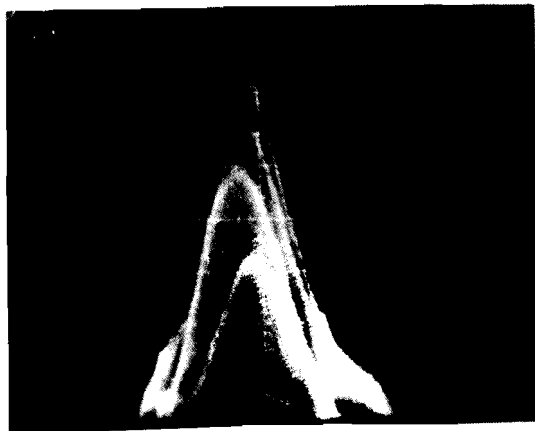
Receiver: Nortec, Collimated Flat 2.25 MHZ  
PZT 3/4 inch diameter J-Z-12-0

Measured Frequency: 2.22 MHZ  
Damping Factor: 14  
Pulse Duration: High 7.0  
Sensitivity: 3.0  
Scope Sensitivity: 1v/div  
Sweep: 10 $\mu$  sec/div  
Water Path: 3.0 inches



A

Sound Beam Profile  
1 div = .037 inches  
Beam Width at 6 db: .052 inch



B

Sound Beam Profile  
1 div = .037 inch  
Beam Width at 6 db: .070 inch

Figure 32. Sound Beam Profile of Focus Transmitter  
Collimated Flat Receiver Combination at 3-Inch Water Path

Table XII

## ULTRASONIC ATTENUATION OF VYB 70 1/2 - SC1008 COMPOSITES

Defect	Material Condition	Average Percentage above No-Intentional-Defect Specimen Attenuation Value
Small voids	Cured	>86%
	Pyrolyzed	162%
	Graphitized	>218%
Large voids	Cured	>131%
	Pyrolyzed	>73%
	Graphitized	231%
Delamination	Cured	12.5%, 382%
	Pyrolyzed	34%, >212%
	Graphitized	64%
Noncarbonaceous	Cured	12%
	Pyrolyzed	213%
	Graphitized	>332%
Lack of wetting	Cured	1%
	Pyrolyzed	202%
	Graphitized	360%
Poor fiber bundle	Cured	12.5%
	Pyrolyzed	176%
	Graphitized	265%
Weave	Cured	146%
	Pyrolyzed	147%
	Graphitized	208%, 296%

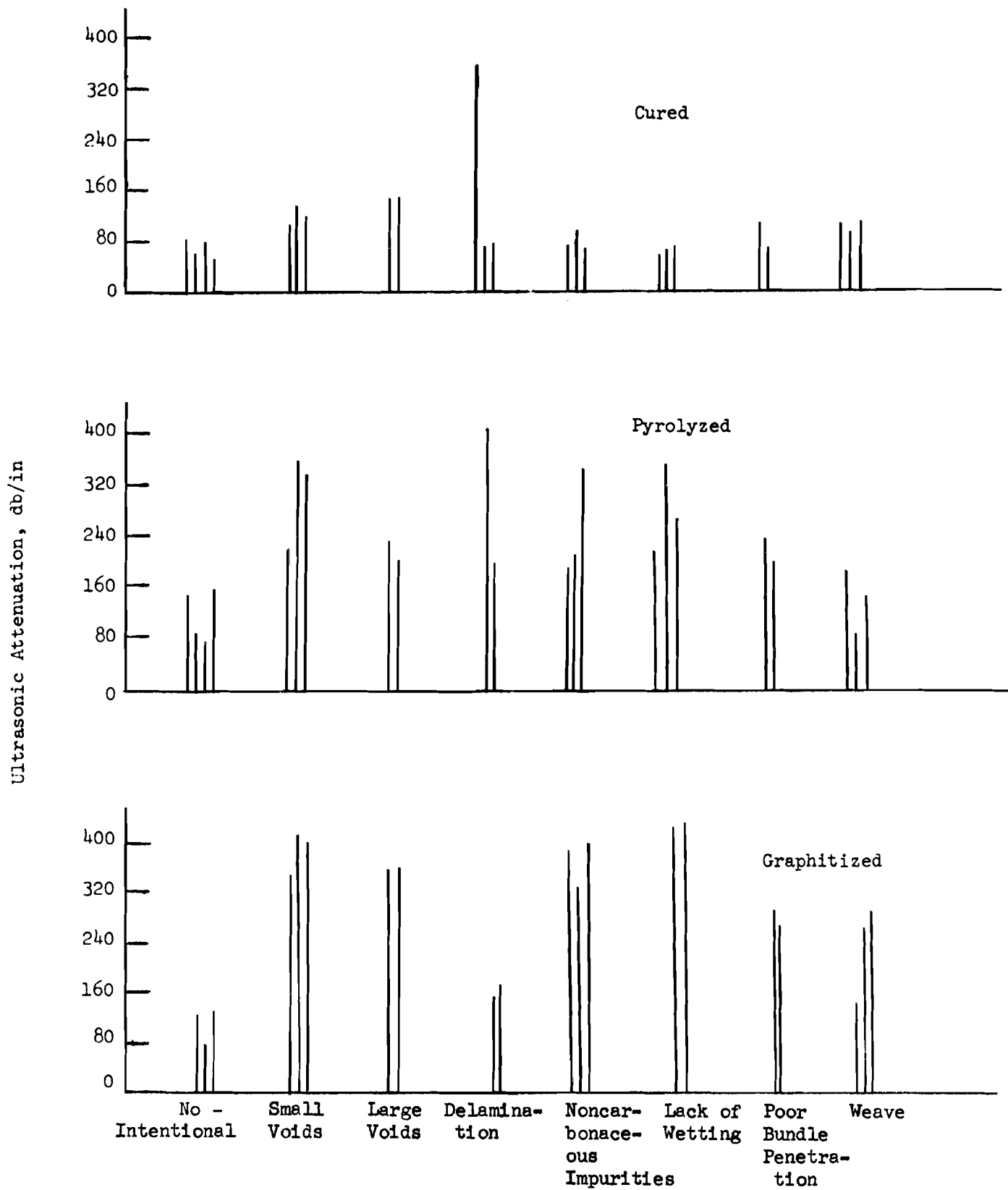


Figure 33. Ultrasonic Attenuation of VYB 70 1/2 - SC1008 Composites



The crack defects which were detected by X-ray radiography were also detected by the attenuation technique (Figure 34). The irregular path of the cracks through the thickness of the specimen provide the reflective area to interfere with the ultrasonic wave transmission. The in-process analysis of the composites has also shown that the attenuation and X-ray techniques generally yielded the same type of map for the next process condition (cure to pyrolyzed or pyrolyzed to graphitized).

The ultrasonic attenuation measured from the C-scan maps was correlated to the measured apparent porosity of the composite system (Figure 35). In four specimens, the actual attenuation was not determined due to a lack of attenuation maps at the higher levels (indicated by arrows on the graph). Apparent in the graph is the trend of higher attenuation corresponding to higher porosity. The attenuation technique can provide a means of inspecting for discrete discontinuities and determining material variability (porosity). A possible trend in the data of the measured apparent porosity of the graphitized composite versus the measured attenuation on the pyrolyzed composite is suggested (Figure 36). This indicates the usefulness of in-process quality control program that would nondestructively measure properties on a pyrolyzed composite and relate them to the final processed product.

The ultrasonic attenuation was found to increase with frequency. However, the relative differences between no-intentional and defective material were essentially constant over the frequency range of 0.7 to 5.0 MHz. This makes the selection of an operating frequency for material uniformity monitoring less critical for the attenuation technique. The operating frequency will be shown to be very critical in the velocity technique.

#### Pulse-Echo Technique

The ultrasonic pulse-echo technique was also evaluated as a method for defect detection in the carbon-carbon composites. The equipment used in the pulse-echo technique (Figure 37) utilized an Automation Industries 725 Immerscope to pulse the transducer, which acts as both the transmitter and receiver. The signals were monitored or gated as an increase in defect signal indications between the front and back surface reflections. The writing current for the Alden hot wire recorder was switched on or off by the signal height of the defect indication.

An evaluation was conducted to select the transducer for the pulse echo study. This evaluation was based on the defect sensitivity response from a test standard of cured VYB 70 1/2 - SC1008 composite. From the results of this study (Reference 1), a 3/8-inch diameter, focused transducer was selected over a flat 3/8-inch diameter transducer because of its narrower front face blind zone (approximately 0.025 inch as compared to 0.033 inch) and the slightly better defect sensitivity (Figure 38). It was found that the general level of noise from the composites was less with the focused transducer.

The selected focused transducer was characterized by the sound beam profiling technique (Reference 1). In order to properly employ a focused transducer for evaluating materials, the focal point and focal zone in water of the transducer must be known to determine correct water distances to be used. The focal point was determined to be 1.3 inches with a frequency of 2.86 MHz and a damping factor of 3.0.

Pulse-Echo Map (Light  
areas are discontinuity  
indications)  
\*Loss of signal

Through-Transmission  
Attenuation Map (Dark  
areas are more attenuating)  
12db

Positive Print of X-ray  
Radiograph (Light areas  
are less dense)

Figure 34. Nondestructive Test Maps for Pyrolyzed VYB 70 1/2-SC1008  
Composite Specimen 18C Containing Crack

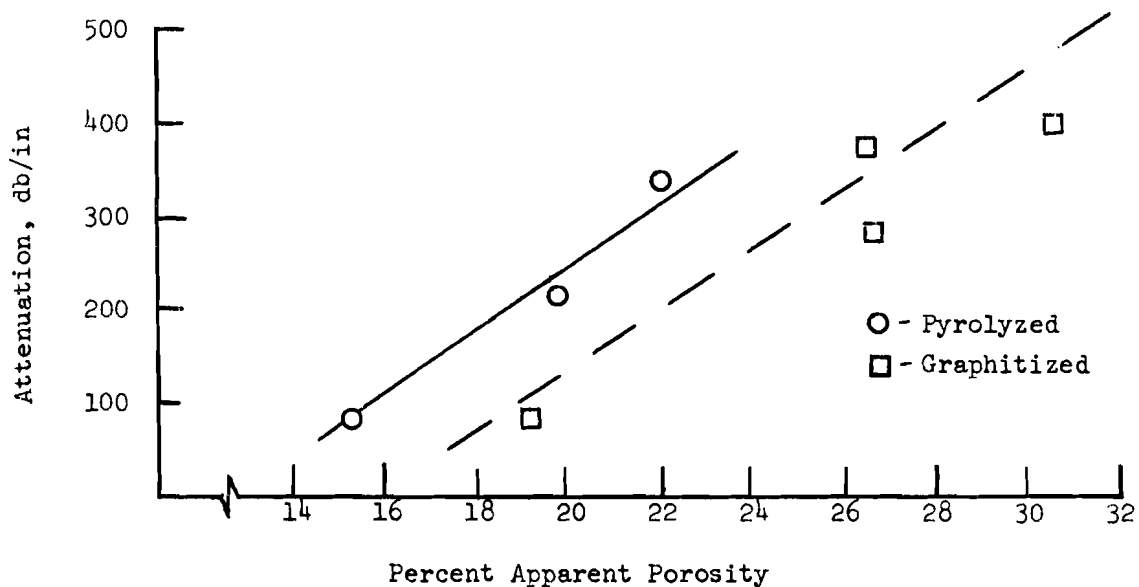


Figure 35. Ultrasonic Attenuation versus Apparent Porosity of VYB 70 1/2 - SC1008 Composite

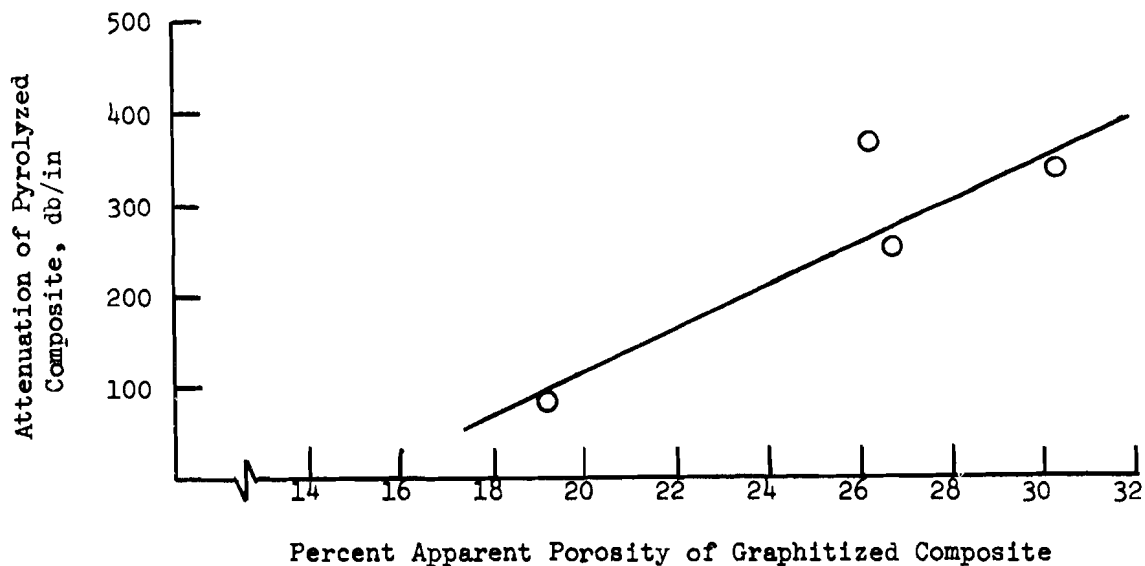


Figure 36. Attenuation of Pyrolyzed Composite versus the Apparent Porosity of Graphitized VYB 70 1/2 - SC1008 Composite

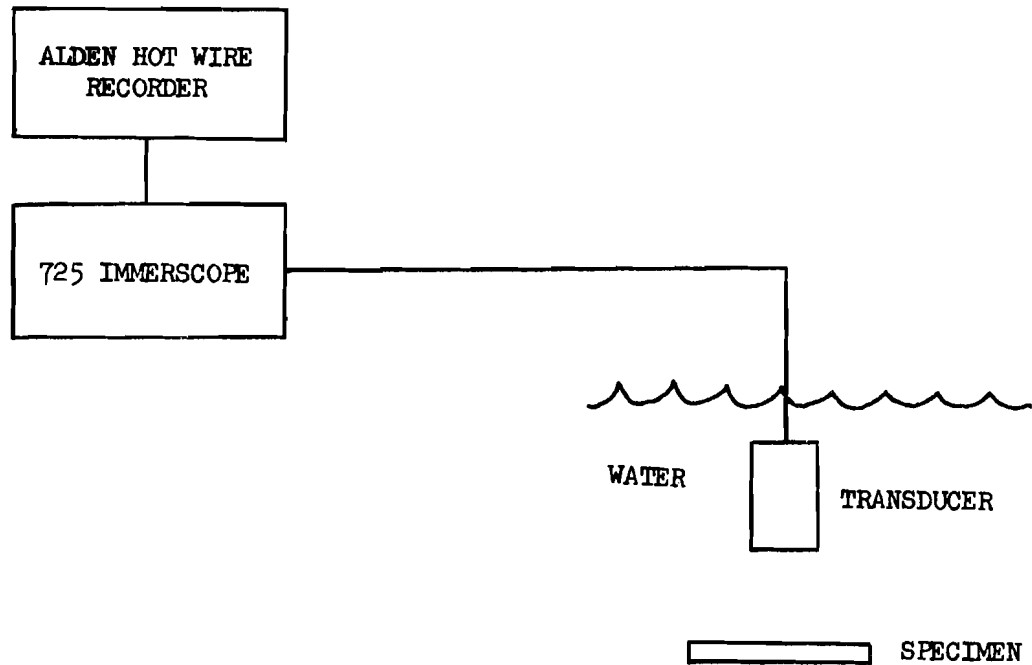
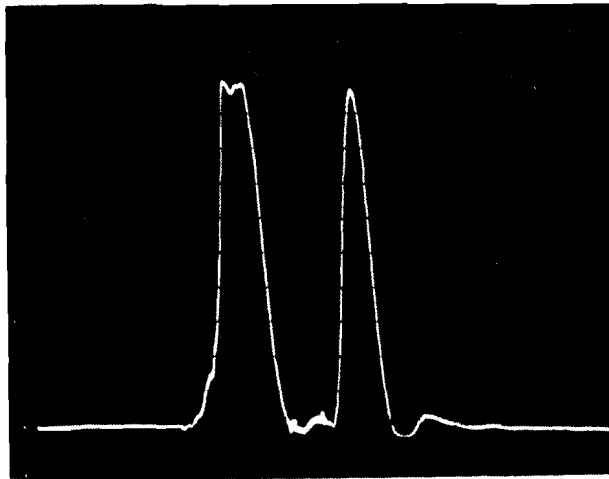
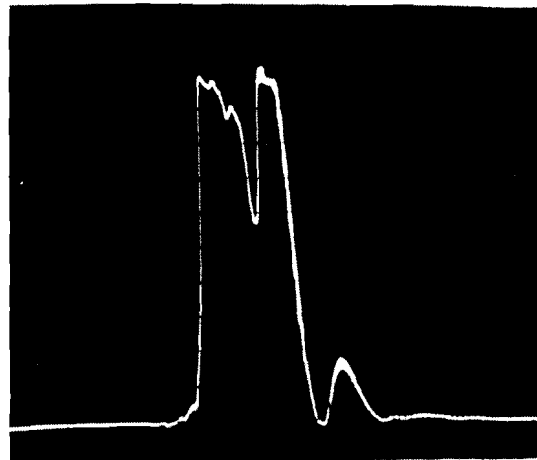


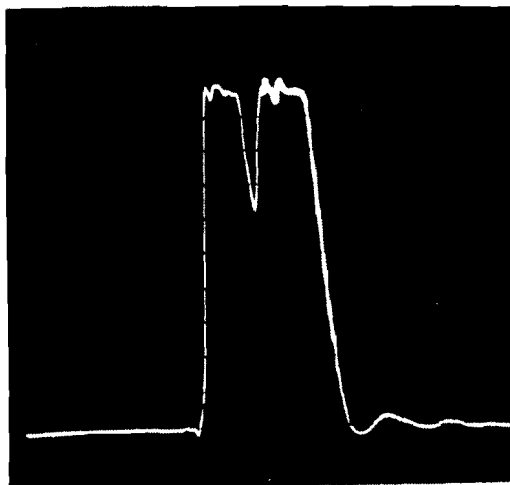
Figure 37. Pulse-Echo Equipment Arrangement



Front and Back Surface  
Indications for No-  
Intentional-Defect  
Area using 3/8-Inch  
Focused Transducer



3/16-Inch Flat-Bottom  
Hole Defect Response  
Using 3/8-Inch Focused  
Transducer



3/16-Inch Flat-Bottom  
Hole Defect Response  
Using 3/8-Inch Flat  
Transducer

Figure 38. Comparison of Pulse-Echo Responses for Focused and Flat Transducers

The optimum location of the transducers focal point with respect to the specimen for the highest defect sensitivity was determined using the same ultrasonic standards employed for the attenuation study. A comparison of the pulse-echo results to the through-transmission data showed that the through-transmission technique was more sensitive as to minimum size detectable defect than the pulse-echo technique (Reference 1). The accuracy of reproduction of defect size for the pulse-echo technique was fairly good for an ideal case of a flat bottom hole with normal orientation. When a defect was at an angle to the normal and/or round bottomed, the pulse-echo technique was either not capable of detecting the defect or it grossly underestimated the defect size (0.188-inch, angled, round bottom hole by 79 percent). In composite materials, the defects encountered are expected to possess a radius of curvature, consequently the round bottom hole may more closely simulate the defects of interest.

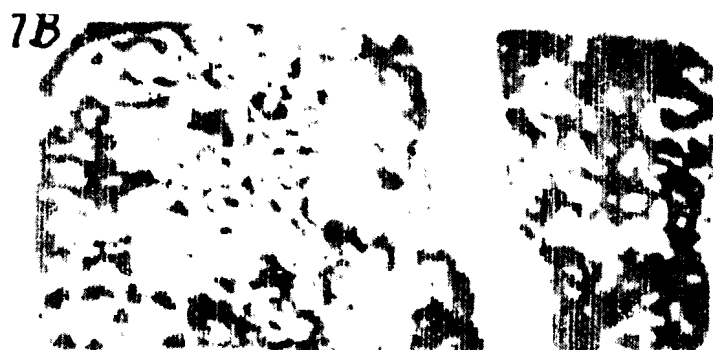
The application of the pulse-echo technique to the pyrolyzed and graphitized VYB 70 1/2 - SC1008 composites was not successful in detecting the intentional defects (Table XI). The pulse-echo technique did not detect the delamination defect during the in-process analysis; however, it did detect it in a machined standard. Using the machined ultrasonic test standard of the graphitized VBY 70 1/2 - SC1008 composite containing the delamination defect, the effect of frequency on the pulse-echo and through-transmission techniques was evaluated. The pulse-echo technique detected the delamination defect at an operating frequency of 2.25 MHz, but not at 5.0 MHz (Figure 39). Many extraneous defect indications on the pulse-echo map made interpretation of the 5.0 MHz pulse-echo map very difficult. However, the through-transmission technique detected the delamination defect at both frequencies. The increase in operating frequency for the pulse-echo technique actually reduced the limits of detection for this defect.

The lack of defect sensitivity of the pulse-echo technique and the sensitivity of this technique to specimen surface roughness as compared to the attenuation technique suggested that the application of this technique to the other unidirectional composites be discontinued. However, the pulse-echo technique may be applicable to higher density composites. This fact will be discussed in the multidirectional composite section.

#### 5.1.2 VYB 70 1/2 - Pitch

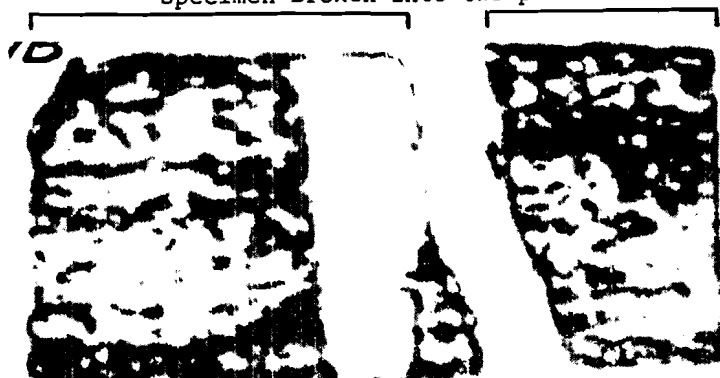
The VYB 70 1/2 - coal tar pitch composites were evaluated on an in-process basis using the radiographic and ultrasonic techniques. The in-process analysis was conducted after impregnation, pyrolysis, and graphitization. The ultrasonic techniques included through-transmission attenuation and velocity measurements. Pulse-echo C-scan mapping was not employed due to the marginal results obtained from the SC1008 composite system. Radiographic techniques included both X-ray and neutron radiography.

The as-impregnated coal tar pitch composites were examined by the X-ray radiography and ultrasonic velocity measurement techniques. The X-ray radiographic parameters for the as-impregnated VYB 70 1/2 - pitch composites were optimized to 20 Kv, 10 ma, 360 sec, 24-inches film-to-focal spot distance. The X-ray radiographs of two specimens, one containing a crack and the other having a complete separation into two halves, are shown in Figure 40 before and after pyrolysis. The examination of the composite after pyrolysis showed that even



5.0 MHz

Specimen broken into two pieces



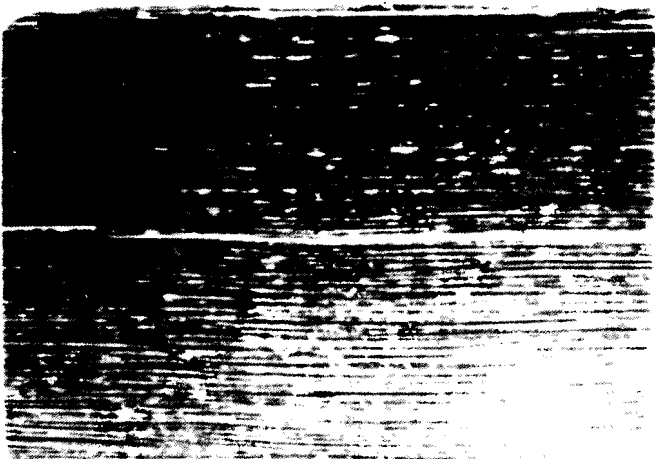
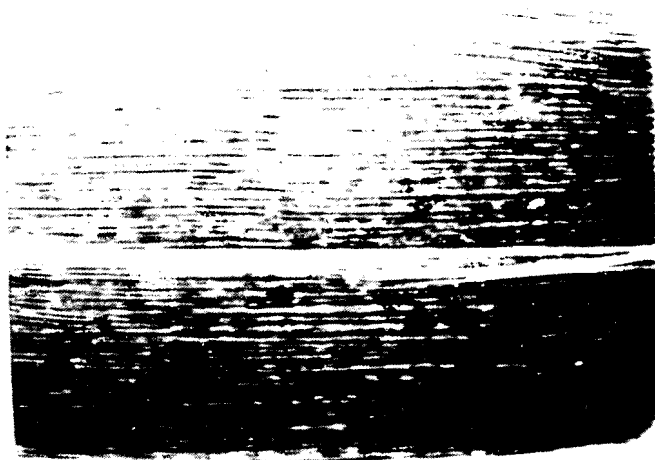
2.25 MHz

Pulse-Echo C-Scan Maps Using a Focused  
Transmitter with Focal Point Located  
within Specimen



Through-Transmission Attenuation C-Scan Map  
Using a Focused Transmitter - Collimated  
Receiver with Focal Point Located within  
Specimen

Figure 39. Ultrasonic Pulse-Echo and Through-Transmission Attenuation C-Scan  
Maps of Graphitized VYB 70 1/2-SC1008 Composite Containing a  
Delamination Defect



As Impregnated

Specimen

8D



8B



Pyrolyzed

Figure 40. Positive Prints of X-ray Radiograph of As-Impregnated and Pyrolyzed VYB 70 1/2-Coal Tar Pitch Composite



the grossest defect, complete separation of the specimen into two halves, could be healed upon pyrolysis due to the fluid nature of the pitch during the initial stages of the cycle. Due to this change in defect structure which occurs with the as-impregnated unidirectional pitch composites, further analysis of the as-impregnated unidirectional composite was not considered necessary.

An attempt was made to measure the ultrasonic longitudinal velocity in the as-impregnated composite by the through-transmission technique previously described. Due to significant amounts of pitch on the surface of the composite, measurements were extremely difficult to make with any degree of accuracy. The only way reliable measurements could be made was if the pitch, which was required for proper processing, was removed. However, this resulted in damage to the specimen. Therefore, further evaluation of the ultrasonic longitudinal velocity techniques for the as-impregnated composite was discontinued.

#### X-ray Radiography

X-ray radiographs were taken of all pyrolyzed and graphitized specimens through the thickness direction. The parameters used for the pyrolyzed condition were (using Type M Film):

Voltage - 20 kv  
Amperage - 10 ma  
Film Focal Distance - 29 in  
Time - 180 sec  
Screen - .004-in polyethylene  
Resulting Film Density - Approximately 3.0

and for the graphitized condition

Voltage - 18 kv  
Amperage - 10 ma  
Film Focal Distance - 29 in  
Time - 180 sec  
Screen - .004-in polyethylene  
Resulting Film Density - Approximately 3.0.

Using a slotted X-ray standard (previously described) of VYB 70 1/2 - pitch composite the sensitivity was determined to be 0.5 percent based on a specimen thickness of 0.100 inches.

The X-ray radiographs of these pyrolyzed samples detected the line defects, cracks, which occurred in all the specimens. It was not possible to differentiate the lack of wetting and small void specimens from the no intentional defect specimens. The weave defect was easily detected by the X-ray radiography. The delamination defect was detected in one of the four composite panels which contained this defect. Upon graphitization the X-ray radiographs contained similar information as on the pyrolyzed composites. A summary of defect detectability for the pyrolyzed and graphitized VYB 70 1/2 - pitch composites is contained in Table XIII.

Selected pyrolyzed and graphitized VYB 70 1/2 - pitch and VYB 70 1/2 - SC1008 composites were used to evaluate the usefulness of neutron radiography as an

Table XIII

SUMMARY OF APPLICABLE NONDESTRUCTIVE TEST TECHNIQUES  
FOR THE VYB 70 1/2 - PITCH COMPOSITE SYSTEM

Defect	Condition	X-Ray	Attenuation	Ultrasonic Velocity
Small Void	Pyrolyzed	No	No	Yes
	Graphitized	No	No	No
Lack of Wetting	Pyrolyzed	No	No (1)	Yes
	Graphitized	No	Yes (1)	Yes
Delamination	Pyrolyzed	No (2)	Yes	Yes
	Graphitized	Yes	Yes	Yes
Weave	Pyrolyzed	Yes	Yes (3)	Yes
	Graphitized	Yes	Yes	Yes

(1) Detected in two of four panels

(2) Detected in one of four panels

(3) Detected as gross nonuniformity in center of panel although attenuation value less than no-intentional-defect panel.

evaluation method (Reference 1). This technique was similar to X-ray radiography in that a test specimen was exposed to radiation to achieve an image of the object on film. The fundamentals of neutron radiography are well documented (Reference 7) and will not be discussed in detail. The evaluation of the neutron radiographs included a direct comparison to the results obtainable with X-ray radiography and also included an evaluation of neutron-absorbing doping agents. The neutron radiography was conducted at the General Electric Vallecitos Nuclear Center at Pleasanton, California, and monitored by MDAC personnel.

A direct exposure technique was used to record the image of the object by using a 0.0005-inch gadolinium screen which is a prompt emission material (little tendency to become radioactive). This screen was placed behind the film such that there was a source-object-film-screen arrangement. This arrangement was used so that the film was in direct contact with that side of the screen which emits the low energy gamma rays. The emulsion side of the film was in direct contact with the gadolinium screen. The film used was Eastman single emulsion Type R which has a very fine grain size. The exposure time was 25 minutes.

The possibility of obtaining greater contrast and definition by temporarily impregnating or diffusing into the composite a strong neutron absorber was evaluated. The two doping agents selected for evaluation were paraffin (high hydrogen content) and gadolinium nitrate,  $Gd_2(NO_3)_3$ .

Prior to conducting the neutron radiography all test samples were X-ray radiographed using the optimized conditions. Reviewing the X-ray and neutron radiographs indicated that the undoped samples were of inferior quality to that of the X-ray radiographs of the VYB 70 1/2 - pitch and VYB 70 1/2 - SC1008 composites. The sensitivity of the neutron radiographic technique for the pyrolyzed SC1008 composite was found to be approximately 4.2 percent using the same slotted standard as used in the X-ray study. Recalling that the sensitivity for the optimized X-ray technique was 0.5 percent, it is apparent that the X-ray technique was considerably more sensitive. It is important to note that the neutron radiographs were not optimized for best exposure parameters (time) and consequently the density of the resulting negative was relatively low.

The other pyrolyzed SC1008 standards containing specific defects which were used in the X-ray study were also evaluated in this neutron radiographic analysis. Generally the results indicated that the neutron radiographs of the undoped standards were of inferior quality to the X-ray radiographs. Two defects which were detected in the X-ray study and not in this study were weave irregularities and noncarbonaceous impurities. The latter was as expected since the silica used for impurity has a much lower absorption coefficient than carbon.

The paraffin-doped pitch composites compared favorably to the X-ray radiographs in the amount of detail present. The neutron radiograph of the  $Gd_2(NO_3)_3$ -doped specimen had extremely high density which necessitated making an extraction. This was done by exposing the negative to ordinary light and obtaining a reverse image negative. The examination of this negative was disappointing in that the dopant actually reduced the detail obtainable. This was due to the

fact that the  $\text{Gd}_2(\text{NO}_3)_3$  which was present in the large crack essentially washed out the image of the small cracks adjacent to the larger one. However, when a positive print was made of this negative, a significant amount of detail was obtained which was better than that contained in the X-ray radiographs (Reference 1).

The results of the neutron radiography indicated that there was not a major improvement over X-ray radiography for evaluation of the unidirectional composites. The evaluation of weave pattern irregularities was best accomplished by X-ray radiographic methods. Neutron radiography did provide some additional information on the composite uniformity when the  $\text{Gd}_2(\text{NO}_3)_3$  dopant was used. However, this slight improvement was obtained only with the best dopant (based on absorption coefficient available). From this standpoint, the technique would be limited in use on production hardware since it is not known at this time how well the doping material can be removed from the composite or what effects residual doping material might have on composite performance. Further, the most efficient sources of thermal neutrons are reactors, and large structures would be difficult to handle if they were to be evaluated by neutron radiography.

#### Ultrasonic Velocity

The longitudinal velocity measurements (at 1.6 MHz) on the pyrolyzed VYB 70 1/2 - pitch composites which contained the intentional defects had slightly lower velocities than those specimens without intentional defects (Figure 41). In the graphitized condition the velocity measurements (at 0.8 MHz) were sensitive to the presence of all defects except the small voids. The no-intentional-defect-specimens, were processed under a different processing procedure from the other composite specimens as described in Section 3.1. It is possible that the graphitized pitch binder properties were of such a significant difference that they out-weighed the 6 percent increase in porosity for the small void specimens. The mechanical test results (Section 6.0) on these specimens indicated a higher strength associated with the graphitized small void specimens which corresponded to the high velocity. However, the mechanical test results indicated that a similar increase in velocity should have been observed for the pyrolyzed specimens. These results indicate that the processing conditions have an important effect on the velocity results. If processing conditions are changed, absolute values of velocity can be misleading when compared to material processed under different conditions.

The longitudinal velocity of the pyrolyzed and graphitized composites increased with increasing density (Figure 27). This trend was attributed to an increase in the porosity of the composite (Subsection 5.1.1). The densities varied over a range of approximately 9 percent which corresponded to a 20 percent range in velocity. Again, the dependence of velocity on density suggests its use in screening low density carbon-carbon composites.

The ultrasonic longitudinal velocity was measured as a function of frequency for the no intentional, small void and lack of wetting defects. The through-transmission technique as previously described was used. As with VYB 70 1/2-SC1008 unidirectional composite system, a frequency dependence of velocity existed (Figure 42). The figure indicates a difference between the velocity

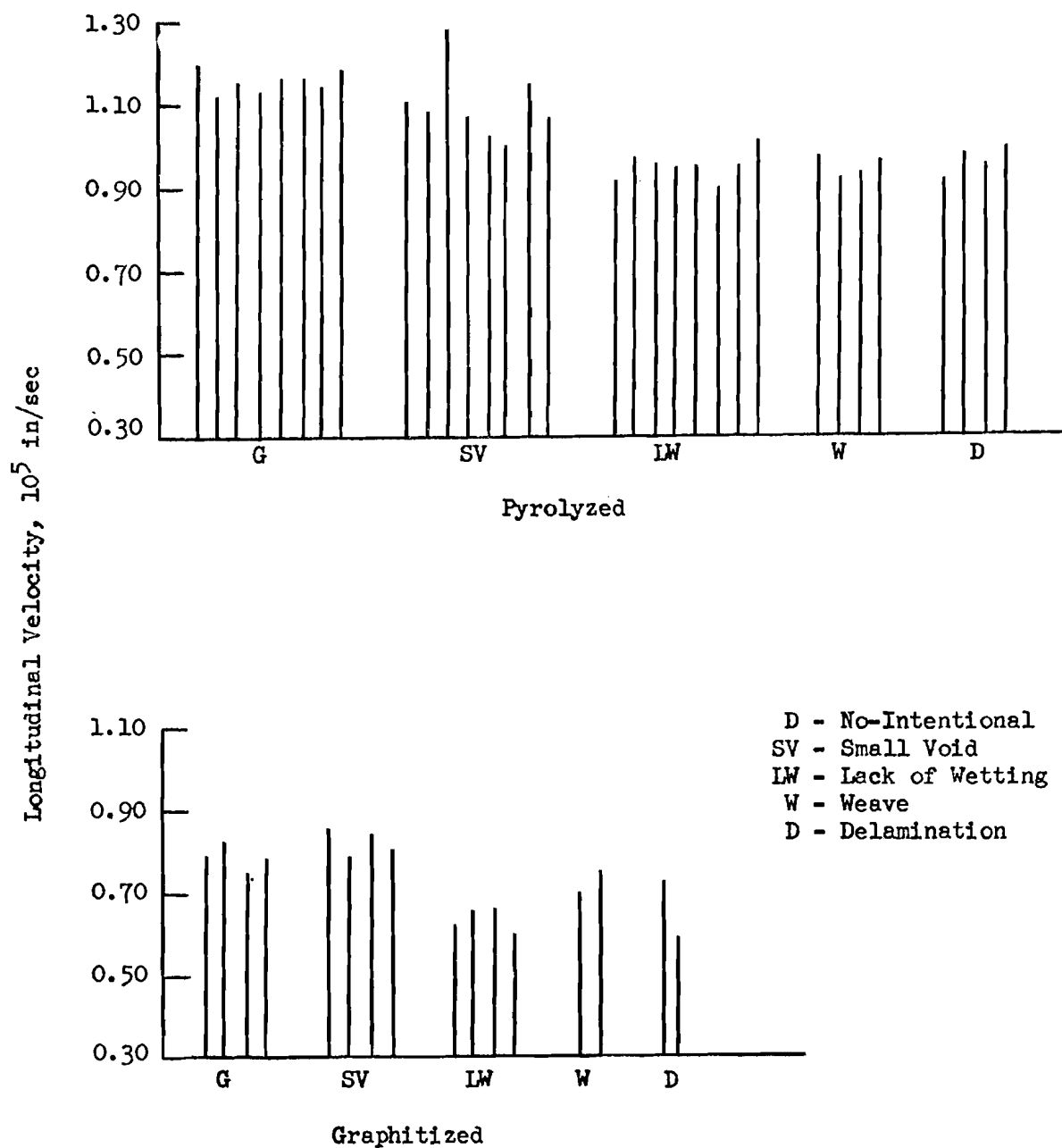


Figure 41. Longitudinal Velocity of VYB 70 1/2 - Pitch Composite

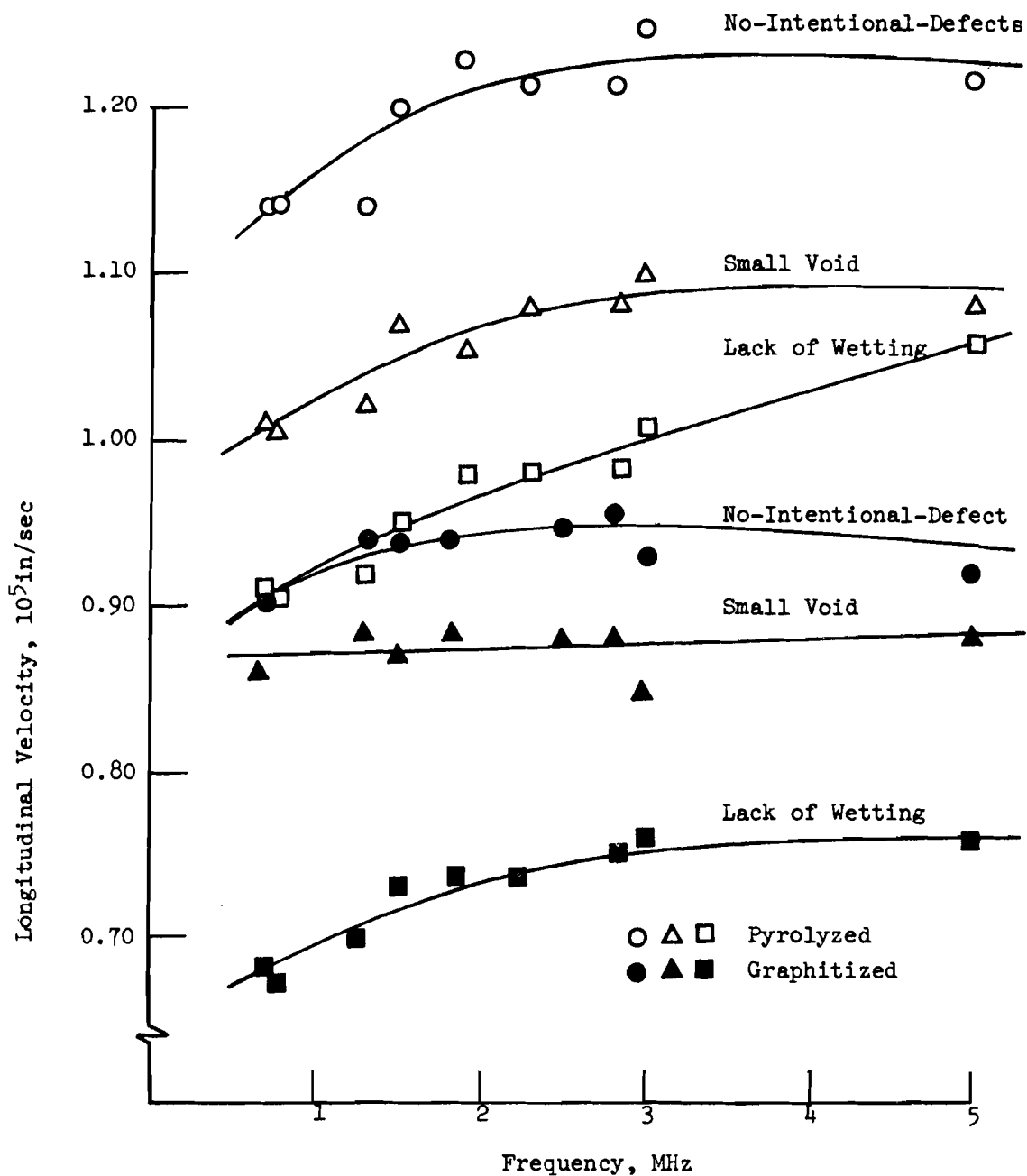


Figure 42. Ultrasonic Longitudinal Velocity versus Frequency for Pyrolyzed and Graphitized VYB 70 1/2 - Pitch Composite

of the no-intentional and defect specimens at all frequencies over the range 0.7 to 5 MHz. Measurements could not be made at higher frequencies due to the attenuation present.

The frequency dependence of velocity for the VYB 70 1/2 - pitch system was significantly different from the VYB 70 1/2 - SC1008 system. At 2.5 MHz the measured velocities were significantly different for each defect group as opposed to being equal in the VYB 70 1/2 - SC1008 system. The difference in the frequency-velocity relationships and the magnitudes of the velocity for these two systems (same yarn but different matrices) may be attributed to the significant difference in pore structure which existed between these two systems. In Section 4.0, the pitch system was shown to have a lower porosity level and a significantly different pore distribution from the SC1008 system as shown by the porosimeter data. The volume fraction of VYB 70 1/2 yarns was approximately the same for both systems. These facts suggest that the binder system in a composite (and the processing procedures) plays a significant role in determining the measured ultrasonic velocities. These differences will also be shown to affect the mechanical properties in Section 6.0.

The selection of the operating frequency depended upon which defect groups were to be screened. Pyrolyzed and graphitized no-intentional defect specimens can be separated from the other defect groups most confidently at approximately 2 MHz. As can be seen from Figures 29 and 42, this selection was not as critical as with the VYB 70 1/2 - SC1008 composites.

The 2 MHz frequency could also be used to select the small void specimens. However, this selection can not be arbitrary for, at 5 MHz, one could not confidently screen the lack of wetting defect from the small void. The importance of having the capability of screening these defect groups will become important when the strengths associated with each group are examined. The point of having the capability of screening the small void specimens was emphasized due to the higher strengths achieved with these autoclave-processed specimens (Section 6.0).

Figure 42 also shows the decrease in velocity upon graphitization as in the SC1008 system. As previously explained, this was attributed to the change in porosity and modulus of the composite materials. The possible introduction of material discontinuities into the composite system was not considered to be the cause of the change in velocity because the wavelength of the ultrasound at these frequencies (0.8 mm at 2.5 MHz and 0.4 mm at 5.0 MHz) is an order of magnitude greater than the maximum size discontinuity present (0.02 mm). Thus, the ultrasonic wave "saw" the composite as a macroscopically homogeneous material rather than an inhomogeneous material containing many discontinuities.

#### Ultrasonic Attenuation

Ultrasonic attenuation measurements were made by the immersed through-transmission technique. Ultrasonic test standards, 0.100-inches thick, containing a 0.064 and 0.032 inch diameter flat bottom hole 0.050 inches from the top surface were fabricated from the pyrolyzed and graphitized composites. The 0.064-inch diameter hole was detected in both the pyrolyzed and graphitized composites; however, it was not possible to detect the 0.032-inch diameter hole in either condition. These test standards also contained three 0.064-inch

diameter holes 0.200 and 0.150 inches apart (center to center). At the 0.150-inch distance, the individual holes could not be identified, that is they were detected as one large defect. A 0.064-inch diameter hole placed 0.150 inch from the test standard edge was not discretely identified. Although the defect was detected, it could not be separated from the edge. The resolution between two artificial defects in this composite system was 0.200 inch.

The analysis of the attenuation C-scan maps of the VYB 70 1/2 - pitch composites indicated that it was difficult to differentiate between the intentional defect and the no-intentional-defect specimens. The attenuation values for each composite panel are summarized in Figure 43 and Appendix I. The main reason for this lack of differentiation is the high attenuation of the no-intentional-defect specimens. These specimens were processed differently from the defect specimens (Section 3.1). Differences in porosity and fiber-matrix bonding are probably the cause of this higher attenuation. The C-scan maps of the pyrolyzed panels indicated the weave and delamination defects as a higher attenuating area in the center of the panel. Porosity present in the weave defect specimen accounts for the high attenuation, rather than the weave defect itself.

Upon graphitization, the attenuation of the specimens increased although the results and interpretation of the maps were the same for all specimens. The smaller increase in attenuation after graphitization as compared to the SC1008 system was attributed to the significantly different porosity levels and pore distribution which existed between these two systems. The attenuation of a material may not only be affected by the porosity level but also by the pore size distribution.

In only one case did a defect, small void defect in graphitized condition, go undetected by the three nondestructive testing techniques (X-ray radiography, ultrasonic attenuation and velocity) initially employed on the composite panels (Table XIII). However, as will be discussed, the ultrasonic longitudinal velocity measured on the graphitized mechanical test coupons showed a difference between no-intentional-defects and the small voids.

A comparison of the measured total porosity and the ultrasonic attenuation of the VYB 70 1/2 - pitch composite specimens processed under different conditions is made in Table XIV. In the VYB 70 1/2 - SC1008 system, a trend between porosity and attenuation indicated higher attenuation corresponding to higher porosity. A similar trend exists between the porosity and attenuation data on composite specimens processed under the same procedures (Figure 44). The no-intentional defect specimens do not follow the same trend as the other specimens. Again, this points out the significant difference that can exist in the NDT data between specimens processed under different conditions.

Specimens were selected from the pyrolyzed VYB 70 1/2 - pitch composite system to evaluate a multi-level or half tone recording system. This system provides an indication of several attenuation levels on one map by having shading gradation between the normal "on - off" condition. In order to assess the potential for such apparatus, contact was made with Automation Industries in Chatsworth, California, and arrangements made to use the Automation "half tone" recording system to evaluate its applicability to through-transmission



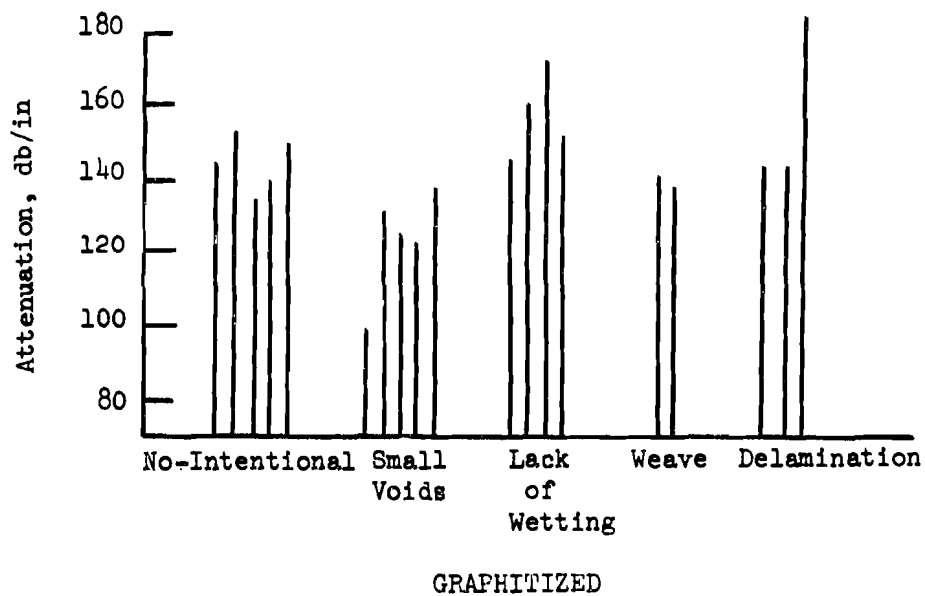
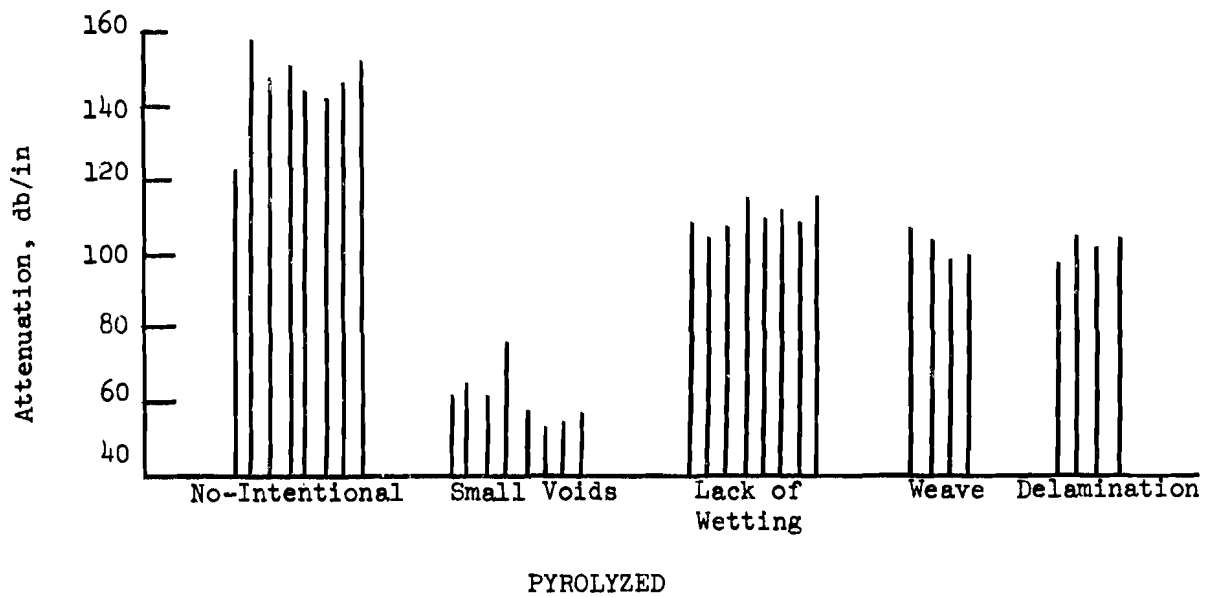


Figure 43. Ultrasonic Attenuation of Pyrolyzed and Graphitized VYB 70 1/2 - Pitch Unidirectional Composites

Table XIV

ULTRASONIC ATTENUATION AND POROSITY OF  
VYB 70 1/2 - PITCH COMPOSITE SPECIMENS

Defect Group	Condition	Total Porosity, %	Attenuation (db/in)
No-Intentional <sup>(1)</sup>	Pyrolyzed	6.1	145
	Graphitized	11.5	146
Small Void <sup>(2)</sup>	Pyrolyzed	11.8	60
	Graphitized	15.1	115
Lack of Wetting <sup>(2)</sup>	Pyrolyzed	14.8	109
	Graphitized	19.6	157

(1) Pressure pyrolysis cycle

(2) Autoclave pyrolysis cycle

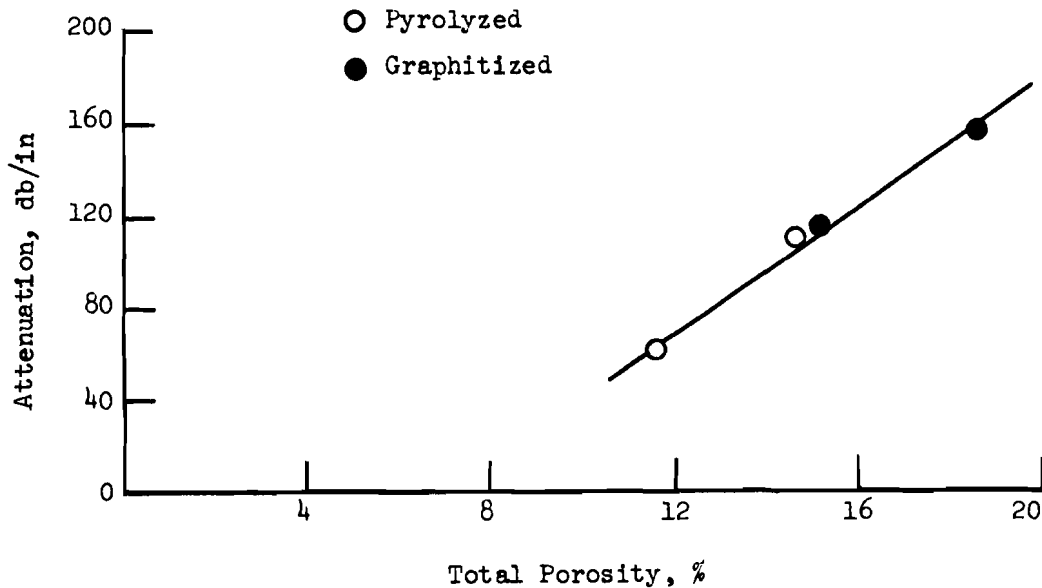


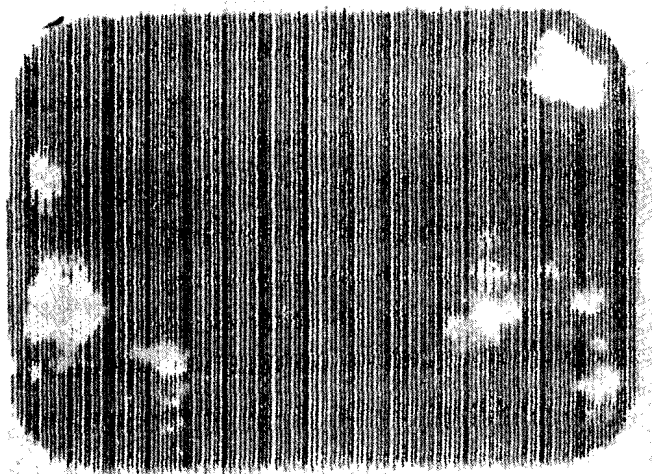
Figure 44. Total Porosity versus Attenuation of VYB 70 1/2 - Pitch Composites Processed Under the Same Conditions

attenuation measurements. The equipment employed was a Model UM721 reflectoscope with a 10N Pulser Receiver, and Fast Transigate and Transigraph Modules. The tank, bridge, recorder, and transducers were all MDAC equipment which have been used for all previous attenuation mapping work.

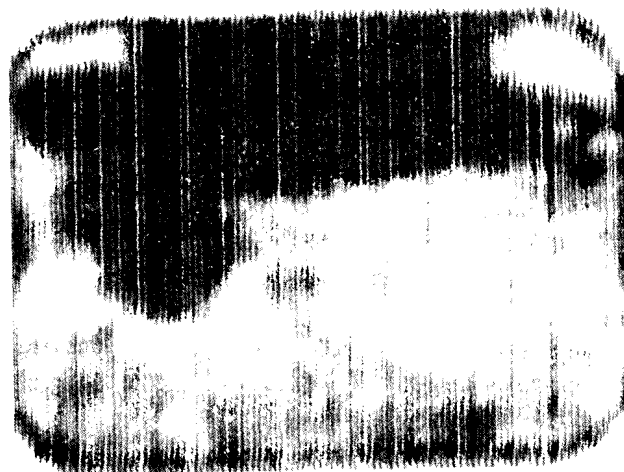
Specimens 10B was C-scan mapped by both the half-tone and normal on-off recording methods. The maps of this specimen are compared in Figure 45. The half-tone recording maps provided useful information on panel uniformity. However, discrete discontinuity detection may be more difficult with this method than with the on-off method. Small discrete defects may be uninterpretable or lost in the different shadings. Possibly, a combination of these two methods may prove useful.

The attenuation maps of three groups of pyrolyzed specimens indicated that the uniformity of the composites were drastically different depending on the location of the specimen in the processing fixture. It was found that the attenuation values of the specimens more than doubled for the two locations. Since the attenuation of a material may be related to the amount of porosity present, it was possible that one location caused an excessive amount of porosity to occur. This lead to an investigation of this processing condition and subsequent changes in procedures. This case in particular indicated the usefulness of applying NDT techniques during a process development program to aid in evaluating the composites.

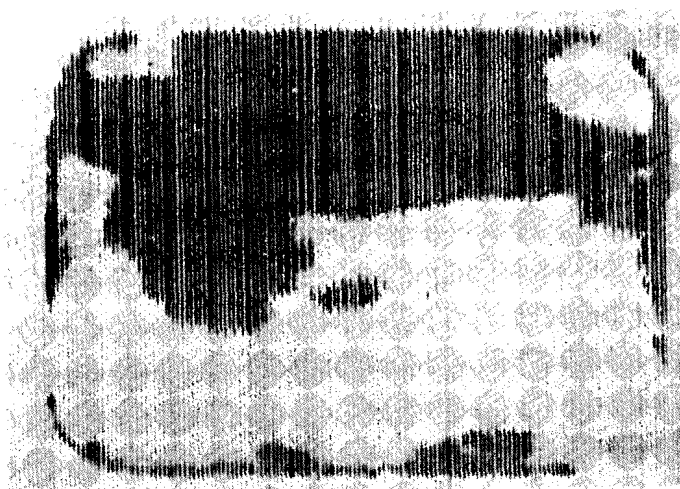
Ultrasonic attenuation maps and X-ray radiographs of flexure-tested composites were correlated to the microscopic evaluation of the material. In order to evaluate the flexure test specimens under the condition of first load-carrying failure, the flexure tests were stopped shortly after the first peak in the load-deflection curve. The X-ray and through-transmission data complemented one another in that the X-ray technique was most sensitive to defects parallel to the X-ray beam while the through-transmission technique was most sensitive to those defects perpendicular to the ultrasonic beam. A positive print of the X-ray radiograph of specimen 1A3 is shown in Figure 46. The portion of the X-ray print which corresponded to the area of the specimen to be sectioned and microscopically evaluated was photographically enlarged by 4X. Due to this enlargement process, the darker areas are of low density. At locations 1, 2, and 3, the negative reveals lines of lower density. These lines should appear as vertical lines on the micrograph of the edge view. These lines have been correlated to cracks present in the composite edge view as seen in Figure 47. The through-transmission C-scan map (Figure 47) indicates that areas 1 and 2 had a much greater attenuation than area 3. It was expected that areas 1 and 2 will have a larger size and number of horizontal cracks through the specimens than area 3. Upon examination of Figure 47, this was seen to be the case. Unlike the X-ray radiograph where single irregularities are detectable, the through-transmission attenuation method will at times rely on the integration of a number of defects to yield a specific attenuation level or map.



16 db



5-20 db



20 db



10-20 db

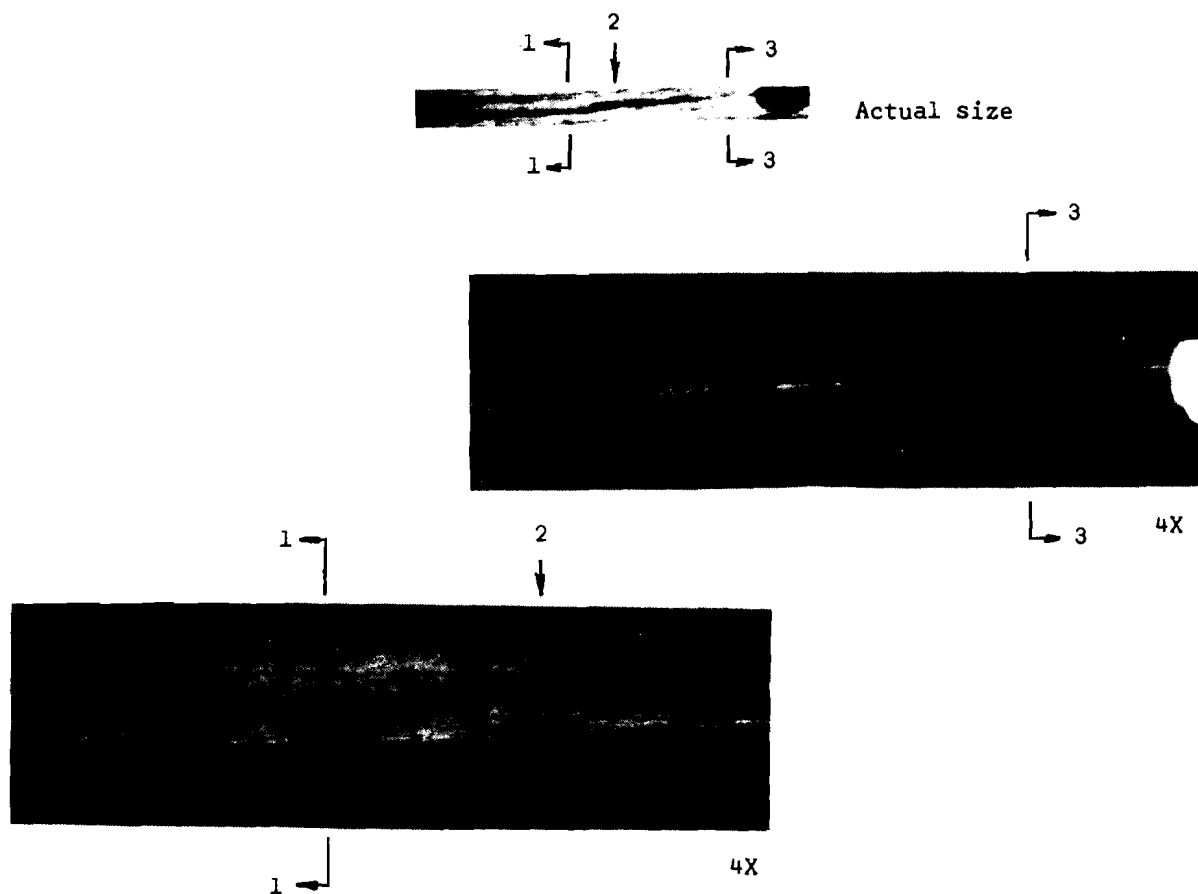
Regular C-Scan Maps

Half-Tone C-Scan Maps

Specimen 10B

VYB 70 1/2-Pitch, Large Voids

Figure 45. Comparison of Half-Tone and Regular Attenuation C-Scan Maps



X-Ray Radiographs

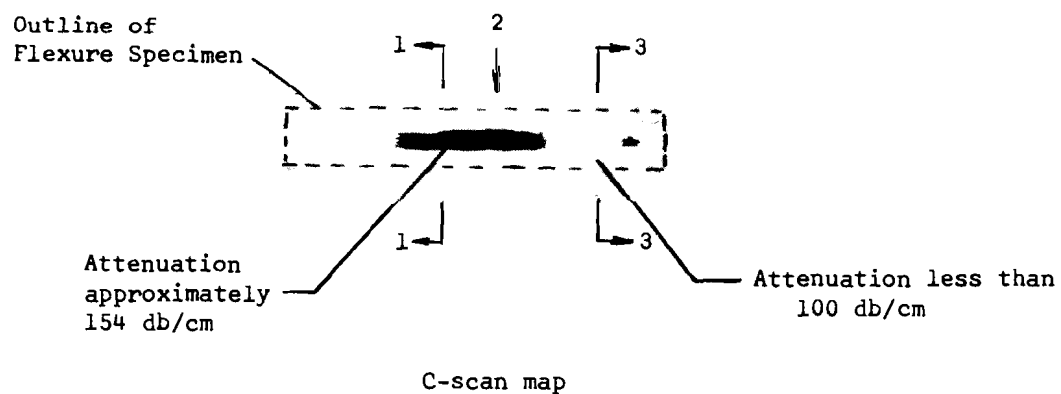
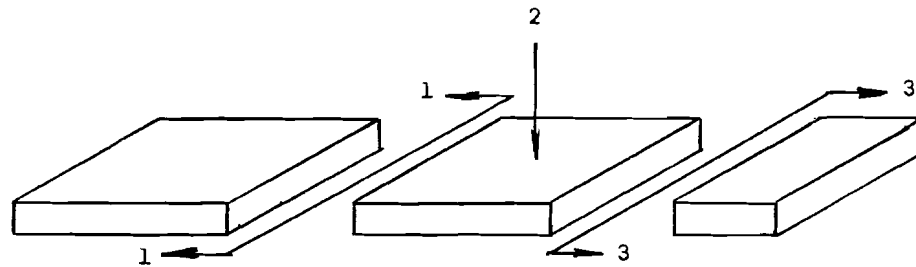


Figure 46. X-Ray Radiographs and Attenuation C-Scan Maps of Graphitized VYB 70 1/2-Pitch Composite Specimen 1A3 after Flexure Test

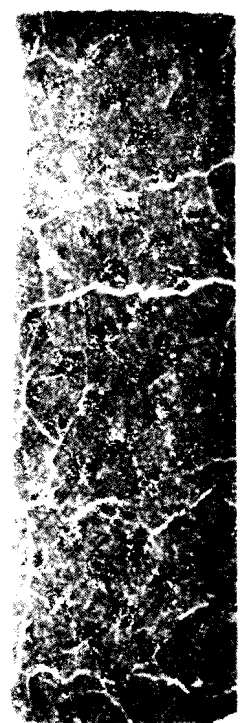


1



2

17X



3

Figure 47. Photomicrographs of Graphitized VYB 70 1/2-Pitch Composite Specimen 1A3 after Flexure Test

### 5.1.3 Modmor II - Pitch

#### X-ray Radiography

X-ray radiographs were taken of all pyrolyzed and graphitized Modmor II - pitch unidirectional specimens through the thickness direction. The parameters used were voltage - 17 kv, current - 10 ma, film-to-source distance - 29 inches, screen - .004-inch polyethylene, and time - 178 seconds (pyrolyzed condition) and 150 seconds (graphitized condition). The sensitivity of the X-ray radiographic technique was determined to be 0.5 percent using a slotted standard. The X-ray technique was only capable of detecting the weave and crack defects within the pyrolyzed and graphitized composites. A summary of defect detectability for the pyrolyzed and graphitized Modmor II - pitch composites is contained in Table XV.

#### Ultrasonic Velocity

The ultrasonic velocity of the pyrolyzed Modmor II composite panels (at 1.6 MHz) showed a decrease for the small void and lack of wetting defects (Figure 48). It was not possible to distinguish the weave defect from these measurements. In the graphitized condition, the velocity measurements (at 0.8 MHz) for the no-intentional-defect-specimens were actually less than that of the defect specimens. The no-intentional-defect specimens had a higher total porosity, approximately 8 percent, than the lack of wetting or small void defect specimens. Increases in total porosity of a material are usually associated with a decrease in ultrasonic longitudinal velocity. Therefore, it can only be suggested that another material property is affecting these results of the graphitized Modmor II - pitch composites.

Table XV

#### SUMMARY OF APPLICABLE NONDESTRUCTIVE TEST TECHNIQUES FOR THE MODMOR II - PITCH COMPOSITE SYSTEM

Defect	Condition	X-Ray	Attenuation	Ultrasonic Velocity
Small Void	Pyrolyzed	No	No	Yes
	Graphitized	No	No	Yes
Lack of Wetting	Pyrolyzed	No	No	Yes
	Graphitized	No	No	Yes
Weave	Pyrolyzed	Yes	Yes <sup>(1)</sup>	No
	Graphitized	Yes	Yes <sup>(1)</sup>	No
Cracks	Pyrolyzed	Yes	Yes	No
	Graphitized	Yes	Yes	No

(1) Detected in two of five panels as a higher attenuating area.

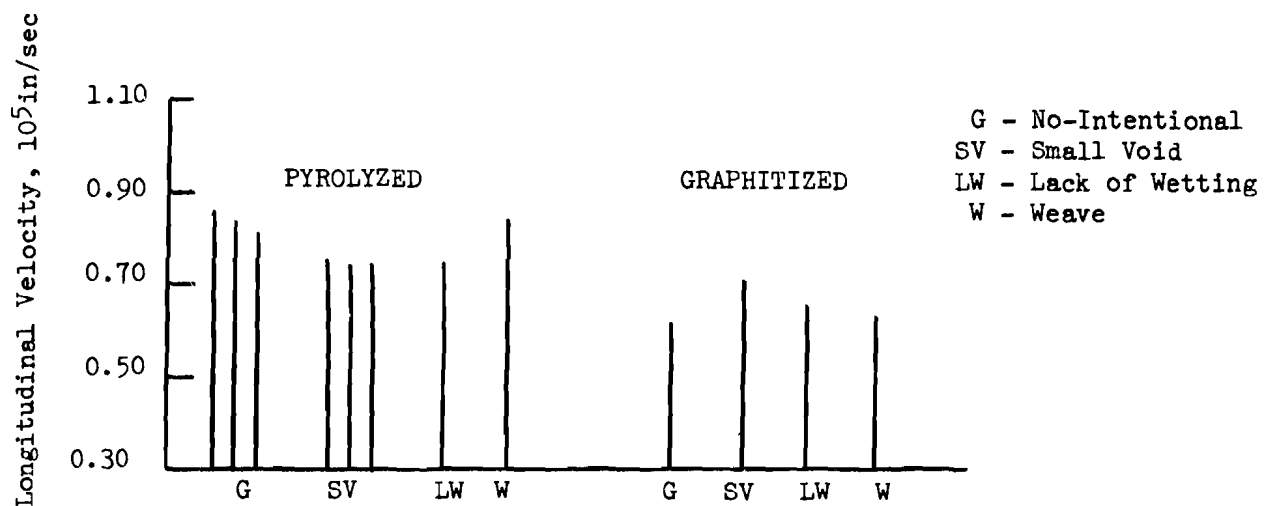


Figure 48. Longitudinal Velocity of Modmor II - Pitch Composite



As with the other unidirectional systems, bulk density (water immersion) of the composite was related to the longitudinal velocity (Figure 27). The trend for the pyrolyzed system was similar to that obtained for the VYB 70 1/2 - SC1008 and VYB 70 1/2 - pitch systems, that is higher velocity corresponding to higher density. However, an exception to this trend was found for the graphitized Modmor II - pitch system. This anomalous result was directly opposite to that observed for the other systems and is not completely understood.

The ultrasonic longitudinal velocity was measured as a function of frequency on selected Modmor II - pitch samples representing no-intentional and small void defect groups. The measurements were made by the through-transmission, technique from 0.8 MHz using the time delay to the peak of the initial cycle. The data suggested that the velocity was frequency dependent (Figure 49). The frequency dependence of velocity was different from that obtained for the VYB 70 1/2 - SC1008 composite. In the VYB 70 1/2 - SC1008 composite system no significant difference existed in the velocity values for the various specimens at 2.5 MHz and a large difference existed at 0.8 MHz. In the Modmor II - pitch system, the velocity values for the small void and no-intentional defect specimens were very close at 0.8 MHz while at 2.5 MHz a large difference existed. Therefore, the selected operating frequency for screening of Modmor II - pitch composites was different from the VYB 70 1/2 - SC1008 system.

On comparing the frequency dependence graphs of the two pitch systems, it is seen that the trends are similar. A difference does exist in the magnitude of the velocity and in the precise shape of the curve in the 0.5-1.5 MHz region. This difference was believed due to the difference between the VYB 70 1/2 and Modmor II yarn properties and the slight difference in pore structure between the two systems.

#### Ultrasonic Attenuation

Attenuation measurements were made by the immersed through-transmission (focused transmitter - collimated receiver) method on the pyrolyzed and graphitized composites (Figure 50). The ultrasonic attenuation values of the weave defect containing specimens were higher than the no-intentional-defect specimens in the pyrolyzed and graphitized conditions. This was due to a local increase in porosity due to the weave irregularity. The small increase in attenuation after graphitization, as compared to the SC1008 systems, was again attributed to the differences in the porosity level and pore distributions (Section 4.0). Direct comparisons for the attenuation values for the small void and lack-of-wetting-defect specimens to the no intentional-defect specimens were not possible because the attenuation maps of the defect specimens were made with a very rough specimen surface as compared to the no-intentional-defect specimens. The attenuation maps showed narrow strips of high attenuation areas which corresponded to irregular cracks through the thickness of the specimens. These differences in surface condition therefore prohibited the correlations of attenuation with porosity for this composite system.

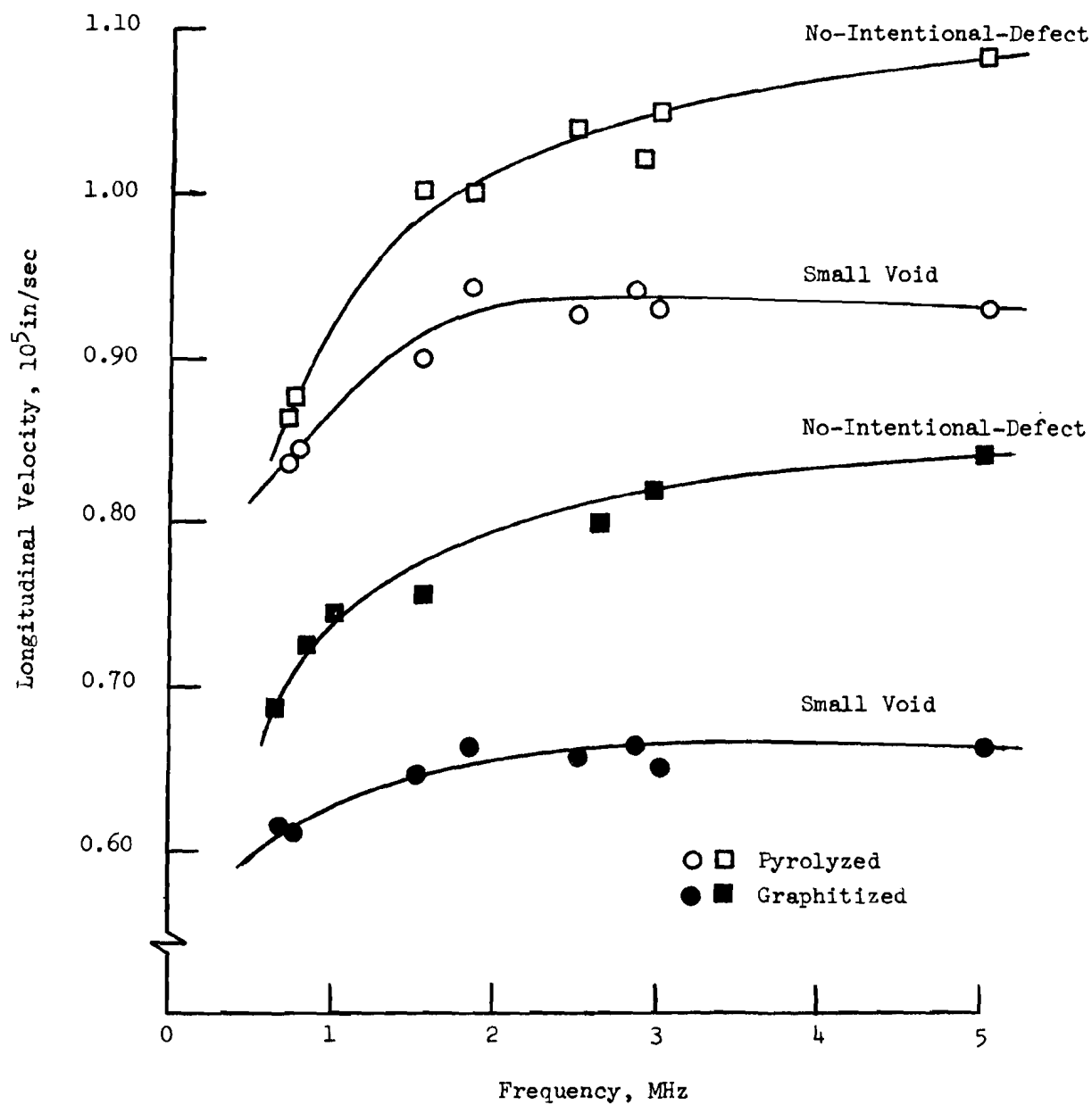


Figure 49. Ultrasonic Longitudinal Velocity versus Frequency for Pyrolyzed and Graphitized Modmor II - Pitch Composites

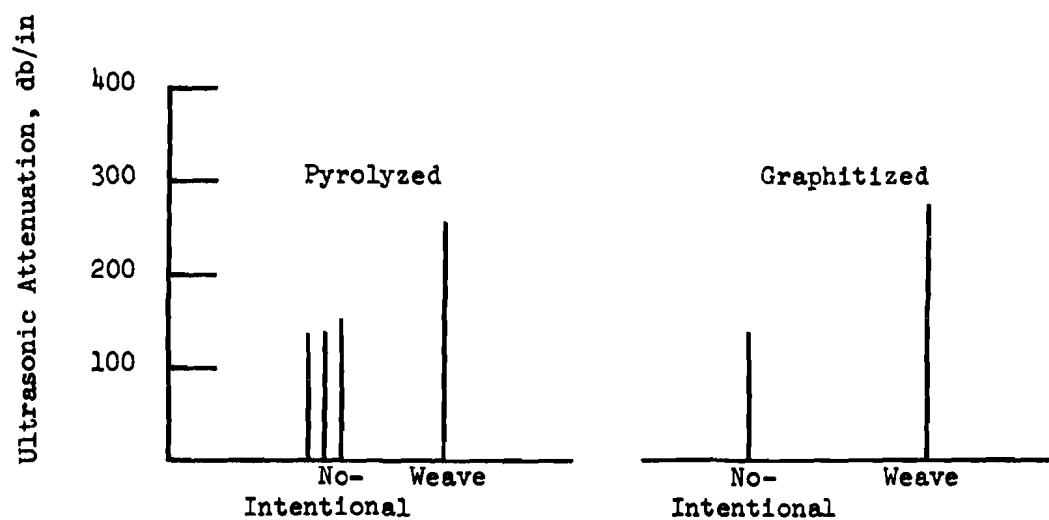


Figure 50. Ultrasonic Attenuation of Pyrolyzed and Graphitized Modmor II - Pitch Composites

#### 5.1.4 Ultrasonic Transverse Velocity

The characterization of the unidirectional composites also included transverse (shear) wave velocity measurements on selected control specimens. The shear wave velocity measurements were made at 0.5 MHz using a 0.5 MHz one-inch diameter transmitter with a 2.0 MHz one-half-inch diameter crystal bonded to a three-inch long, one-inch diameter aluminum buffer rod for the receiver. Both transducers used a polarized lead-zirconate-titanate element. The buffer rod was used to separate the longitudinal and shear wave components of the received signal. This eliminated the difficulty in measuring the shear wave component delay (arrival) time which was caused by a longitudinal wave mode arriving at approximately the same time as the shear wave component. A water-soluble, high-viscosity couplant was used to couple the transducers to the vinyl-coated specimens. The shear velocity measurements were made in the transverse (thickness) direction with the polarization directions parallel and perpendicular to the fiber direction. A shear velocity measurement was made on the quartz standard to establish a level of confidence. The measured shear velocity of  $1.49 \times 10^5$  in/sec compares to the value of  $1.48 \times 10^5$  in/sec given in Reference 3.

The shear wave velocities were generally higher for the no-intentional-defect-composite-specimens (Table XVI and Figures 51-52). One exception is the shear velocity polarized perpendicular to the fiber direction for the pyrolyzed composites containing small voids which was higher than the velocity for the no-intentional-defect-specimens. The shear wave velocities polarized perpendicular to the fiber direction ( $V_{66}^*$ ) were consistently less than those parallel to the fiber direction ( $V_{44}^*$ ). For an ideal unidirectional composite with good transverse properties,  $V_{66}$  should be greater than  $V_{44}$ . The shear velocity  $V_{66}$  is proportional, in part, to the transverse extensional modulus, whereas the shear velocity  $V_{44}$  is proportional to the in-plane shear modulus. The lower shear velocity in the transverse plane ( $V_{66}$ ) suggests that the transverse modulus for these composites is low. One possible explanation for the low transverse properties is that the basal planes of both the matrix and fibers are oriented parallel to the fiber direction such that their weakest direction is in the transverse direction of the composite.

A comparison of the transverse velocity versus the longitudinal velocity measurements for defect detection is summarized in Table XVII. The results do not indicate any advantage of using shear wave velocity measurements over the longitudinal velocity measurements for defect detection.

#### 5.2 Multidirectional Composites

The multidirectional composites evaluated by the nondestructive techniques included the 0.500-inch thick DACLOCK 120 (D120) and 1.0-inch thick orthogonal flat goods, the 1.0-inch thick (wall) woven cylinder, and a 4.0-inch thick AVCO

---

\* The notation here corresponds to that used for the elastic stiffness constants for a material with hexagonal symmetry [ $V_{66} = (C_{66}/\rho)^{1/2}$ ,  $V_{44} = (C_{44}/\rho)^{1/2}$ ].

Table XVI

## SHEAR WAVE VELOCITY MEASUREMENTS

Material System	Specimen	Defect	Condition	Shear Velocity, $10^5$ in/sec	
				Parallel to Fibers	Perpendicular to Fibers
VYB 70 1/2 - SC1008	31C	No-Intentional	Pyrolyzed	0.678	0.467
	14A		Graphitized	0.736	0.420
	26A	Small Void	Pyrolyzed	0.665	0.482
	26C		Graphitized	0.629	0.328
	27C	Large Void	Pyrolyzed	0.594	0.438
	27D		Graphitized	0.613	0.317
VYB 70 1/2 - Pitch	12B	No-Intentional	Pyrolyzed	0.920	0.613
	13		Graphitized	0.778	0.448
	21D	Small Void	Pyrolyzed	0.852	0.659
	22B		Graphitized	0.691	0.466
	6C	Lack of Wetting	Pyrolyzed	0.767	0.570
	5B		Graphitized	0.669	0.393
Modmor II - Pitch	2-3	No-Intentional	Pyrolyzed	0.750	0.474
	2-5		Graphitized	0.705	0.325
	14D2	Small Void	Pyrolyzed	0.643	0.498
	14C		Graphitized	0.609	0.375

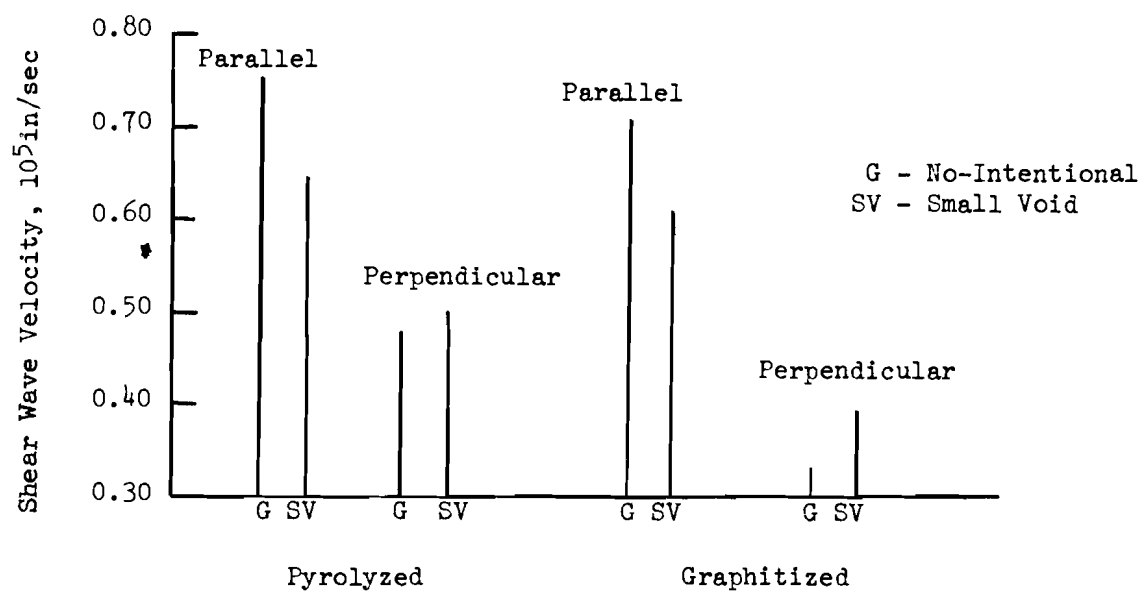


Figure 51. Polarized Shear Wave Velocity of Modmor II - Pitch Composite

VYB 70 1/2 - SC1008

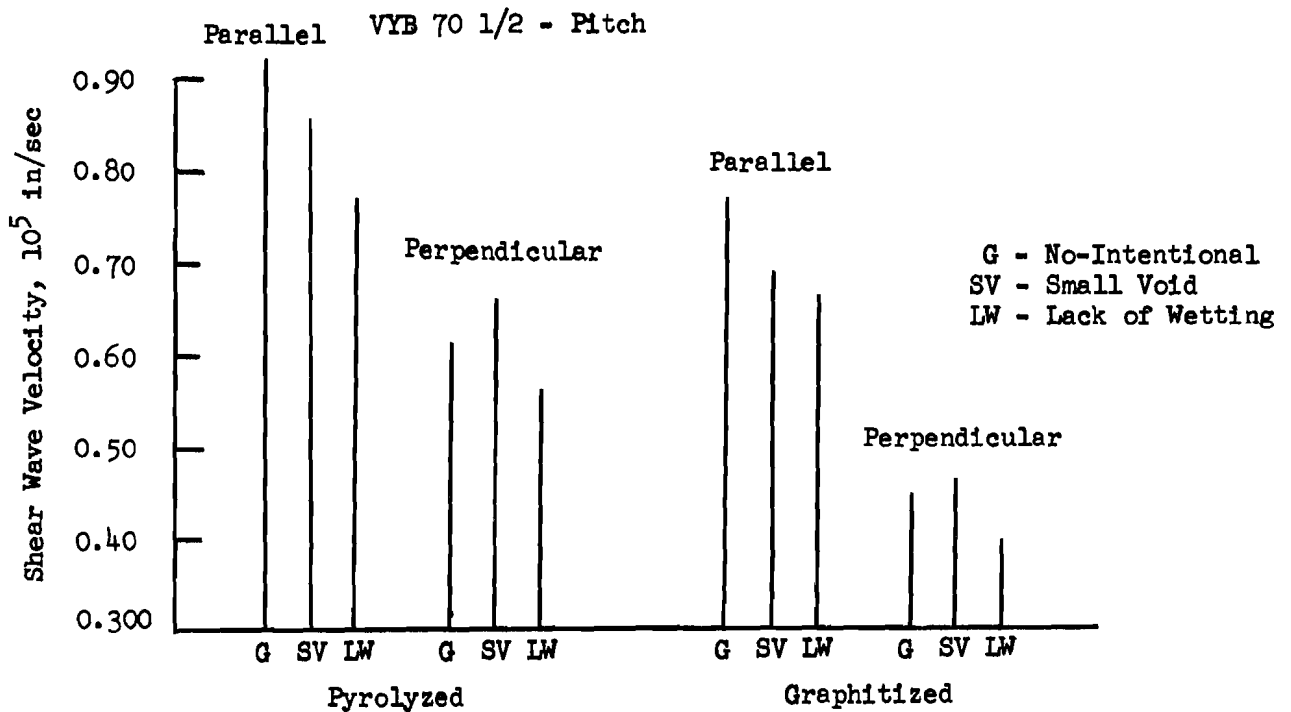
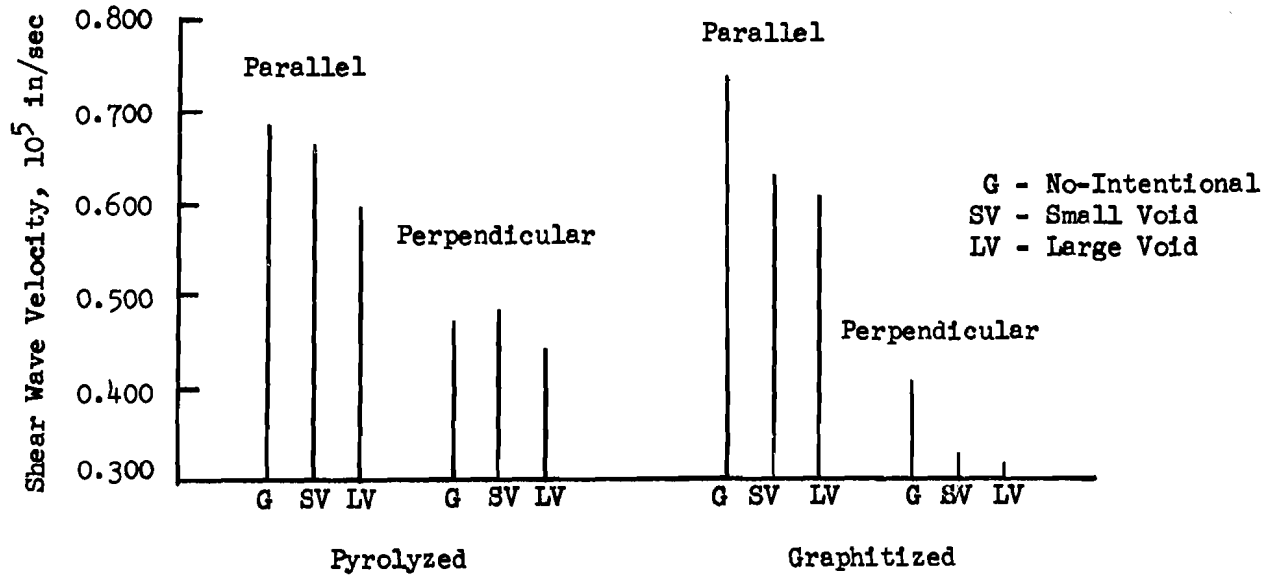


Figure 52. Polarized Shear Wave Velocity of VYB 70 1/2 - SC1008 and VYB 70 1/2 - Pitch Composites

Table XVII

## PERCENTAGE CHANGE IN VELOCITY MEASUREMENTS\*

System	Defect	Orientation	Pyrolyzed		Graphitized	
			%V <sub>T</sub>	%V <sub>L</sub>	%V <sub>T</sub>	%V <sub>L</sub>
VYB 70 1/2 - SC1008	Small Void	Parallel	-2	-8	-15	0
		Perpendicular	+3		-20	
	Large Void	Parallel	-12	-10	-17	-7
		Perpendicular	-6		-25	
VYB 70 1/2 - Pitch	Small Void	Parallel	-7	-4	-11	+2
		Perpendicular	+7		+3	
	Lack of Wetting	Parallel	-17	-18	-14	+15
		Perpendicular	-7		-12	
Modmor II - Pitch	Small Void	Parallel	-14	-10	-14	+15
		Perpendicular	+5		+15	

\*Percentage change with respect to no-intentional-defect specimen velocity.



MOD III billet. The DACLOCK 120 and orthogonal composite materials were evaluated in the as-woven, impregnated and pyrolyzed, and graphitized conditions. The combination of nondestructive analysis techniques, ultrasonic attenuation and velocity and X-ray radiography, were able to detect the intentional discontinuities of interest (Table XVIII).

#### 5.2.1 DACLOCK 120 X-Ray Radiography

Low voltage X-ray radiographic techniques were applied to the as-woven D120 multidirectional fabric. The study included the selection of radiographic parameters to obtain satisfactory sensitivity and definition of weave detail. The voltage of the X-ray beam was varied to measure the lowest voltage (beam energy) consistent with practical operating times. The source-to-film distance was varied in an air atmosphere. In general, the greatest distance practical would be the best for maximum image sharpness but would be offset by increasing air scatter of the low energy end of the X-ray beam spectrum. It was found that image sharpness increased as distance increased from 24 to 29 inches (due to improving geometric sharpness), but with further increase in the distance, image sharpness was slightly reduced (due to increased air scatter).

Three types of film, Kodak R, M, and AA, were examined. The improvement in image definition using bare type R film was marginal. The type AA film resulted in inferior quality image definition. The selected parameters were 30kv, 29-inch film-to-focal spot distance, 10 ma, and 180 sec giving a film density of approximately 3.4 using Kodak Type M film.

Table XVIII

#### APPLICABILITY OF NONDESTRUCTIVE TEST TECHNIQUES FOR DACLOCK 120 PYROLYZED MULTIDIRECTIONAL COMPOSITE

Defect	Condition	X-ray	Ultrasonic	
			Attenuation	Velocity
Small Void	Pyrolyzed	Yes	Yes	Yes
Lack of Wetting	Pyrolyzed	No	Yes	Yes
Weave	Pyrolyzed	Yes	Yes	Yes <sup>(1)</sup>
	As Woven	Yes	---	---

(1) Detected due to higher porosity associated at weave defect.

A helium chamber was evaluated as a means of reducing the effects of radiation scatter (mainly film fogging and loss of contrast). The chamber was filled with helium gas to one atmosphere to replace the air between the X-ray source and the film. The scatter from helium is only 1.5 percent of that experienced with air. The results of these studies showed that improvement in image definition was negligible (Reference 1). The use of screens for the removal of low energy, air-scattered X-rays was evaluated. At the condition of 29 inches of air path for the beam, it was found that a sheet of polyethylene (0.008-inch thick), when placed directly over the sample, did effectively improve image sharpness and radiographic sensitivity (Reference 1).

The application of X-ray radiography to the as-woven multidirectional flat goods has shown that X-ray negative indications can be directly related to weaving irregularities present within the fabric. It has been demonstrated that this technique, when employed by a weaver, can greatly reduce the number and frequency of defects occurring (Reference 8). Specific X-ray radiographic indications were correlated to the actual irregularities by sectioning the woven fabric which had been cast in a clear resin, and visually observing the irregularities. These results are discussed in detail in Reference 1. Figure 53 shows the most pronounced weave irregularity found, broken yarns which protruded straight up through the fabric. These broken yarns appeared on the X-ray radiograph as large dark spots. Other broken yarns, which were shorter (and possible slanted), were not detected on the radiograph.

The X-ray radiographic analysis of the D120 fabric after the various processing steps (after the initial impregnation and pyrolysis steps, first graphitization, final impregnation and pyrolysis steps and again after the final graphitization) detected the weave defects which were initially observed in the as-woven condition and those areas which did not receive a thorough impregnation. It was not possible to detect the lack of wetting defect. The ability of the X-ray radiographic technique to detect areas of matrix nonuniformities provides a rapid in-process technique for monitoring the impregnation steps.

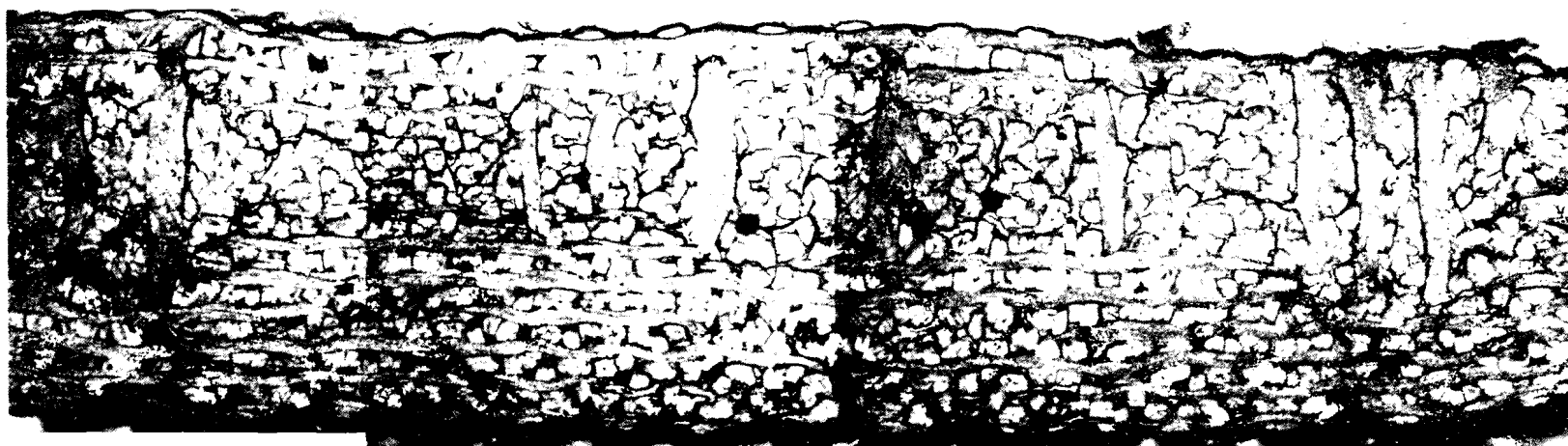
The X-ray radiographs after each processing step were very similar (Figure 54); however, as the density of the composite panels increased the ability to identify the weave defects became more difficult. This was particularly true of the no-intentional-defect specimens which received the full processing sequence and had the highest density.

To determine the sensitivity of the X-ray technique, a slotted standard (previously described) was machined from the no-intentional-defect multidirectional composites after the final pyrolysis. The sensitivity was 0.8 percent (ability to detect a .004-inch defect in .50-inch thick material) with the following exposure parameters:

Voltage: 27kv  
Film to Focal Spot Distance: 29 in.  
Current: 10 ma  
Time: 180 secs  
Screen: .008 in polyethylene

A

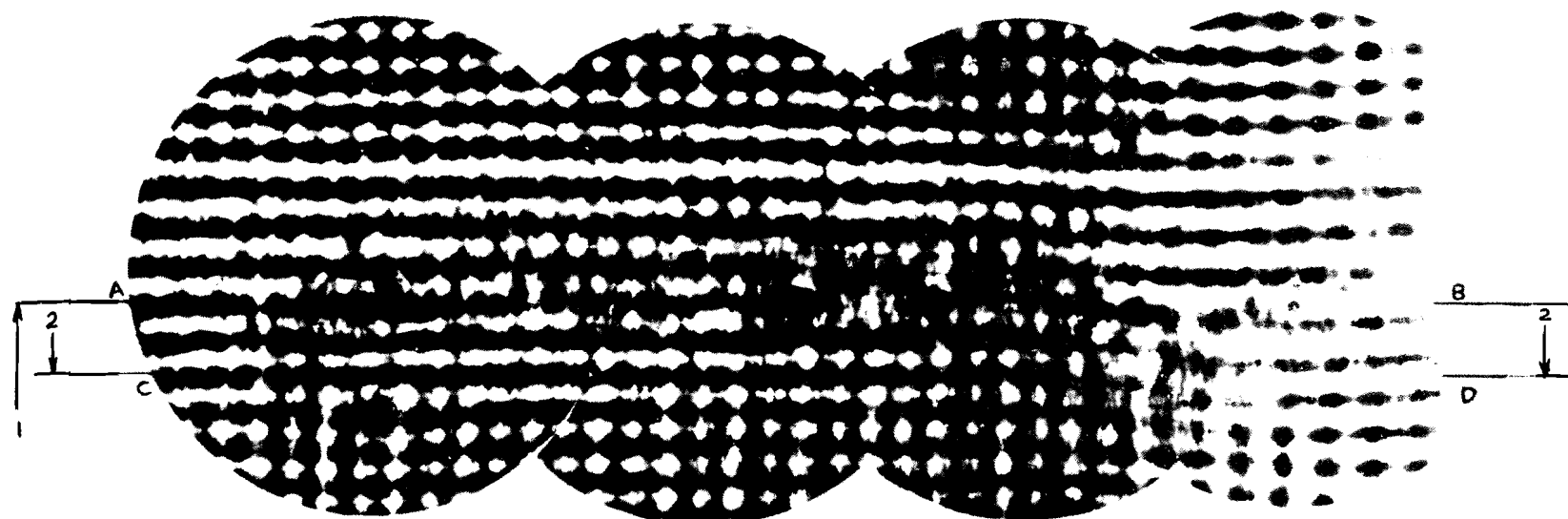
B



5X

Irregularity - broken weaving warps

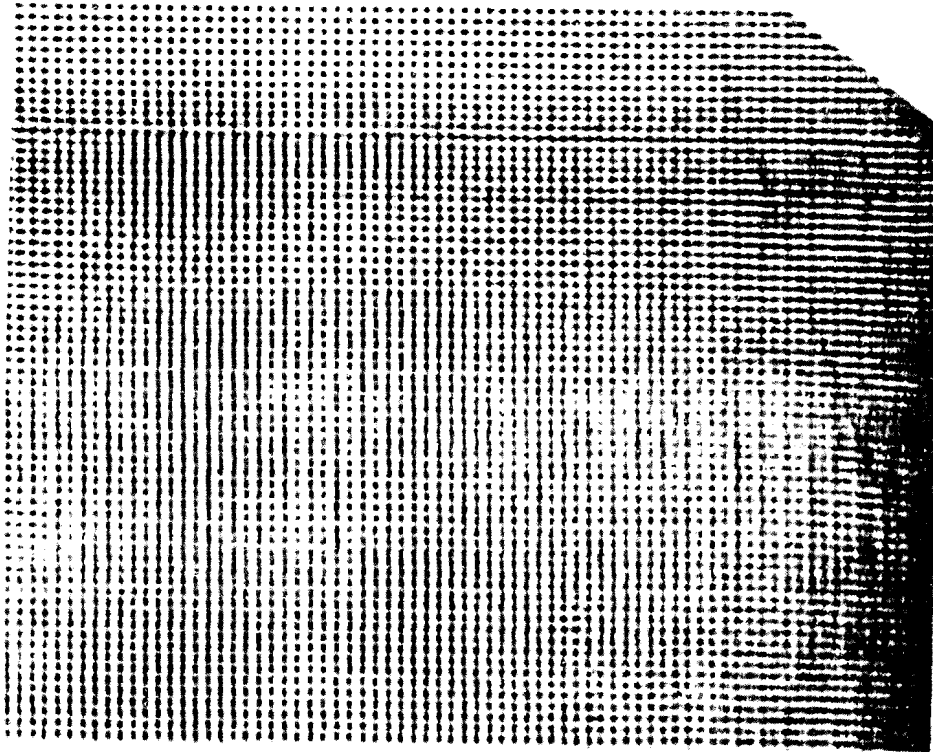
96



Radiograph Appearance - wide band in fill direction

Figure 53. Photomicrograph and X-ray Radiograph of DACLOCK 120 As-woven Fabric

as-received



Pyrolyzed

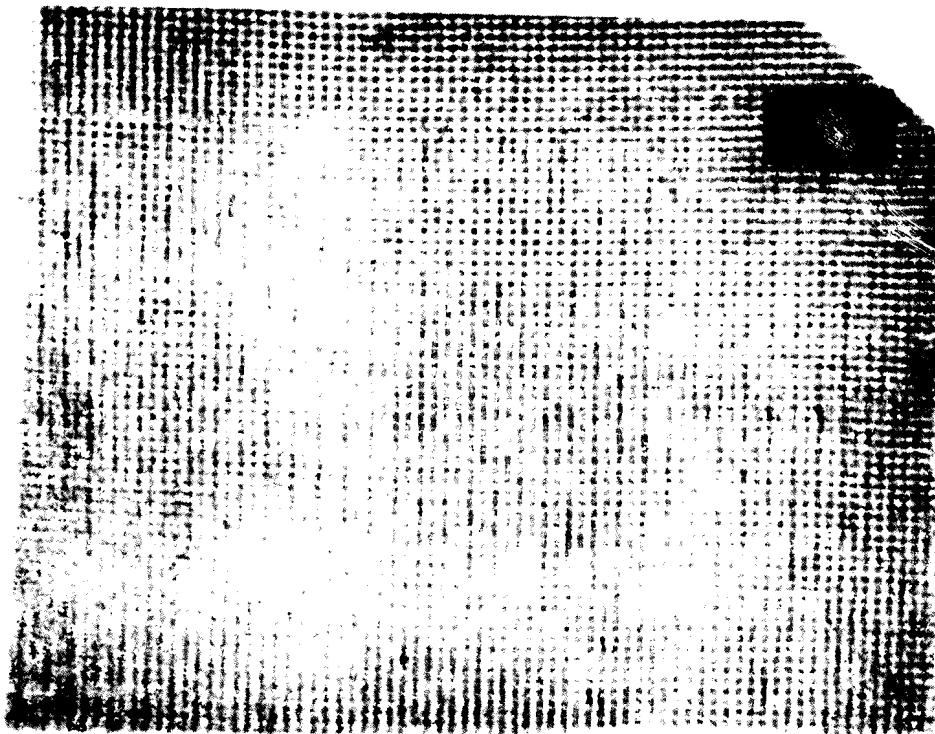


Figure 54. Positive Prints of X-Ray Radiographs of Specimen 98-7 Multidirectional DACLOCK 120 Before and After Three Impregnations and Pyrolysis (Dark areas represent higher density)

### Ultrasonic Velocity

The ultrasonic longitudinal velocities measured by the through-transmission technique on the pyrolyzed and graphitized DACLOCK 120 are summarized in Figure 55. The velocity measurements were made at 0.8 MHz for the pyrolyzed and 0.5 MHz for the graphitized composite. The velocity measurements on the pyrolyzed composites containing intentional defects were less than the no-intentional-defect specimens. The velocity measurements were reduced by 19 percent, 19 percent, and 17 percent for the small void, lack of wetting and weave defects. Upon graphitization, the velocity of the no-intentional-defect specimens decreased by 28 percent. As in the unidirectional composites, this decrease in velocity was attributed to the higher porosity of the graphitized composite.

The bulk density as measured by water immersion was related to the measured ultrasonic longitudinal velocity (Figure 56). The data indicated a trend of higher velocity corresponding to higher density. A plot of porosity as measured by mercury porosimetry versus velocity yielded similar results, higher velocity corresponding to lower porosity. These results strongly suggest the use of ultrasonic longitudinal velocity measurements for the selection or screening of material having density variability.

The ultrasonic longitudinal velocity through the thickness direction was also measured as a function of frequency for the pyrolyzed DACLOCK 120 composite. As in the unidirectional composites, a frequency dependence existed (Figure 57). The figure shows an increase in velocity of approximately 7 percent for all specimens over the 0.2 to 0.5 MHz range. Measurements could not be made at higher frequencies due to the attenuation present. The selection of an operating frequency over this frequency range was not as critical as in the unidirectional composites.

### Ultrasonic Attenuation

Ultrasonic attenuation measurements were made on the multidirectional composites after the initial and final impregnation and pyrolysis cycles and after the final graphitization. After the initial graphitization step, the composites possessed an extremely high attenuation which prohibited C-scan mapping. The attenuation of the pyrolyzed multidirectional composites were greater for the defect containing specimens as compared to the no-intentional defect specimens (Table XIX). As with the unidirectional composites the attenuation of the pyrolyzed composites increased with increasing total porosity (Figure 58).

A typical through-transmission attenuation C-scan map is shown in Figure 59. The map displays areas of higher attenuation (dark areas) which are distributed throughout the panels.

The limit of detectability or defect sensitivity of the through-transmission attenuation technique was determined for the pyrolyzed multidirectional D120 composite. Several holes, ranging in diameter from 0.1 to 0.2 inches and depth from 0.1 to 0.3 inches, were drilled in a 0.4-inch thick standard. Various transducer combinations and operating frequencies were used in C-scan mapping this standard (Table XX). The resulting maps indicated that a 0.5 MHz focused

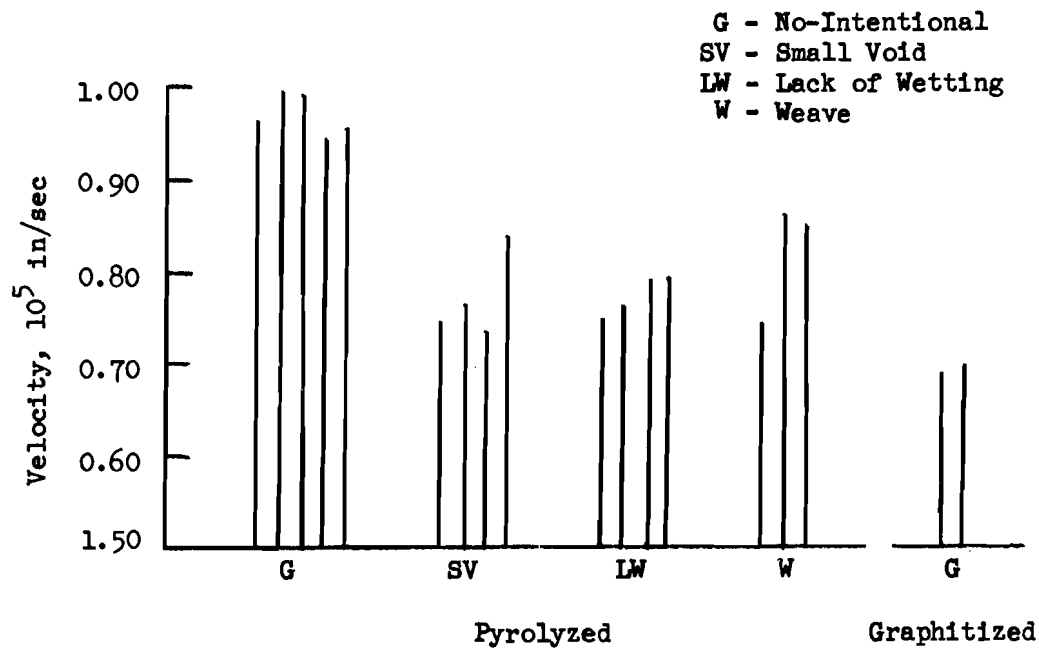


Figure 55. Ultrasonic Longitudinal Velocity of Pyrolyzed and Graphitized DACLOCK 120 Multidirectional Composite

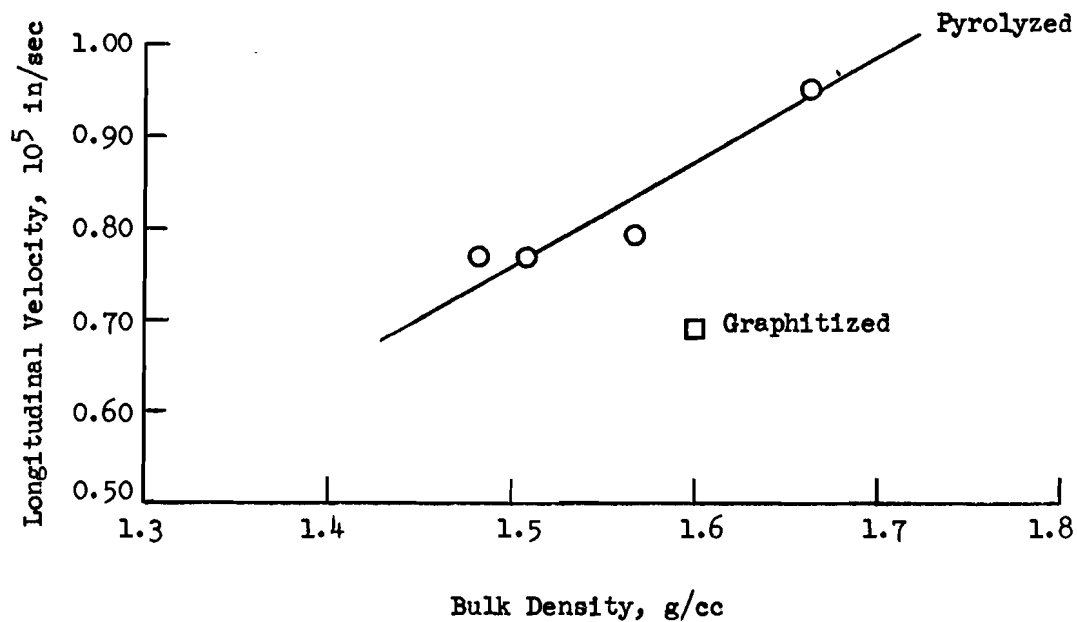


Figure 56. Ultrasonic Longitudinal Velocity Versus Bulk Density of DACLOCK 120 Multidirectional Composite

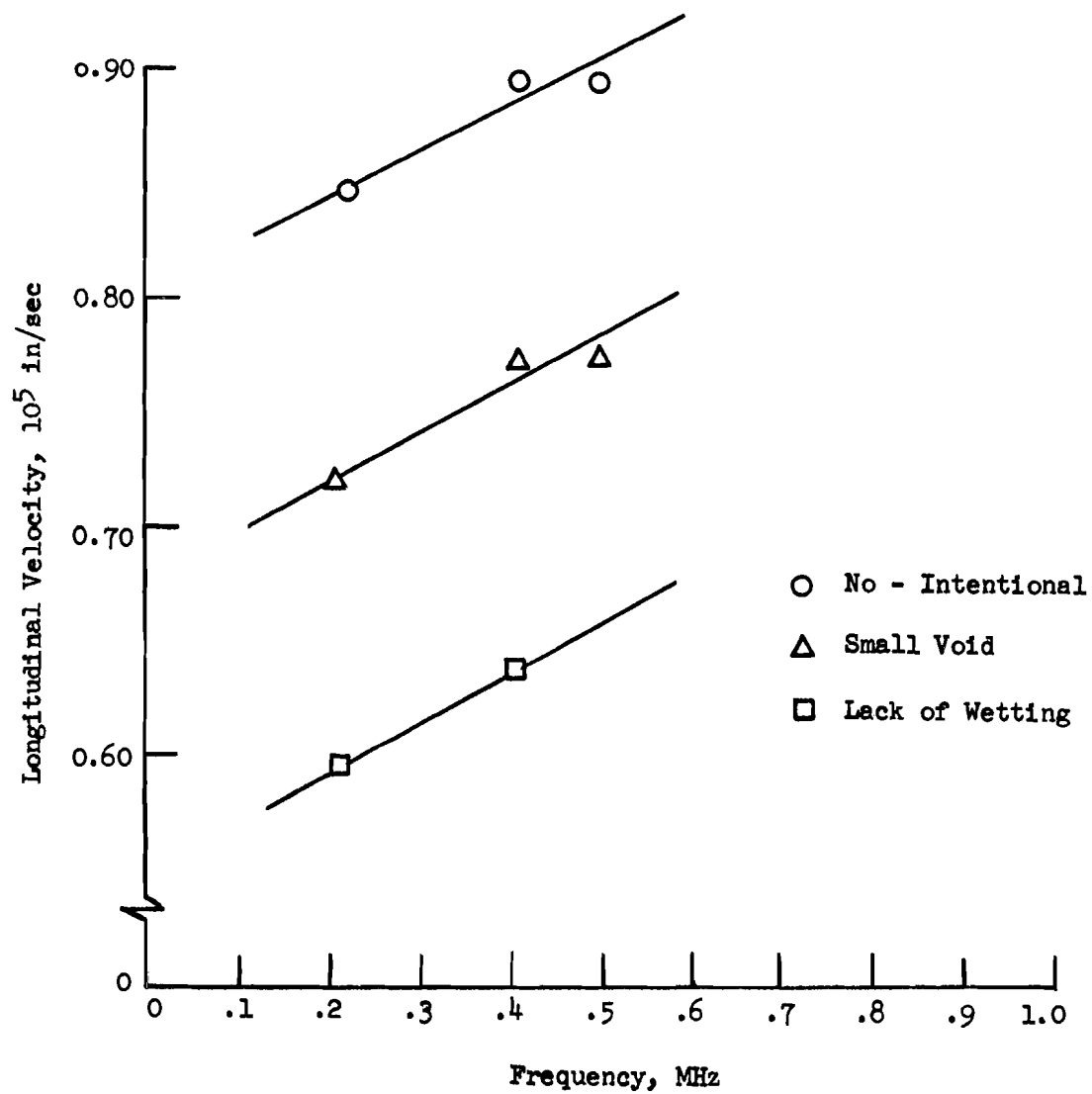


Figure 57. Frequency Dependence of Longitudinal Velocity for Pyrolyzed DACLOCK 120 Multidirectional Composite

Table XIX

## ATTENUATION OF DACLOCK 120 MULTIDIRECTIONAL COMPOSITES

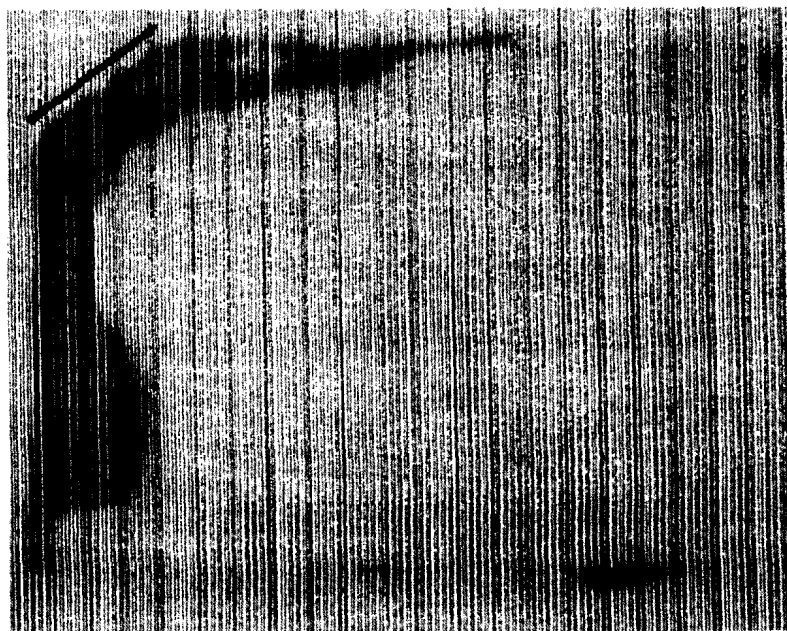
Specimen	Condition	Defect	Attenuation (db/in)
71	Pyrolyzed	No-Intentional	92
72			96
73			96
74			87
75			96(93) <sup>(1)</sup>
67	Pyrolyzed	Small Void	110
68			124
69			115
70			111(115)
60	Pyrolyzed	Lack of Wetting	118
61			124
62			114
63			116(118)
64	Pyrolyzed	Weave	108
65			102
66			115(118)
72	Graphitized	No-Intentional	92
75			74(83)

(1) Average value





36 db



41 db

Figure 58. Through Transmission C-Scan Map at 0.5 MHz of Multidirectional DACLOCK 120 Specimen 98-7 After Three Impregnations and Pyrolysis

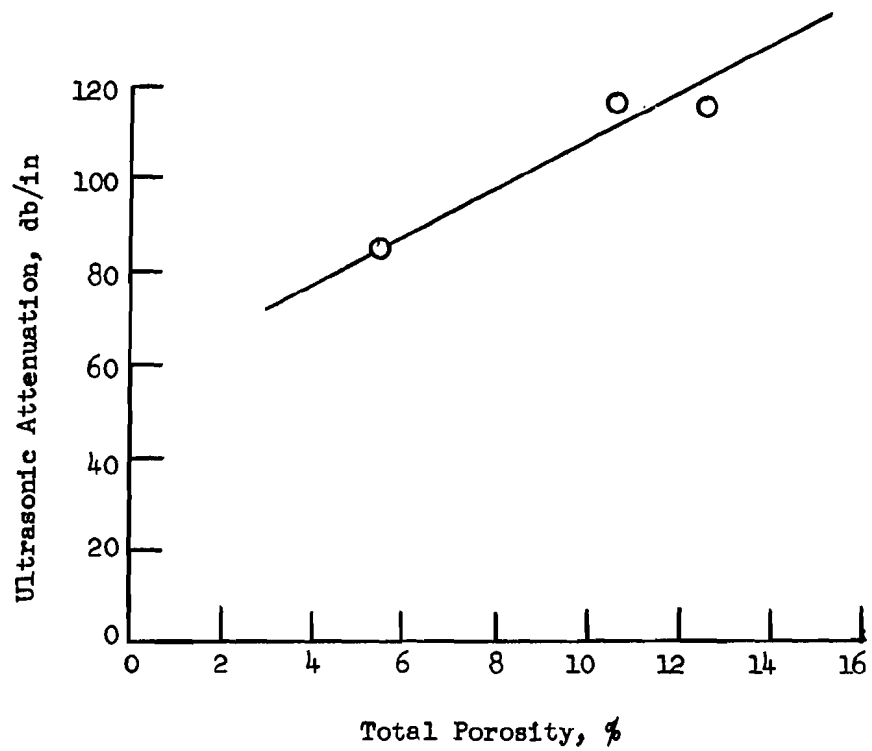


Figure 59. Attenuation Versus Total Porosity for  
DACLOCK 120 Composite

Table XX

TRANSDUCER COMBINATION FOR THROUGH-TRANSMISSION  
ATTENUATION EVALUATION

Combination Number	Transmitter	Receiver
1	Focused (3-inch) PZT-5 1.0 MHz 1-inch Diameter Focal Point .4" below Top Surface	Flat Collimated 1.0 MHz 3/4-inch Diameter
2	Focused (3-inch) PZT-5 1.0 MHz 1-inch Diameter Focal Point .3" below Top Surface	Flat Collimated 1.0 MHz 3/4-inch Diameter
3	Focused (3-inch) PZT-5 0.5 MHz 1-inch Diameter Focal Point .25" below Top Surface	Flat Collimated 0.5 MHz 3/4-inch Diameter
4	Focused (3-inch) PZT-5 0.5 MHz 1-inch Diameter Focal Point .25" below Top Surface	Flat 0.5 MHz 3/4-inch Diameter
5	Focused (3-inch) PZT-5 0.5 MHz 1-inch Diameter Focal Point .25" below Top Surface	Flat 1.0 MHz 3/4-inch Diameter

transmitter - 0.5 MHz collimated receiver combination provided the best defect detection. The smallest defect (hole) detected was a 0.2-inch diameter, 0.2-inch deep hole. This sensitivity was significantly lower than the unidirectional composites (sensitivity was 0.032-inch diameter hole for the VYB 70 1/2 - SC1008 and 0.064-inch diameter hole for the VYB 70 1/2 - pitch). This indicates the drastic effect of material thickness and weave geometry on defect sensitivity.

The pulse-echo technique operating at 0.5 or 1.0 MHz was not capable of providing any useful information on these coarse weave composite samples. In a subsequent section the pulse-echo technique will be shown to be useful for evaluating fine weave-high density carbon-carbon composites, the AVCO Mod III material.

### 5.2.2 Orthogonal Composite

The one-inch thick orthogonally woven flat fabric was evaluated by the X-ray radiographic and attenuation and pulse-echo C-scan techniques after the initial impregnation and pyrolysis cycles, graphitization, and the final impregnation and pyrolysis cycles. This material was fabricated without intentional defects to determine the applicability of the NDT techniques to thicker multidirectional composites. The X-ray radiographs were similar after each processing step, detecting a low density area between the yarns over a portion of the specimen. The radiographs were also similar to the as-woven condition in that the same weave defects were detected.

The sensitivity of the X-ray technique was determined to be approximately 2.0 percent for the 1.0 inch thick (.020 inch defect in a 1.0 inch thick material) composite using a slotted X-ray standard. The increase in material caused a substantial decrease in sensitivity.

Ultrasonic attenuation C-scan maps were made at 0.5 MHz on the one-inch thick orthogonal flat goods. The attenuation maps were similar after the three processing cycles. The maps indicated higher attenuating areas in the center of the specimen. After the final impregnation and pyrolysis cycles the center area had an attenuation greater than 33 db/in while the outer portions of the specimen had an attenuation of approximately 29 db/in (Figure 60).

An orthogonal one-inch thick standard containing artificial defects was evaluated by the attenuation and pulse-echo techniques. Two different size flat bottom holes, 0.388 and 0.250-inch diameter at 0.450 inches from the surface, were evaluated. Using a 0.5 MHz focus (3 inch focal length) transmitter with 0.2 MHz flat receiver, the 0.388 inch diameter hole was detected. A number of areas within the composite were highly attenuating and some equally as high as the 0.388 inch hole (Figure 61). The pulse-echo technique applied to this coarse weave composite was not capable of detecting either defect. Actually it was not possible to receive any interpretable reflected signal from the material.

### 5.2.3 AVCO MOD III Composites

The Air Force Materials Laboratory submitted two samples of AVCO Mod III carbon-carbon composite for nondestructive evaluation. These billets, 4 x 4 x 7 inches, provided the opportunity to apply the nondestructive techniques used in this

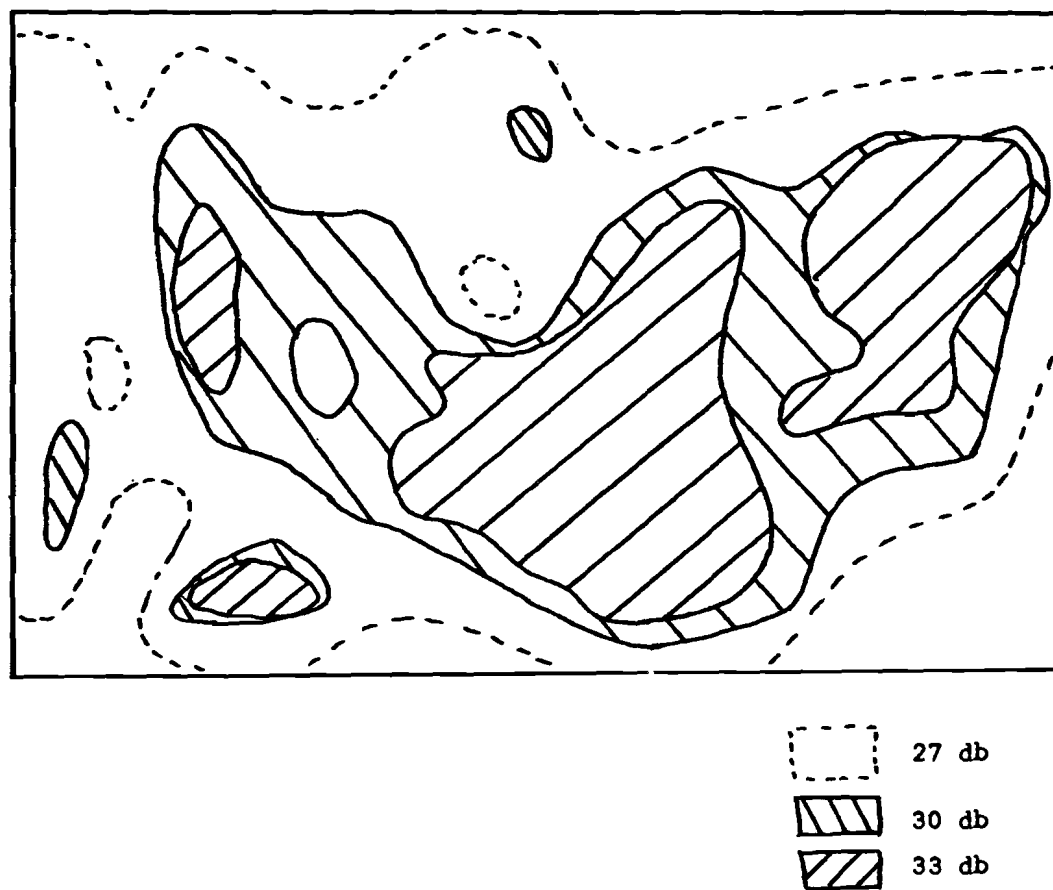
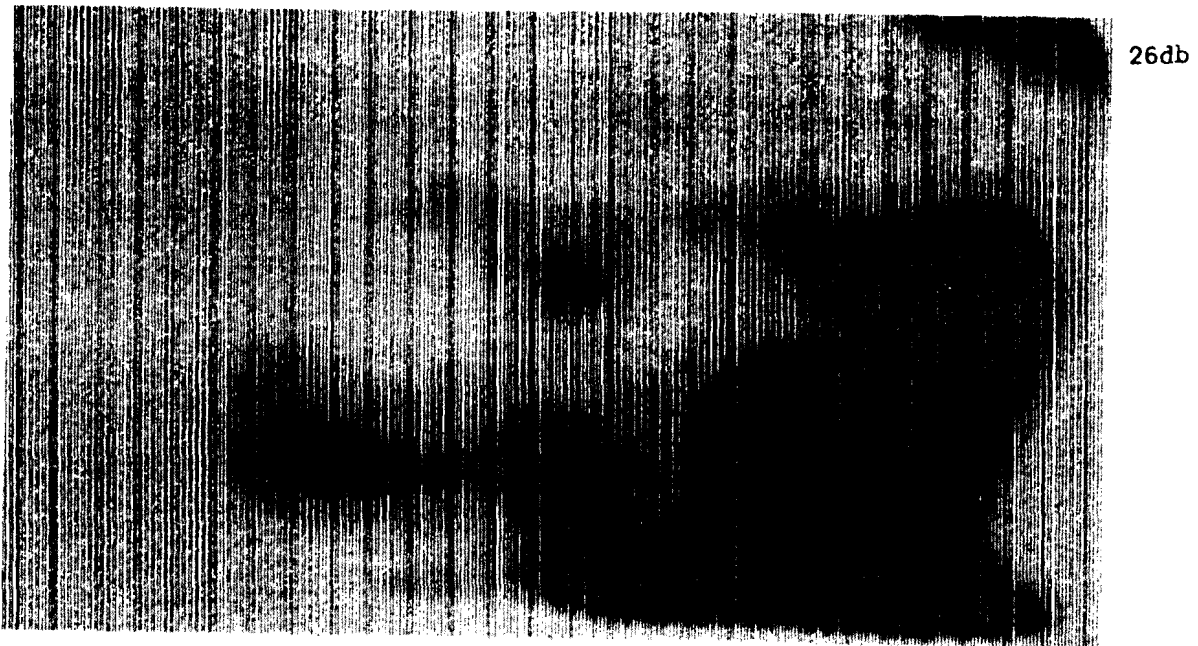


Figure 60. Sketch of Attenuation C-Scan Maps of Orthogonal Composite



0.388-Inch Hole

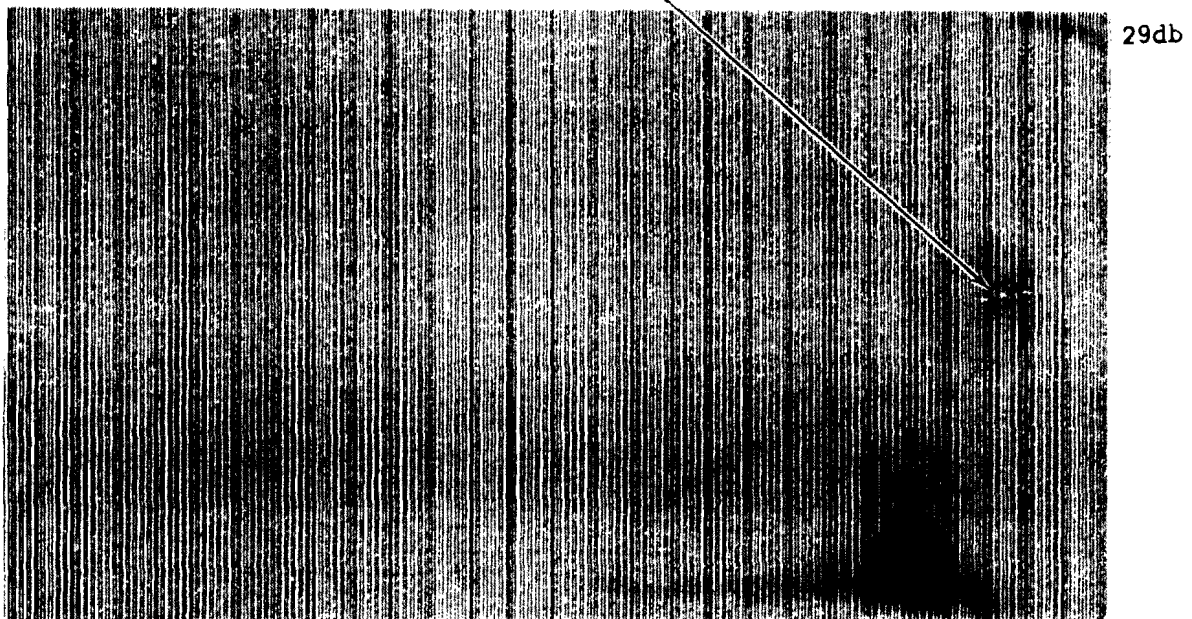


Figure 61. Ultrasonic Through Transmission Attenuation C-Scan Map of 1.00 inch Thick Orthogonally Woven Multidirectional Composite with Intentional Defects Present (Dark areas more attenuating).

program to a fine weave, thick (4-inch) composite. The results of this evaluation demonstrated the usefulness and applicability of the nondestructive techniques for providing detailed information on material uniformity and discrete discontinuities.

X-ray radiographs were taken of all three views using the following parameters:

Thickness view

- 80 kv-voltage
- 5 ma-current
- 36 inches-source to film distance
- 30 sec-time
- Type M film

Length view

- 100 kv-voltage
- 10 ma-current
- 36 inches-source to film distance
- 60 sec-time
- Type M film

The X-ray radiographs revealed a film density variability across the thickness direction of approximately 20 to 29 percent for billets 715 and 709 respectively. The bulk density (weight-scalar) of these billets were 1.62 g/cc and 1.59 g/cc for 715 and 709. It was not permitted to extract samples from the billets to determine the actual values of density (or porosity) fluctuations which would be related to the film density differences. The fluctuations indicated that higher material density existed at the edges which decreased on approaching the center. The radiographs also revealed a number of line irregularities across the thickness direction of both billets (Figure 62).

The ultrasonic through-transmission attenuation maps were made using a 3.125-inch diameter, 1.0 MHz focused transmitter having a 10.5 inch focal length with a .375 inch diameter, 1.0 MHz flat receiver. The transducer was positioned so that the focal point was located at a depth of 1.6 inches below the top surface. The typical through-transmission map of a billet showing material nonuniformities is shown in Figure 63. The dark areas in the C-scan map refer to higher attenuating areas, larger amount of scattering from anomalous areas within the material. The C-scan maps of opposite sides of the same specimens were similar. The wide strip of higher attenuation in the figure corresponded to the area of line irregularities in the X-ray radiograph of the billet. The higher attenuating areas along the edges of the billet are due to sound beam scattering from the irregular corners of the billet.

The ultrasonic attenuation values measured by this immersed through-transmission technique were between 12 and 18 db/in. This low value for attenuation made it feasible to apply the pulse-echo technique. The finer weave higher density composites as the AVCO Mod III composite may be evaluated with the pulse-echo technique even though the coarser weave, lower density composites could not. Using a 1.0 MHz flat, .750-inch diameter transducer, pulse-echo maps were made of each side. A typical map is shown in Figure 64. Since a flat bottom hole could not be drilled into the billets, a standard was sought

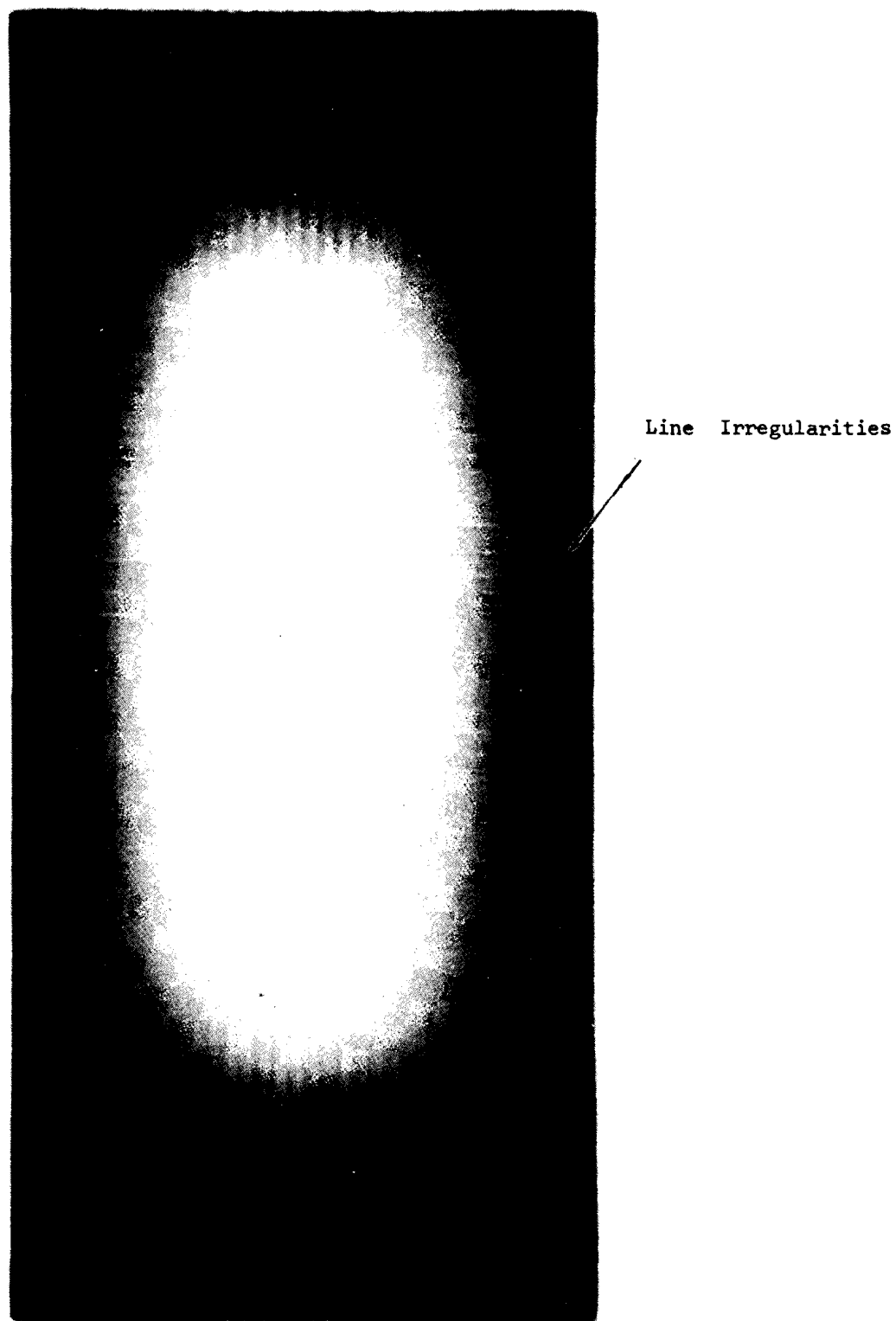


Figure 62. Positive Print of X-Ray Radiograph of AVCO Mod III  
Billet 715



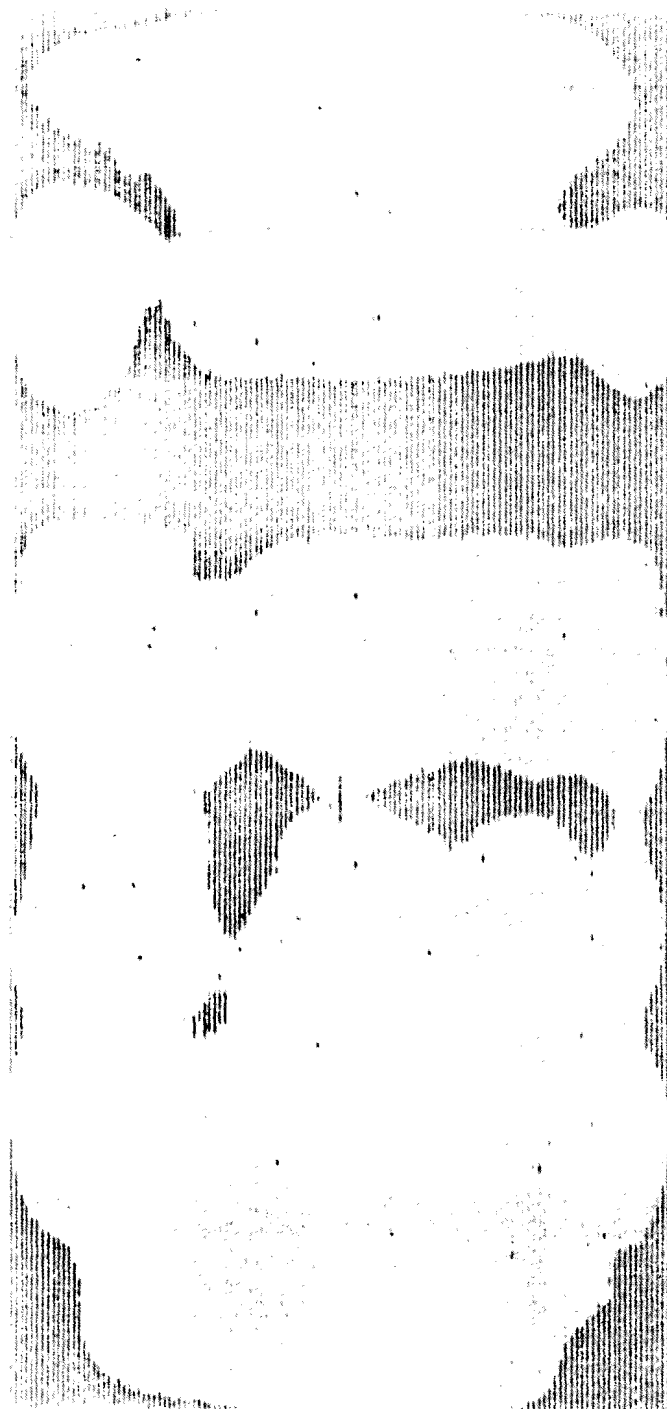


Figure 63. Ultrasonic Through-Transmission Attenuation Map of Billet 709 Through View B (Recording level 65 db or 16 db/in).

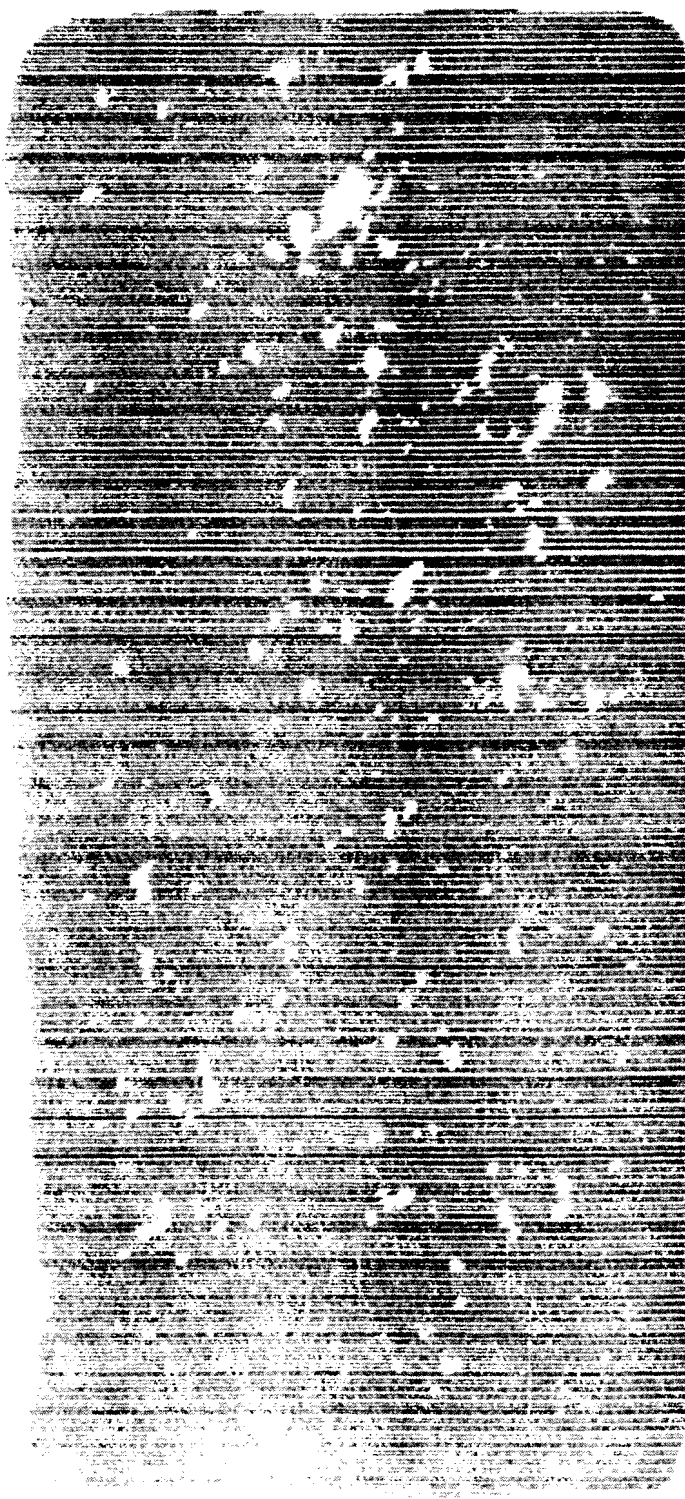


Figure 64. Positive Print of Pulse-Echo C-Scan Map of Billet 715

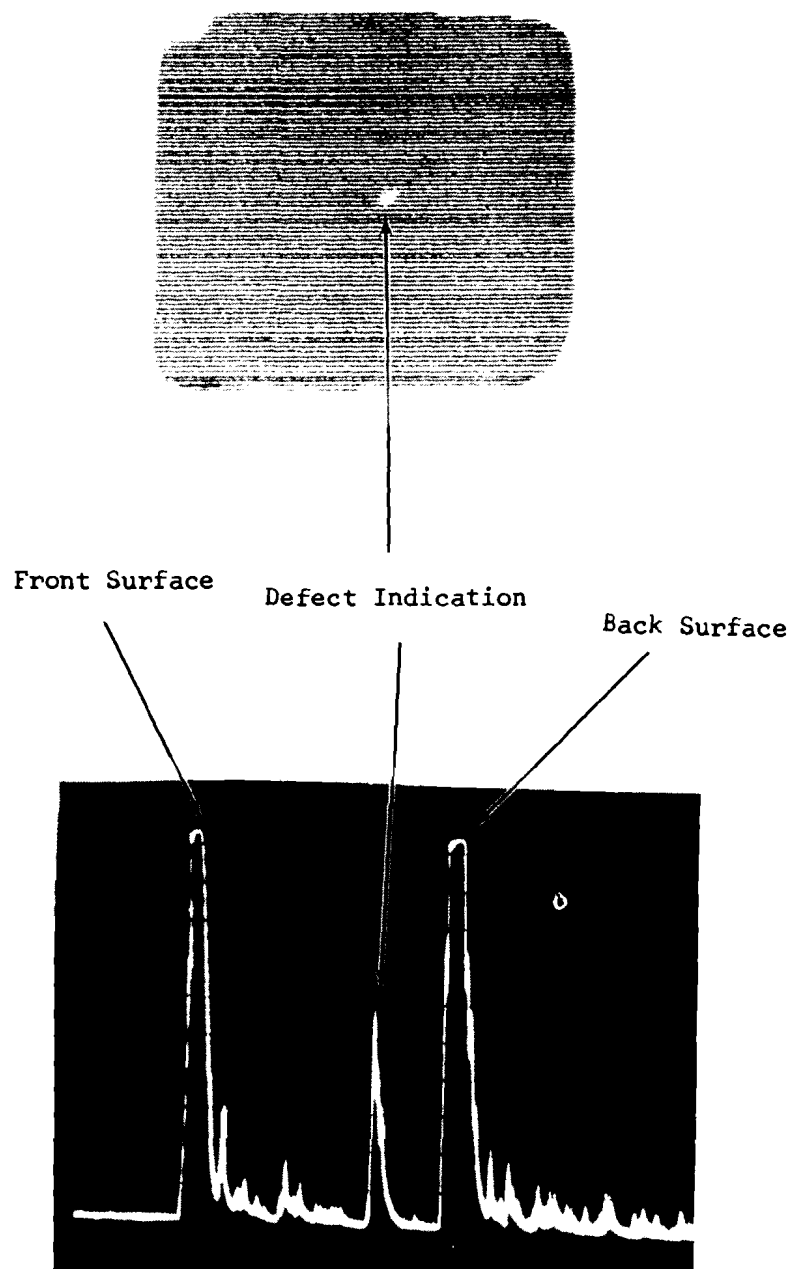


Figure 65. Pulse-Echo Test Standard ATJ-S Graphite C-Scan Map and A-Scan of 1/16" Flat Bottom Hole

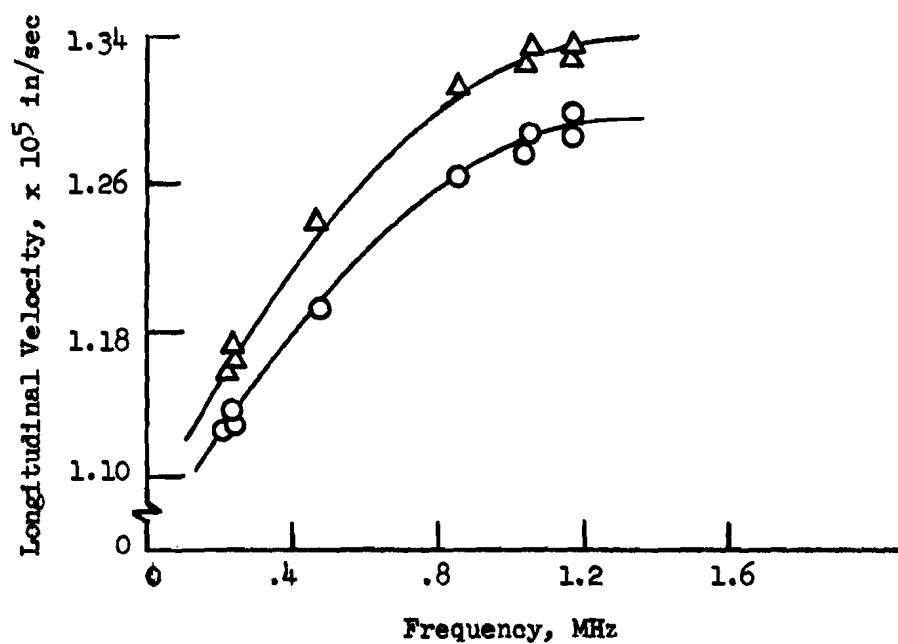


Figure 66. Graph of Ultrasonic Longitudinal Velocity versus Frequency for AVCO Mod III Multi-directional Carbon-Carbon Composite

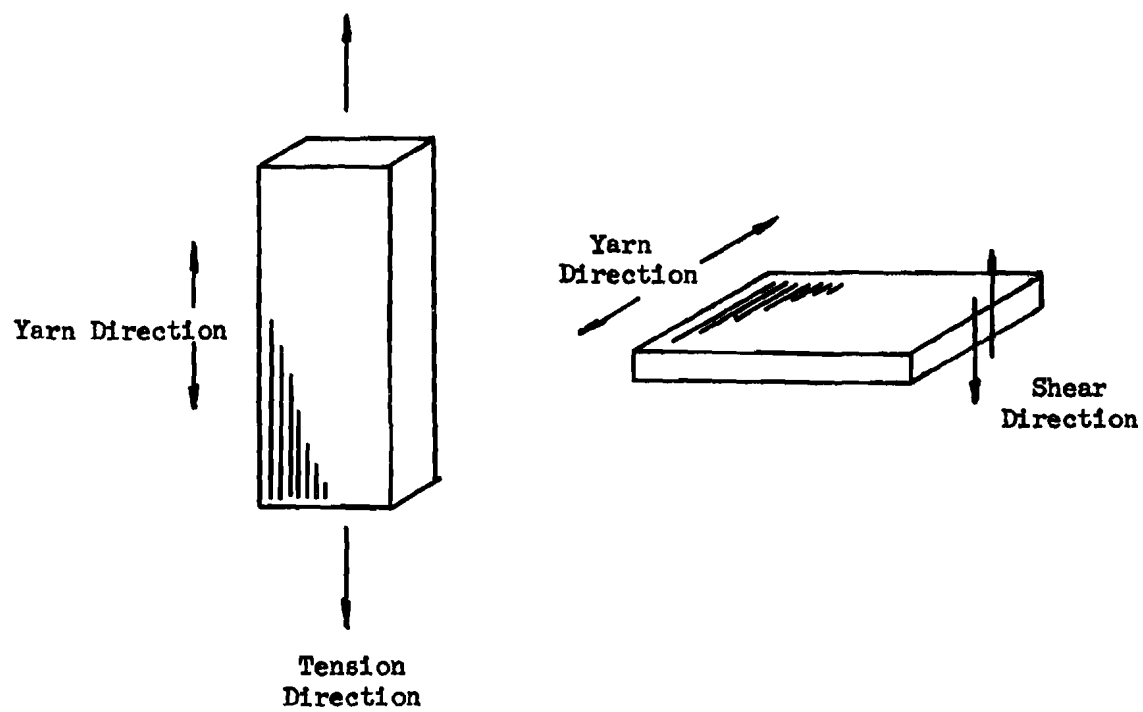


Figure 67. Stress Directions for Mechanical Testing of Unidirectional Composites

data was also taken on the mechanical test specimens to characterize the uniformity of the specimen with respect to the defect of interest. This data was then compared to the mechanical test results to determine what relationships existed.

## 6.1 Unidirectional Composites

### 6.1.1 Uniaxial Tension Test Techniques

Efforts have been devoted to establishing appropriate tension test techniques. The techniques being evaluated reflected a departure from standard mechanical test practice for unidirectional composites because of constraints imposed by the dimensions of the available material samples. The resulting tension measurements were expected to be adequate to judge the severity of flaws and for comparison of the different material systems. The material samples from which the tension specimens were excised permitted a maximum specimen length of 3.0 inches. The thickness of the panels was approximately 0.10 inch and the width of the tension specimens was limited to approximately 3/8 inch.

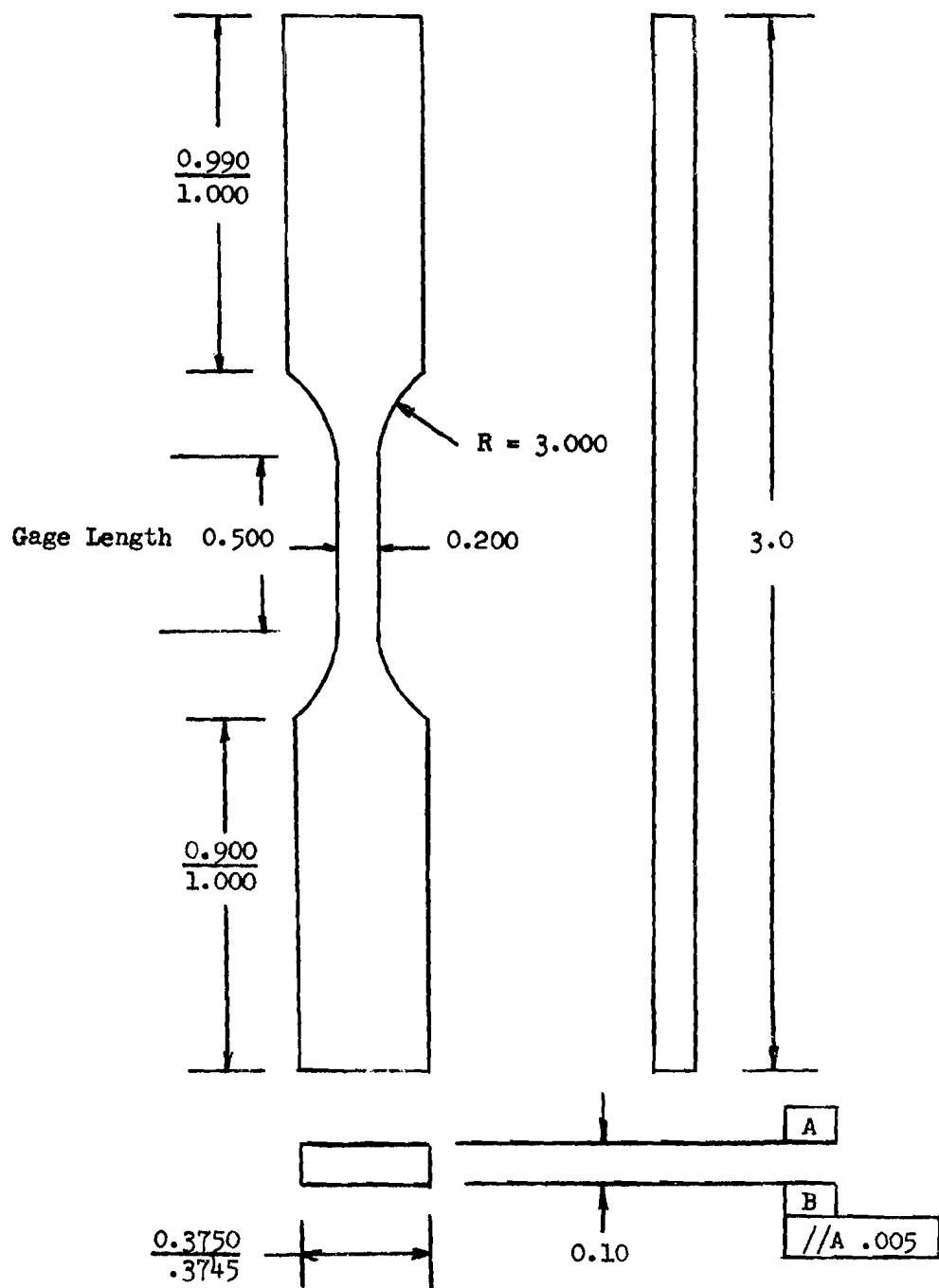
The principal problem associated with tension testing of unidirectional composites was that of introducing the load to the gage section in a manner that resulted in uniform stress without the presence of stress concentrations, which may cause premature failure outside the gage section. The problem of load introduction was made more difficult by the limitation on the length of the specimen.

Load may be introduced by shear tractions at the surfaces of the specimen ends either by friction-gripping or via bonded doublers. The doublers might be loaded by friction, pins, or other means. Friction loading was eliminated from further consideration because measurements on typical composite samples showed the transverse crushing strength to be too low (Reference 1).

The use of pin-loaded bonded doublers was first investigated by applying the technique to tension tests of Poco AXF 5Q grade bulk graphite specimens which were sized to conform to the carbon-carbon samples. The specimen configuration is shown in Figure 68. The pin-loaded doublers, which were aligned using the special bonding fixture (Figure 69), provided adequate load alignment. The results were encouraging in that the measured strengths (Table XXI) were in the range of data obtained with larger standard specimens of the same material tested with a rigid fixturing system. A 1/2-inch extensometer was used, and the test run at a crosshead rate of 0.02 in/min. The average tensile strength, 7240 psi, for the bonded doubler graphite specimens was within 6 percent of the average tensile strength of 7700 psi, for a standard tension specimen.

The same specimen/doubler configuration was then used to test specimens of unidirectional VYB 70 1/2 - coal tar pitch composite. The tension test results are given in Table XXII. The stress-strain curves for all the specimens were linear to failure. Examination of the fractured specimens (Figure 70) shows that failure appears to be associated with the tangent point region where the fillet radius meets the gage section.

Next, some strip-style specimens (with no reduced section) excised from the same batch of VYB 70 1/2 composite panels were tested using the same doubler installation. Figure 71 shows the failed specimens; failure now seemed to



All Dimensions in Inches

Figure 68. Dogbone Specimen Configuration

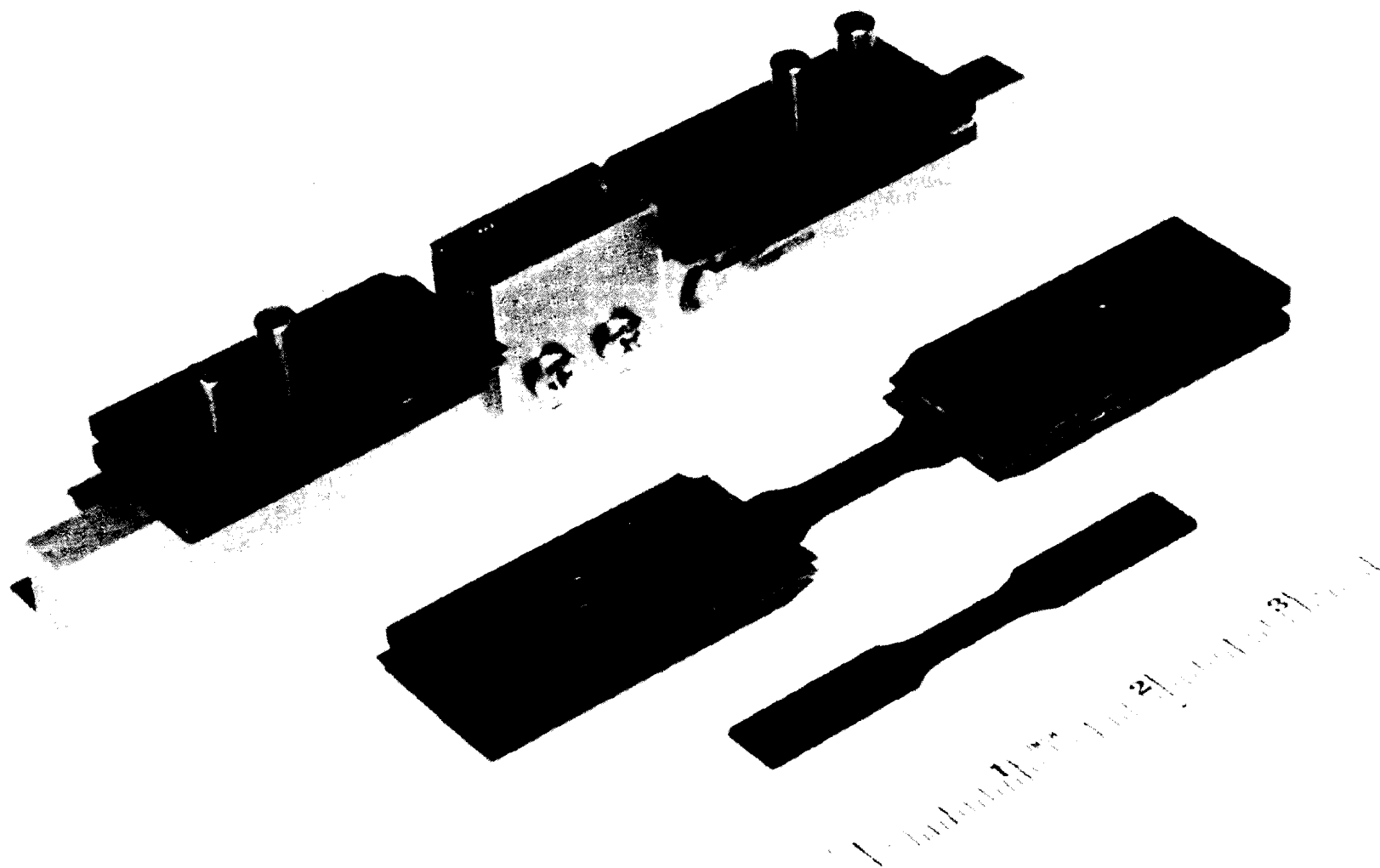


Figure 69. Specially Designed Assembly Fixture for the Bonding of Test Specimens and Doublers



Table XXI

TENSION TEST RESULTS OF POCO AXF-5Q GRAPHITE BONDED-DOUBLER SPECIMENS

Specimen	Area (in <sup>2</sup> )	Maximum Load (lb)	Maximum Stress at Failure (psi)	Total Strain at Failure (in/in)	Modulus (10 <sup>6</sup> psi)	Remarks
1	0.01755	121	6900	.0061	2.25	Large pore on fracture surface
2	0.01745	130	7450	.0063	2.15	
3	0.01761	130	7380	.0065	1.87	Failed at doubler- lack of adhesive

Table XXII

MECHANICAL TEST RESULTS OF UNIDIRECTIONAL  
VYB 70 1/2 - PITCH COMPOSITE, BATCH No. 8

Specimen Type	Specimen Number	Ultimate Tensile Strength, Ksi	Strain to Failure, percent	Young's Modulus 10 <sup>6</sup> psi
Dogbone Tensile	8B2	10.5	0.14	7.14
	8A2	12.7	0.29	4.25
	8A1	16.3	0.28	5.44
Strip Tensile	8A3	19.0	no data	no data
	8A4	18.3	0.42	4.60
	8C1	17.2	0.40	4.63
4-pt Flexure	8C1	25.6	no data	no data
	8C2	27.1	no data	no data
	8C3	27.6	no data	no data

Table XXIII

MECHANICAL TEST RESULTS FOR PYROLYZED  
VYB 70 1/2 - SC1008 COMPOSITE

Specimen Type	Specimen Number	Ultimate Tensile Strength, Ksi	Strain to Failure, percent	Young's Modulus 10 <sup>6</sup> psi
Strip	14D3	11.0	.15	7.3
	14D1	11.6	.25	4.6
Dogbone Thickness	14C4	13.5	.27	5.0
	14C5	13.7	.17	5.9

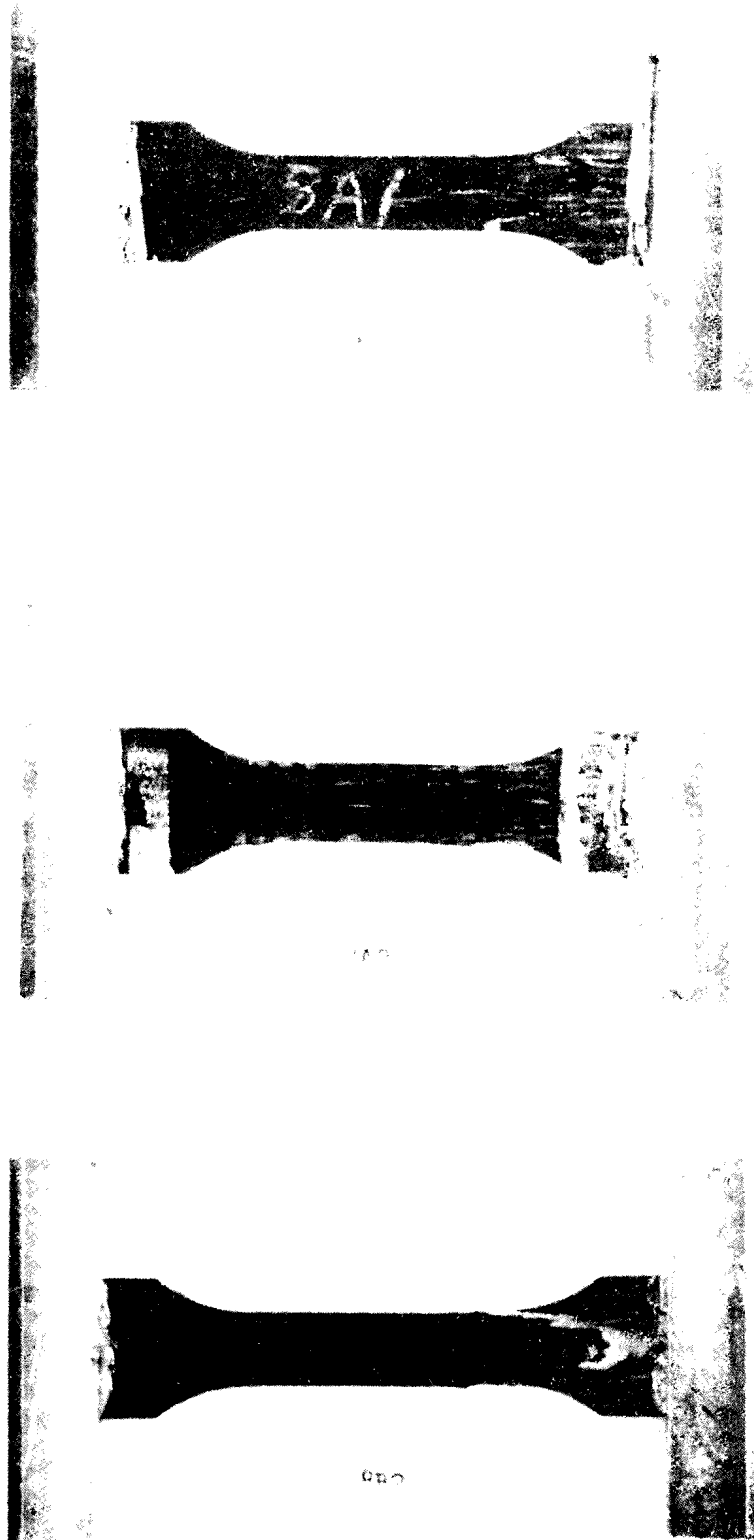
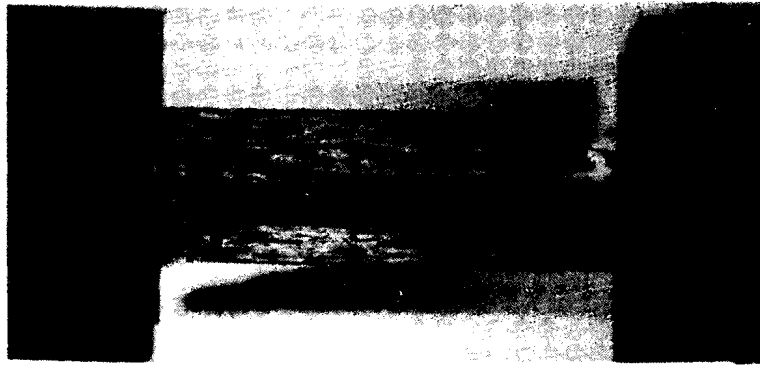


Figure 70. Photomacrographs of Pyrolyzed VYB 70 1/2-Coal Tar Pitch Composite Specimens after Tensile Testing (2X)



Specimen 8A4



Specimen 8A3



Specimen 8C1

2X

Figure 71. Posttest Photographs of Strip Tension Specimens of Unidirectional Composite

be associated with the stress concentrations occurring in the vicinity of the doublers. However, as Table XXII shows, the measured strengths were significantly higher for the strip specimens than for the reduced-section dogbone-style specimens. This implies that "dogboning" by reducing the gage section width imposes a more severe stress concentration than was caused by the doublers.

To give a rough measure of the "true" tensile strength of the composite, additional specimens excised from the same batch of VYB 70 1/2 composite were tested in flexure. Since the load introduction problems with the flexure test minor, the measured flexural strength for brittle materials, and for most composites, is usually higher than the tensile strength measured by the best available tension techniques.

The flexure results are also given in Table XXII. It is seen that the flexural strength is approximately 40 percent higher than the strength measured for the strip specimens. In addition to the aforementioned problems with load introduction in the tension test, which gave rise to stress concentrations of unknown magnitude, there are a number of other factors which may account for the increase in flexural strength over tensile strength:

1. Volume Effects

Statistical strength theory (e.g., the Weibull approach) predicts lower strength for large volumes of stressed material. The highly stressed volume in the flexure test is smaller than in a uniaxial tension test; therefore, one might expect higher strength results from the flexure test.

2. Frictional Restraint

In the flexure test, friction between the specimen and the loading points introduces a bending moment which opposes the applied loading. Thus, the actual net moment applied to the specimen may be less than that calculated from the vertical loads and point spacing by an amount which may range from one to ten percent (depending on the effective coefficient of friction) for the configuration tested.

3. Nonlinear Stress-Strain Response

The flexural strength is calculated on the assumption that the stress-strain curve is linear. A typical stress-strain curve measured for a strip specimen showed a slight departure from linearity observed near failure which would result in the calculated flexural strength being a few percent higher than the true stress at failure.

In view of these considerations it was believed that the tensile strength measured using the strip specimen was probably close to the maximum obtainable with specimens that conform to the dimensional limitations imposed by the available material samples. However, further modifications to the specimen design were studied since failure under the grip is an indication of premature fracture from specimen design.

Initial tension testing of the pyrolyzed VYB 70 1/2 - SC1008 composites involved the strip tensile specimen design. This design was unsatisfactory since failure occurred at the doublers. At this point, the specimen configuration was changed to a dogbone specimen reduced in the thickness direction as shown in Figure 72. This design combines the features of strip specimen with the advantage of a reduced gage section. By reducing the thickness rather than the width, it was possible to use a large fillet radius that reduced the stress concentration at the fillet. Failed tensile specimens using this current design are shown in Figure 73. Failure occurred in the center of the gage section in all cases. This specimen design also resulted in higher strength values as shown in Table XXIII. The doubler material selected was aluminum, rather than steel as previously used, so that a closer matching of transverse moduli between the specimen and the doubler could be provided.

#### 6.1.2 Shear Test Technique

Shear tests were conducted in a "double shear" fixture similar to the Johnson-type shear test of Method 1041, Federal Test Method Standard No. 4060. The fixture is schematically indicated in Figure 74. The specimens were approximately 1.5 inches long, 0.375-inches wide, and 0.08 to 0.13-inches thick. Loads were applied by an Instron machine operating at 0.05 in/min crosshead speed. Load was recorded as a function of time during each test. The shear strength was calculated according to the relation:

$$\tau = \frac{P}{2wt}$$

Where

P = maximum recorded load  
w = specimen width  
t = specimen thickness

#### 6.1.3 Mechanical Test Results

The mechanical test results for the unidirectional composites, VYB 70 1/2 - SC1008, VYB 70 1/2 - pitch, Modmor II - pitch and Thornel 50 - pitch, are summarized in Tables XXIV and XXV. A complete tabulation of the mechanical test results is presented in Appendix II. The Thornel 50 - pitch composites were used to evaluate the effect of a tetrabromoethane (TBE) impregnate which was used to enhance the detail of the X-ray radiographic technique. Five Thornel 50 - pitch specimens were tensile tested without the TBE impregnate and five after the TBE had been applied and removed. The usefulness of this X-ray dopant method will be discussed in a following section.

The effect of the particular defects on the tensile and shear strengths of the VYB 70 1/2 - SC1008 composites are shown in Figures 75 and 76. The tensile strength, modulus, and strain to failure of the graphitized VYB 70 1/2 - SC1008 composites were significantly reduced with the presence of all intentional defects except for two specimens containing cracks (Figure 77). For the composite specimens containing cracks, the cracks ran parallel to the stress direction (parallel to the fibers) and the tensile properties could be expected to be

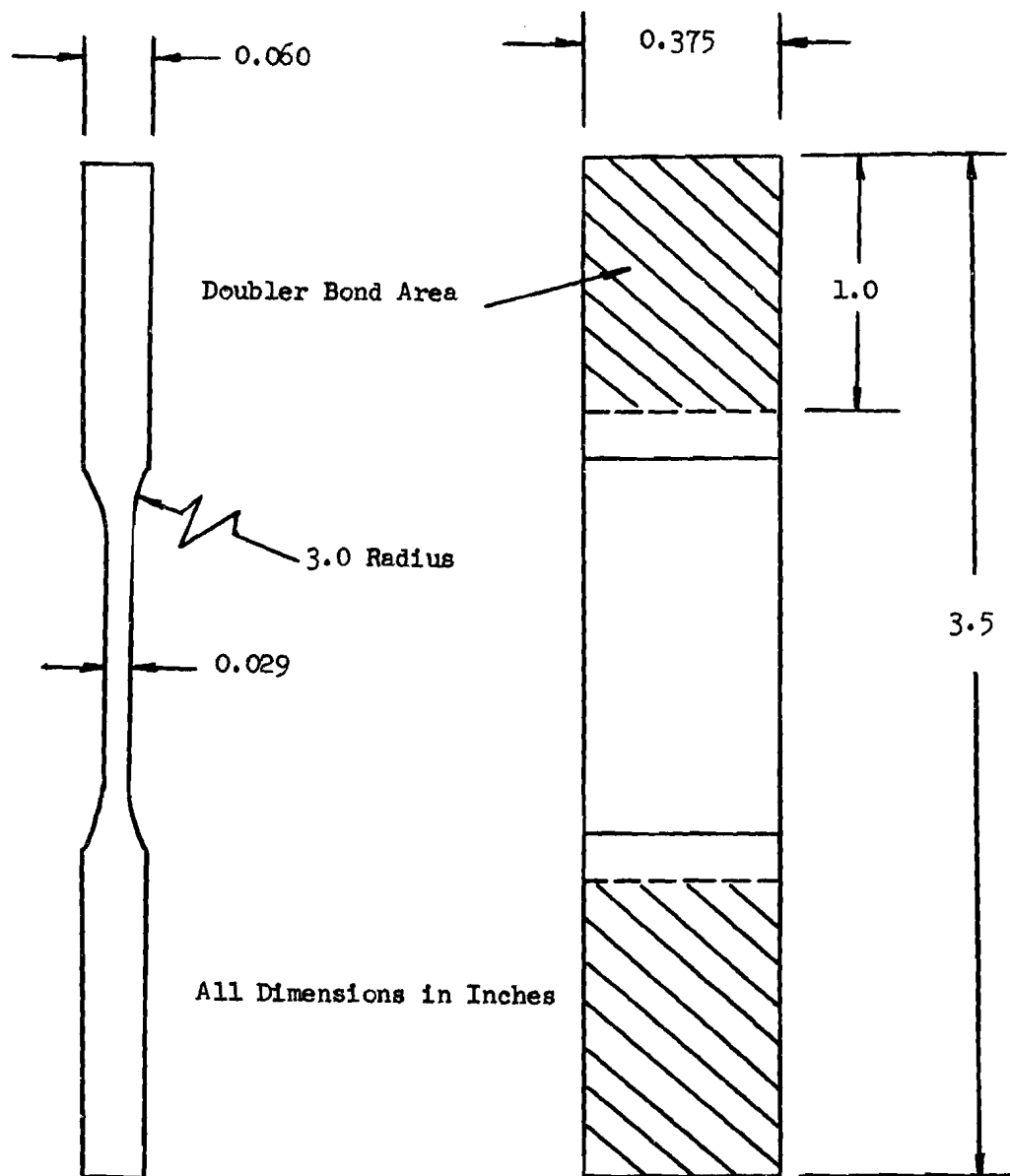
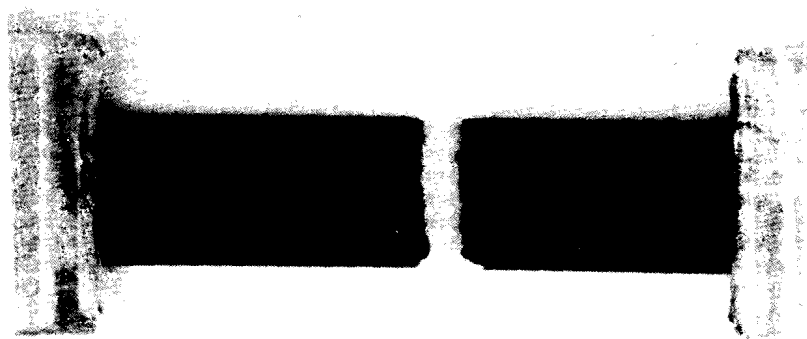


Figure 72. Current Tension Specimen Design



No-Intentional-Defect

2X



Small void

Figure 73. Failed Tensile Specimens of Pyrolyzed VYB 70 1/2-SC1008 Composite Using Current Specimen Design



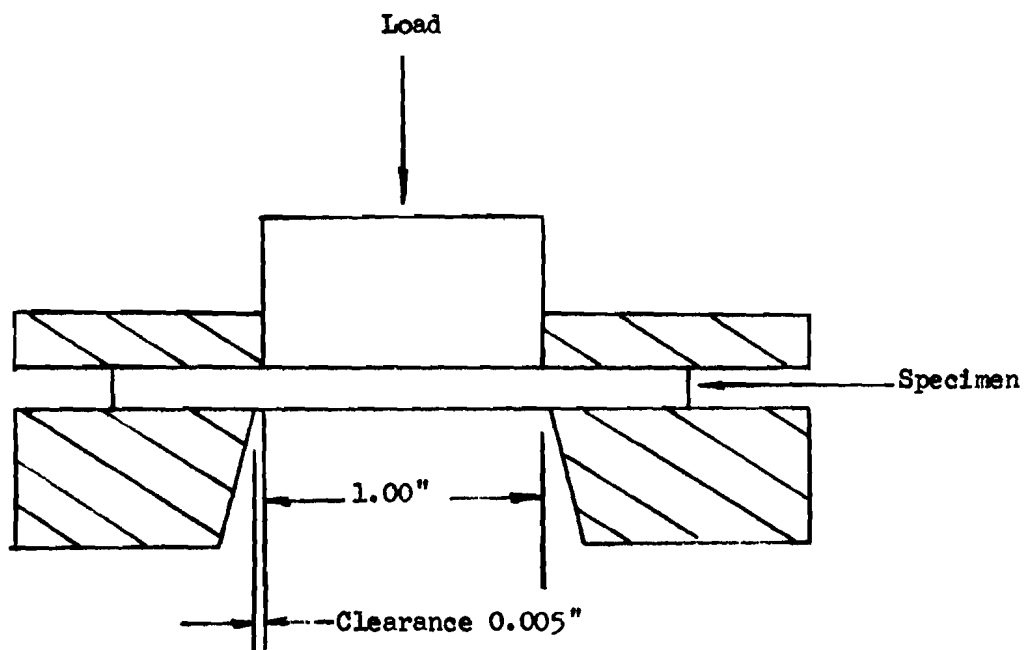


Figure 74. Double Shear Fixture Schematic

Table XXIV

## SUMMARY OF AVERAGE MECHANICAL PROPERTIES

Composite System	Defect Group	Condition	Modulus, $10^6$ psi			Strain- to- Failure (%)	Ultimate Tensile Strength (ksi)	Ultimate Shear Strength (psi)
			Initial	Final	Secant			
VYB 70 1/2 - SC1008	No-Intentional	Pyrolyzed	5.2	6.5	5.4	.22	13.6	1105
	Small Void	Pyrolyzed	4.8	3.8	3.8	.19	7.3	934
	Lack of Wetting	Pyrolyzed	4.0	4.4	4.4	.28	11.3	663
	Weave	Pyrolyzed	6.5	7.0	7.0	.10	6.9	698
	Crack	Pyrolyzed	-	-	-	-	-	1385
	Delamination	Pyrolyzed	-	-	-	-	-	1630
	Large Voids	Pyrolyzed	-	-	-	-	-	746
	Poor Bundle	Pyrolyzed	-	-	-	-	-	481
	Noncarbonaceous	Pyrolyzed	-	-	-	-	-	663
	No-Intentional	Graphitized	6.0	6.8	7.0	.33	17.0	462
	Small Void	Graphitized	2.8	2.9	2.8	.18	4.2	294
	Lack of Wetting	Graphitized	2.3	2.4	2.3	.24	5.8	210
	Weave	Graphitized	2.1	4.5	2.9	.36	9.8	339
	Large Void	Graphitized	-	-	-	-	-	115
	Cracks	Graphitized	5.3	8.8	6.4	.32	21.0	-
VYB 70 1/2 - Pitch	No-Intentional	Pyrolyzed	12.6	12.6	12.6	.07	8.6	770
	Small Void	Pyrolyzed	8.3	16.7	-	-	15.4	1770
	Lack of Wetting	Pyrolyzed	11.1	12.2	11.7	.13	15.2	1780
	Weave	Pyrolyzed	6.0	8.0	8.0	.09	7.4	850
	No-Intentional	Graphitized	8.1	14.5	9.6	.23	20.2	690
	Small Void	Graphitized	5.1	12.5	7.3	.40	29.2	880
	Lack of Wetting	Graphitized	-	-	-	-	24.0	940
	Weave	Graphitized	5.6	10.7	5.7	.31	19.4	740

Table XXIV (Continued)

Composite System	Defect Group	Condition	Modulus, $10^6$ psi			Strain- to- Failure (%)	Ultimate Tensile Strength (ksi)	Ultimate Shear Strength (psi)
			Initial	Final	Secant			
Modmor II - Pitch	No-Intentional	Pyrolyzed	24.3	24.3	24.3	.07	16.2	2380
	Small Void	Pyrolyzed	-	-	-	-	-	1260
	Lack of Wetting	Pyrolyzed	20.3	20.3	20.3	.06	12.0	1210
	Weave	Pyrolyzed	-	-	-	-	4.5	1110
	No-Intentional	Graphitized	-	38.9	51.6	.04	19.9	970
	Small Void	Graphitized	-	18.4	25.3	.04	10.0	1410
	Lack of Wetting	Graphitized	24.5	24.5	24.5	.11	26.3	1270
	Weave	Graphitized	29.0	29.0	29.0	-	4.4	1070

Table XXV

MECHANICAL TEST DATA ON THORNEL 50 - PITCH COMPOSITE NO-INTENTIONAL-DEFECT  
SPECIMENS AFTER GRAPHITIZATION

Description	Modulus, $10^6$ psi			Strain- to- Failure (%)	Ultimate Tensile Strength (ksi)	Remarks
	Initial	Final	Secant			
Untreated	21	5	9.5	.37	35.0	Failed in Gage Section
	20	20	20	.13	25.7	Failed in Gage Section
	58	58	58	.10	58.0(1)	Pulled out of Doublers
	18	-	16	.18	30.0(1)	Pulled out of Doublers
	29	29	29	.14	40.5(1)	Pulled out of Doublers
Treated with Tetrabromoethane	25	0.7	-	1.04	28.4	Failed in Gage Section
	27	2.5	-	1.01	32.2	Failed in Gage Section
	35	35	35	.01	31.8	Failed in Gage Section
	28	28	28	.16	45.8(1)	Pulled out of Doublers
	33	-	17	.20	51.2(1)	Pulled out of Doublers

(1) No failure

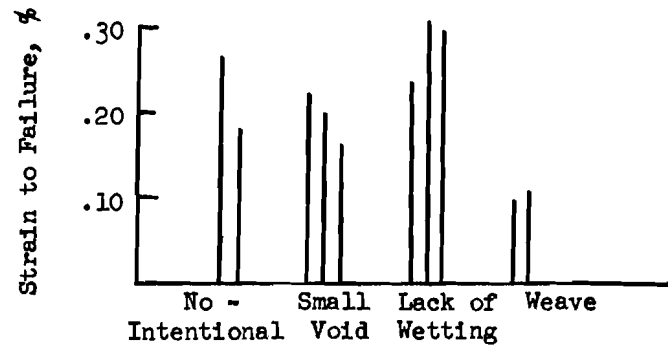
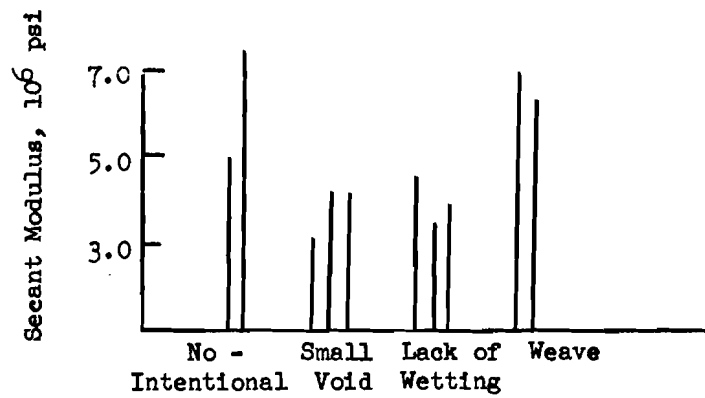
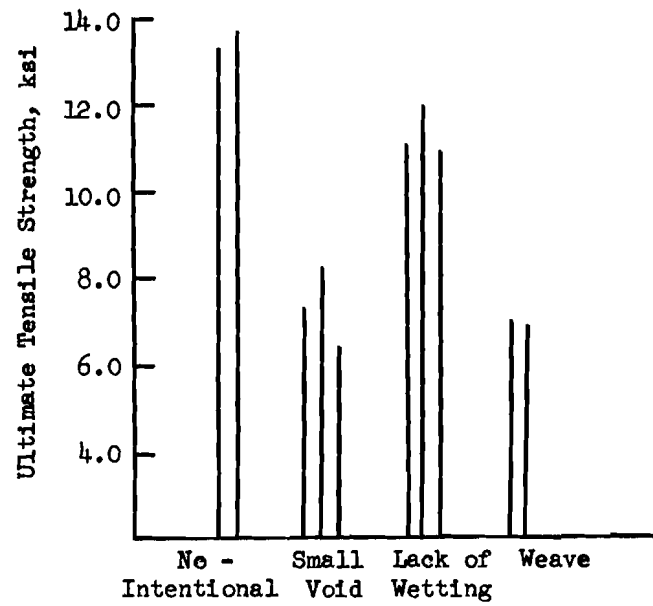


Figure 75. Uniaxial Tensile Test Results on Pyrolyzed VYB 70 1/2 - SC1008 Composite

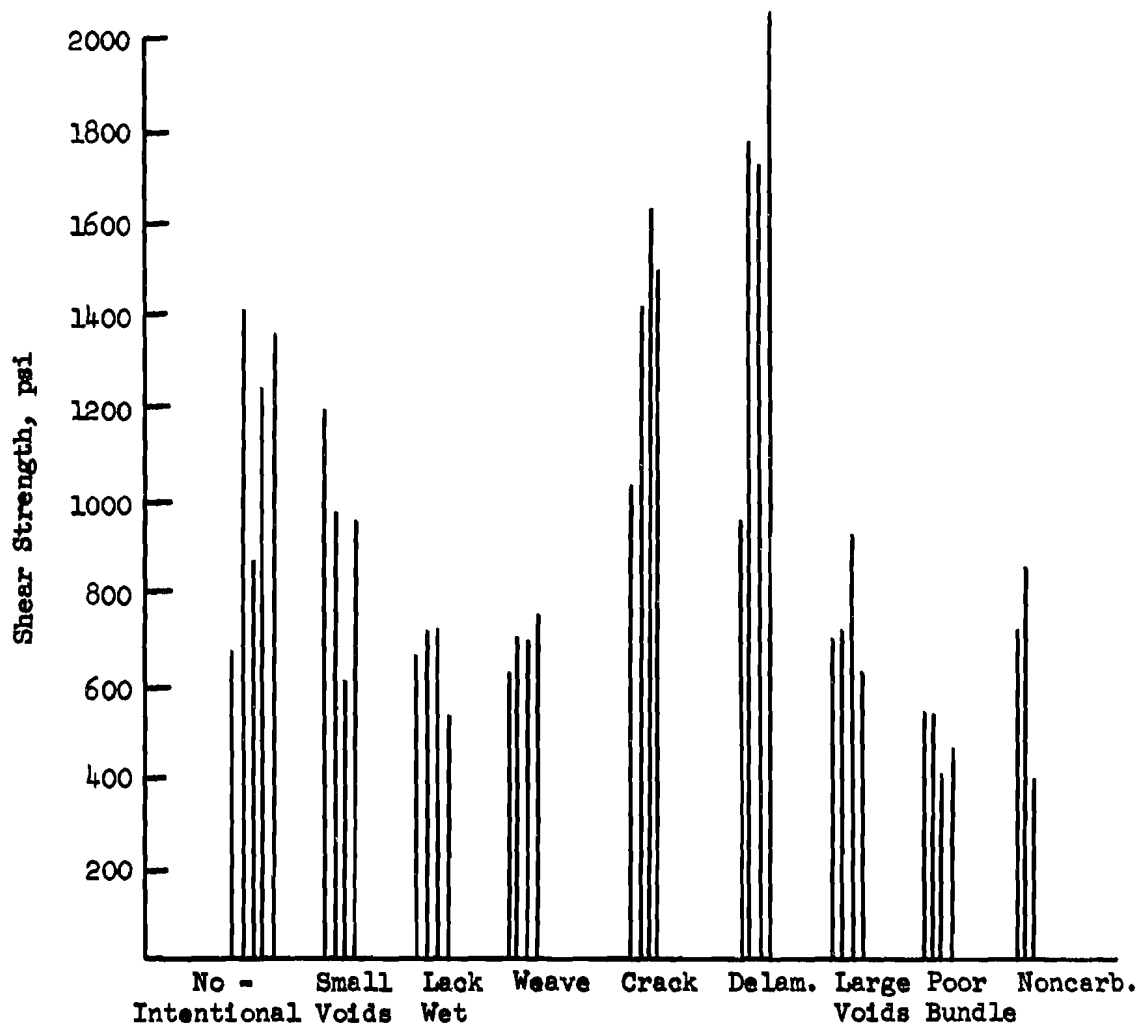


Figure 76. Shear Strength of Pyrolyzed VYB 70 1/2 - SC1008 Composite

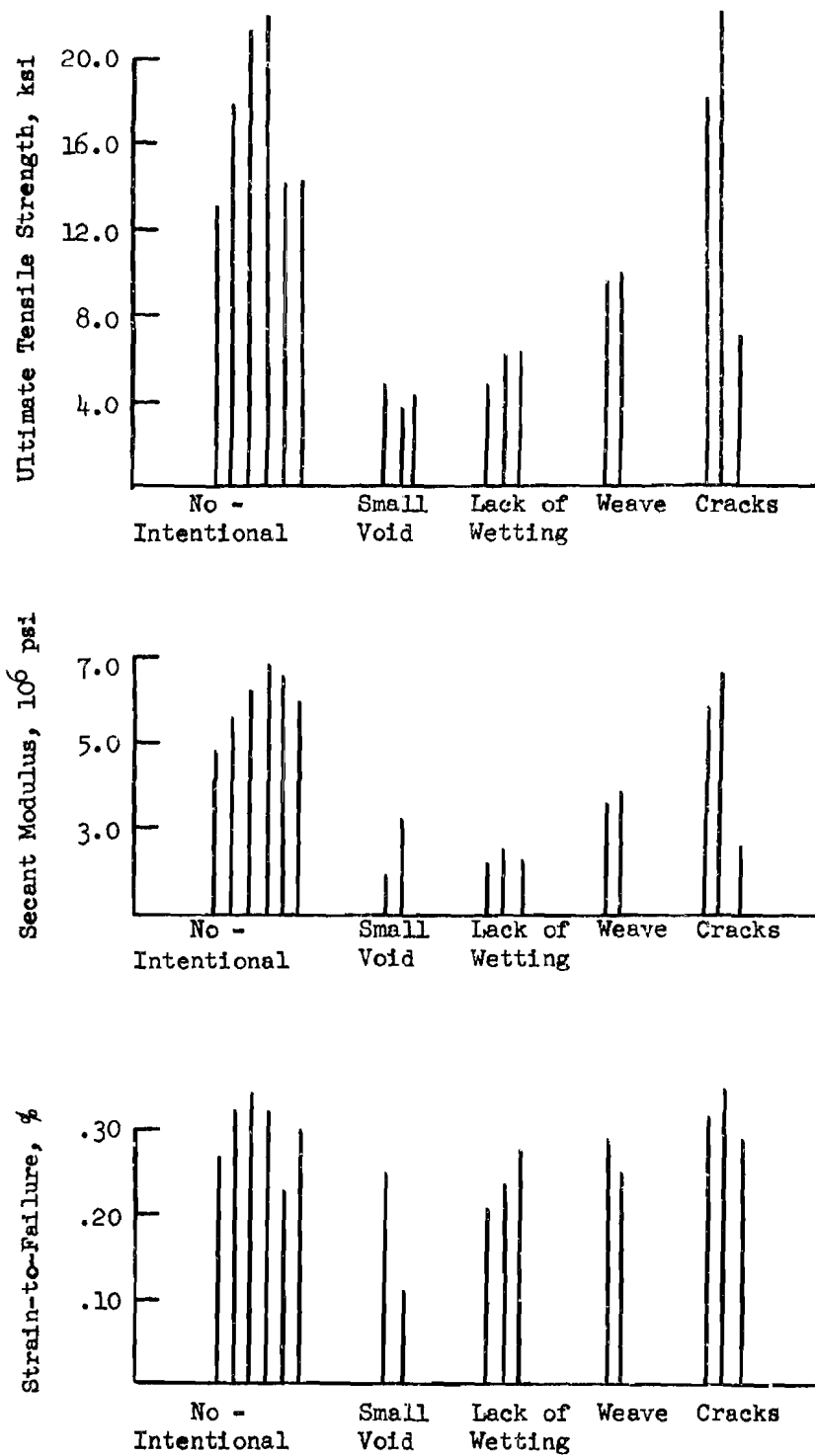


Figure 77. Uniaxial Tensile Test Results for Graphitized VYB 70 1/2 - SC1008 Composite

approximately the same as the no-intentional-defect samples. The low strength cracked specimen (UTS = 7.7 ksi,  $E = 2.7 \times 10^6$  psi, strain to failure = .29 percent) had an extremely large crack along the center of the specimen. The other two higher strength specimens (UTS = 18.2 and 23.1 ksi,  $E = 5.9$  and  $6.8 \times 10^6$  psi, strain to failure = .31 and .34 percent) had smaller cracks present along the fibers. The small void and lack of wetting defects had larger effect on the tensile strength of the graphitized than the pyrolyzed composite. The weave defect caused approximately the same reduction in strength for both material conditions.

The tensile test results for the VYB 70 1/2 - pitch composites are shown in Figure 78. The small void and lack of wetting defects actually had about a 50 percent higher tensile strength and strain to failure than the no-intentional defect specimen (Table XXIV). The secant moduli were less for the defects. The weave defect reduced both the tensile strength and modulus of the composites. The change in processing procedure from the pressure pyrolysis for the no-intentional defect specimens to the autoclave pyrolysis for the defect specimens may be the cause of the increase in mechanical properties. The higher strength of small void and lack of wetting defects may be partially associated with a stronger matrix to fiber bond than that for the no-intentional defect samples.

Upon graphitization, the tensile strength and strains for the VYB 70 1/2 - pitch and SC1008 composites greatly increased. This increase in strain was due both to the increase in strength and also a decrease in the initial modulus.

The influence of binder type with and without defects is shown in the tensile stress-strain curves in Figure 79 for both the pyrolyzed and graphitized conditions. In both cases, the volume percent of yarn was 65 percent. In the pyrolyzed condition, it appears that the no-intentional-defect specimens were stronger and had greater strain capacity with the SC1008 than the pitch binder (14,000 psi vs 9,000 psi and 0.3 percent vs 0.1 percent). However, on graphitization, the relative effects were nearly equalized; strength and strain increased for both binder systems (20,000 psi and 0.3 percent).

For the graphitized composites, an increase in stiffness with increasing load was measured for both binders (Figure 79). The initial modulus was about  $6 \times 10^6$  psi up to 0.2 percent strain, and the tangent modulus at higher strains was  $12 \times 10^6$  psi. It should be noted that the initial modulus is equivalent to the published value for the as-received yarn. Apparently there was a stiffening of the yarns on being stressed.

The introduction of defects also had a profound effect. The pyrolyzed pitch defect strengths were comparable to the SC1008 composites, but the strains were only one-half that for the SC1008. On graphitization, this influence of defects was more notable for the SC1008 binder for the strengths were reduced to less than 5,000 psi and strain to about 0.2 percent. Thus, the less graphitic binder appears to be more sensitive to defects.

The highest strength and strain values were obtained for the pitch-graphitized system with small voids. The double modulus was again evident. The initial modulus was slightly less ( $4$  vs  $6 \times 10^6$  psi) although the "knee" occurred at about the same stress level (10,000 psi). The final modulus values are comparable for both the no-intentional-defect and small void specimens. The



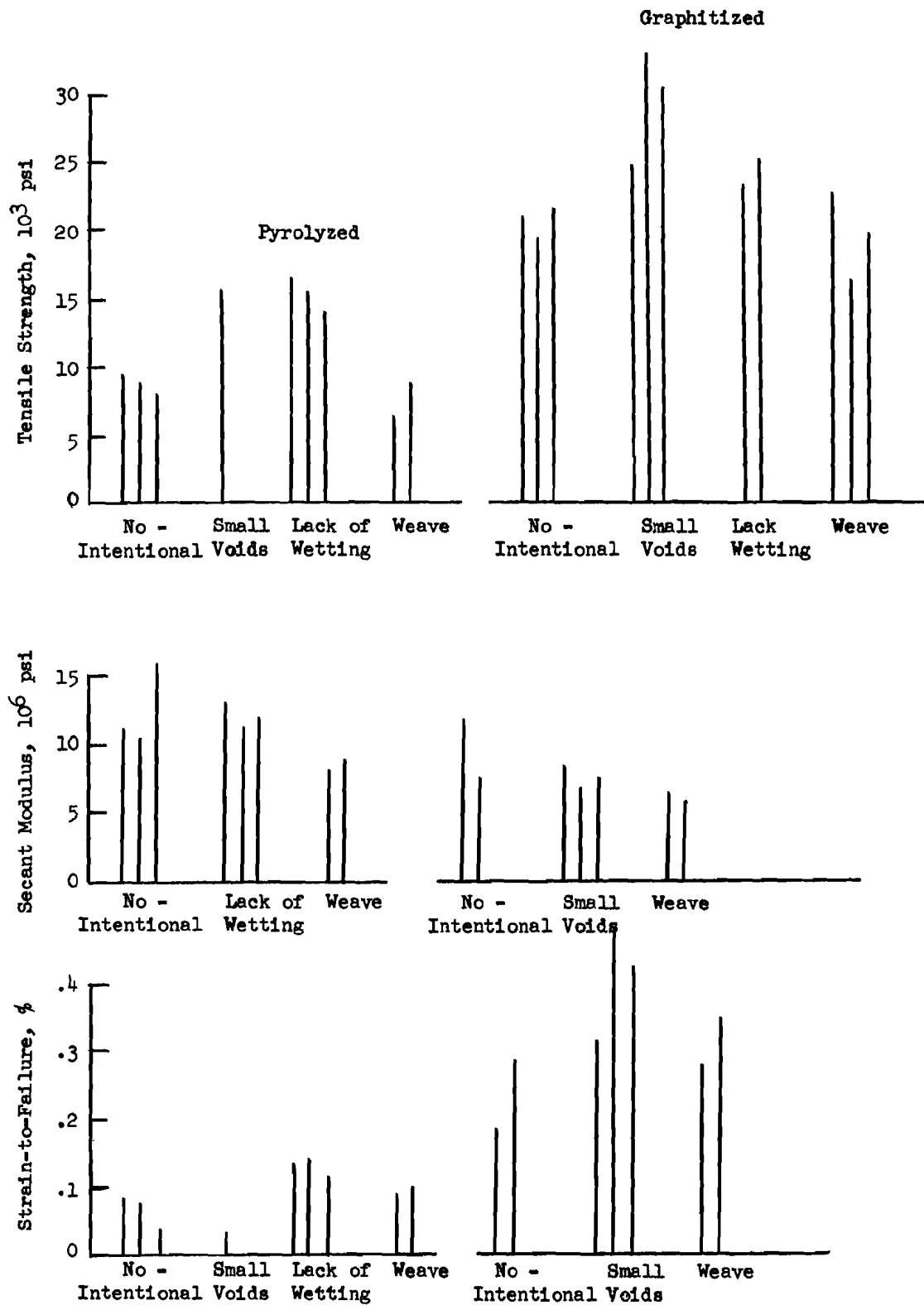


Figure 78. Uniaxial Tensile Test Results on Pyrolyzed and Graphitized VYB 70 1/2 - Pitch Composites

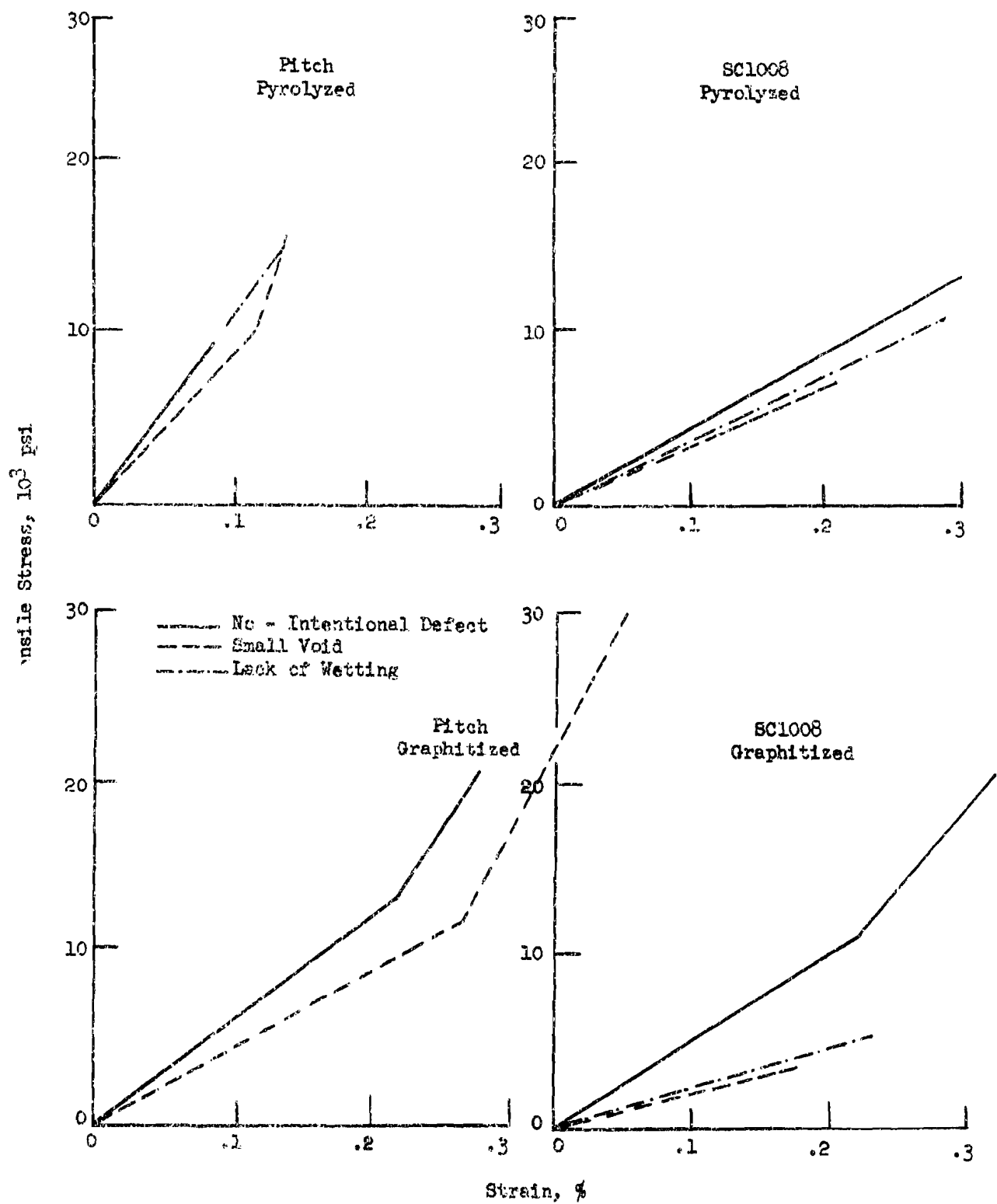


Figure 79. Effect of Binder on the Tensile Properties of the VYB 70 1/2 Composites

small void specimens had strength values of about 30,000 psi and strains of 0.4 percent. It is interesting that upon graphitization, the strain increased by a factor of 4 and the strength increased by a factor of 3. The utilization of the yarn strength within the composite is an indication of the influence of the matrix. It is estimated that 65 percent of each sample is composed of yarns. Metallographic examination has shown that each VYB 70 1/2 yarn is fluted with a maximum diameter of 6 $\mu$ . Because of the fluting, the effective cross section of a yarn is only 80 percent of its circular cross section. Therefore, the effective volume percent of yarns is the product of the estimated yarn volume and the effective cross section, that is, 50 percent. After graphitization, the yarn strength is reported to be 90,000 psi. Thus, the maximum tensile strength of a sample should be about 45,000 psi. The measured strengths were 30,000 psi or 3/4 of the theoretical strength, a relatively good value.

A conceptual model is shown in Figures 80 and 81 for possible changes in the microstructure for these different systems. The pitch-pyrolyzed diagram shows the pitch between two yarns. Generally, it is amorphous in structure except near the interface between the matrix and the yarn. Some orientation is shown by the dashed lines. Evidence for this effect is available since the microscope examination of pyrolyzed (at 600°C) specimens under polarized light showed a highly reflective thin region next to the fibers. It is to be noted that the fibers are crooked as pyrolysis occurs and are apparently straightened out during the graphitization step for the pitch binder. The contraction of the pitch during pyrolysis may cause the yarns to contract. Measurements of the the composites before and after graphitization have shown that they lengthen 1 percent in the direction parallel to the fibers and contract 5 percent in directions perpendicular to the axis of the fibers. Thus, the proposed model suggests a straightening of the yarns as the pitch structure becomes more oriented especially in the region next to the fibers. As the graphite plates enlarge, densification will occur so the fibers are pulled together in the transverse direction.

In contrast, the SC1008 binder is not oriented during pyrolysis and may not cause the yarns to become crooked as the pyrolysis occurs. There is no observable structuring at the yarn-matrix interface. However, on graphitization there is some evidence that a slight degree of ordering occurs; for example Fitzer et al (Reference 10) have observed ordering at the yarn-matrix interface. Also, it is conjectured that the yarns are made slightly crooked although not as much as for pitch, since there was a double modulus measured for the graphitized SC1008 no-intentional-defect specimens.

If small voids are introduced into the binder, it is proposed that the structures are altered according to Figure 81. The effect of the small voids is particularly evident for the pitch binder both in the pyrolyzed and graphitized states. A double modulus was measured for the pyrolyzed case and it is conjectured that the voids permit the contoured yarns to move laterally and straighten during the latter portions of the tensile test. This effect is noted particularly for the graphitized state where both the strain and stress values were increased to the highest values. The voids may also provide a means for stopping cracks that might be initiated in the matrix while under tension, thus allowing a higher utilization of the yarn strengths.

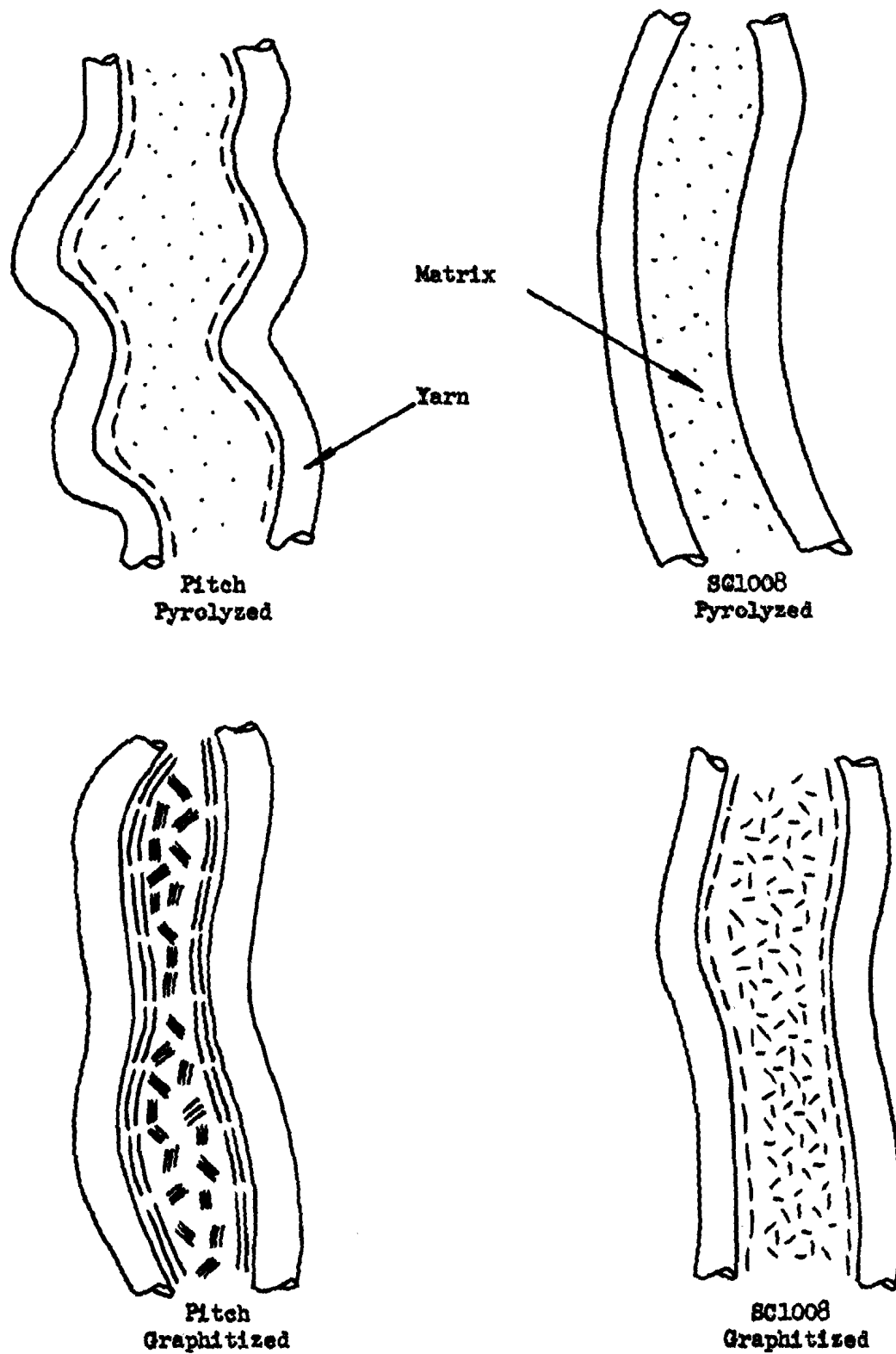


Figure 80. Model of No-Intentional - Defect Composite

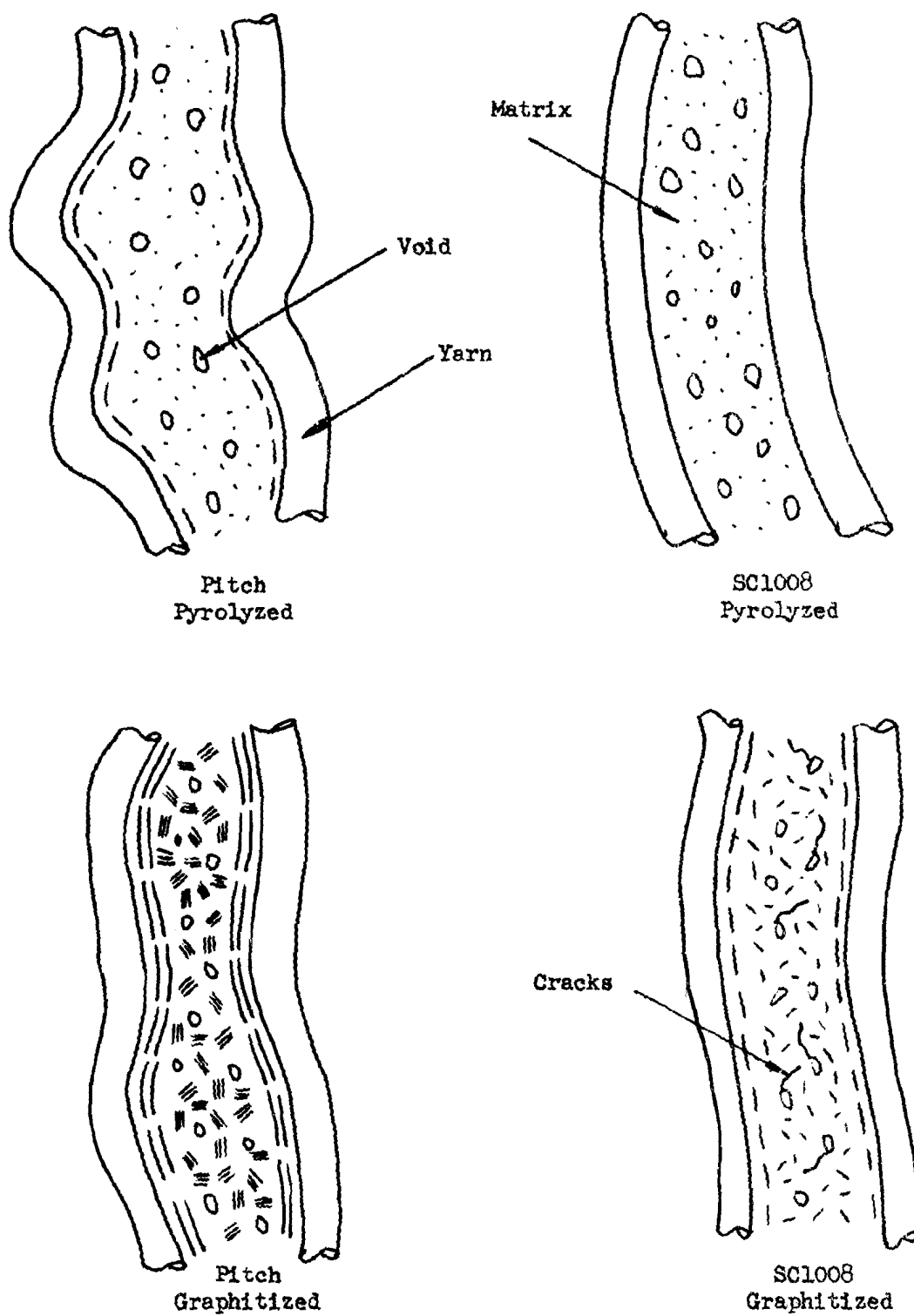


Figure 81. Model for Small Void Composite

In contrast, the voids in the less graphitic binder SC1008 appeared to enhance cracking for the strengths and strains were reduced in both the pyrolyzed and graphitized cases. This was particularly evident for the graphitized case where the strength was only one-eighth and strain one-half that for the no-intentional-defect specimens. No double modulus was observed for either material condition nor for the lack of wetting defect. The lack of wetting defect appears to have extended the strength and strain values for the pitch-pyrolyzed composites beyond the no-intentional-defect specimens. The lack of wetting defect for the graphitized pitch composite also extended the strength, however, not as far as the small void specimen (Table XXIV). The lack of wetting specimen strengths were almost as high as the no-intentional-defect samples for the SC1008, pyrolyzed, but the values were greatly reduced for the graphitized condition, indicating the brittle nature of the SC1008 compared to the pitch system.

The tensile results for the Modmor II - pitch composites are shown in Figure 82. An indication of the yarn-strength effect was made by comparing the tensile properties of the Modmor II (untreated) and VYB 70 1/2 - pitch unidirectional composites (Figure 83). In the pyrolyzed condition, this figure shows that the strengths for the VYB 70 1/2 and Modmor yarns composites were similar. This suggests that the composite strengths were not solely a function of the strengths of the yarns. The strain values of the lower modulus yarn composites were larger than for the high modulus yarns for the no-intentional-defect, small void, and lack of wetting specimens.

In the graphitized state, again, there was very little difference in the strength values for the no-intentional-defect specimens, but a large difference between the small void samples. The low modulus yarn composite was almost 30 ksi versus 12 ksi for the high modulus, small void composite. The strain values at failure were 2 to 3 times larger than for the Modmor yarn.

Another high modulus fiber, Thornel 50, was used to study the effect of types of high modulus yarns and to determine the effect of a TBE (x-ray dopant) impregnation. Half the samples were sent to AFML for TBE impregnation treatment to enhance any defects and half were not treated. After the x-ray evaluation was completed, the TBE was removed from the specimen by heating. All samples were then mechanically tested at MDAC.

The uniaxial tensile tests on the treated and untreated Thornel 50 - pitch composites was inconclusive as to the effect of the TBE on composite tensile properties (Table XXV). The data for treated specimens ranged from 23,000 to 51,200 psi and 25,700 to 58,000 psi for the untreated specimens. The moduli and strains were also similar. The higher strength specimens for both groups actually did not fail but were pulled out of the doublers due to a failure in the adhesive bond. Uniaxial tensile tests performed on Poco graphite specimens which had been impregnated and then treated to remove the TBE showed no reduction in tensile properties (Reference 11).

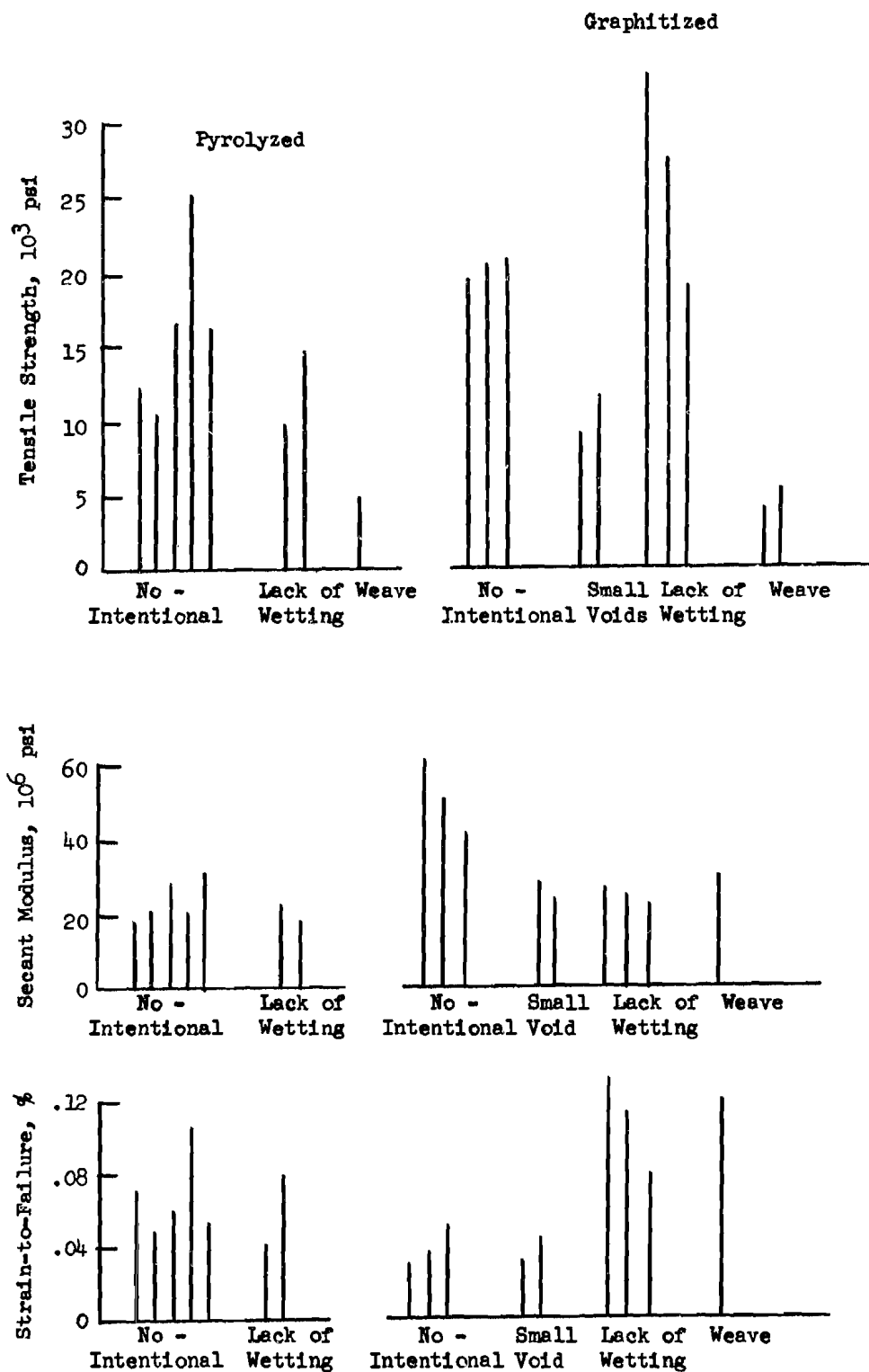


Figure 82. Tensile Test Results for Pyrolyzed and Graphitized Modmer II - Pitch Composites

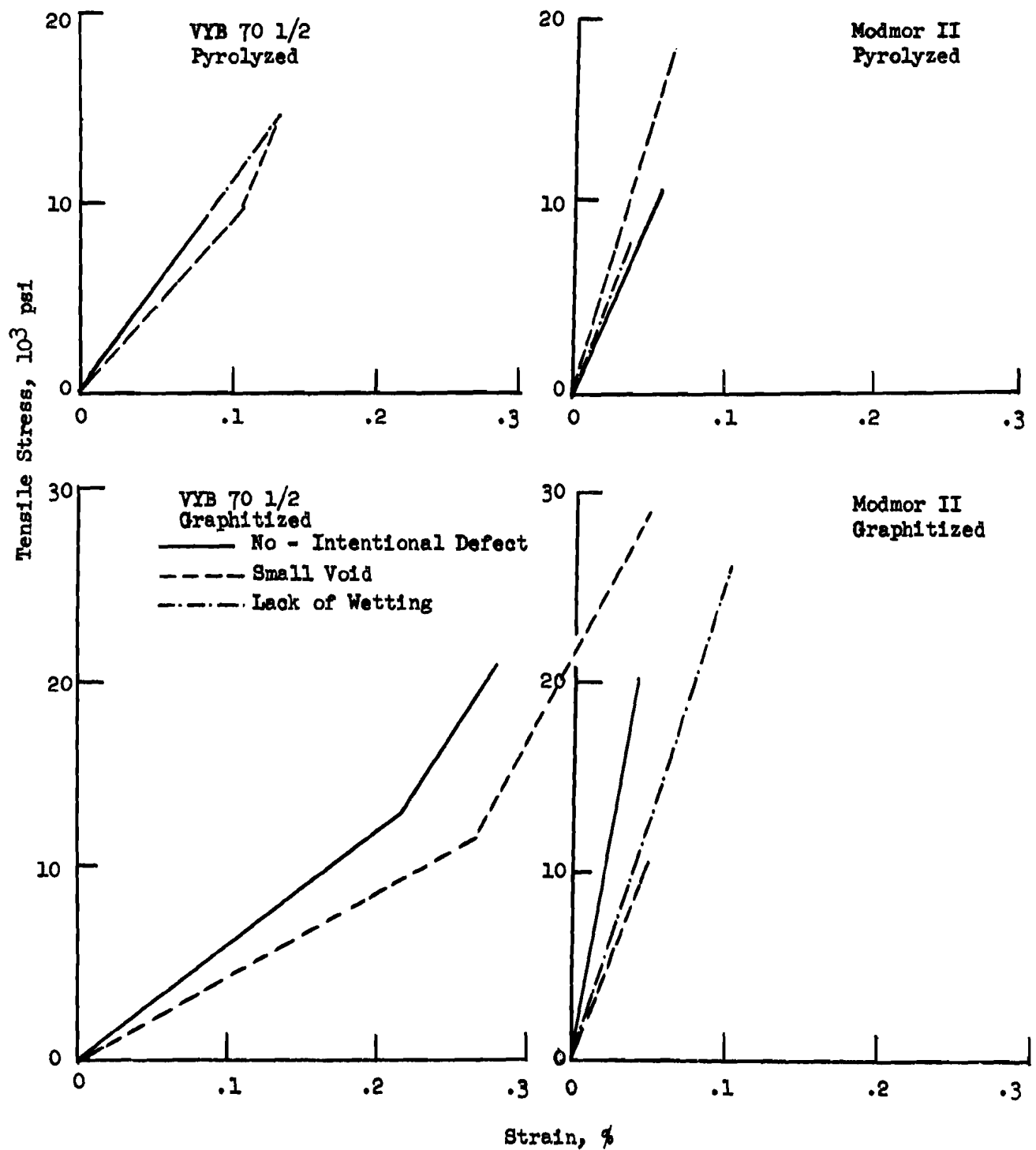


Figure 83. Effect of Yarn on the Tensile Properties of the Pitch Binder Composites



The graphitized Thornel samples showed at least double the strength values of the Modmor samples and several samples had almost triple the strengths. In all cases, the moduli remained constant throughout the test. The maximum strength and strain values were inconclusive because of the influence of the failure in the doublers.

The Modmor yarn with its untreated surface resulted in composites with lower strength than for composites containing Thornel 50. Thus, consideration should be given to the wetting of the binders and the type of surfaces of the different yarns. Apparently, there was sufficient difference between the surfaces of these yarns to obtain a higher utilization from the Thornel yarn. The lack of a double modulus may indicate that the Thornel and Modmor yarns have sufficient stiffness to prevent the yarns from becoming crooked as was the case for the VYB 70 1/2 yarns.

The effect of yarn and binder type, material condition, and defects on the shear strengths of the unidirectional samples was investigated. The shear test results are shown in Figure 84. In general, the values were between 800 psi and 1200 psi.

The shear strength of the pyrolyzed and graphitized VYB 70 1/2 - SC1008 were reduced from the intentional defect specimens. In the pyrolyzed condition, the specimens containing cracks and delamination defects had a higher shear strength than the no-intentional-defect specimens. In the case of the specimens containing cracks, the cracks were not located directly on the shear plane and therefore, the results should be similar to the no-intentional-defect specimens. The delamination defect was perpendicular to the loading direction and therefore may have very little effect on the shear strength. The microscopic evaluation of these specimens showed that the fibers were not parallel to the shear plane at one end of the specimen. This nonparallelism at one of the two shear planes can result in high shear strength values. The graphitization sequence greatly reduced the shear strength of the SC1008 composites.

The two high values of 1800 psi were obtained for the pyrolyzed VYB - pitch with small voids and lack of wetting defects. These values were higher than the no-intentional defect specimens. This supports the suggestion that the autoclave process increased the yarn-binder bond (compared to pressure cycle) as discussed in the tensile test results. As in the SC1008 binder system, the shear strengths were reduced upon graphitization.

For the high modulus Modmor yarn, the highest values of 2200 psi was obtained with the no-intentional-defect specimens. The presence of defects again reduced the shear strengths of the composite. The unusually high shear strength values for the graphitized small void defect specimens were attributed to the orientation of the fibers at the shear plane. The X-ray radiographs of the shear specimens showed that the fibers were at approximately a 5 degree angle to the shear plane. The high shear strengths, thus, were associated with shear of both the fibers and matrix, whereas the other strength values were more associated with shear of the matrix.

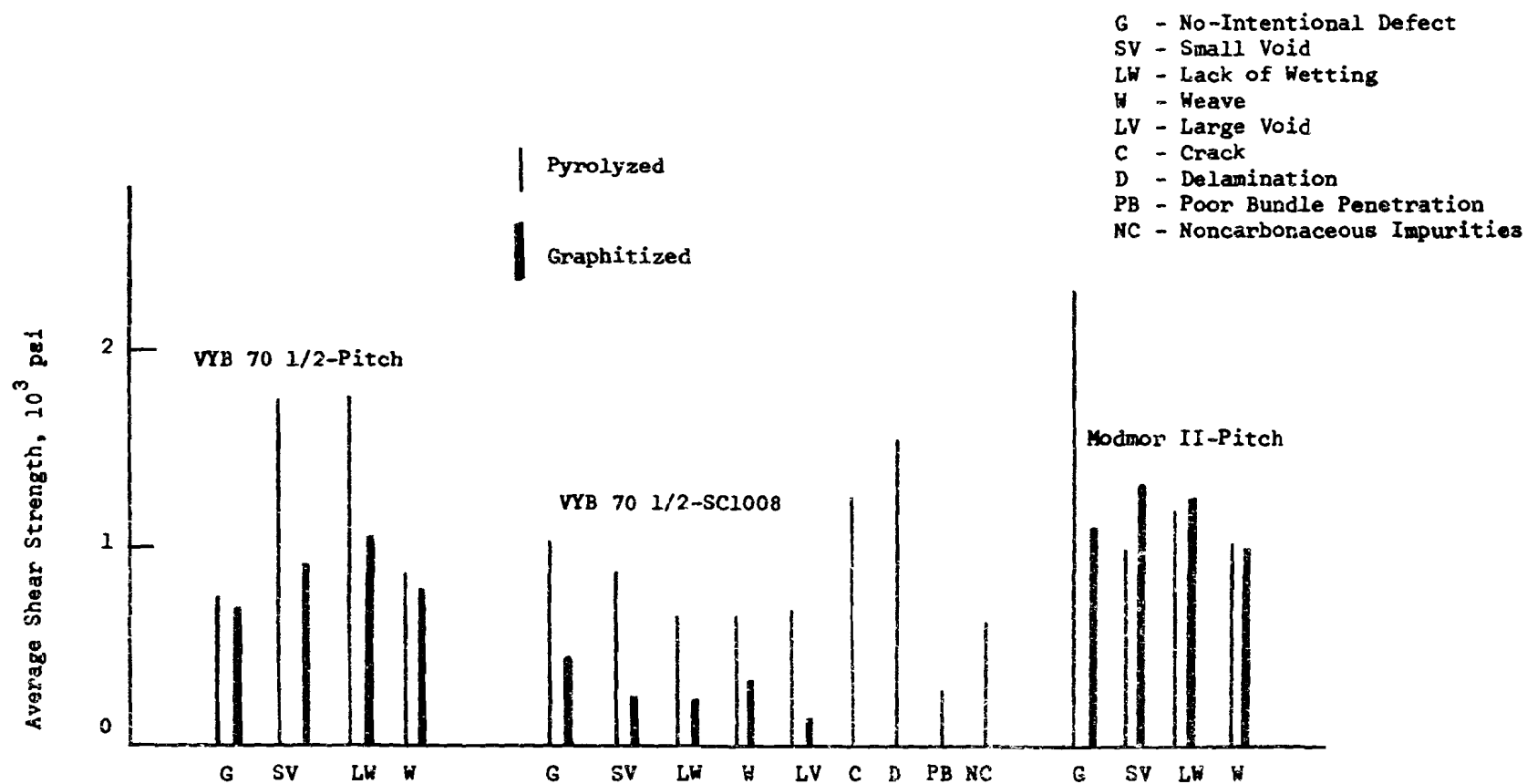


Figure 84. Average Shear Strength of Unidirectional Composites

Analysis of the mechanical test data involved correlation of the mechanical properties to physical property measurements. The porosity and bulk density data obtained from mercury porosimetry measurements (Section 4.0) was correlated to the tensile strength and moduli of the pyrolyzed and graphitized composites (Figures 85 and 86). The graphs for the VYB 70 1/2 - SC1008 composite system indicated higher strength and moduli were associated with lower porosity values over the 16 to 30 percent range. Similar trends existed for the bulk density measurements, higher strengths and moduli corresponded to higher densities. For the VYB 70 1/2 - pitch and Modmor II - pitch systems (Figure 86) the tensile strength - porosity data suggested that the strengths increased as the total porosity decreased up to a point and then decreased with a further decrease in porosity. Inconclusive data was obtained for the pyrolyzed samples. The proposed trends are indicated as dotted lines since additional data would be required to confirm the suggested porosity effect. Sufficient moduli data was not available to evaluate the effect of porosity on the VYB 70 1/2 - pitch and Modmor II - pitch systems. This was due to the lack of data points for the small void defect specimens in the pyrolyzed condition.

For the VYB 70 1/2 yarn systems, it was noted that for the SC1008 binder with a porosity level of 16 to 30 percent, a continual increase in strength was noted with a decrease in porosity while for the pitch binder with a porosity range of 6 to 16 percent the strength reached a maximum and then decreased. This suggested that the highest density composites may not imply highest tensile strengths. The small pores present may provide a means of dissipating the energy associated with a fiber failure which leads to a rapid crack propagation causing a catastrophe failure. This can be interpreted as implying that the small pores provided a means of "blunting" an advancing crack.

The shear strengths of the pyrolyzed and graphitized SC1008 composite showed a trend indicating lower porosity or higher density corresponding to higher strengths (Figure 87). The shear strengths of the pitch binder composites did not show the same trend as the SC1008 system (Figure 88). The values for the VYB 70 1/2 - pitch system showed an increase in strength with porosity. This fact was difficult to interpret for it was contradictory to the expected effect of porosity and cracks which existed upon graphitization. However, it must be recalled that some of the specimens were processed by the die process while others were processed by the autoclave. This suggested that the change in processing increased the yarn-binder bond strength. The increase in shear strength with porosity for the graphitized Modmor II - pitch composites was due to the misorientation of yarns in the small void defects. In the pyrolyzed composites where proper orientation of fibers existed, a decrease in shear strength with porosity was observed.

The porosity and density values measured on the pyrolyzed composite were compared to the tensile strength and moduli values measured on the graphitized composite. The VYB 70 1/2 - SC1008 composite strengths and moduli again increased with decreasing porosity (Figure 89). Although only three points (each an average of five specimens) were available, a trend was suggested. The tensile strengths of the graphitized VYB 70 1/2 - pitch composite were related to the porosity of the pyrolyzed composite (Figure 90).

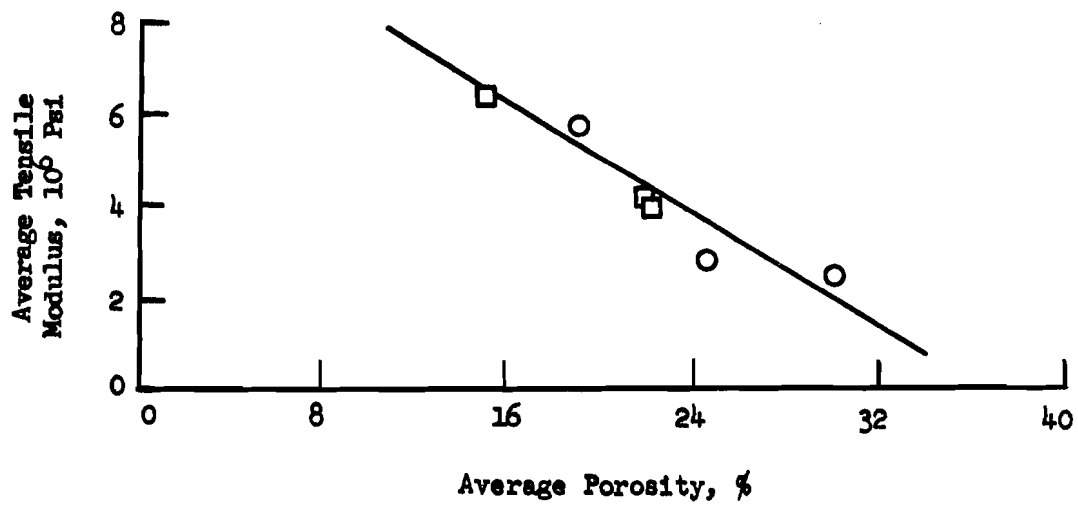
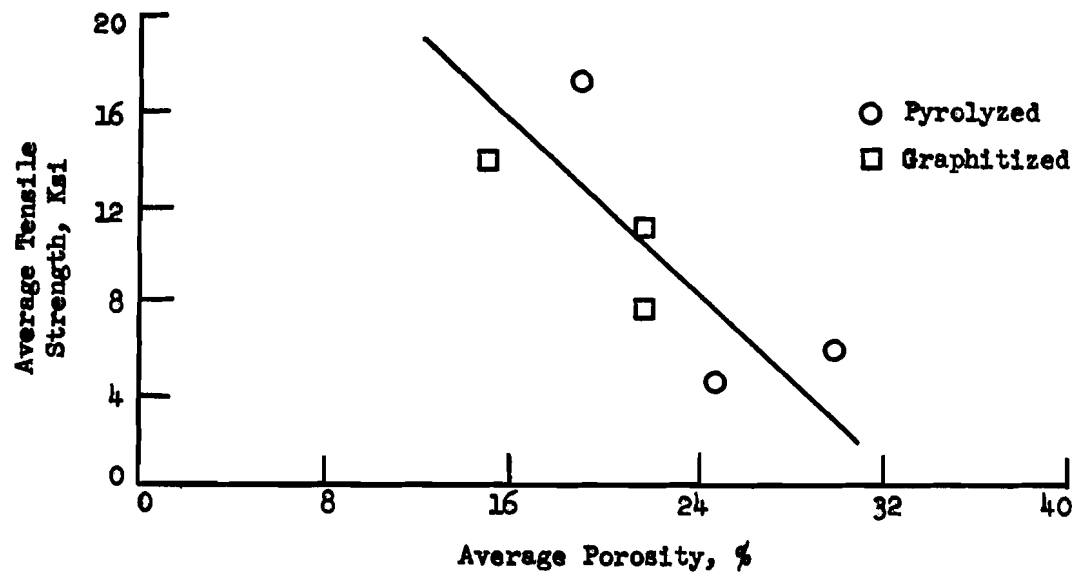


Figure 85. Average Tensile Strength and Modulus of VYB 70 1/2 - SC1008 Composite System

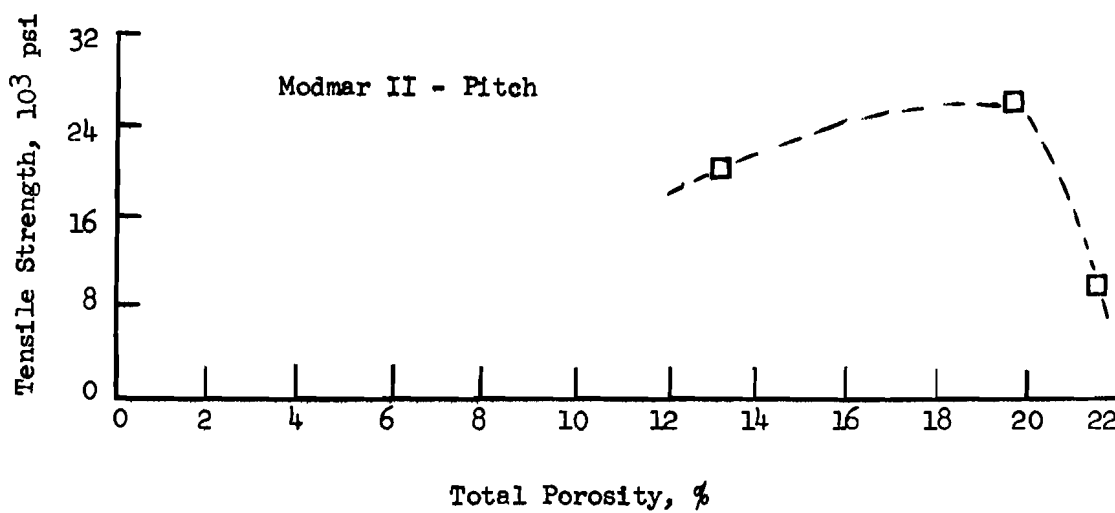
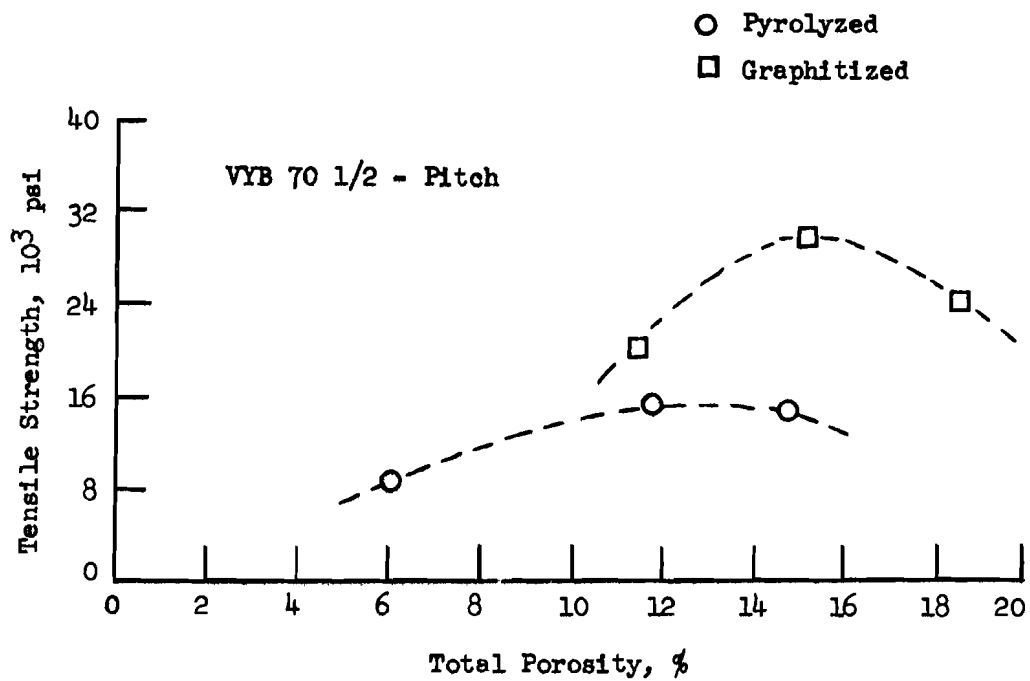


Figure 86. Average Tensile Strength Versus Total Porosity

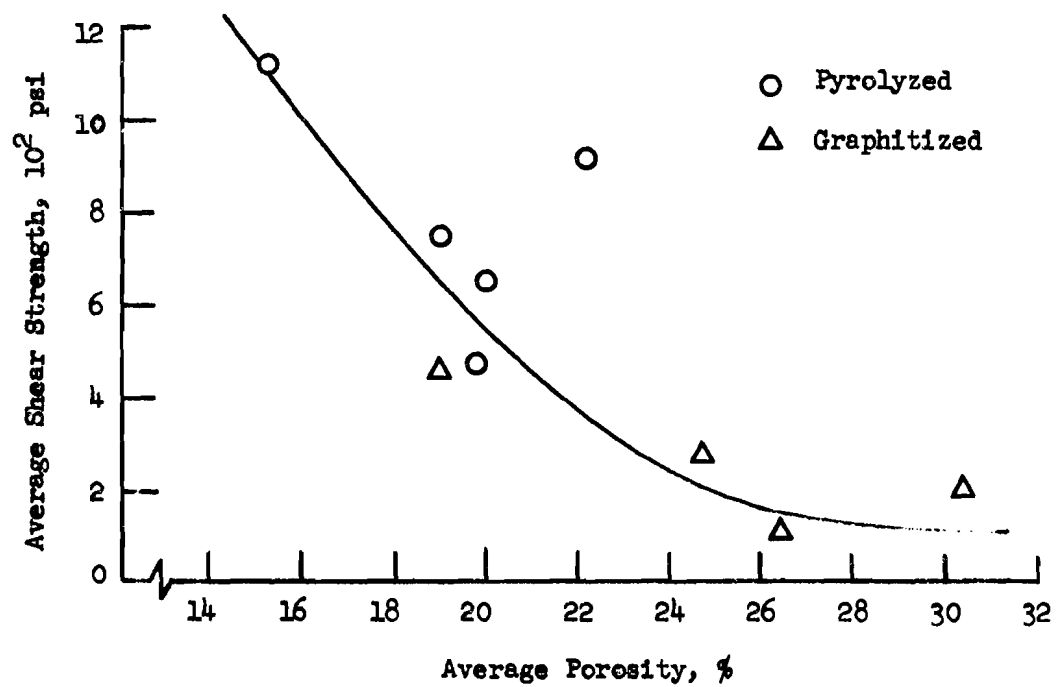


Figure 87. Graph of Average Shear Strength Versus Average Porosity of Pyrolyzed and Graphitized VYB 70 1/2 - SC1008 Composite

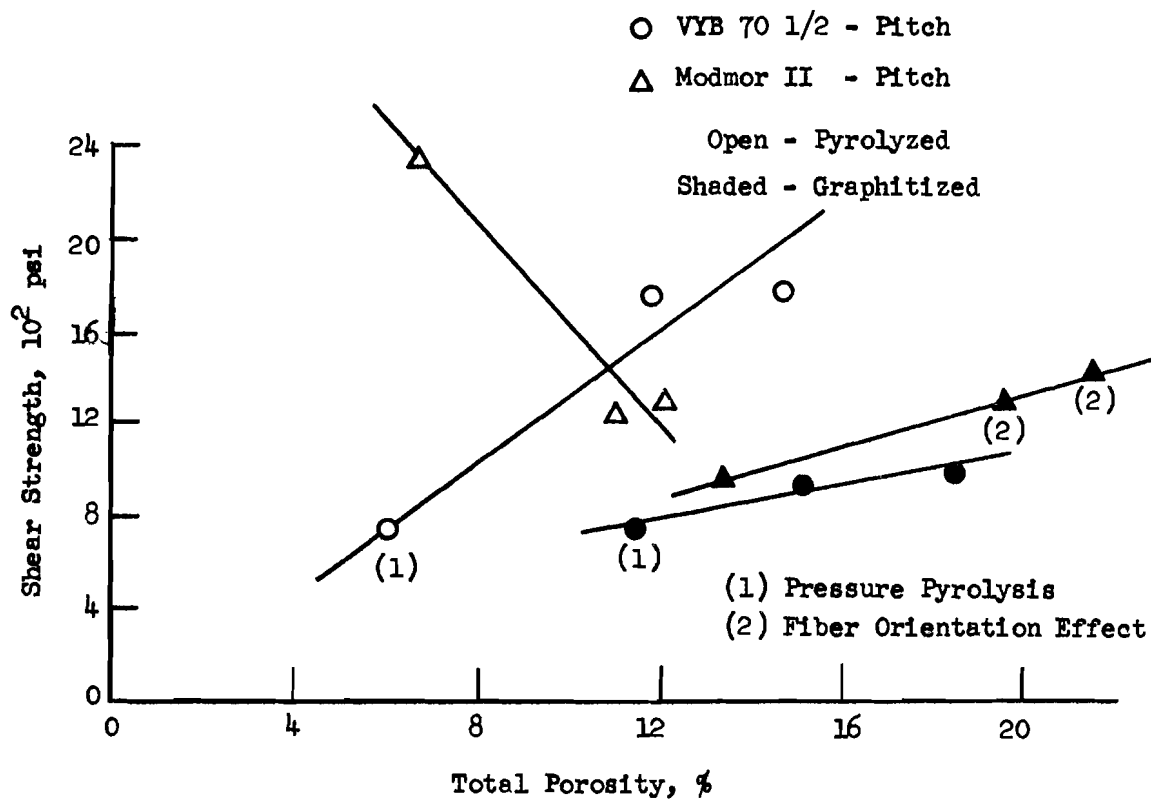


Figure 88. Total Porosity Versus Shear Strengths of VYB 70 1/2 - Pitch, Modmor II - Pitch Composites

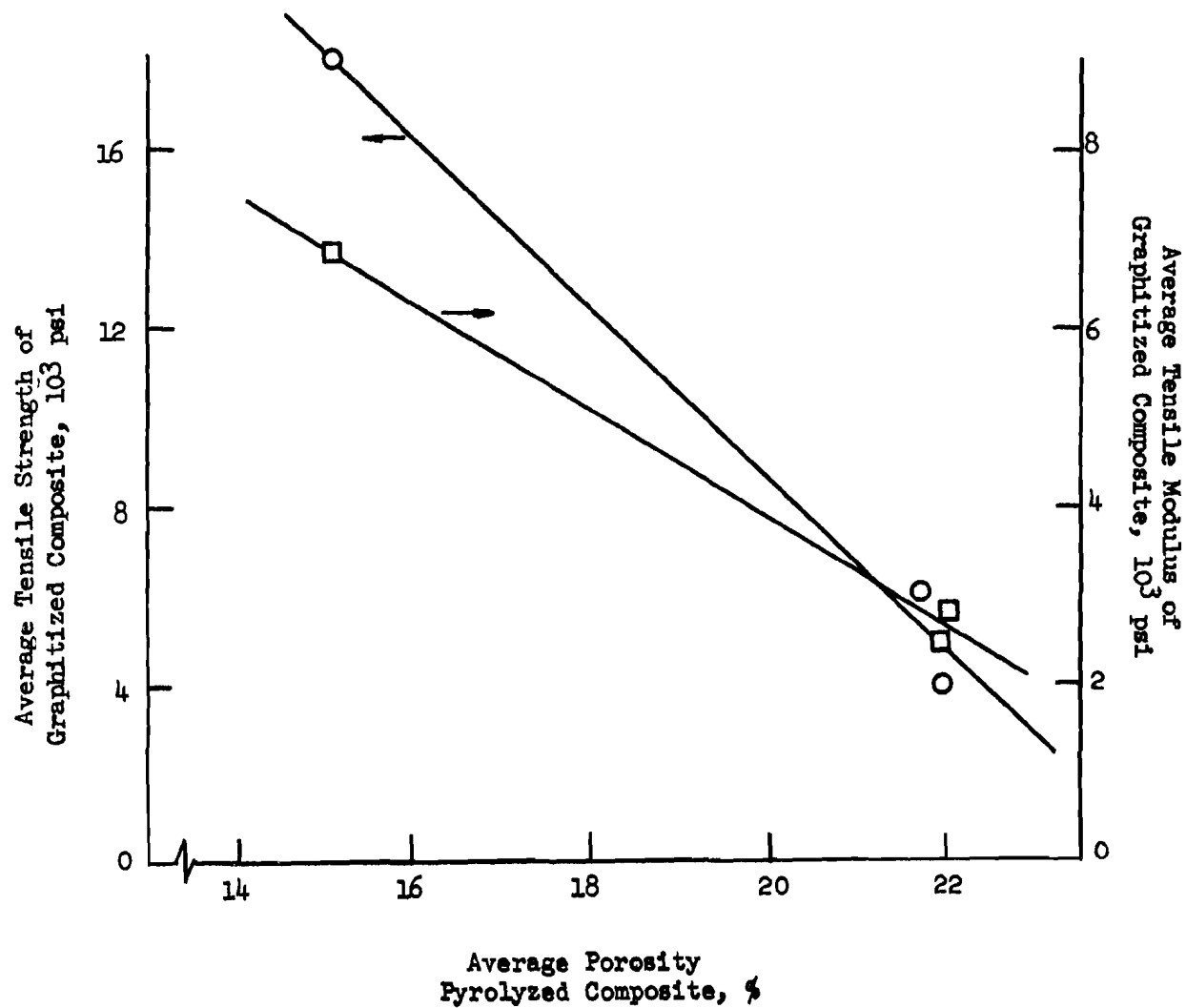


Figure 89. Prediction of Tensile Strength and Modulus of Graphitized VYB 70 1/2 - SC1008 Composite from Average Porosity of Pyrolyzed Composite



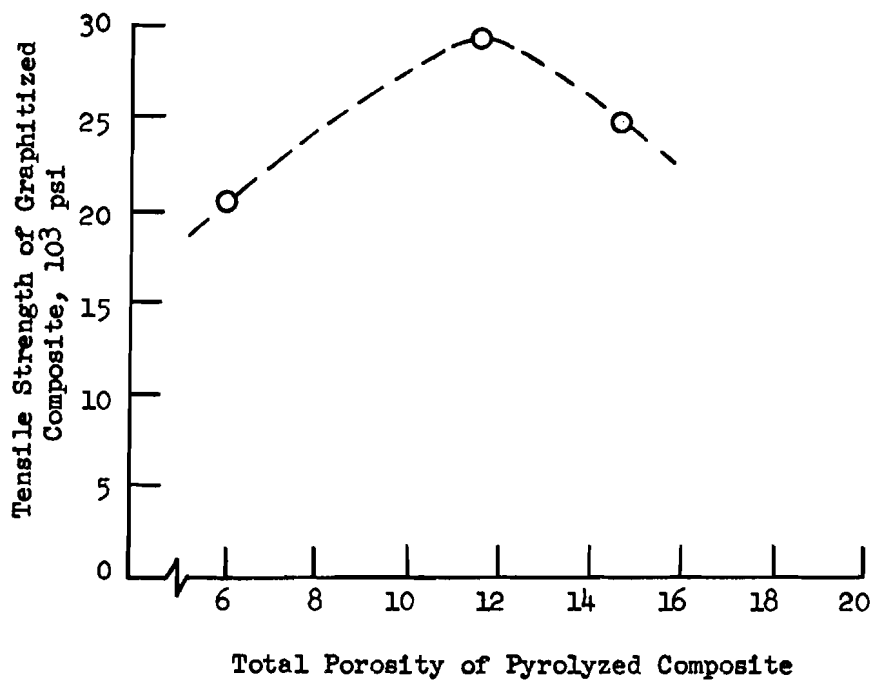


Figure 90. Prediction of Tensile Strength of Graphitized VYB 70 1/2 - Pitch Composite from the Porosity of Pyrolyzed Composite

The in-process prediction of shear strengths from the porosity of the pyrolyzed composites is suggested in Figure 91. The VYB 70 1/2 - SC1008 shear strengths of the graphitized composite increased with decreasing porosity of the pyrolyzed composite. The VYB 70 1/2 - pitch showed an increase in shear strength with porosity and, as explained previously, this may be attributed to an increase in the yarn-binder bond strength.

The examination of the tensile test results for the graphitized, no-intentional defect specimens showed a large amount of scatter. Two tensile tested specimens were selected from this group (10A5 and 14A3) for electron fractography and scanning electron microscopy to determine the cause of the scatter. The fracture surface was examined by plastic/carbon replicas with a chromium shadow at 45°. The surfaces of the fractured unidirectional samples were examined to evaluate the mode of failure and interrelationship between the binder and the VYB 70 1/2 filaments. The scanning electron microscope, with its great depth of focus, was particularly useful for examination of the ends of the fractured unidirectional samples. The electron fractography was most useful in studying the yarn-binder interface.

The results indicated that the higher strength specimen (14A3) had a larger amount of yarn-matrix bonding taking place than the lower strength specimen (10A5). This was indicated by the large amount of matrix remaining on the filament surface of specimen 14A3 as shown in the electron fractographs of Figures 92 and 93. The black areas or spots in the micrographs are folds in the plastic replica or dust particles from the fracture surface. The VYB 70 1/2 filament diameter is approximately 6.0 microns. The scanning electron micrographs of specimens 10A5 and 10A3 are shown in Figures 94 and 95. These results indicated the importance of the yarn-matrix bond or specifically the wetting of the yarn by the matrix. Electron fractographs of the VYB 70 1/2 filament showed the brittle filament fracture present in both these composite specimens (Figure 96).

The nondestructive test data on the two graphitized no-intentional-defect tensile specimens (10A5 and 14A3) were examined to determine if a difference existed. The ultrasonic velocity and attenuation measurements were not successful in differentiating between these two specimens. However, examination of the X-ray radiographs did reveal significant differences between specimens 10A5 and 14A3. Figure 97 shows the large difference in uniformity between the two specimens. Specimen 10A5 had a significantly large number of discontinuities running parallel to the fiber direction. Although it was not possible to quantitatively determine the difference between these two specimens, it was possible to nondestructively detect the lower strength composite specimen by one of the techniques employed.

In order to evaluate the quality of the VYB 70 1/2 - pitch yarn, interface, and the mode of failure, electron fractographic and scanning electron microscopy were also conducted on the fractured surfaces of the VYB 70 1/2 - pitch tensile specimens. The two specimens selected for discussion were a graphitized no-intentional-defect with an ultimate strength of 20.8 ksi, strain to failure of 0.18 percent, and a modulus of  $11.6 \times 10^6$  psi, and a small void specimen with an ultimate strength of 32.6 ksi, strain to failure of 0.4 percent and a modulus of  $6.9 \times 10^6$  psi.

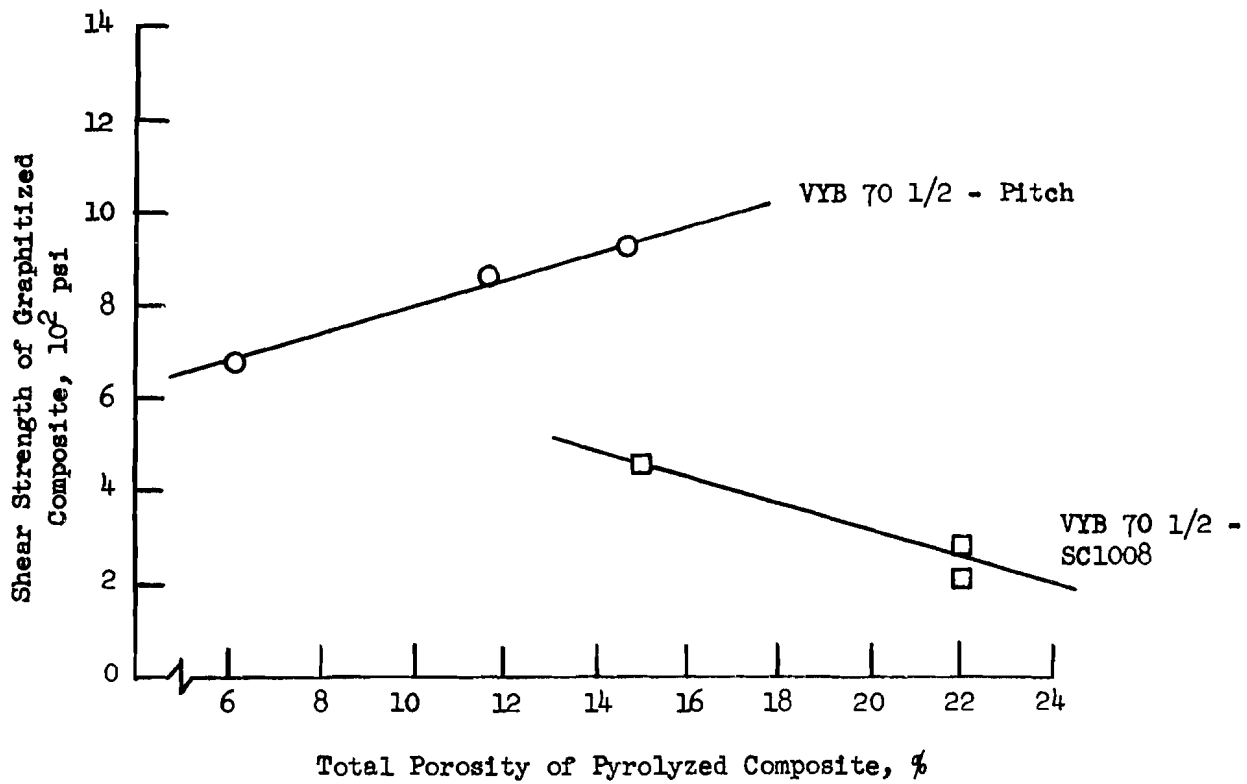


Figure 91. Shear Strength of Graphitized Composite Versus Total Porosity of Pyrolyzed Composite

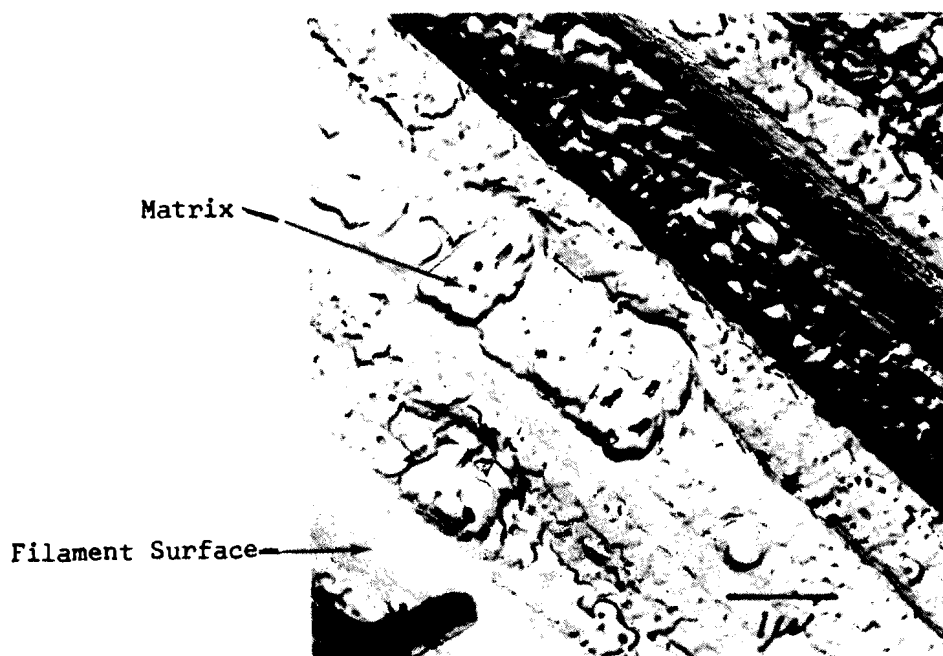
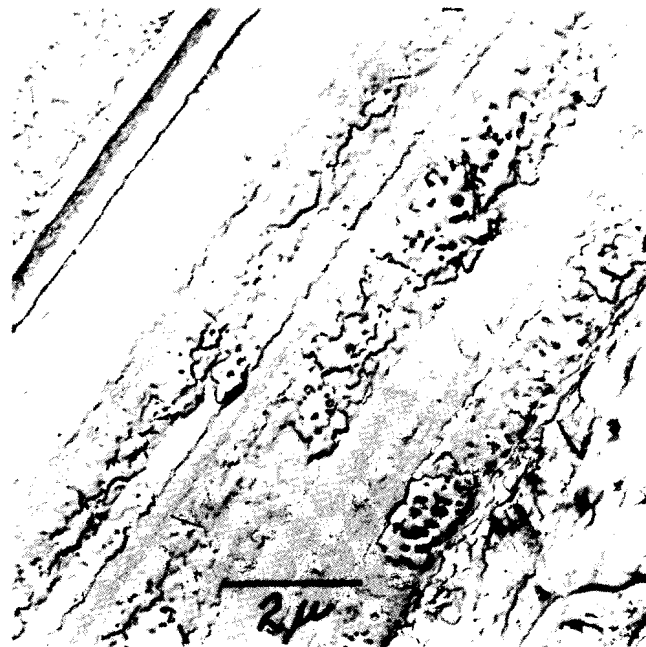


Figure 92. Electron Fractographs of Graphitized VYB 70 1/2-SC1008 Tensile Specimen 14A3

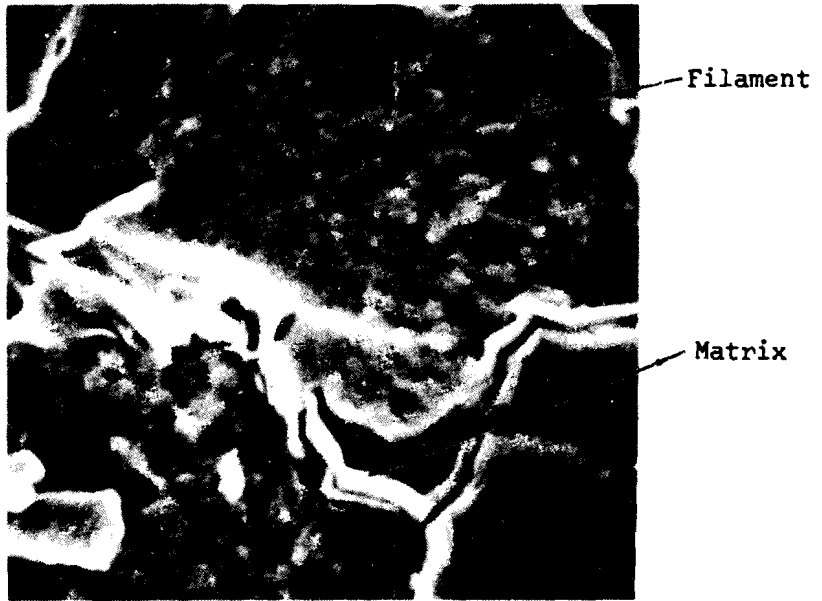


Matrix

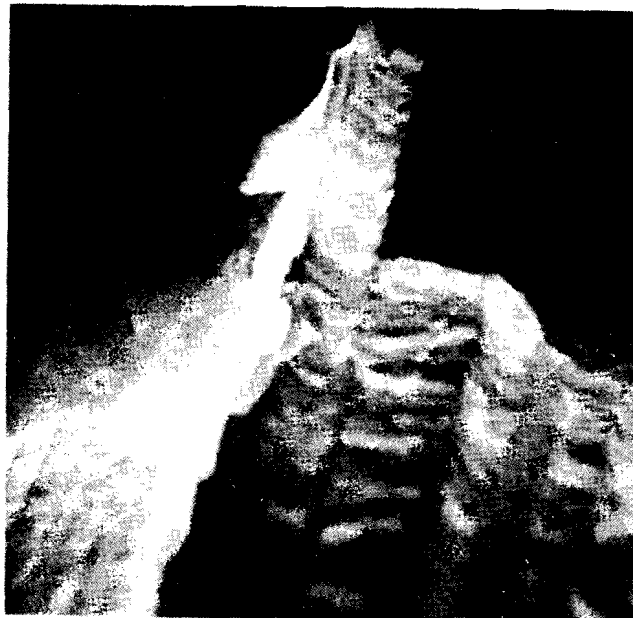


Filament Surface

Figure 93. Electron Fractographs of Graphitized VYB 70 1/2-SC1008 Tensile Specimen 10A5



MAGN. 8,970X



MAGN. 13,900X

Figure 94. Scanning Electron Micrographs of Graphitized  
VYB 70 1/2-SC1008 Tensile Specimen 14A3



Filament

MAGN. 570X



MAGN. 2550X

Matrix



MAGN. 6100X

Figure 95. Scanning Electron Micrographs of Graphitized  
VYB 70 1/2-SC1008 Tensile Specimen 10A5.

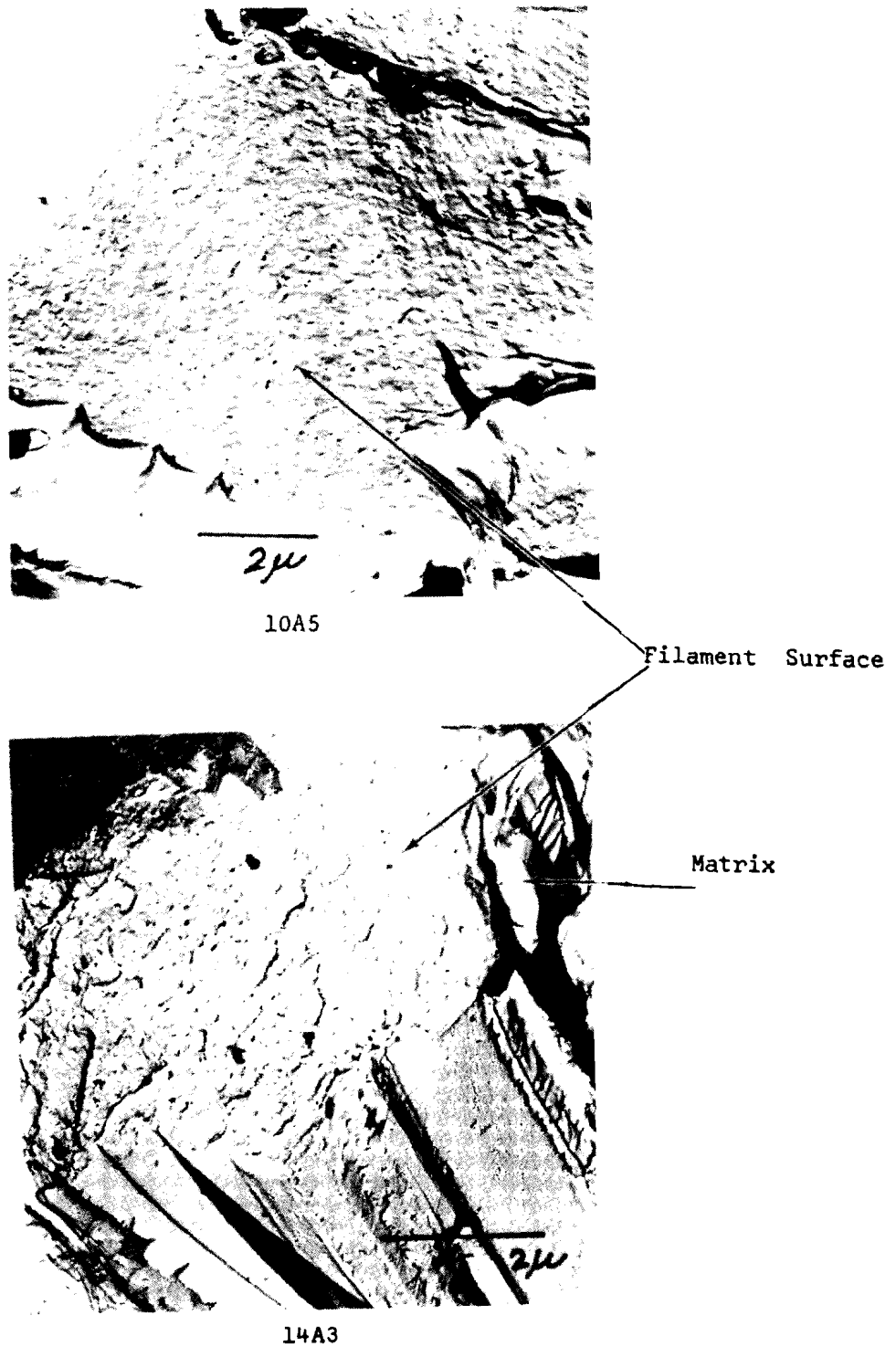
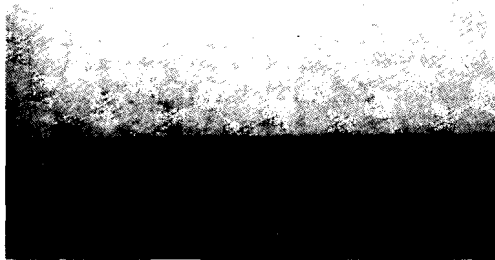


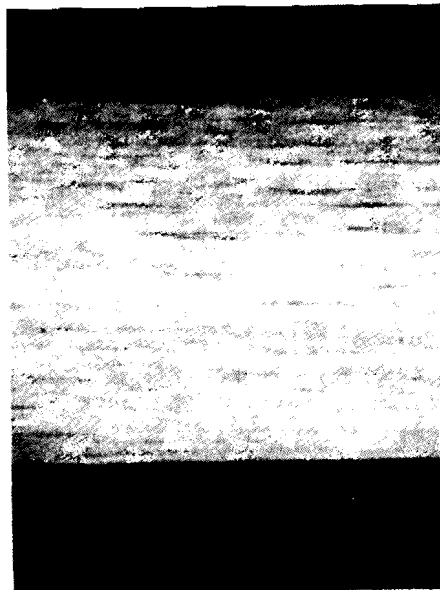
Figure 96. Electron Fractographs of Graphitized VYB 70 1/2-SC1008 Tensile Specimens 10A5 and 14A3





5X

Specimen 14A-3 (21,000 psi)



5X

Specimen 10A5 (13,100 psi)

Figure 97. Positive Print of X-Ray Radiograph of Graphitized VYB 70 1/2-SC1008 Tensile Specimens

From the SEM pictures, there was evidence of multiple fracture within a single filament (along its length) for the no-intentional defect specimen (Figure 98). There were numerous short lengths of filaments that were in different orientations. In contrast, the micrographs of the small void specimen showed no mis-oriented broken filaments (Figure 99).

A more detailed view of the binder-filament distribution is shown in Figure 100 for the small void specimen. Similar effects were observed in other specimens both of the no-intentional and small void defect types. A layering of matrix is evident between filaments. The apparent voids between layers may either be those present before testing or may have been created where the matrix had been sheared and removed with the other section of the tensile specimen. Since the matrix has penetrated into the crevices that exist for each filament, excellent penetration seems to have occurred. These SEM photomicrographs, and the light microscopy studies, indicate that an orientation of the binder matrix with the a-b planes parallel to the filament axis is present.

Replicas were made of the surfaces of filaments to determine the continuity of the matrix that appears to be attached to the filament surface. The filaments were well covered by the pitch binder since bare filament surfaces were not visible (Figure 101). This figure did not show the bare filament surfaces (slightly striated) as seen in Figure 92. The different binder appearances or textures in Figure 101 are due to the layering and different orientation of the pitch. This suggests that wetting and bonding to the filament surface as occurred with the pitch.

On comparing the electron fractographs of the pitch and SC1008 binders, it was apparent that the pitch binder did indeed wet the filaments to a greater degree than the SC1008 binder. This is shown most clearly in Figure 101, 92, and 93.

Local cracking of the pitch binder is shown on Figure 102 where the orientation of the cracking was normal to the axis of the filaments. It appears that the two cracks across the matrix segment do not propagate into the adjacent filaments. In the top portion of the figure, this may be due to a separation between the matrix and yarn prohibiting any penetration.

There was no major significant difference in microstructure as observed in the electron fractographs between the no-intentional-defects and the small void samples. This suggests that small voids were relatively large compared to the scale of these pictures. If crack initiation begins at the ends of the bonded regions, then the increase in voids might be a lack of complete coverage by the matrix. These local regions may then permit local redistribution of the loads between yarns. The no-intentional-defects may mean better coverage and a loss of the ability to locally relieve itself. These observations are consistent with the previously proposed model.



HS-260

1600X

No-Intentional-  
Defect Specimen



HS-262

1600X

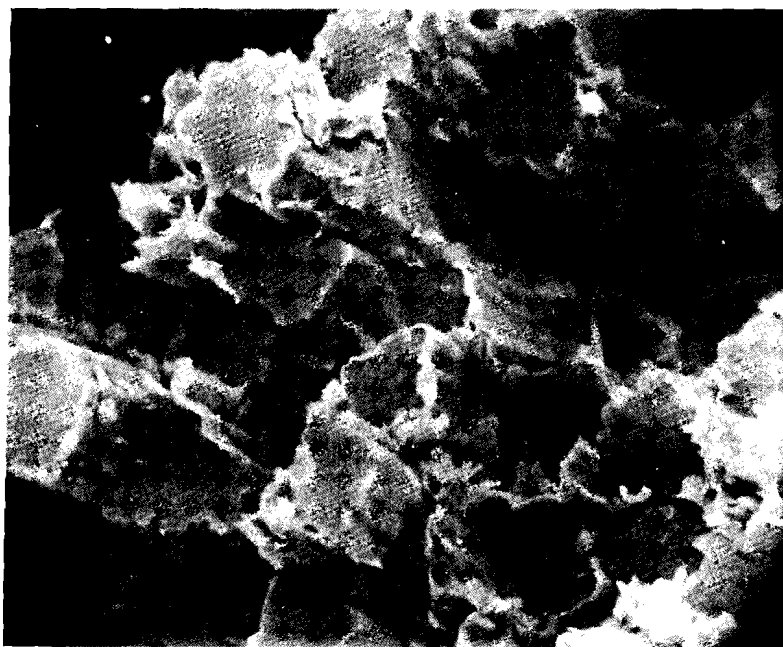
Figure 98. Scanning Electron Micrographs of Graphitized VYB 70 1/2-Pitch Tensile Specimen



HS-266

1700X

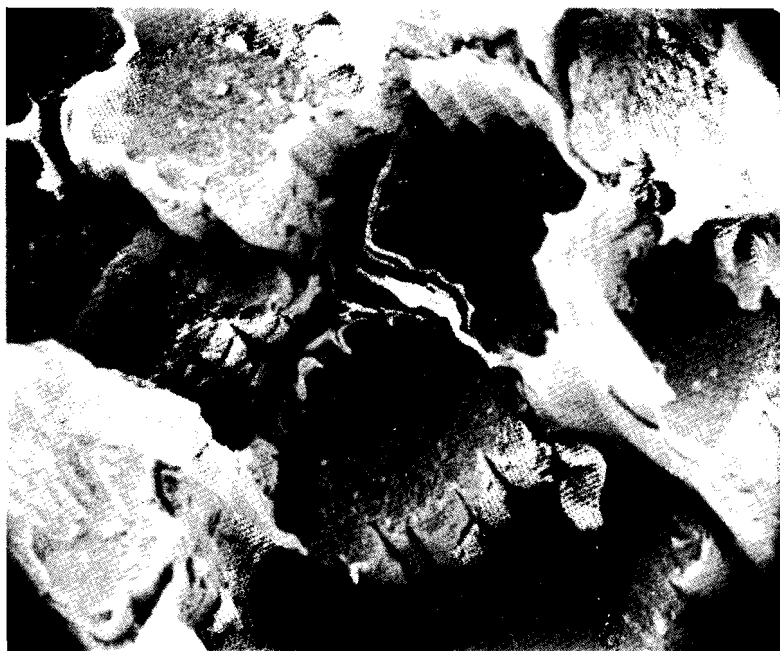
Small Void  
Specimen



HS-265

1700X

Figure 99. Scanning Electron Micrographs of Graphitized  
VYB 70 1/2-Pitch Tensile Specimen



HS 301

3500X

Small Void  
Specimen



HS-302

8700X

Figure 100. Scanning Electron Micrographs of Graphitized  
VYB 70 1/2-Pitch Tensile Specimen



No-Intentional-  
Defect Specimen



Small Void  
Specimen

Figure 101. Electron Fractographs of Graphitized VYB 70 1/2-  
Pitch Tensile Specimen



Figure 102. Electron Fractograph of Graphitized VYB 70 1/2-Pitch  
Tensile Specimen

#### 6.1.4 Relationship of Mechanical Properties to NDT Measurements

The nondestructive analysis of the mechanical test specimens included ultrasonic longitudinal velocity, bulk density, and electrical resistivity measurements and X-ray radiography. Along with the ultrasonic velocity measurements, attenuation measurements were made by the through-transmission method using a dry coupling method. A 0.0156-inch thick neoprene rubber film was used between the specimen and the transducers. A modified press arrangement was used to provide a constant pressure between the specimen and transducer (Figure 103). The bulk density was a weight-scalar measurement.

The attempts at measuring the ultrasonic attenuation by dry coupling methods were not completely successful due to specimen surface conditions. The amount of pressure applied to the transducer-specimen combination was also found to significantly effect the measured value. In a previous study, a comparison of dry and liquid couplant methods for carbon-carbon composites demonstrated that dry methods were inadequate (Reference 9). The attenuation values used for the material property correlations were those obtained by the immersed through-transmission method on the composite panels from which the test coupons were excised.

The frequency selected for the velocity measurements on the pyrolyzed and graphitized composites was 1.6 MHz and 0.8 MHz, respectively. These frequencies were selected for the ultrasonic measurements because they gave a strong transmitted signal through the specimens while still giving a difference in velocity between good and defective material as determined from the frequency dependence study. The nondestructive test data from the shear and tensile test specimens are shown graphically in Figures 104 to 115 and listed in Appendix III. The nondestructive test data on the mechanical test coupons generally had the same relationships between no-intentional and intentional defect specimens as previously discussed in Section 5.0.

The electrical resistivity measurements were made on the pyrolyzed and graphitized VYB 70 1/2 - SC1008 composites to determine if any correlations existed between resistivity and the defects introduced, bulk density, and process condition (either pyrolyzed or graphitized). Eddy current studies of graphites have suggested that increases in resistivity were associated with increases in density (Reference 12). The resistivity values obtained on the composites (Figures 116 and 117) were found to fluctuate among the defects. However, the resistivity measurements were very sensitive to material condition, pyrolyzed or graphitized, for all composite specimens. The pyrolyzed values were 6 to 11 times larger than the graphitized material value (Table XXVI). The electrical resistivity varied with the measured bulk density of each specimen such that no trend in the data was apparent.

The average ultrasonic attenuation, (as measured on the composite panels) was related to the ultimate tensile and shear strengths of the composites (Figure 118). The correlation between attenuation of the pyrolyzed composites and the tensile and shear strengths of the graphitized composites (Figure 119), suggests that in-process screening of these composites with the use of attenuation measurements is possible. The trend of higher attenuation with lower strength corresponded to the increase in attenuation which was observed with porosity (Section 5.0). The sensitivity of the attenuation technique is 1 db



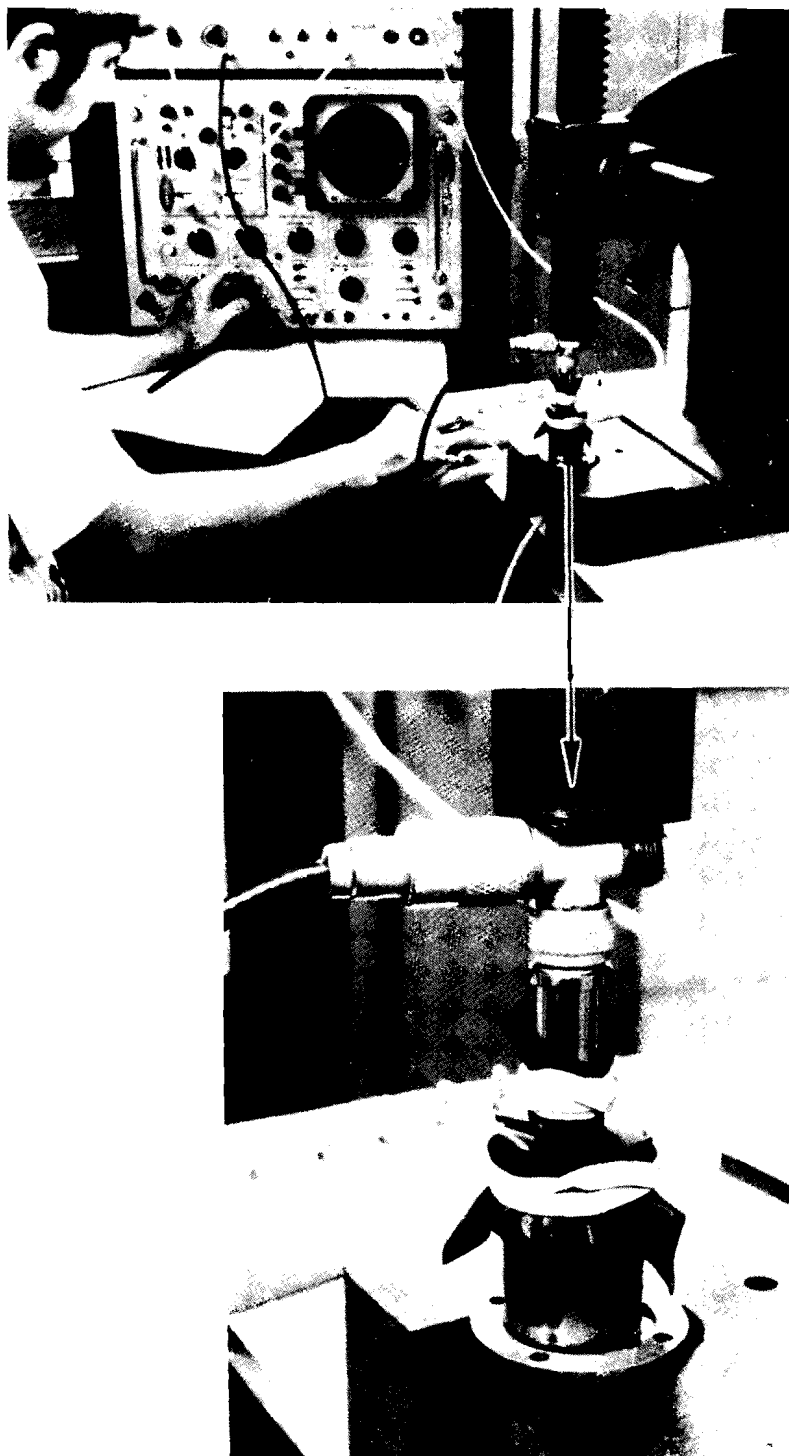


Figure 103. Photograph of Ultrasonic Longitudinal Velocity and Attenuation Measurement Apparatus by Dry Coupling Methods

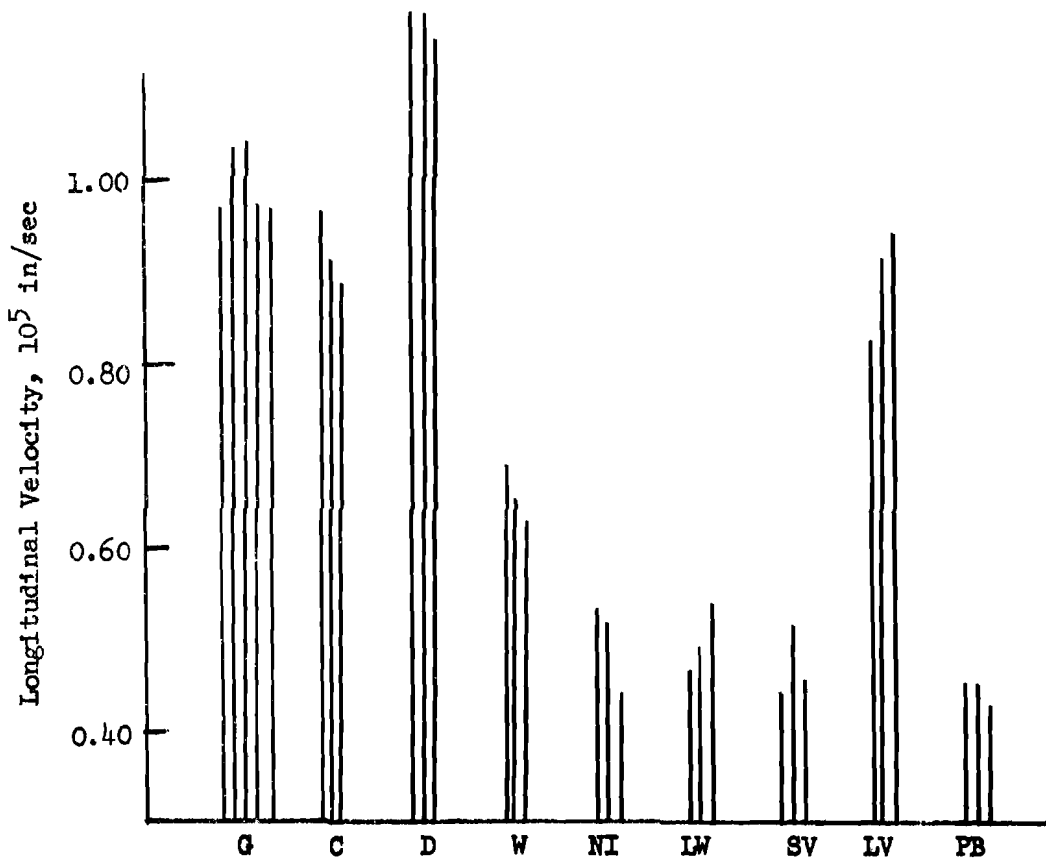
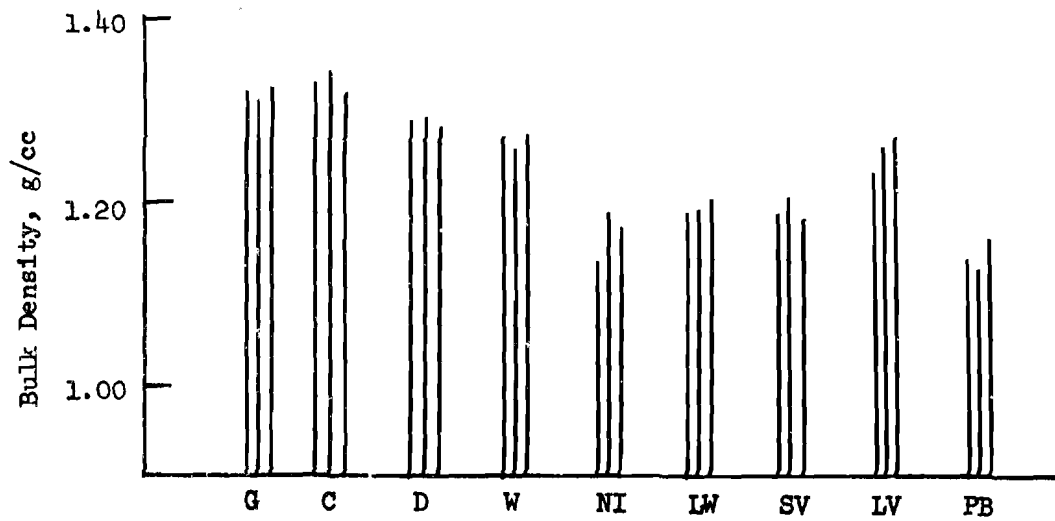


Figure 104. Bar Graph of Nondestructive Test Measurements on Pyrolyzed VYB 70 1/2 - SC1008 Tensile Specimens

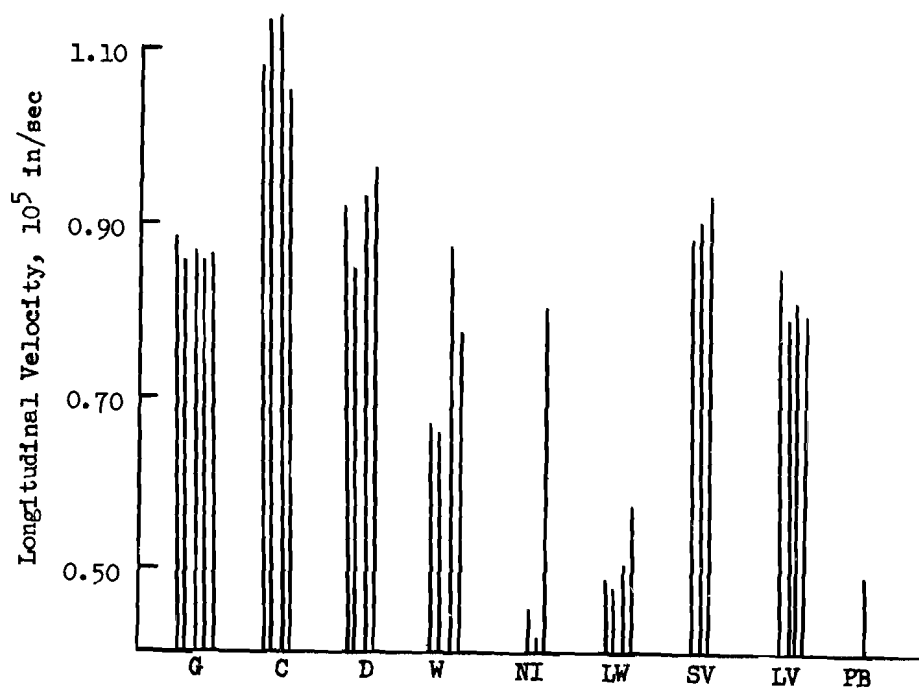
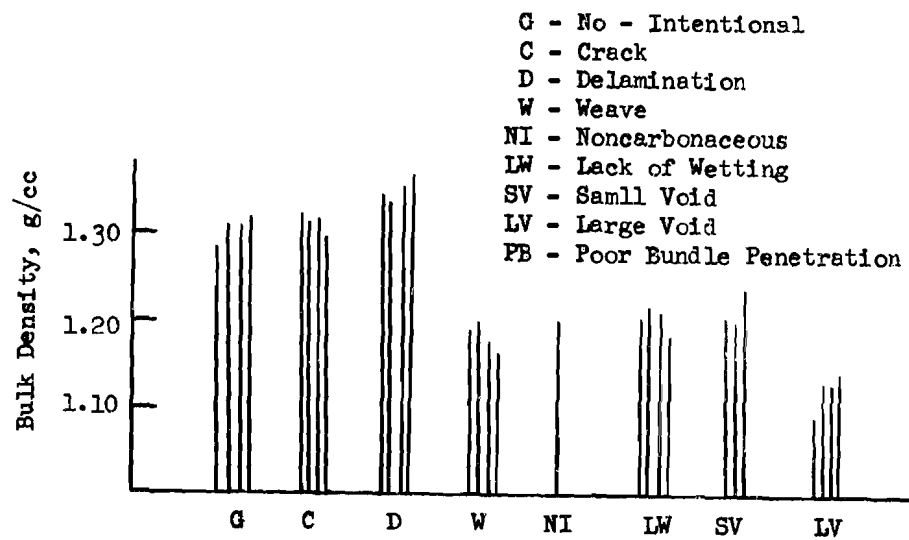


Figure 105. Bar Graph of Nondestructive Test Measurements on Pyrolyzed VYB 70 1/2 - SC1008 Shear Test Specimens

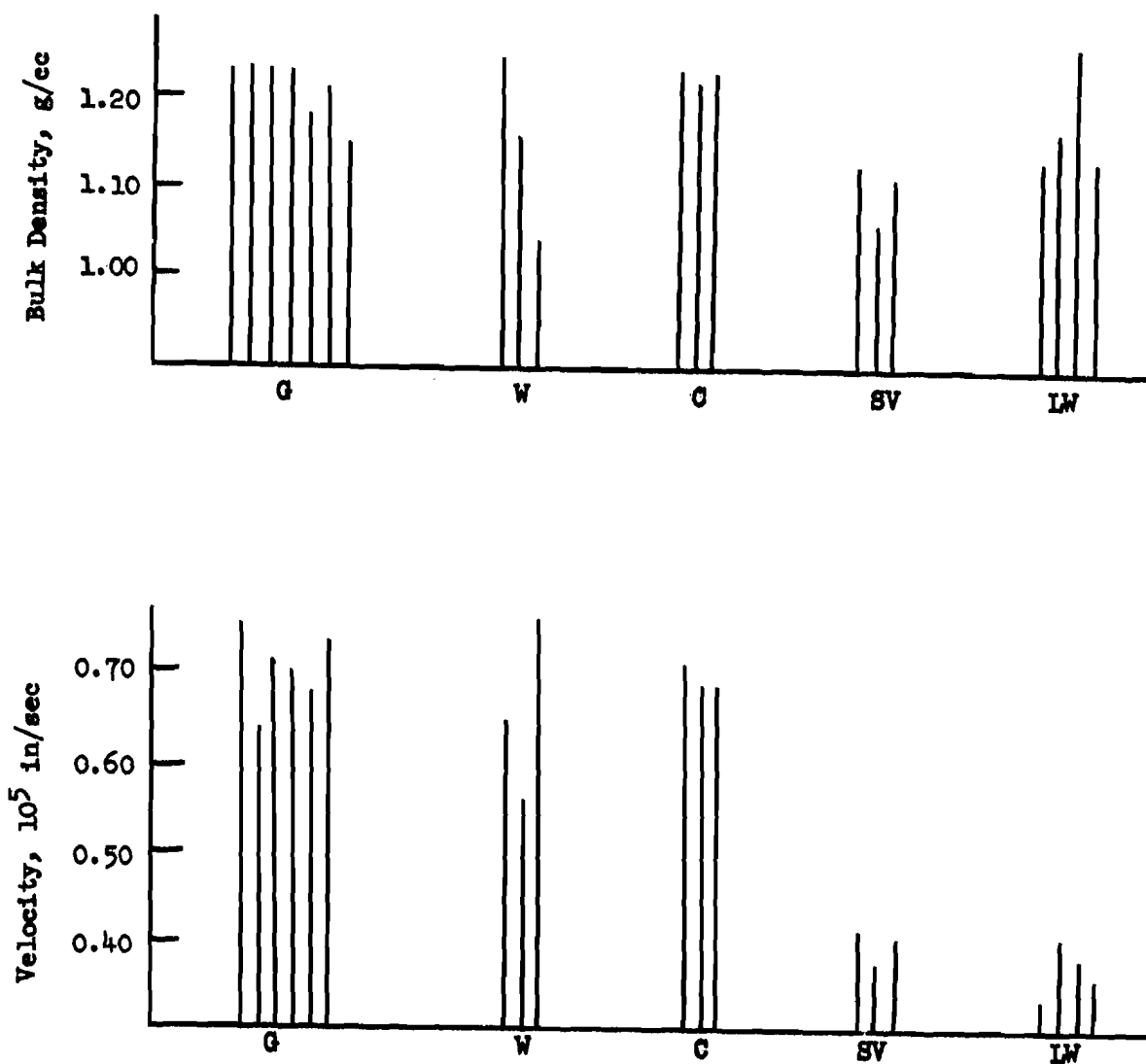


Figure 106, Bar Graph of Nondestructive Test Measurements of Graphitized VYB 70 1/2 - SC1008 Tensile Specimens



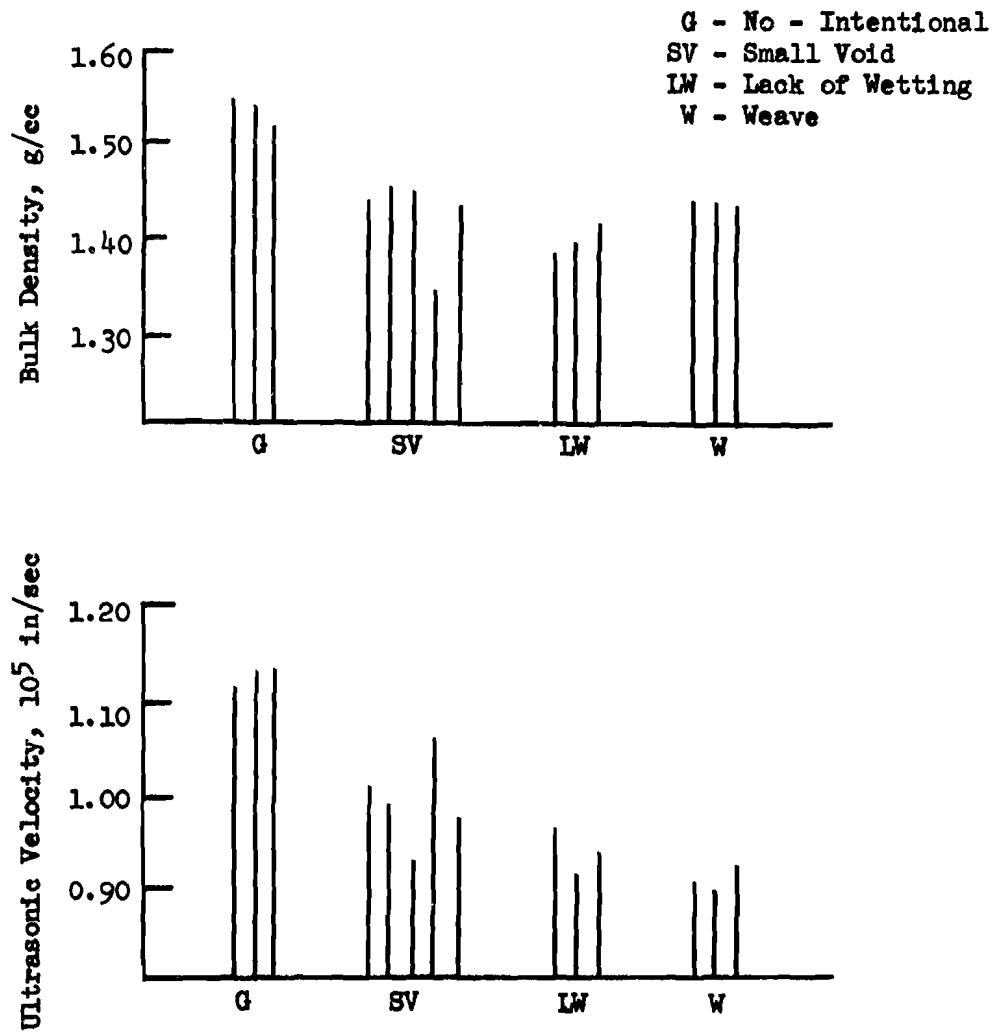


Figure 108. Nondestructive Test Measurements on Pyrolyzed  
VYB 70 1/2 - Pitch Tensile Specimens

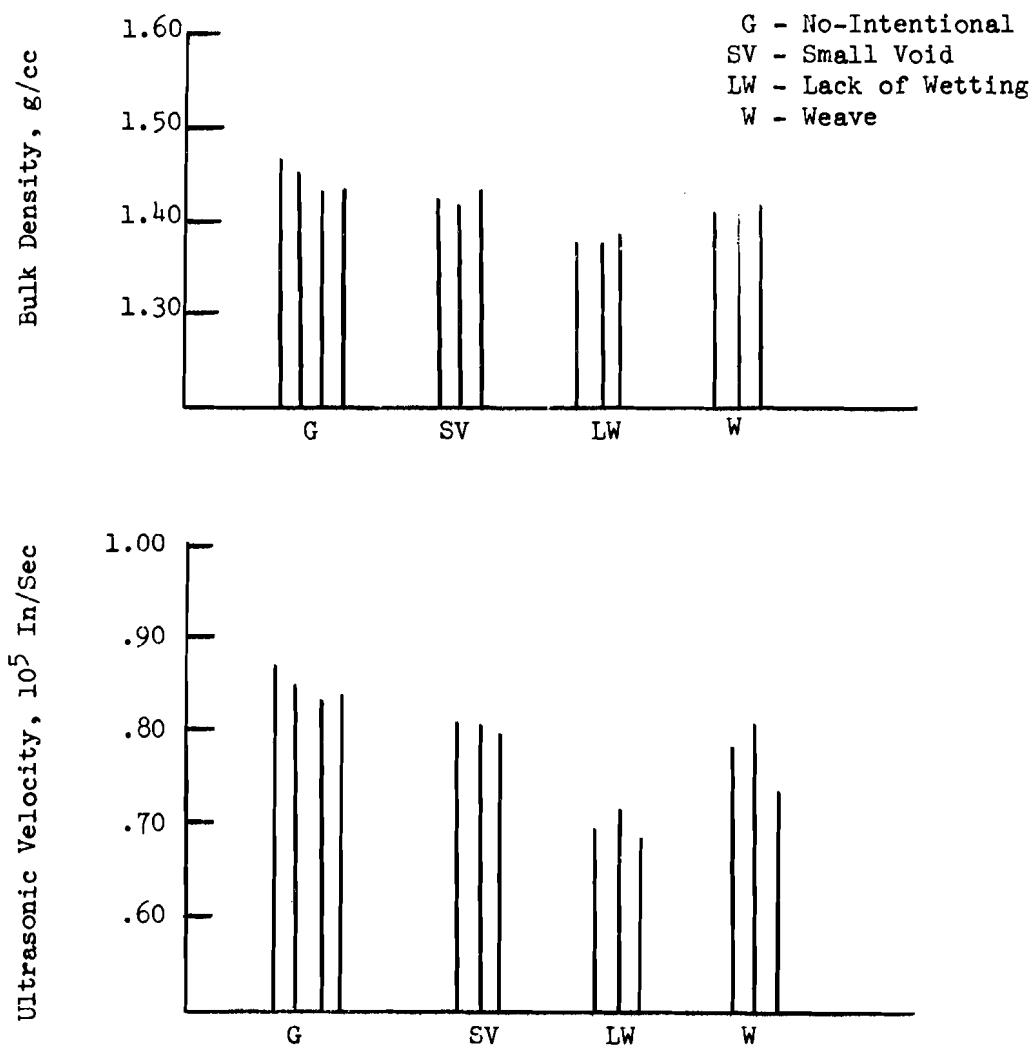


Figure 109. Nondestructive Test Data on Graphitized  
VYB 70 1/2 - Pitch Tensile Specimens

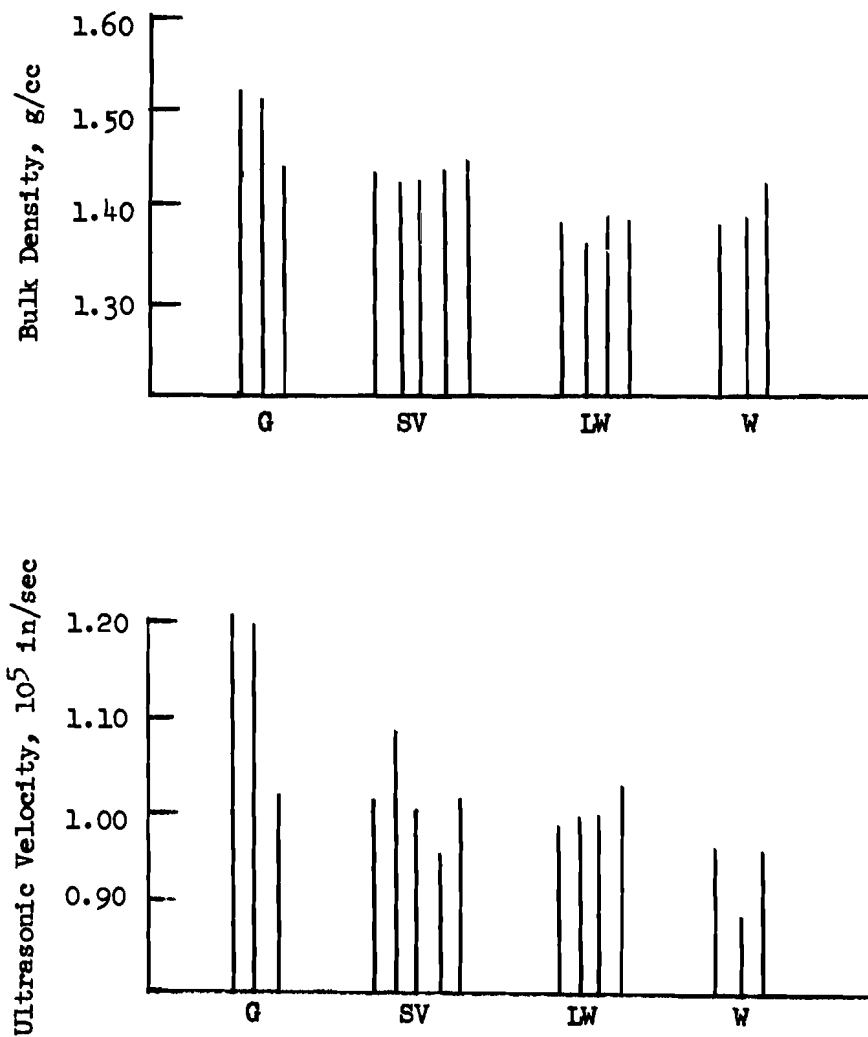


Figure 110. Nondestructive Test Measurements on Pyrolyzed VYB 70 1/2 - Pitch Shear Specimens



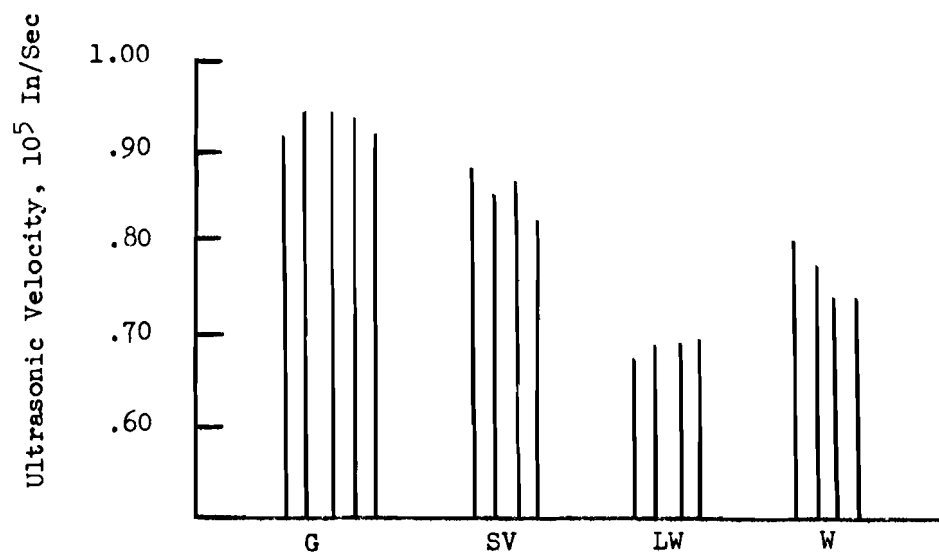
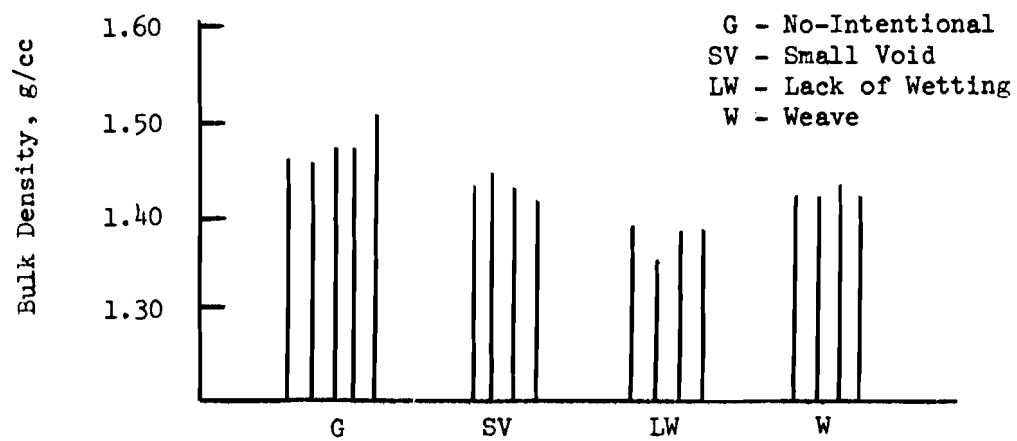


Figure 111. Nondestructive Test Data on Graphitized VYB 70 1/2 - Pitch Shear Specimens

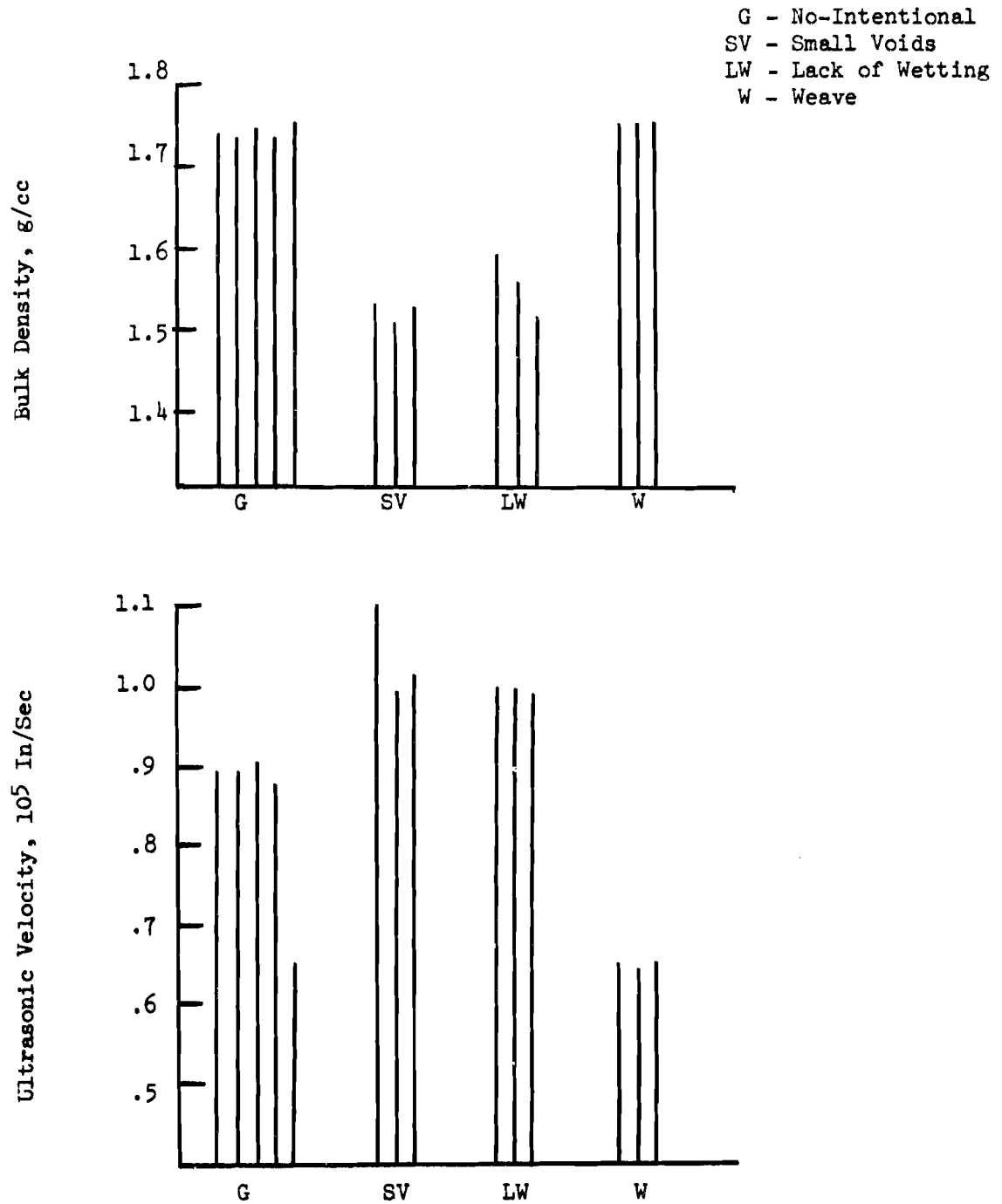


Figure 112. Nondestructive Test Data on Pyrolyzed  
Modmor II - Pitch Tensile Specimens

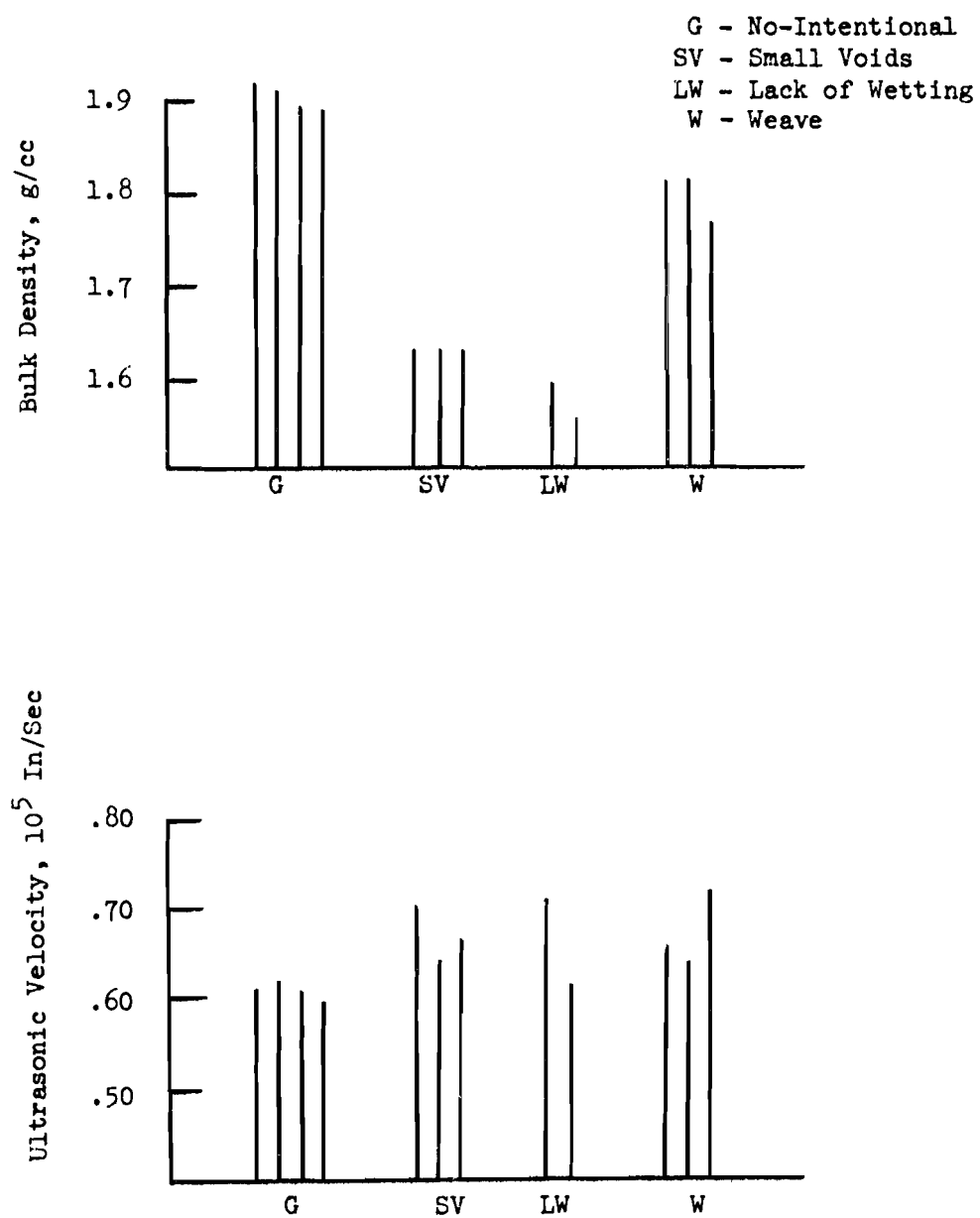


Figure 113. Nondestructive Test Data on Graphitized  
Modmor II - Pitch Tensile Specimens

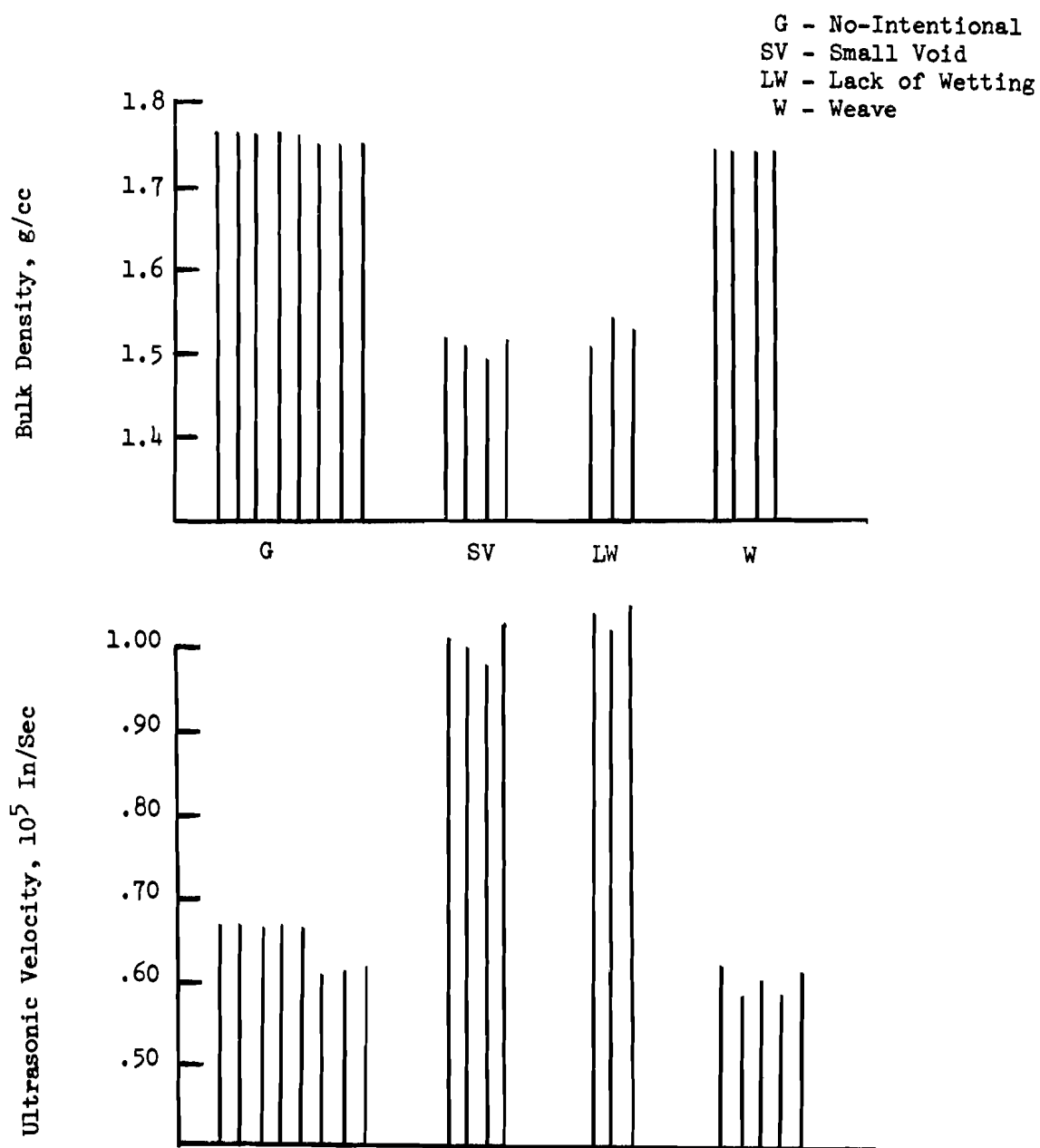


Figure 114. Nondestructive Test Data on Pyrolyzed  
Modmor II - Pitch Shear Specimens

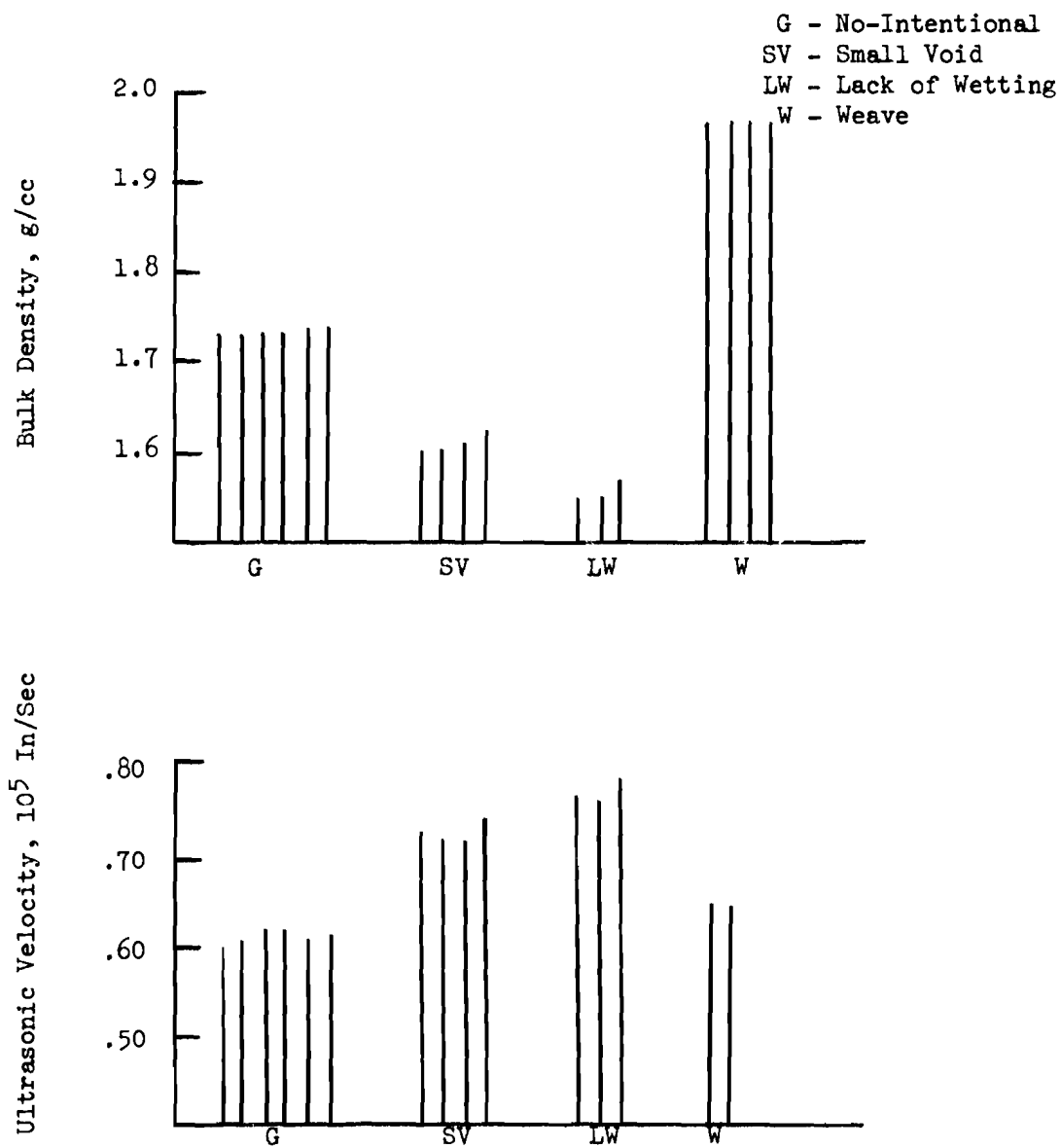


Figure 115. Nondestructive Test Data on Graphitized  
Modmor II - Pitch Shear Specimens

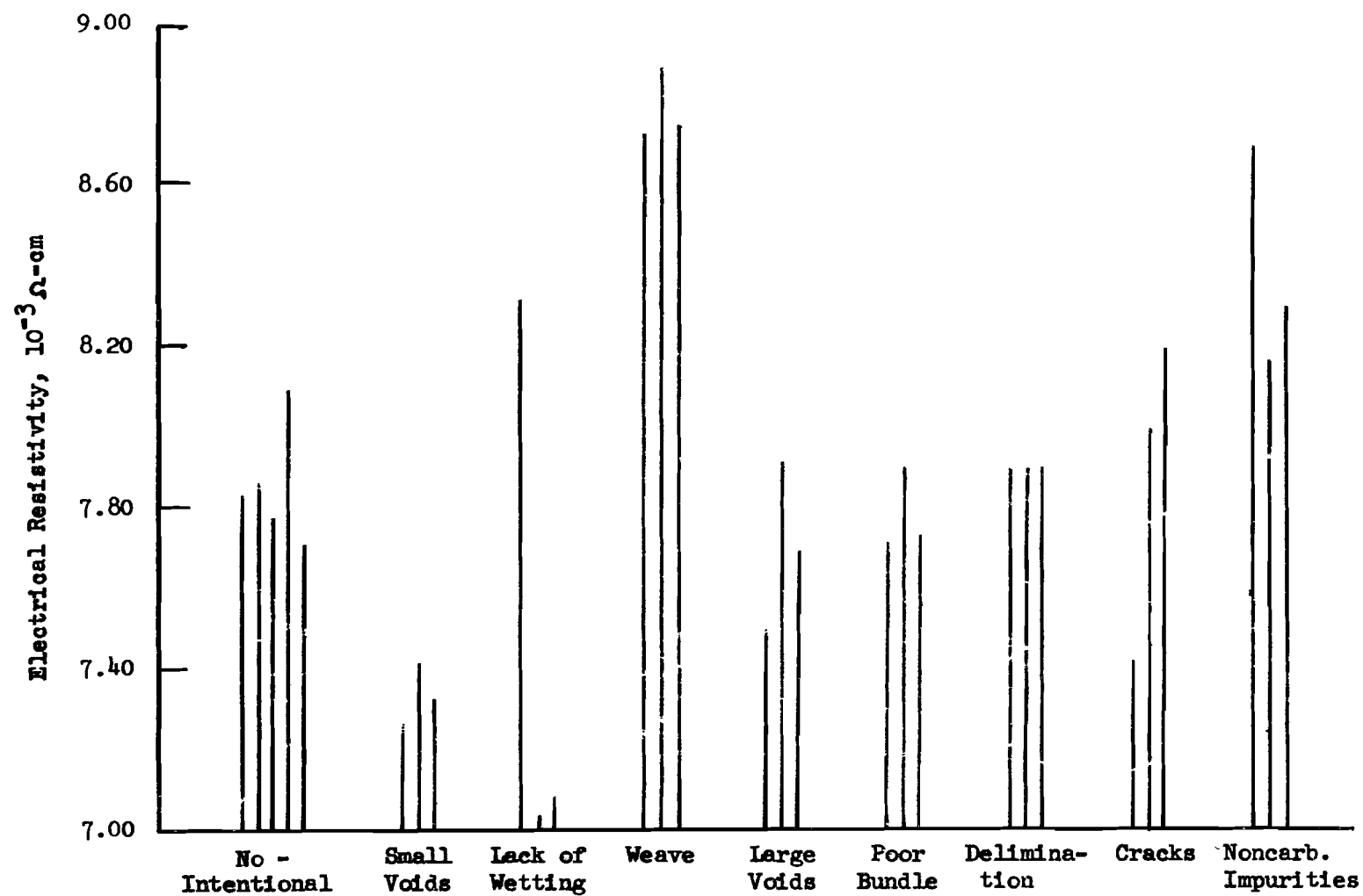


Figure 116. Electrical Resistivity of Pyrolyzed VYB 70 1/2 - SC1008 Composite Tensile Specimens

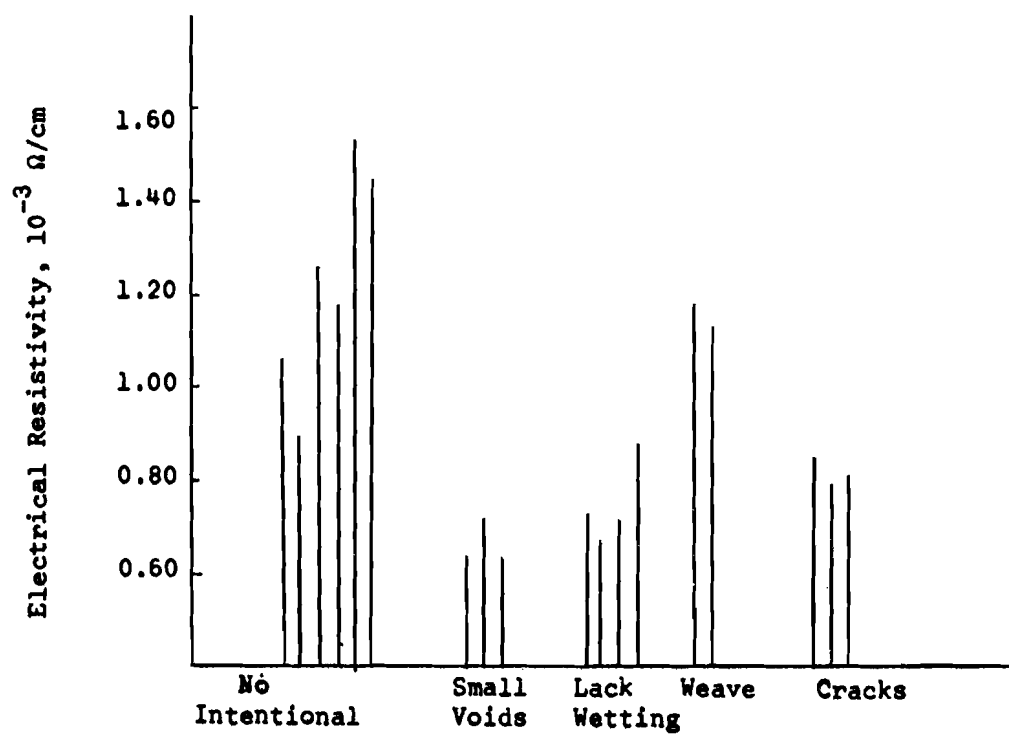


Figure 117. Electrical Resistivity of Graphitized  
SC1008-VYB 70 1/2 Tensile Specimens

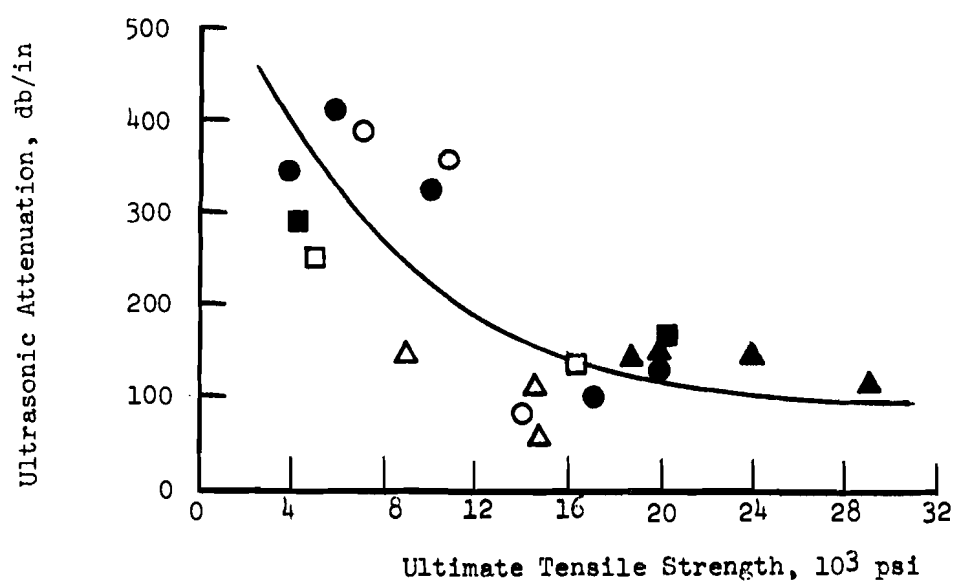
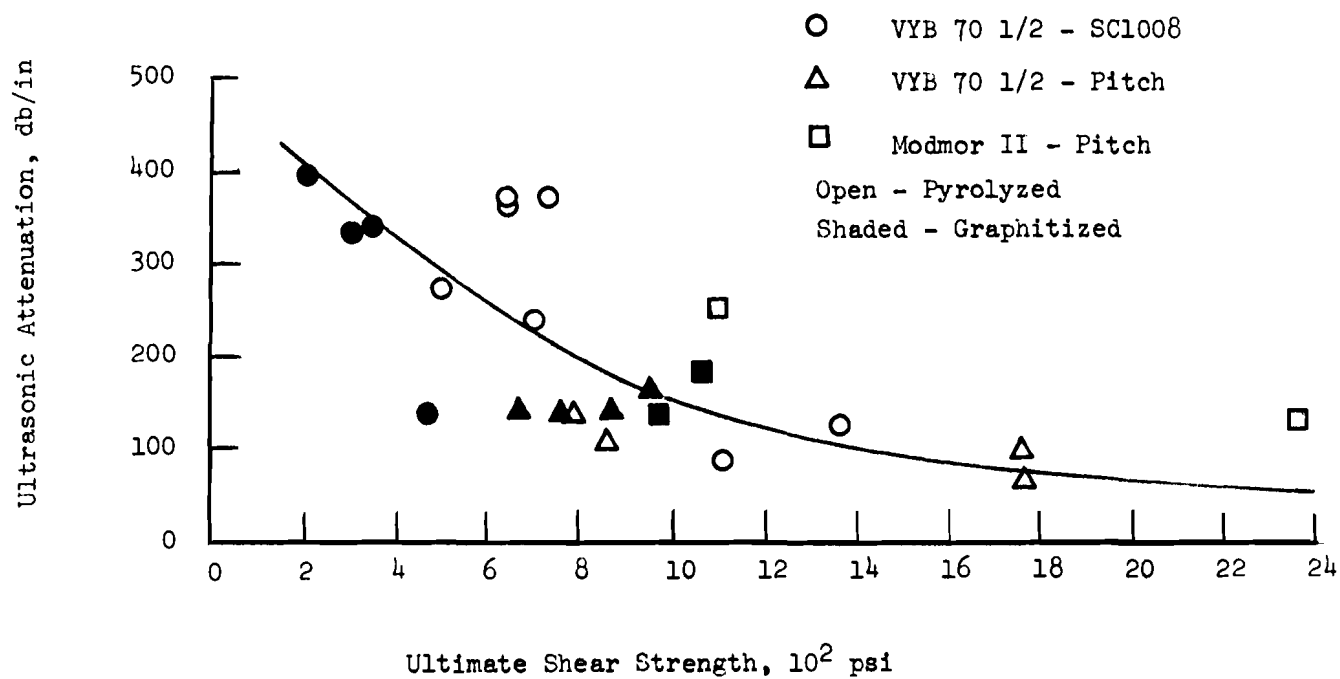


Figure 118. Attenuation Versus Composite Strengths



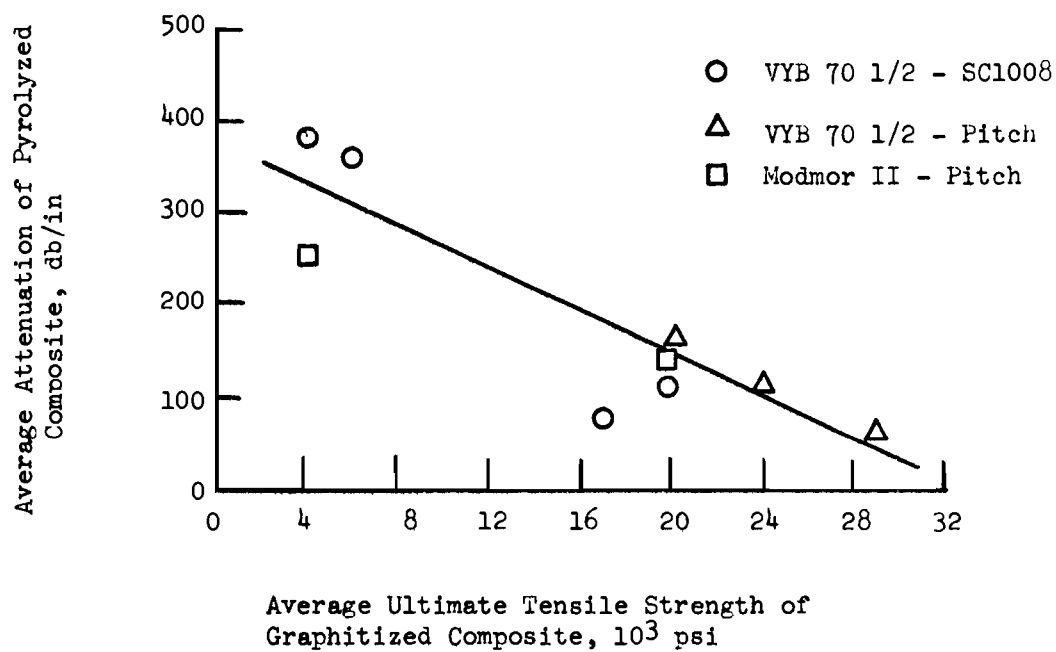
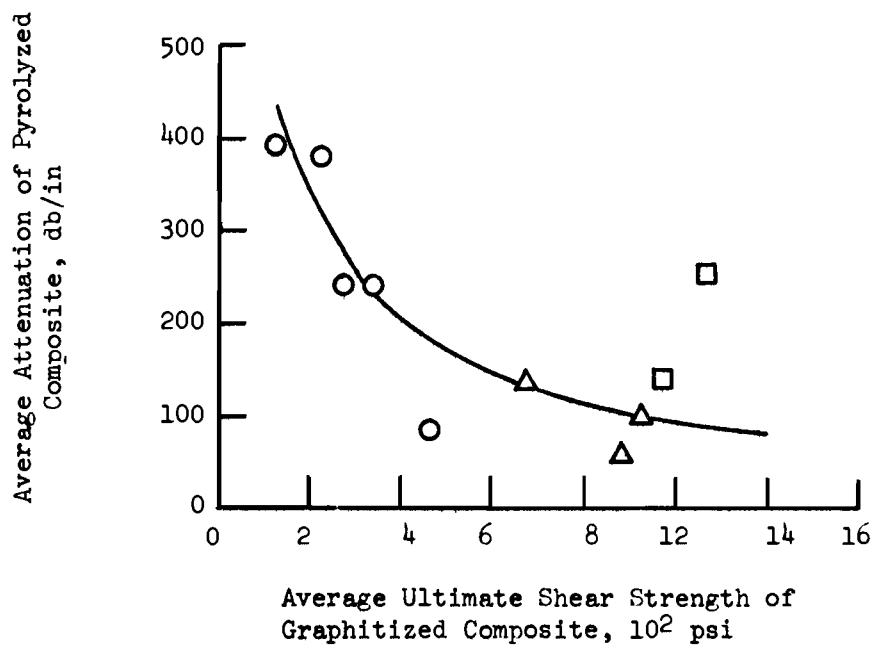


Figure 119. Attenuation of Pyrolyzed Composite Versus Strength of Graphitized Composite

TABLE XXVI

PERCENTAGE CHANGE IN AVERAGE ELECTRICAL RESISTIVITY VALUES  
FOR PYROLYZED AND GRAPHITIZED VYB 70 1/2 - SC1008 COMPOSITE

Average Electrical Resistivity, $10^{-3}$ $\Omega$ -cm			
Defect	Pyrolyzed	Graphitized	Percentage Change, %
No-Intentional	7.86	1.23	640
Small Void	7.34	.67	1100
Lack of Wetting	7.46	.75	990
Weave	8.80	1.26	700
Cracks	7.87	1.02	770

(approximately 10 db/in for these specimens); thus, for Figures 118 and 119, a difference in the attenuation values of 30 db/in is significant.

Relationships between the ultrasonic longitudinal velocity measured through the thickness direction (perpendicular to fibers) and the tensile properties in the fiber direction were not apparent. The scatter in the data obscured any trends. The properties which may be controlling the tensile properties of the composites, such as the amount and strength of the bond between matrix and filament, are difficult to detect by velocity measurements. The controlling effect of the fiber-matrix bond was suggested in the scanning and electron fractography results obtained on the SC1008 and pitch composites. (A subtle difference exists between monitoring lack of fiber bundle wetting by velocity measurements which was successful and monitoring the amount and strength of the bond between each individual filament of the bundle. In the former case the lack of wetting of the fiber bundle refers to voids immediately adjacent to the fiber bundles).

The velocity measurements were related to the shear strength of the VYB 70 1/2 - SC1008 and Modmor II - pitch unidirectional composites (Figure 120). The scatter in the VYB 70 1/2 - pitch composite data did not suggest any trends. This was partly due the change in processing procedures for these composites. The trends that existed suggested higher velocity corresponding to higher strengths.

The ultrasonic longitudinal velocity ( $V_{11}$ ) measured through the thickness of the composite was correlated to Young's modulus in the fiber direction. It is important to realize that theory states that the elastic stiffness constant in the fiber direction is calculated from the longitudinal velocity measured in the fiber direction (Reference 13).

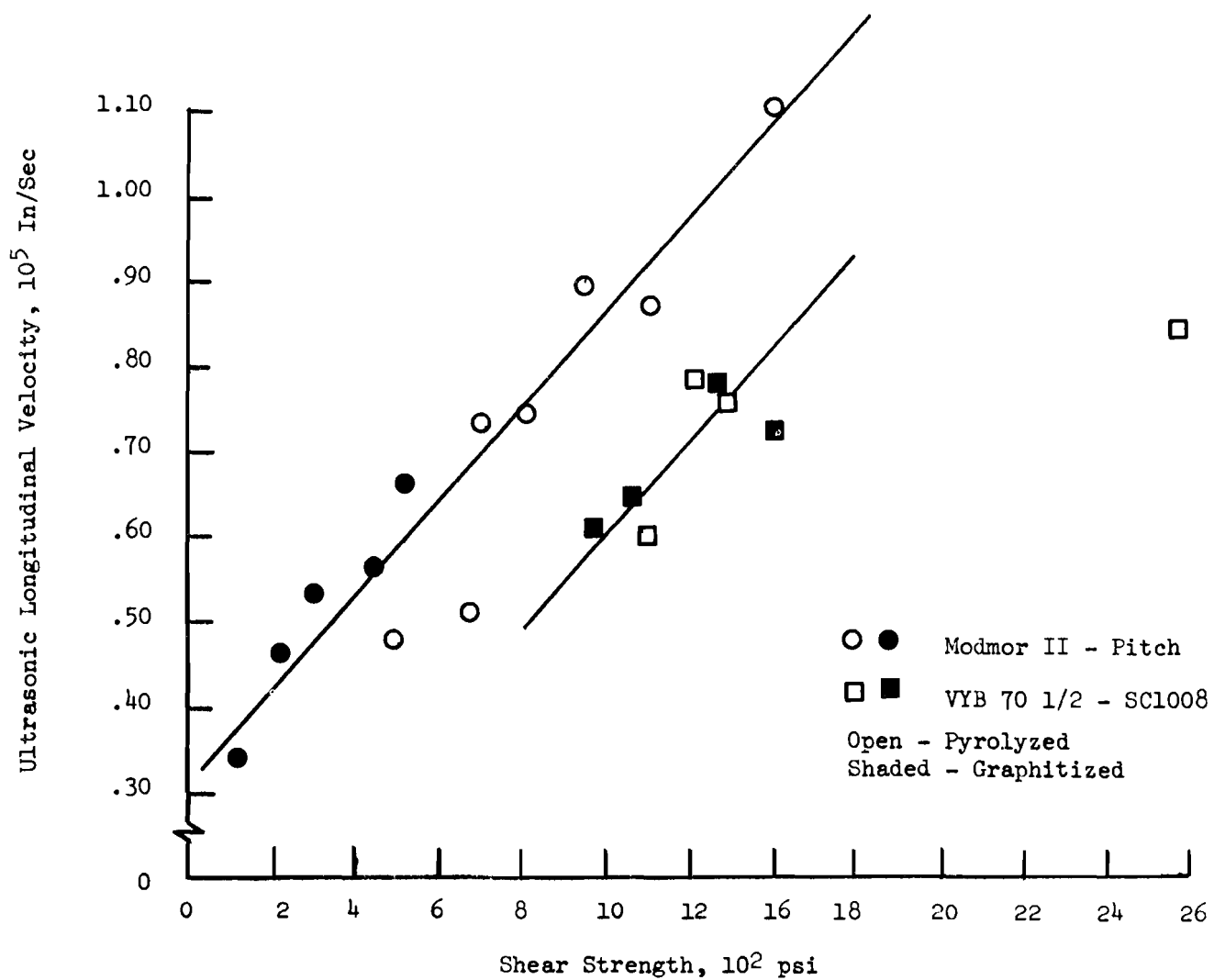


Figure 120. Ultrasonic Longitudinal Velocity Versus Shear Strength  
 For The VYB 70 1/2 - SC1008 and Modmor II - Pitch Composites

The equation for this calculation is

$$V_{33} = (C_{33}/\rho)^{1/2}$$

were

$V_{33}$  = longitudinal velocity in fiber direction

$C_{33}$  = elastic stiffness constant in fiber direction

$\rho$  = density

To calculate Young's modulus, the inverse of the elastic compliance constant,  $1/E = S_{33}$ , it is necessary to obtain all the elastic stiffness constants,  $C_{11}$ ,  $C_{12}$ ,  $C_{13}$ ,  $C_{44}$  and  $C_{33}$ , for the unidirectional fiber composite. Five constants are necessary since the unidirectional composite possesses hexagonal symmetry. The elastic compliance matrix is the inverse of the elastic stiffness matrix. It is expected that the ratio of  $C_{33}/C_{11}$ , where  $C_{11} = \rho V_{11}^2$  is the stiffness constant normal to the fibers, should remain constant for a given composite of constant fiber volume fraction and fiber and matrix Poisson's ratio. Therefore, velocity values,  $V_{11}$ , may be related to the modulus in the fiber direction by a proportionality constant. With the introduction of defects the ratio  $C_{33}/C_{11}$  is not expected to remain the same (since changes in Poisson's ratio of the matrix occur), however, the magnitude of the changes may be small enough to allow correlations between velocity ( $V_{11}$ ) and modulus ( $1/S_{33}$ ) to be made.

The graph of dynamic modulus ( $\rho V_{11}^2$ ) normal to the fiber direction versus Young's modulus as determined by mechanical testing for the pyrolyzed and graphitized composites is shown in Figure 121. No trends were evident for the Modmor II - pitch composites. The in-process prediction of Young's modulus of the graphitized composite from measurements of the dynamic modulus ( $\rho V_{11}^2$ ) on the pyrolyzed composites was very successful (Figure 122). It is suggested that the in-process prediction of material properties using velocity measurements is possible.

A limited evaluation of the Thornel 50 - pitch composites was conducted to determine the merit and effect of using an X-ray absorbing doping agent or electronic processing for improving X-ray sensitivity. The use of a tetrabromoethane (TBE) dopant was very successful in providing increased detect sensitivity in Poco graphites (Reference 11). Therefore, the TBE dopant was selected for evaluation in the carbon-carbon composites. The method of electronic processing of the X-ray negatives was by a commercial unit (LogEtronic). The experimental work in performing the electronic enhancement and X-ray dopant impregnation and X-ray radiography was accomplished at the Air Force Materials Laboratory.

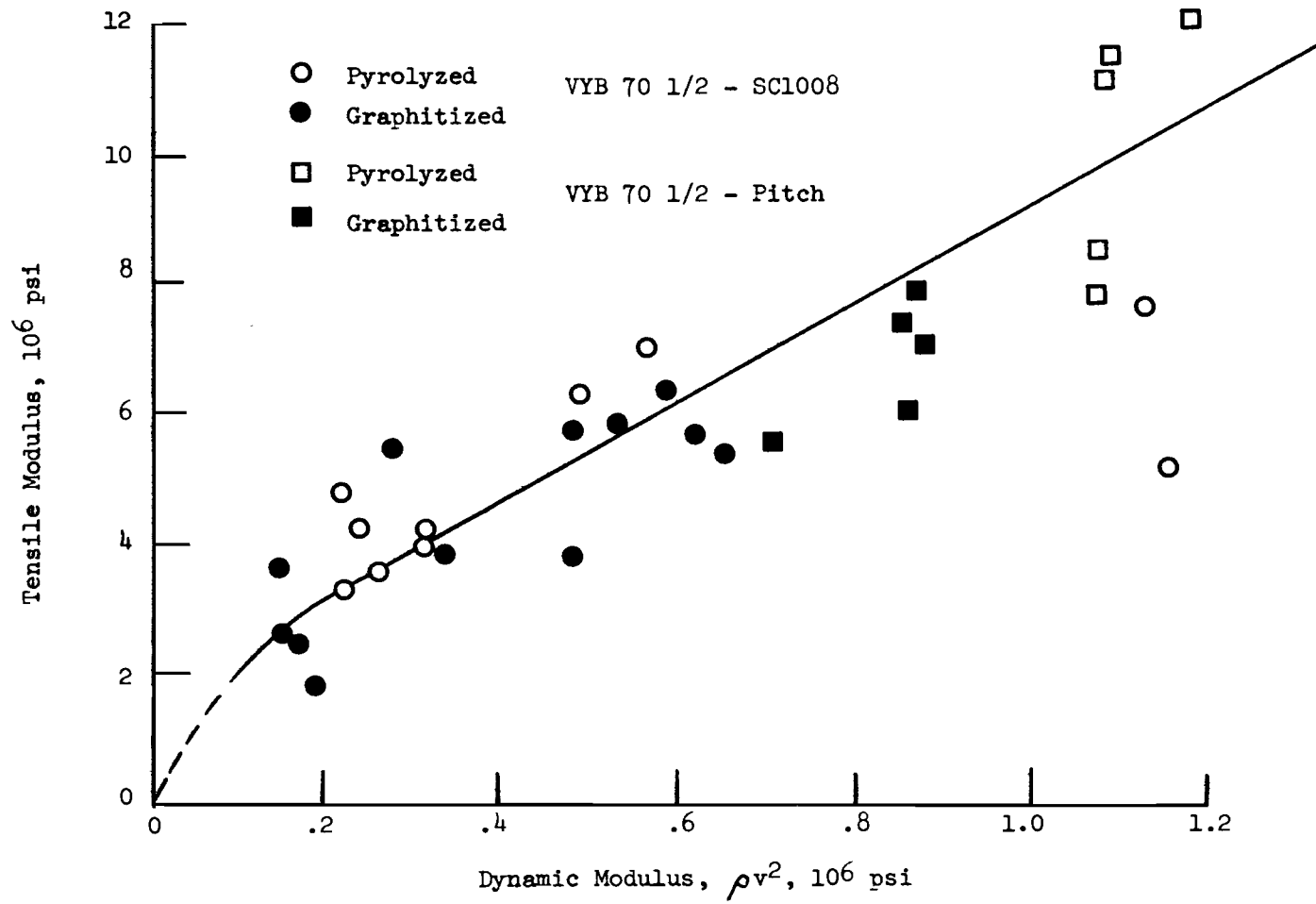


Figure 121. Dynamic Modulus Versus Tensile Modulus of VYB 70 1/2 - SC1008 and Modmor II - Pitch Composites

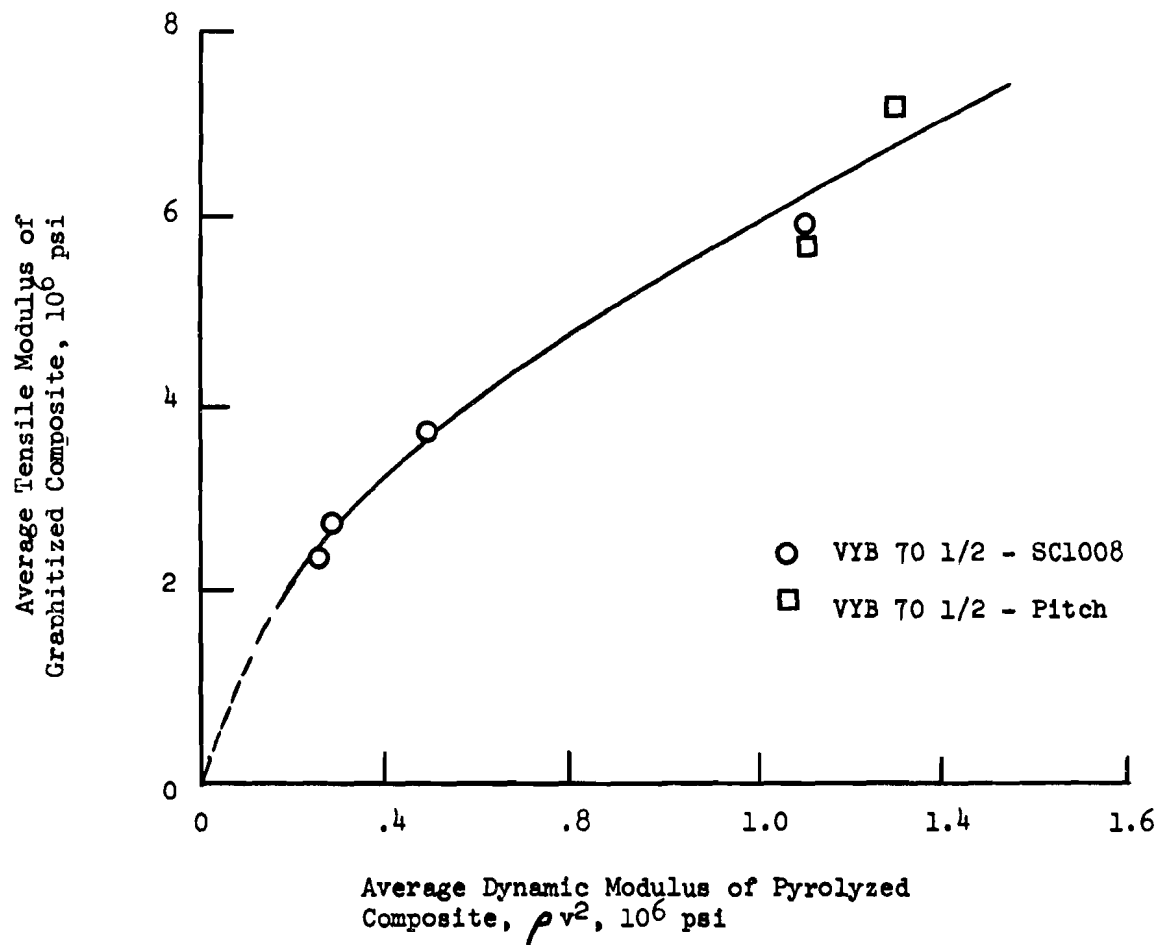


Figure 122. Dynamic Modulus of Pyrolyzed Composite Versus Tensile Modulus of Graphitized VYB 70 1/2 - SC1008 and VYB 70 1/2 - Pitch Composites

Figure 123 shows a comparison of a normal X-ray radiograph (prior to TBE treatment), LogEtronic enhancement of the normal X-ray and TBE doped X-ray radiographs. The specimens included in this figure were a low-strength (17) and a higher strength (32) specimen. The interpretation of the radiographs suggested that the LogEtronic processing offered some additional defect information and the TBE more. The use of the TBE dopant was limited when gross defects existed. These defects absorbed a large amount of dopant and washed out detail which would otherwise be present. However, when a more uniform specimen was examined, the TBE provided significantly more defect information than normal X-ray radiography techniques.

## 6.2 Multidirectional Composites

The mechanical testing of the DACLOCK 120 multidirectional composite consisted of tension tests in the warp direction and compression tests in the fill direction. The warp and fill composite directions have been described in Figure 2. The tests were conducted on the no-intentional-defect specimens after final pyrolysis and after final graphitization while the defect specimens were tested only after the final pyrolysis.

### 6.2.1 Test Techniques

The uniaxial tension tests were performed by friction gripping of dog bone tensile specimens in an Instron Universal Testing machine. The test specimen was designed to provide a cross-sectional area which would include a minimum of three unit cells of the composite (Figure 124) in the thickness.

The friction gripping technique was possible due to the increased strength in the third direction provided by the multidirectional reinforcement. Strains were monitored by averaging the response of two strain gages located on opposite sides of the specimen at the midpoint of the gage section. The tests were conducted at a crosshead rate of 0.02 inches per minute.

Compression tests were conducted in an Instron machine using an ASTM D695-63T compression test fixture to insure proper alignment. A rectangular test specimen 1.00 x 0.40 x 0.40 inches was used. The tests were conducted at a crosshead rate of 0.02 inches per minute. As in the tension tests, two strain gages on opposite sides of the specimen were used to monitor strain.

### 6.2.2 Mechanical Test Results

The tension and compression test results are presented (Table XXVII) and discussed with respect to correlations which existed with the porosity and non-destructive test data. A complete tabulation of mechanical test results is presented in Appendix II.

Specimen 17



a) Normal X-Ray Radiograph



b) LogEtronic Enhancement



c) Tetrabromoethane Dopant

Specimen 32



a) Normal X-Ray Radiograph



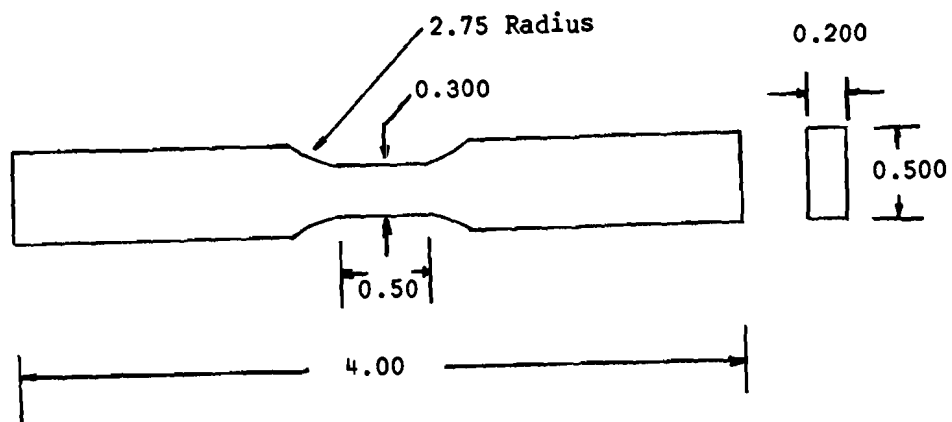
b) LogEtronic Enhancement



c) Tetrabromoethane Dopant

Figure 123. X-Ray Radiographic Enhancement Evaluation





All Dimensions in Inches

Tolerances

.XX  $\pm$  .03

.XXX  $\pm$  .005

Figure 124. Tension Test Specimen Design for  
Multidirectional Composite

Table XXVII

AVERAGE MECHANICAL PROPERTIES OF MULTIDIRECTIONAL  
DACLOCK 120 COMPOSITE

Defect Group	Condition	Tension			Compression		
		Strength, (psi)	Secant <sup>(1)</sup> Modulus, (10 <sup>6</sup> psi)	Strain to Failure, (%)	Strength, (psi)	Secant Modulus, (10 <sup>6</sup> psi) <sup>(1)</sup>	Strain to Failure (%)
No-Intentional <sup>(2)</sup>	Pyrolyzed	3200	2.6	.13	16,300	1.2	1.4
	Graphitized	3960	2.6	.15	9,400	0.8	1.2
Small Void <sup>(3)</sup>	Pyrolyzed	4260	3.6	.12	6,200	1.0	0.7
Lack of Wetting <sup>(3)</sup>	Pyrolyzed	5100	2.3	.20	9,100	1.0	0.9
Weave <sup>(3)</sup>	Pyrolyzed	4440	2.9	.15	10,200	1.2	0.9

(1) Calculated from Strain-to-Failure.

(2) Average of five tests.

(3) Average of three tensile and four compression tests.

The tensile stress-strain curves were all essentially linear to failure. The compression curves, however, deviated slightly from linearity. Typical compression stress-strain curves for each defect group are shown in Figure 125.

The compressive strengths and strains-to-failure were reduced by the presence of all defects, small void, lack of wetting and weave. The modulus decreased slightly for the small void and lack of wetting specimens. The weave defect examined in these tests was the irregular (wider) spacing of the fill yarns (Reference 1). This irregular spacing was parallel to the compressive load axis. Upon final graphitization, the compressive strengths of the no-intentional-defect specimens decreased 42 percent, the modulus decreased 35 percent, and the strain to failure 14 percent.

In addition to the mechanical tests on the defect study specimens, compressive tests were conducted on specimens which had undergone other pyrolysis-graphitization sequences. This study consisted of evaluating the effect of the number of impregnation and pyrolysis sequences, the graphitization step and the location of graphitization steps in the sequence (midpoint in cycle, final or both). A detailed discussion of this effort is contained in Reference 1; however, the main conclusions will be presented below. A summary of the data and processing sequences evaluated is contained in Table XXVIII.

The compression tests were conducted in the three principal composite directions from selected process systems. The results indicated that the compressive properties in the warp, fill and radial directions were very similar. This suggests that the pores present within the composite were not oriented along any one direction.

The influence of the graphitization step is clearly shown by Figure 126 where failure stress is plotted as a function of failure strain. The process evaluation test specimens are indicated by the squares while the specimens devoted to the intentional defect study are indicated by circles in the figure. The trade-off is clearly shown between doubling the strength with half the strain capability for the pyrolyzed composites or doubling the strain and halving the strength for the pyrolyzed and graphitized composites. The lower values of strain and stress were usually for samples that received fewer impregnations. The compressive strengths of the highest strength pyrolyzed composites ranged from 23,000 to 29,000 psi with strains of 0.8 to 0.9 percent. The highest strength graphitized composites had compressive strengths ranging from 15,000 to 18,000 psi with strains of 1.1 to 1.6 percent. These specimens were processed by the two pyrolysis (2P) - graphitization (G) - three pyrolysis (3P) sequence described in Section 3.0.

The graphitization step, whether at the midpoint of the processing cycle or at the end, reduced the compressive strengths below the pyrolyzed values. A final graphitization step reduced the strengths more than a midpoint graphitization.

The tensile properties, strength and modulus, actually increased with the presence of the intentional defects (Table XXIX). The highest strengths were achieved with the lack of wetting defect, 5100 psi average tensile strength. The strain to failures values were approximately the same for the defect groups except for the small void. The weave defect, irregular spacing, was oriented perpendicular to the loading axis.

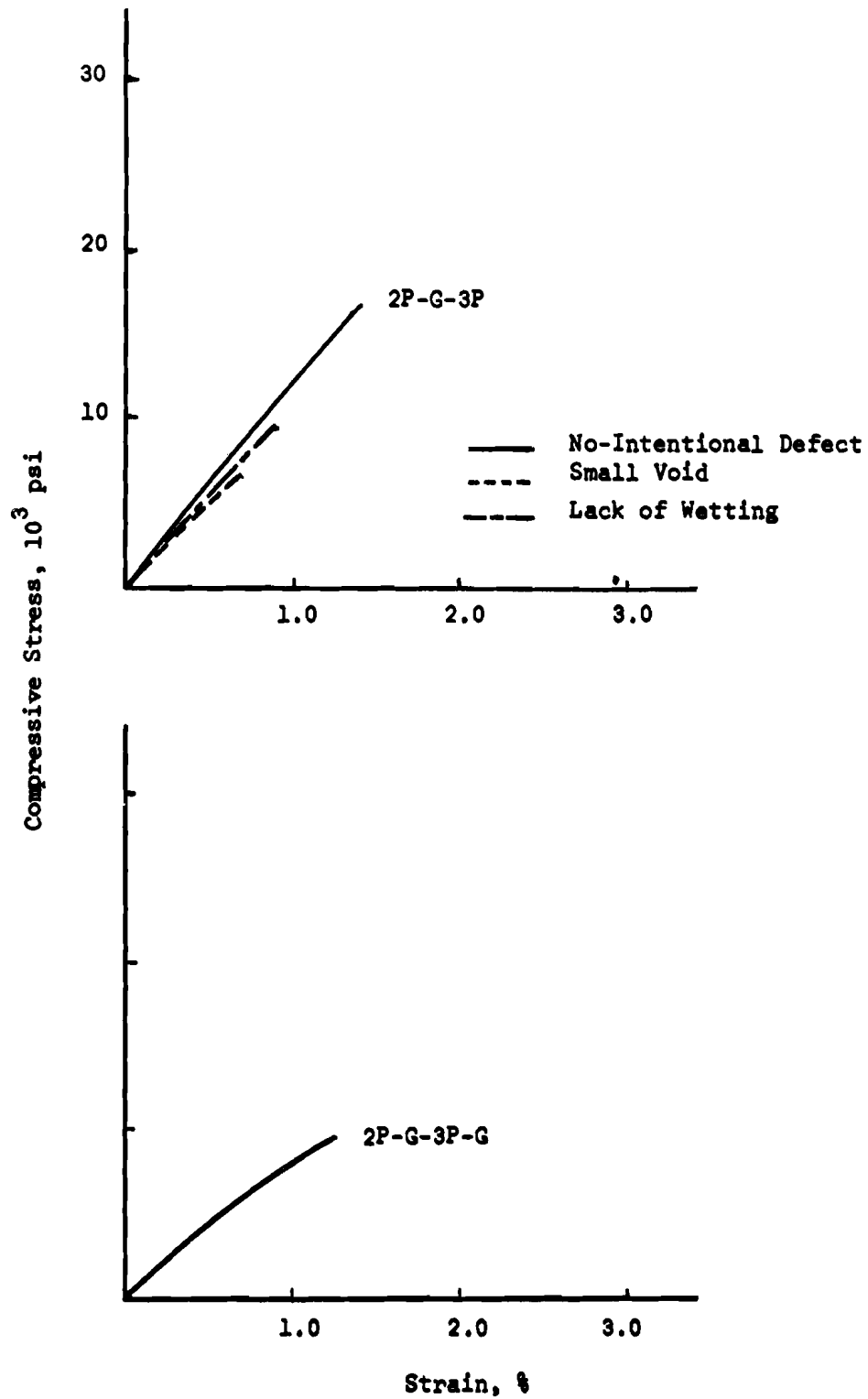


Figure 125. Compressive Stress-Strain Curves for VYB 70 1/2-Pitch Multidirectional Composite

Table XXVIII

## SUMMARY OF PROCESS CHARACTERIZATION DATA FOR MULTIDIRECTIONAL COMPOSITE

Processing <sup>(1)</sup> Conditions	Mercury Porosimetry			Ultimate Compression Strength		Compressive Modulus		Strain to Failure	
	Bulk Density (gm/cc)	Apparent Density (gm/cc)	Porosity (%)	Average (psi)	Range (psi)	Average (10 <sup>6</sup> psi)	Range (10 <sup>6</sup> psi)	Average (in/in)	Range (in/in)
2P	--	--	--	17,100	15,900 to 18,800	--	--	--	--
2P	--	--	--	4,300	3,300 to 6,200	1.20	0.41 to 2.8	0.0069	0.0018 to 0.0120
1P	--	--	--	12,600	10,300 to 15,000	3.3	2.0 to 4.5	0.0025	0.0015 to 0.0035
4P	1.57	1.70	7.4	11,900	10,300 to 13,700	2.9	1.7 to 2.3	0.0069	0.0052 to 0.0108
3P	1.50	1.56	3.9	21,900	19,000 to 25,400	2.5	2.3 to 2.7	0.0038	0.0012 to 0.0055
4P	1.62	1.68	3.7	24,000	22,600 to 25,800	3.1	2.8 to 3.2	0.0071	0.0068 to 0.0076

(1) P - Impregnation and Pyrolysis

G - Graphitization

Table XXVIII (Continued)

Processing Conditions <sup>(1)</sup>	Mercury Porosimetry			Ultimate Compression Strength		Compressive Modulus		Strain to Failure	
	Bulk Density (gm/cc)	Apparent Density (gm/cc)	Porosity (%)	Average (psi)	Range (psi)	Average (10 <sup>6</sup> psi)	Range (10 <sup>6</sup> psi)	Average (in/in)	Range (in/in)
4P	1.56	1.64	4.7	26,000	23,300 to 28,800	3.2	3.1 to 3.4	0.0087	0.0076 to 0.0094
2P-G-2P	1.55	1.65	6.1	9,700	8,700 to 10,200	1.3	1.3	0.0077	0.0048 to 0.0106
3P-G-P	1.67	1.82	8.0	13,000	12,300 to 13,500	0.87	0.85 to 0.89	0.0154	0.0136 to 0.0172
2P-G	—	—	—	9,500	7,400 to 11,600	—	—	—	—
2P-G	—	—	—	3,100	3,000 to 3,200	2.0	1.7 to 2.3	0.0043	0.0020 to 0.0066
1P-G	—	—	—	3,200	—	0.80	—	0.0041	—
4P-G	1.62	1.87	13.5	4,000	3,200 to 4,300	0.87	0.60 to 1.1	0.0061	0.0036 to 0.0104

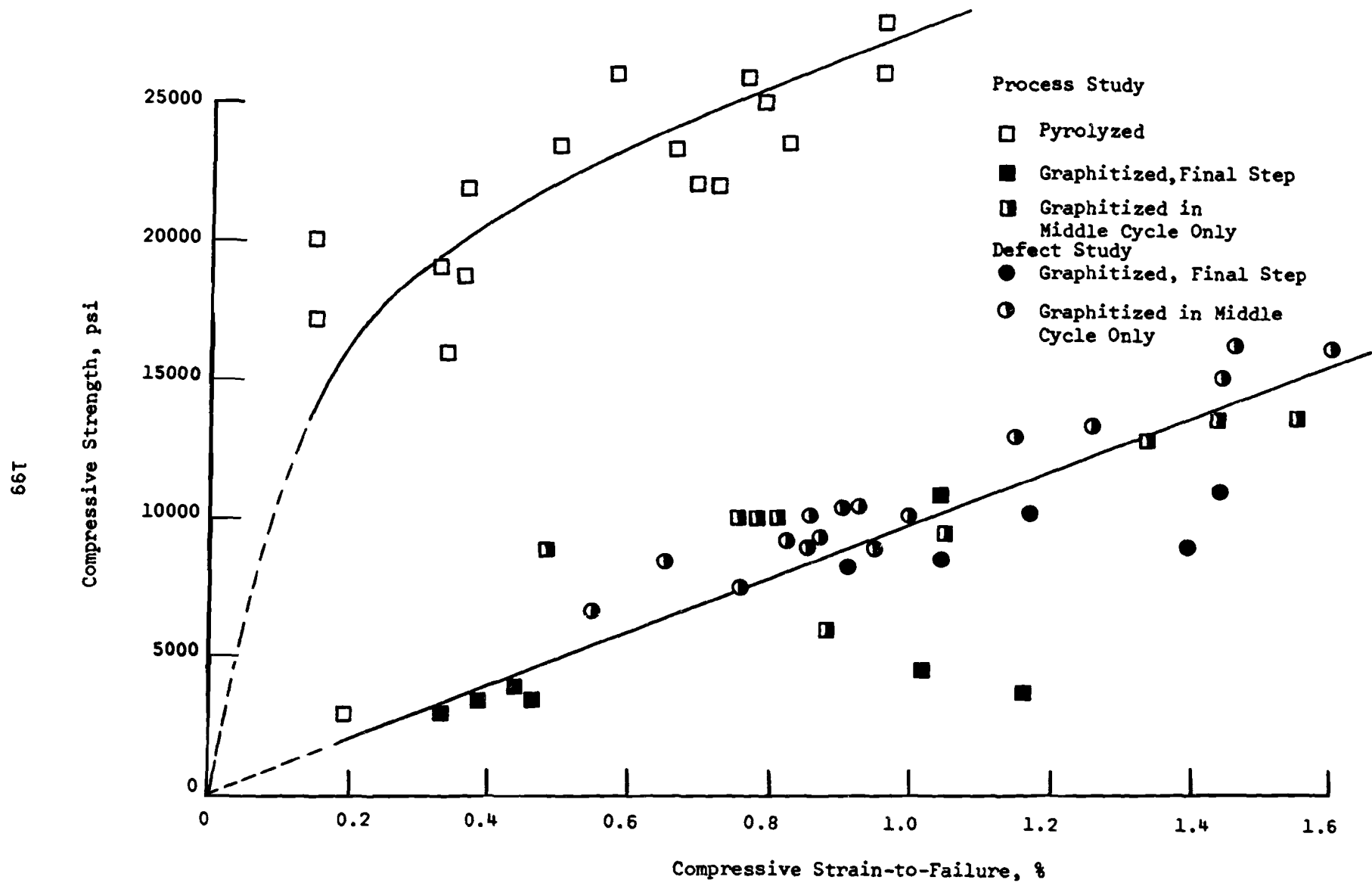


Figure 126. Compressive Strength Versus Strain-to-Failure for Multidirectional Composite

Table XXIX

## NONDESTRUCTIVE TEST DATA ON MULTIDIRECTIONAL TEST SPECIMENS

Specimen	Condition	Description	Defect	Longitudinal Velocity, ( $10^5$ in/sec)	Bulk Density, (g/cc)
3D74 T1	Pyrolyzed	Tension	No-Intentional	0.88	1.60(1)
T2				0.85	1.60
3D71 T3				0.81	1.60
T4				0.82	1.60
T5				0.80	1.60
3D69 T1	Pyrolyzed		Small Void	0.49	1.30(1)
T2				0.58	1.30
T3				0.48	1.30
3D61 T1	Pyrolyzed		Lack of Wetting	0.48	1.42(1)
T2				0.49	1.42
T3				0.50	1.42
3D64 T1	Pyrolyzed		Weave	0.58	1.47(1)
T2				0.67	1.47
T3				0.69	1.47
3D75 T1	Graphitized		No-Intentional	0.70	1.60(1)
T2				0.71	1.60
T3				0.73	1.60
3D72 T4				(2)	1.60
T5				(2)	1.60

(1) Average of four or five compression specimens.

(2) Material attenuation prohibited measurement.



Table XXIX (Continued)

Specimen	Condition	Description	Defect	Longitudinal Velocity (10 <sup>5</sup> in/sec)	Bulk Density, (g/cc)
3D74 C1	Pyrolyzed	Compression	No-Intentional	0.85	1.56
C2				0.86	1.60
3D71 C3				0.87	1.60
C4				0.88	1.61
C5				0.92	1.60
3D68 C1	Pyrolyzed		Small Void	(2)	1.31
C2				(2)	1.33
C3				(2)	1.27
C4				(2)	1.28
3D61 C1	Pyrolyzed		Lack of Wetting	(2)	1.42
C2				(2)	1.43
C3				(2)	1.42
C4				(2)	1.42
3D64 C1	Pyrolyzed		Weave	0.69	1.46
C2				0.71	1.47
C3				0.71	1.48
3D75 C1	Graphitized		No-Intentional	0.78	1.60
C2				0.74	1.60
C3				0.80	1.60
3D72 C4				(2)	1.60
C5				(2)	1.60

As in the unidirectional samples, ability to strain plays an important role in determining the utilization of the composites physical characteristics. The defects appear to permit some homogenization of the local stresses and more utilization of the yarn's strength.

Upon graphitization, the tensile properties increased by approximately 20 percent (Figure 127). These samples received two impregnations and pyrolysis (2P), a graphitization (G), impregnations and pyrolysis (3P), and a final graphitization step (G). As in the unidirectional composites this increase was attributed to the yarn-binder interactions.

The total porosity data obtained from the mercury porosimetry measurements and theoretical density estimates (Section 4.0) were correlated to the compressive and tensile properties of the composites. The trends suggested higher compressive strengths associated with lower porosity (Figure 128). Those composite specimens from the process study which were processed under similar procedures as the defect study specimens are also shown in the figure as square points. However, the moduli did not change significantly over the porosity range and no trend was observed.

In the case of the tensile strengths, the data suggested that an optimum porosity level may exist (Figure 129). Admittedly, a larger effort in this area is required to substantiate or determine the effect of porosity on strength. This trend was similar to that obtained for the unidirectional VYB 70 1/2 - pitch composites.

In general, it was found that different physical strength characteristics could be obtained depending on the type of binders and yarns and their compatibility. Furthermore, the material condition, pyrolysis or graphitization, plays an important role. The more graphitic binder was less sensitive to defects. In fact, there appears to be an optimum density for the best tensile results. If compressive loads are more important, the highest density should be obtained in the matrix.

These results showed that detailed consideration must be given to the total processing system. Furthermore, more detailed investigations are required to better understand the role of binder and yarn in the failure modes involved both for compressive, shear and tensile loading conditions.

### 6.2.3 Relationship of Mechanical Properties to NDT Measurements

The nondestructive analysis of the mechanical test specimens included ultrasonic longitudinal velocity and bulk density measurements and X-ray radiography. The velocity measurements were made through the thickness or radial direction by the dry coupling method described in Section 6.1.4. The longitudinal velocity was measured at 0.5 MHz for the pyrolyzed and graphitized composites. The nondestructive test data is listed in Table XXIX for the tension and compression specimens. The data obtained on these specimens had the same relationships between no-intentional and intentional defect specimens as discussed in Section 5.2.

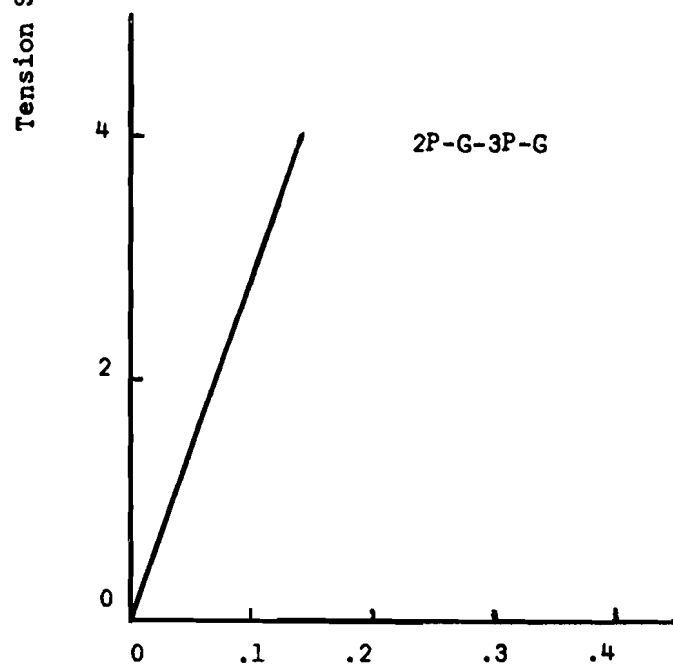
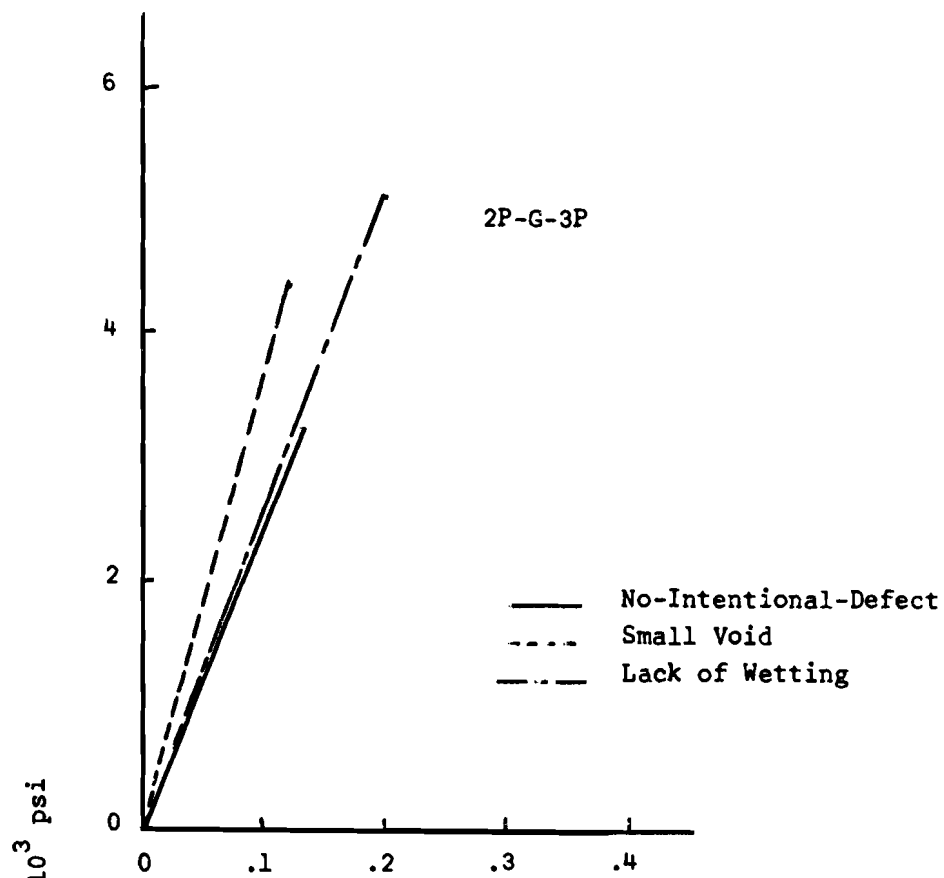


Figure 127. Tension Stress-Strain Curves for VYB 70 1/2-Pitch Multidirectional Composite

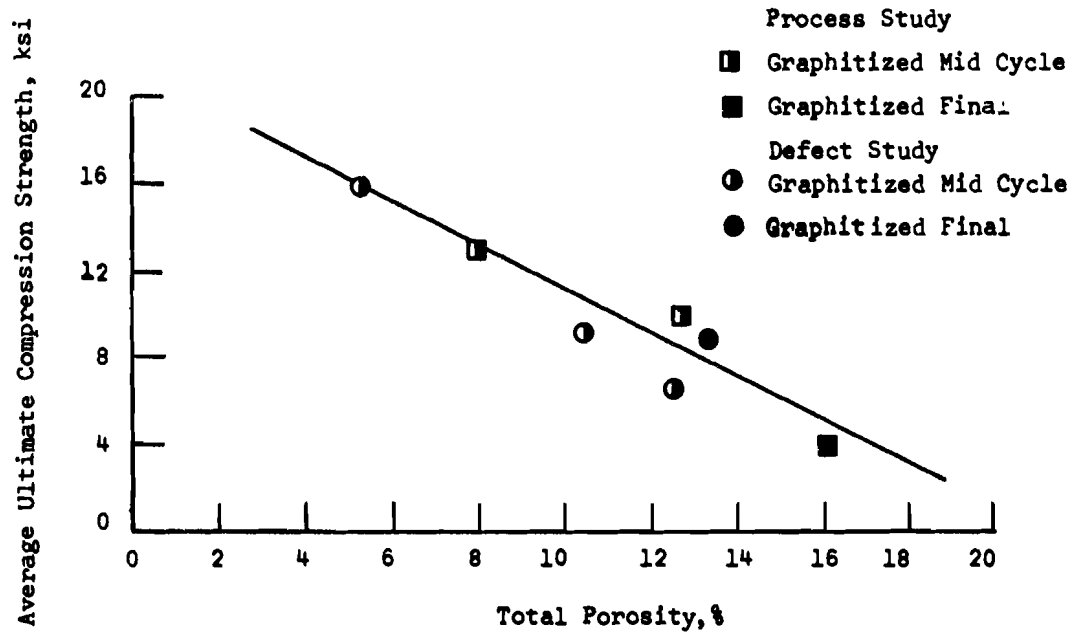


Figure 128. Average Ultimate Compression Strengths Versus Total Porosity of DACLOCK 120 Multidirectional Composite

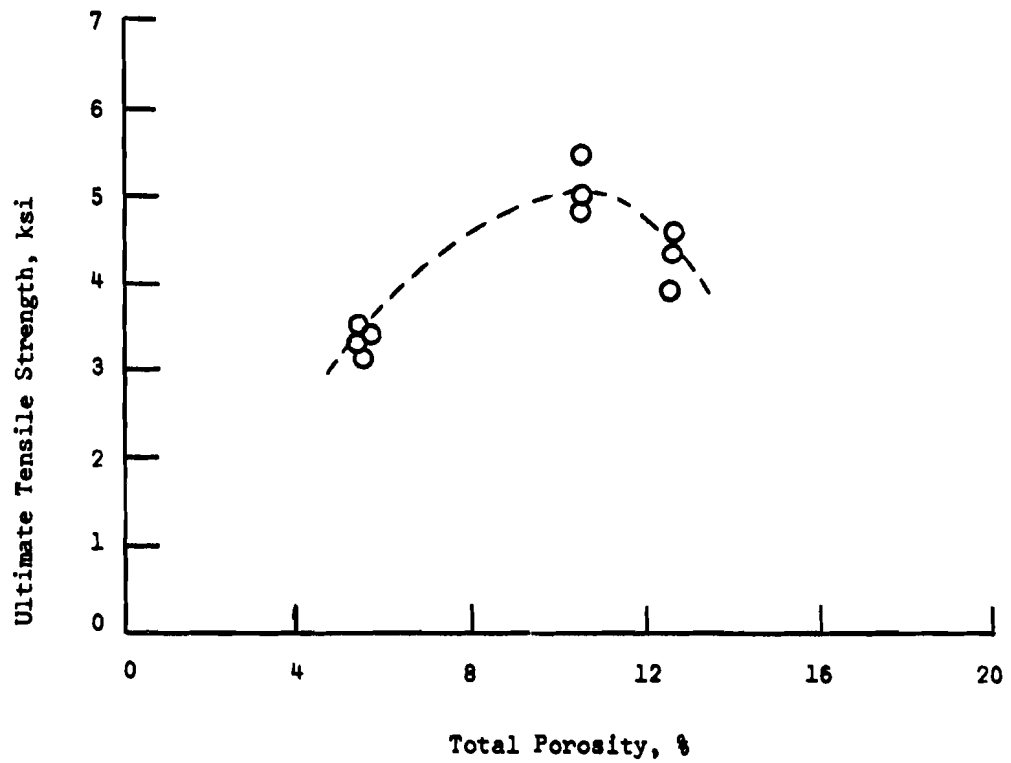


Figure 129. Ultimate Tensile Strength Versus Total Porosity of DACLOCK 120 Multidirectional Composite

The velocity data indicated higher tensile strengths were associated with lower velocity measurements (Figure 130). This can be expected since the strengths were higher for the higher porosity samples. The velocity-strength data did not have the peak as in the porosity-strength curve (Figure 129). Similar results were obtained for the strain to failure values since the porosity sample had the higher strength to failure.

The average ultrasonic attenuation (as measured on the composite panels) is plotted versus tensile strength in Figure 131. Again this trend was attributed to the higher porosity of the stronger composite. Similar results were obtained for the strain to failures.

Higher compressive strengths (and strain to failure) were associated with higher velocity and lower attenuation (Figure 132 and 133). This was expected since the strengths were found to increase with decreasing porosity.

The dynamic modulus values,  $\rho V_{11}^2$  (Section 6.1.4), in the thickness direction were significantly different for each composite defect group (no-intentional -  $1.08 \times 10^6$  psi, small void -  $0.33 \times 10^6$  psi, lack of wetting, -  $0.32 \times 10^6$  psi and weave -  $0.60 \times 10^6$  psi). Since the tensile moduli fluctuated with the porosity and the compression moduli were essentially unchanged, no relationship between these two parameters could be established for the multidirectional composite.

The test results, nondestructive and mechanical, on the multidirectional composite emphasized the importance of determining the effect of physical properties such as porosity, on both NDT and mechanical properties prior to attempting a material screening program. For the compression strengths, the lower attenuation or high velocities were indicative of higher strengths while for the tensile strengths the opposite was observed due to the effects of porosity. These conflicting trends show that a thorough understanding of NDT - property correlations is necessary before NDT can be rationally applied to material screening.

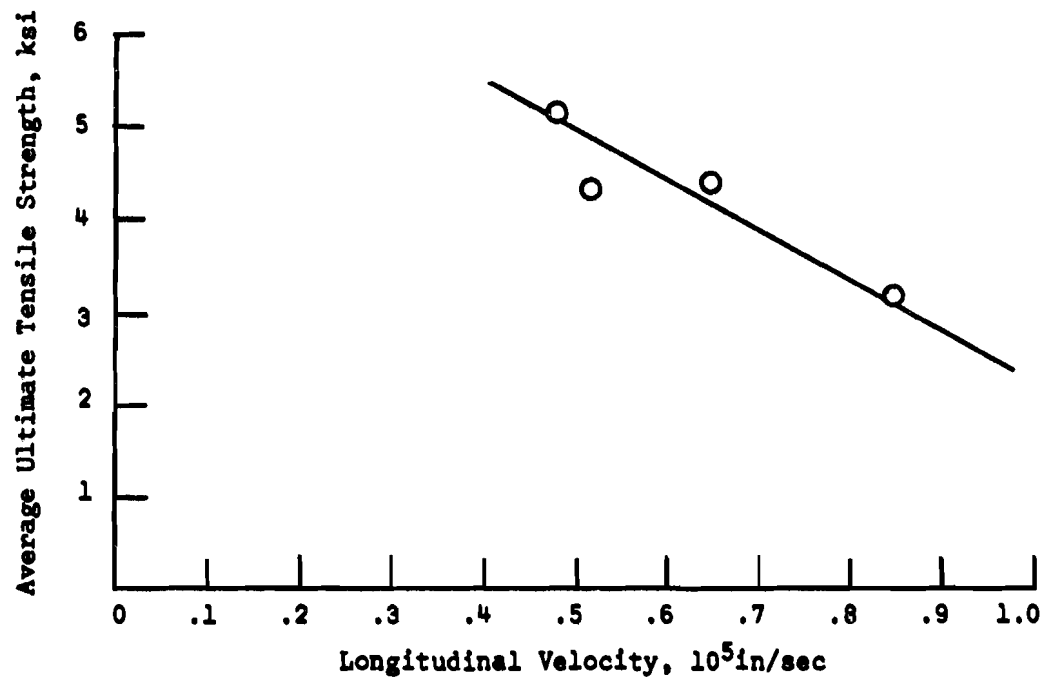


Figure 130. Longitudinal Velocity Versus Ultimate Tensile Strength of DACLOCK 120 Composite

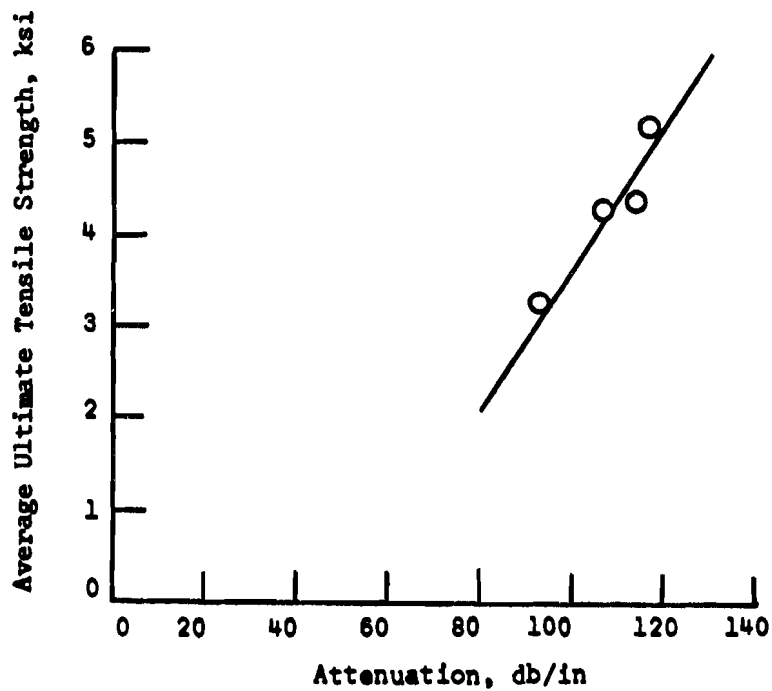


Figure 131. Attenuation Versus Ultimate Tensile Strength of DACLOCK 120 Multidirectional Composite

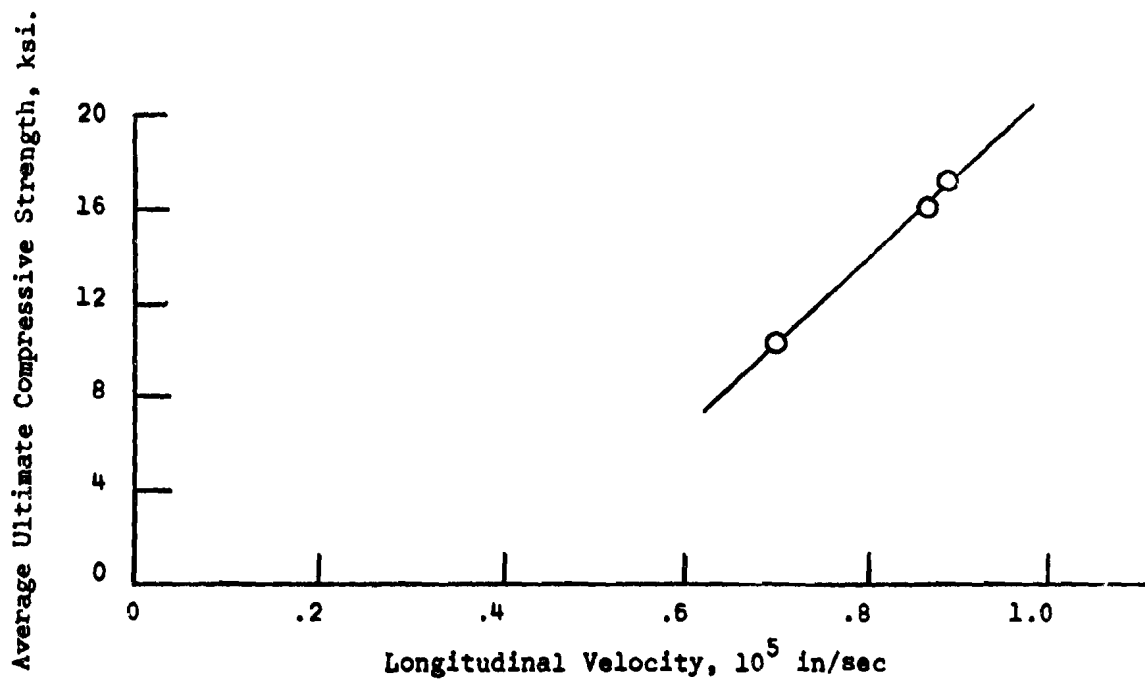


Figure 132. Longitudinal Velocity Versus Ultimate Compressive Strength of DACLOCK 120 Composite

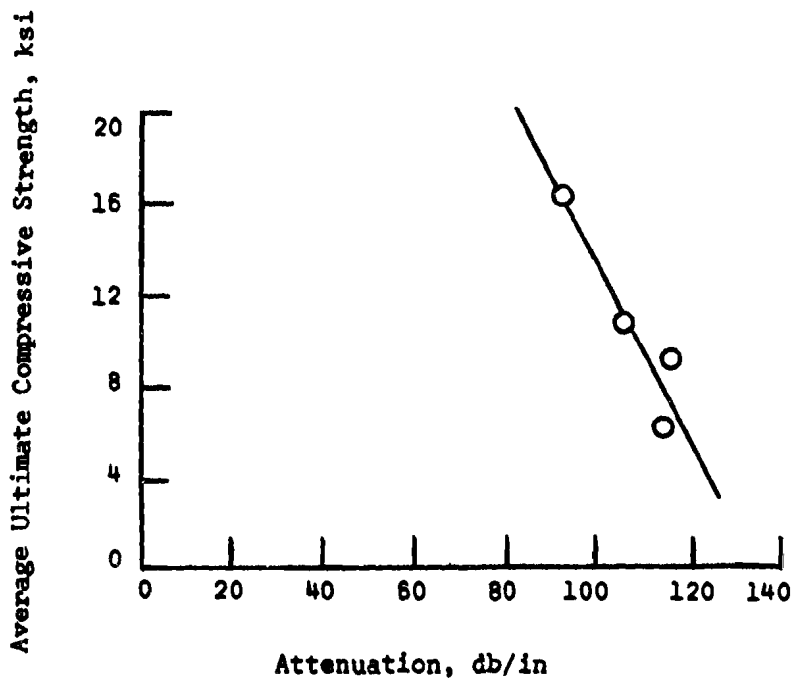


Figure 133. Attenuation Versus Ultimate Compressive Strength of DACLOCK 120 Composite

#### IV. CONCLUSIONS AND RECOMMENDATIONS

Monitoring material uniformities and detecting discrete discontinuities in unidirectional and multidirectional carbon-carbon composites on an in-process basis can be successfully accomplished using nondestructive analyses. The precursor materials, processing variables, and defects can each have a significant effect on the mechanical properties of these carbon-carbon composites. Nondestructive test measurements can be correlated to porosity and mechanical properties of the composite. The application of nondestructive test methods during a materials development or characterization program is helpful to the understanding of material property relationships, and can aid in the development of optimum material processing.

The following recommendations are made based on the results and analyses performed on the carbon-carbon composites:

1. This program dealt only with small samples of materials. Non-destructive testing of actual components may pose problems relating to thickness and geometrical configurations. A study of NDT applicability to hardware configurations appears justified.
2. Further mechanical testing should be conducted to obtain statistical confidence in the NDT-mechanical property correlations reported here. Such a program should make use of larger blocks of material so that better mechanical test specimen designs could be employed.
3. Detailed studies on the mechanical properties of carbon-carbon composites should be conducted to evaluate the effect of porosity and to determine optimum processing procedures.
4. Scanning electron microscopy and electron fractography should be applied to study the yarn-binder interface characteristics in carbon-carbon composites.



APPENDIX I

NONDESTRUCTIVE CHARACTERIZATION MEASUREMENTS  
ON UNIDIRECTIONAL AND MULTIDIRECTIONAL COMPOSITES

NDT CHARACTERIZATION DATA ON CURED, PYROLYZED, AND GRAPHITIZED  
VYB 70 1/2 - SC1008 UNIDIRECTIONAL COMPOSITES

Specimen Group	Defect Type	Cured <sup>(1)</sup>		Pyrolyzed <sup>(1)</sup>	
		Average <sup>(2)</sup> Velocity (10 <sup>5</sup> in/sec)	Average <sup>(3)</sup> Density (g/cc)	Average <sup>(2)</sup> Velocity (10 <sup>5</sup> in/sec)	Average <sup>(3)</sup> Density (g/cc)
9	Delamination	1.10	1.42	(4)	1.25
10	No Intentional	1.20	1.37	1.06	1.27
11	Weave	1.16	1.37	1.08	1.28
12	Noncarbonaceous	1.13	1.35	1.01	1.26
13	Lack of wetting	1.31	--	1.13	1.31
14	No Intentional	1.17	1.36	1.02	1.23
15	Weave	1.20	1.35	0.86	1.22
16	Weave	1.09	1.30	0.87	1.17
17	Delamination	--	1.32	1.23	1.26
18	No Intentional	1.12	1.36	1.07	1.26
19	Delamination	1.10	1.40	0.95	1.31
20	Noncarbonaceous	1.08	1.29	0.58 (5)	1.15
21	Noncarbonaceous	1.09	1.30	0.47	1.15
22	Lack of wetting	1.09	1.30	0.52	1.16
23	Lack of wetting	1.10	1.31	0.58	1.17
24	Small voids	1.13	1.30	0.52	1.16
25	Small voids	1.15	1.26	0.52	1.13
26	Small voids	1.09	1.32	0.96	1.22
27	Large voids	1.10	1.29	0.94	1.17
28	Large voids	1.09	1.28	0.94	1.18
29	Poor bundle	1.03	1.29	0.50	1.10
30	Poor bundle	1.08	1.32	0.48	1.12
31	No Intentional	1.28	1.40	1.00 (5)	1.30

(1) Average of four specimens

(2) Longitudinal velocity at 2.5 MHz

(3) Bulk density by water immersion

(4) Material attenuation too high for accurate measurement of velocity

(5) Measurement made at 5.0 MHz

NDT CHARACTERIZATION DATA ON CURED, PYROLYZED, AND GRAPHITIZED  
VYB 70 1/2 - SC1008 UNIDIRECTIONAL COMPOSITES (Continued)

Specimen	Defect	Graphitized <sup>(6)</sup>	
		Average Velocity <sup>(2)</sup> (10 <sup>5</sup> in/sec)	Average Density <sup>(3)</sup> (g/cc)
10	No-Intentional	0.76	1.24
11	Weave	0.71	1.25
12	Noncarbonaceous	0.71	1.23
14	No-Intentional	0.67	1.24
15	Weave	0.58	1.20
16	Weave	0.59	1.14
18	No-Intentional	0.66	1.25
19	Delamination	0.61	1.22
20	Noncarbonaceous	(4)	1.09
21	Noncarbonaceous	(4)	1.13
22	Lack of wetting	(4)	1.15
23	Lack of wetting	(4)	1.17
24	Small void	(4)	
25	Small void	(4)	1.12
26	Small void	0.71	1.26
27	Large void	0.63	1.13
28	Large void	0.66	1.15
29	Poor bundle	(4)	1.10
30	Poor bundle	(4)	1.09
Quartz		2.30 x 10 <sup>5</sup>	

(6) Average of Two Specimens

NDT CHARACTERIZATION DATA ON PYROLYZED AND GRAPHITIZED  
VYB 70 1/2 - PITCH UNIDIRECTIONAL COMPOSITES

Specimen	Condition	Defect	Bulk <sup>(1)</sup> Density, (g/cc)	Ultrasonic Longitudinal Velocity <sup>(2)</sup> , (10 <sup>5</sup> in/sec)	Ultrasonic Attenuation <sup>(3)</sup> , (db/in)
WPC 12A <sup>(4)</sup>	Pyrolyzed	No-Intentional	1.51	1.19	122
B			1.52	1.11	158
C			1.52	1.15	148
D			1.52	1.13	150
WPC 13A <sup>(4)</sup>		No-Intentional	1.52	1.16	143
B			1.52	1.16	142
C			1.52	1.14	147
D			1.51 (1.52) <sup>(5)</sup>	1.18 (1.15)	152
MDPC 21A		Small Voids	1.48	1.10	63
B			1.48	1.08	64
C			1.48	1.28	60
D			1.48	1.06	77
MDPC 22A		Small Voids	1.51	1.02	57
B			1.51	1.00	53
C			1.51	1.14	54
D			1.51 (1.50)	1.06 (1.10)	56
MDPC 5A		Lack of Wetting	1.44	0.91	110
B			1.44	0.97	105
C			1.43	0.95	108
D			1.43	0.94	115

(1) By water immersion.

(2) Measurements made at 1.6 MHz for pyrolyzed composites and 0.8 MHz for graphitized composites.

(3) Measurements made at 2.25 MHz.

(4) This group was processed under different pyrolysis conditions from other specimens

(5) Average.

NDT CHARACTERIZATION DATA ON PYROLYZED AND GRAPHITIZED  
VYB 70 1/2 - PITCH UNIDIRECTIONAL COMPOSITES (Continued)

Specimen	Condition	Defect	Bulk Density, (g/cc)	Ultrasonic Longitudinal Velocity <sup>(2)</sup> , (10 <sup>5</sup> in/cc)	Ultrasonic Attenuation <sup>(3)</sup> , (db/in)
MDPC 6A	Pyrolyzed	Lack of Wetting	1.43	0.96	100
B			1.47	0.90	115
C			1.46	0.95	99
D			1.45 (1.44)	1.01 (0.94)	116
MDPC 24A		Weave	1.47	0.97	>108
B			1.49	0.92	106
C			1.50	0.93	99
D			1.49 (1.49)	0.96 (0.95)	>100
MDPC 2A		Delamination	1.49	0.91	> 98
B			1.48	0.98	>107
C			1.48	0.96	>103
D			1.47 (1.48)	0.99 (0.96)	>104
WPC 12C	Graphitized	No-Intentional	1.52	0.80	145
D2			1.53	0.82	152
WPC 13A		No-Intentional	1.52	0.75	138
C1			1.52	-	142
C2			1.51 (1.52)	0.78 (0.80)	150
MDPC 21A		Small Voids	1.46	0.85	100
MDPC 22A1		Small Voids	1.47	0.79	131
A2			1.48	-	125
C			1.48	0.84	122
D			1.47 (1.47)	0.81 (0.82)	142

NDT CHARACTERIZATION DATA ON PYROLYZED AND GRAPHITIZED  
VYB 70 1/2 - PITCH UNIDIRECTIONAL COMPOSITES (Continued)

Specimen	Condition	Defect	Bulk Density, (g/cc)	Ultrasonic Longitudinal Velocity <sup>(2)</sup> , (10 <sup>5</sup> in/cc)	Ultrasonic Attenuation <sup>(3)</sup> , (db/in)
MDPC 5A	Graphitized	Lack of Wetting	-	0.61	147
B			-	0.64	160
C			-	0.65	171
D			-	0.60 (0.62)	151
MDPC 24B2		Weave	1.47	0.70	141
C2			1.48 (1.48)	0.75 (0.73)	129
MDPC 2C1		Delamination	1.46	0.72	145
C2			1.45	-	145
D			1.45 (1.45)	0.59 (0.65)	186

NDT CHARACTERIZATION DATA ON PYROLYZED AND GRAPHITIZED  
MODMOR II - PITCH UNIDIRECTIONAL COMPOSITES

Specimens	Condition	Defect	Ultrasonic Longitudinal <sup>(1)</sup> (Velocity, $10^5$ in/sec)	Ultrasonic Attenuation <sup>(2)</sup> (db/in)	Bulk Density <sup>(3)</sup> (g/cc)
M1-1	Pyrolyzed	No-Intentional	.863	135	1.74
2			.848	135	1.76
3			.870	135	1.76
4			.848	135	1.76
5			.847	140	1.78
6			.839	135	1.73
7			.849	135	1.73
8			.889	135	1.74
9			.845	180	1.75
10			.829	135	1.74
11			.818 (.850) <sup>(4)</sup>	135 (140)	1.75 (1.75)
M2-1	Pyrolyzed	No-Intentional	.846	135	1.75
2			.862	135	1.73
3			.836	135	1.76
4			.827	135	1.74
5			.839	135	1.78
6			.837	135	1.75
7			.828	135	1.75
8			.800	135	1.78
9			.872	135	1.75
10			.796	135	1.77
11			.778	140	1.76
12			.828 (.829)	160 (140)	1.73 (1.75)

(1) Ultrasonic longitudinal velocity measured at 1.6 MHz for pyrolyzed material and 0.8 MHz for graphitized material.

(2) Measurements made at 2.25 MHz

(3) By water immersion.

(4) Average

NDT CHARACTERIZATION DATA ON PYROLYZED AND GRAPHITIZED  
MODMOR II - PITCH UNIDIRECTIONAL COMPOSITES (Continued)

Specimens	Condition	Defect	Ultrasonic Longitudinal <sup>(1)</sup> Velocity, (10 <sup>5</sup> in/sec)	Ultrasonic Attenuation <sup>(2)</sup> (db/in)	Bulk Density <sup>(3)</sup> , (g/cc)
M3-1	Pyrolyzed	No-Intentional	.843	140	1.76
2			.818	145	1.75
3			.803	140	1.75
4			.814	135	1.75
5			.835	135	1.76
6			.836	135	1.75
7			.787	185	1.76
8			.827 (.820)	200 (150)	---- (1.75)
M-561	Pyrolyzed	Weave	.804	250	1.74
2			.850	260	1.75
3			.884	250	1.75
4			.877	260	1.73
5			.818	170	1.76
6			.837	350	1.73
7			.753	370	1.75
8			.856	170	1.76
9			.833	180	1.64
10			.828	370	1.75 (1.75)
11			.801 (.831)	250 (260)	
M13A	Pyrolyzed	Lack of Wetting	.733	---	1.68
B			.786	---	1.68
C			.780	---	1.69
D			.790 (.776)	---	1.67 (1.68)
M14A	Pyrolyzed	Small Void	.779	---	1.66
B			.719	---	1.66
C			.744	---	1.66
D			.756 (.750)	---	1.65 (1.66)



NDT CHARACTERIZATION DATA ON PYROLYZED AND GRAPHITIZED  
MODMOR II - PITCH UNIDIRECTIONAL COMPOSITES (Continued)

Specimens	Condition	Defect	Ultrasonic Longitudinal <sup>(2)</sup> Velocity, 10 <sup>5</sup> in/sec	Ultrasonic <sup>(2)</sup> Attenuation (db/in)	Bulk Density <sup>(3)</sup> , (g/cc)
M2-1	Graphitized	No-Intentional	.607	140	1.92
2			.619	140	1.87
3			---	135	1.83
4			.597	140	1.91
5			.630	140	1.99
7			.609	145	1.91
9			.607	145	1.89
10			.586	140	1.96
11			.600	145	1.89
12			.583 (.606)	145 (140)	1.88 (1.91)
M56-2	Graphitized	Weave	.630	280	1.94
4			.658	290	1.82
5			.688	285	1.76
9			.579 (.639)	230 (270)	1.97 (1.88)
M13-A	Graphitized	Lack of Wetting	.661	---	1.70
B			.693 (.672)	---	1.73 (1.72)
M14-B	Graphitized	Small Void	.707	---	1.65
C			.719 (.713)	---	1.66 (1.66)

NDT CHARACTERIZATION DATA ON PYROLYZED AND GRAPHITIZED  
DACLOCK 120 MULTIDIRECTIONAL COMPOSITES

Specimen	Defect Type	Condition	Longitudinal <sup>(1)</sup> Velocity (10 <sup>5</sup> in/sec)	Ultrasonic <sup>(3)</sup> Attenuation (db/in)	Bulk <sup>(2)</sup> Density (g/cc)
71	No-Intentional	2P-G-2P	-	-	1.61
72			-	-	1.60
73			-	-	1.62
74			-	-	1.57
75			-	-	1.64 (1.61)
71	No-Intentional	2P-G-3P	0.96	92	1.65
72			0.98	96	1.67
73			0.98	96	1.66
74			0.93	87	1.64
75			0.90 (0.95) <sup>(4)</sup>	96 (93)	1.67 (1.66)
72	No-Intentional	2P-G-3P-G	0.69	92	1.61
75			0.69 (0.69)	94 (83)	1.59 (1.60)
67	Small Void	2P-G-2P	0.75	110	1.46
68			0.76	124	1.48
69			0.73	115	1.46
70			0.83 (0.77)	111 (115)	1.51 (1.48)
60	Lack of Wetting	2P-G-2P	0.75	118	1.52
61			0.75	124	1.53
62			0.78	114	1.50
63			0.79 (0.77)	116 (118)	1.49 (1.51)
64	Weave	2P-G-2P	-	-	1.48
65			-	-	1.47
66			-	-	1.50 (1.48)
64	Weave	2P-G-3P	0.74	108	1.55
65			0.86	102	1.57
66			0.85 (0.79)	115 (108)	1.58 (1.57)

(1) Measured at 0.5 MHz

(2) By water immersion

(3) Measured at 0.5 MHz

(4) Average

APPENDIX II

MECHANICAL TEST RESULTS ON UNIDIRECTIONAL AND  
MULTIDIRECTIONAL COMPOSITES

UNIAXIAL TENSILE TEST RESU. FOR PYROLYZED AND GRAPHITIZED  
VYB 70 1/2 - SC1008 UNIDIRECTIONAL COMPOSITES

Specimen	Defect	Condition	Ultimate Tensile Strength, (psi)	Strain to Failure, (%)	Secant <sup>(4)</sup> Modulus, (10 <sup>6</sup> psi)	Initial Modulus, (10 <sup>6</sup> psi)	Final Modulus, (10 <sup>6</sup> psi)
14D1 <sup>(1)</sup>	No-Intentional	Pyrolyzed	11.6	.25	4.6	4.6	4.6
D2 <sup>(1)</sup>			4.6	.07	6.5	6.5	6.5
D3 <sup>(1)</sup>			11.0	.15	7.3	5.9	9.1
14C4 <sup>(2)</sup>	Small Void	Pyrolyzed	13.5	.27	5.0	5.0	5.0
C5 <sup>(2)</sup>			13.7 (13.6) <sup>(5)</sup>	.17 (.21)	5.9 (5.4)	5.3 (5.2)	8.0 (6.5)
25B1 <sup>(2)</sup>			7.2	.22	3.3	3.3	3.3
B2 <sup>(2)</sup>	Lack of Wetting	Pyrolyzed	8.4	.20	4.2	4.2	4.2
B3 <sup>(2)</sup>			6.4 (7.3)	.16 (.19)	4.2 (3.9)	— (3.8)	4.0 (3.8)
22A1 <sup>(2)</sup>			10.9	.24	4.5	4.5	4.5
A2 <sup>(2)</sup>	Weave	Pyrolyzed	11.0	.31	3.5	3.5	3.5
A3 <sup>(2)</sup>			11.9 (11.2)	.29 (.28)	4.1 (4.0)	4.1 (4.0)	4.1 (4.0)
15D1 <sup>(3)</sup>			7.0	.10	7.0	7.0	7.0
D3 <sup>(3)</sup>	Cracks	Pyrolyzed	6.8 (7.0)	.11 (.11)	6.3 (6.7)	—	—
18D1 <sup>(1)</sup>			5.2	—	—	—	—
17A1 <sup>(1)</sup>			4.9	.11	4.4	4.4	4.4
29D <sup>(1)</sup>	Poor Bundle	Pyrolyzed	8.3	.14	5.9	5.9	5.9

(1) Strip specimen failed at doublers.

(2) Dogbone thickness specimen.

(3) Strip specimen failed in gage section.

(4) Calculated using strain-to-failure.

(5) Average values of dogbone thickness specimens or strip failure in gage section only.

UNIAXIAL TENSILE TEST RESULTS FOR PYROLYZED AND GRAPHITIZED  
VYB 70 1/2 - SC1008 UNIDIRECTIONAL COMPOSITES

Specimen <sup>(2)</sup>	Defect	Condition	Ultimate Tensile Strength, (psi)	Strain to Failure, (%)	Secant <sup>(4)</sup> Modulus, (10 <sup>6</sup> psi)	Initial Modulus, (10 <sup>6</sup> psi)	Final Modulus, (10 <sup>6</sup> psi)
18A1	No-Intentional	Graphitized	13.0	.40	3.3	--	4.5
A2			18.0	.40	4.5	--	7.7
14A3			21.3	.34	6.4	5.5	7.7
A4			22.0	.32	6.9	5.6	9.1
10A5			13.1	.23	6.0	6.0	6.0
A6			14.4 (17.0)	.30 (.33)	4.8 (5.3)	4.5 (5.4)	5.5 (6.8)
24A3	Small Voids	Graphitized	4.8	.25	1.9	1.7	2.3
25C1			3.7	.11	3.4	3.4 (2.5)	3.4 (2.8)
C2			4.2 (4.2)	-- (.19)	-- (2.7)	--	--
22B2	Lack of Wetting	Graphitized	4.8	0.22	2.2	2.2	2.2
C3			6.3	0.24	2.6	2.4	2.9
23B4			6.1 (5.8)	0.28 (.24)	2.2 (2.6)	2.2 (2.3)	2.2 (2.4)
16D1	Weave	Graphitized	9.4	.47	2.0	2.5	5.0
D2			10.2 (9.8)	.28 (.37)	3.7 (2.9)	2.1 (2.3)	3.9 (4.4)
18B1	Cracks	Graphitized	18.1	0.31	5.9	4.8	8.3
B2			23.0 (20.7)	0.34 (.33)	6.8 (6.4)	5.9	9.1
B3 <sup>(6)</sup>			7.7	0.29	2.7	2.2 (4.3)	3.6 (7.0)

(2) Dogbone thickness specimen.

(4) Calculated using strain-to-failure.

(6) Large crack in center (.024 inches wide).

SHEAR TEST RESULTS FOR PYROLYZED AND GRAPHITIZED  
VYB 70 1/2 - SC1008 UNIDIRECTIONAL COMPOSITES

Specimen	Defect	Condition	Shear Strength, psi
14B1	No Intentional	Pyrolyzed	666
B2			1420
B3			848
B4			1236
31C5			1355 (1105)(1)
26D1	Small Voids	Pyrolyzed	1190
D2			975
26A3			610
A4			960 (934)
22D1	Lack of Wetting	Pyrolyzed	688
D2			715
D3			720
D4			530 (663)
16C1	Weave	Pyrolyzed	622
C2			718
C3			708
C4			745 (698)
18C1	Crack	Pyrolyzed	1027
C2			1405
C3			1626
C4			1483 (1385)
19B1	Delamination	Pyrolyzed	958
B2			1770
B3			1718
B4			2073 (1630)(1)
27C1	Large Voids	Pyrolyzed	710
C2			720
C3			925
C4			630 (746)(1)
29B1	Poor Bundle	Pyrolyzed	545
B2			505
B3			405
B4			470 (481)
21A2	Noncarbonaceous	Pyrolyzed	725
A3			863
A4			400 (663)

(1) Average Value.

SHEAR TEST RESULTS FOR PYROLYZED AND GRAPHITIZED  
VYB 70 1/2 - SC1008 UNIDIRECTIONAL COMPOSITES (Continued)

Specimen	Defect	Condition	Shear Strength, psi
18A1	No-Intentional	Graphitized	299
A2			456
A3			516
A4			326
A5			391
A6			238
A7			1011 (462)
26B1	Small Voids	Graphitized	325
B2			270
B3			240
26C4			340 (294)
23D1	Lack of Wetting	Graphitized	140
D2			255
D3			270
D4			175 (210)
16B1	Weave	Graphitized	279
B2			501
B3			361
B4			214 (339)
15B1	Large Void	Graphitized	234
B2			73
B3			135
B4			119 (115)

UNIAXIAL TENSILE TEST RESULTS FOR PYROLYZED AND GRAPHITIZED  
VYB 70 1/2 - PITCH UNIDIRECTIONAL COMPOSITES

Specimen	Defect	Condition	Ultimate Tensile Strength, (psi)	Strain to Failure, (%)	Secant <sup>(1)</sup> Modulus, (10 <sup>6</sup> psi)	Initial Modulus, (10 <sup>6</sup> psi)	Final Modulus, (10 <sup>6</sup> psi)
13D1	No-Intentional	Pyrolyzed	9.5	.08	11.9	11.9	11.9
D2			8.5	.08	10.6	10.6	10.6
D3			7.7 (8.6) <sup>(2)</sup>	.05 (.07)	15.4 (12.6)	15.4 (12.6)	15.4 (12.6)
21B1	Small Voids	Pyrolyzed	2.4	.03	8.0	5.5	10.0
B3			15.4	—	—	8.3	16.7
6B1	Lack of Wetting	Pyrolyzed	16.4	.13	12.6	11.0	14.3
B2			15.5	.14	11.1	11.1	11.1
B3			13.6 (15.2)	.12 (.13)	11.3 (11.7)	11.3 (11.1)	11.3 (12.2)
26A1	Weave	Pyrolyzed	6.2	.08	7.7	7.7	7.7
A2			8.5	.10	8.5	4.2	8.4
A3			3.0 (7.4)	.12 (.09)	2.5 (8.1)	0.6 (5.9)	10.0 (8.0)
12C1	No-Intentional	Graphitized	20.8	.18	11.6	10.0	16.5
C2			18.9	—	—	—	—
C3			21.0 (20.2)	.28 (.23)	7.5 (9.6)	6.2 (8.1)	12.5 (16.5)
22C1	Small Void	Graphitized	26.5	.31	7.9	6.2	12.5
C2			32.6	.47	6.9	4.3	12.5
C3			30.4 (29.1)	.42 (.40)	7.2 (7.3)	4.8 (5.1)	12.5 (12.5)
5A1	Lack of Wetting	Graphitized	22.8	—	—	—	—
A3			24.9 (23.8)	—	—	—	—
24B1	Weave	Graphitized	22.5	—	—	7.1	16.7
B2			16.7	.28	6.0	5.3	8.3
B3			19.1 (19.6)	.35 (.31)	5.5 (5.8)	4.2 (5.6)	7.1 (10.7)

(1) Calculated using strain to failure.

(2) Average value.

(3) Does not include low value.



SHEAR STRENGTHS OF PYROLYZED AND GRAPHITIZED  
VYB 70 1/2 - PITCH UNIDIRECTIONAL COMPOSITES

Specimen	Defect	Condition	Shear Strength, psi
13BS1 4	No-Intentional	Pyrolyzed	790 750 (770)(1)
21CS1 2 3 4 5	Small Void	Pyrolyzed	770 1410 1200 2270 2180 (1770)
24DS1 2 3	Weave	Pyrolyzed	780 490 1280 (850)
6AS1 2 3 4	Lack of Wetting	Pyrolyzed	1990 1910 1330 1900 (1780)
13AS1 2 3 4 5	No-Intentional	Graphitized	730 460 750 770 750 (690)
22DS1 2 3 4	Small Void	Graphitized	1000 840 770 910 (880)
24C51 2 3 4	Weave	Graphitized	690 780 530 940 (740)
5BS1 3 4	Lack of Wetting	Graphitized	1020 1010 790 (940)

(1) Average value

UNIAXIAL TENSILE TEST RESULTS FOR PYROLYZED AND GRAPHITIZED  
MODMOR II - PITCH UNIDIRECTIONAL COMPOSITES

Specimen	Defect	Condition	Ultimate Tensile Strength, (psi)	Strain to Failure, (%)	Secant <sup>(1)</sup> Modulus, (10 <sup>6</sup> psi)	Initial Modulus, (10 <sup>6</sup> psi)	Final Modulus, (10 <sup>6</sup> psi)
3-7	No-Intentional	Pyrolyzed	12.5	.07	17.8	17.8	17.8
2-6			10.6	.05	21.2	21.2	21.2
1-6			17.5	.06	29.2	29.2	29.2
1-7			25.2	.11	22.8	22.8	22.8
1-10			15.3 (16.2) <sup>(2)</sup>	.05 (.07)	30.6 (24.3)	30.6 (24.3)	30.6 (24.3)
13-2	Lack of Wetting	Pyrolyzed	9.3	.04	23.1	23.1	23.1
13-3			14.7 (12.0)	.08 (.06)	17.5 (20.8)	17.5 (20.8)	17.5 (20.8)
56-3	Weave	Pyrolyzed	4.5	—	—	—	—
2-11	No-Intentional	Graphitized	19.3	.03	64	—	33.3
2-9			20.2	.04	50	—	50.0
2-4			20.2 (19.9)	.05 (.04)	40 (51.6)	—	33.3 (38.9)
14-1	Small Void	Graphitized	8.0	.03	26.6	—	16.7
-2			12.0 (10.0)	.05 (.04)	24.0 (25.3)	—	20.0 (18.4)
13-2	Lack of Wetting	Graphitized	33.0	.13	25.2	25.2	25.2
-3			27.4	.11	25.0	25.0	25.0
-1			18.5 (26.3)	.08 (.11)	23.2 (24.5)	23.2 (24.5)	23.2 (24.5)
56-5	Weave	Graphitized	3.5	.12	29.0	29.0	29.0
56-4			5.2 (4.4)	—	—	—	—

(1) Calculated using strain to failure.

(2) Average value.

SHEAR STRENGTHS OF PYROLYZED AND GRAPHITIZED  
MODMOR II - PITCH UNIDIRECTIONAL COMPOSITES

Specimen	Defect	Condition	Shear Strength, psi
3-1S1	No-Intentional	Pyrolyzed	2750
2			1980
3			3550
4			1790
5			1835 (2380)(1)
14DS1	Small Void	Pyrolyzed	1325
2			1405
3			970
4			1355 (1260)
13D2S1	Lack of Wetting	Pyrolyzed	1050
2			1475
3			1090 (1205)
56-1S1	Weave	Pyrolyzed	1210
2			1225
3			885
4			1070
5			1135 (1105)
2-2S1	No-Intentional	Graphitized	835
2			1270
3			855
4			605
5			980
6			1270 (970)
14S1	Small Void	Graphitized	2190
2			1150
3			890 (1410)
13BS1	Lack of Wetting	Graphitized	830
2			1420
3			1250
4			1670 (1270)
56-9S1	Weave	Graphitized	770
2			1360 (1070)

(1) Average value

UNIAXIAL TENSILE TEST RESULTS FOR PYROLYZED AND GRAPHITIZED  
DACLOCK 120 MULTIDIRECTIONAL COMPOSITES

Specimen	Defect	Condition	Ultimate Tensile Strength, (psi)	Strain To Failure	Secant <sup>(1)</sup> Modulus, (10 <sup>6</sup> psi)
3D74-1	No-Intentional	Pyrolyzed	2600	.11	2.4
2			3505	.13	2.7
3			3085	.11	2.8
4			3500	.14	2.5
5			3300 (3200) <sup>(2)</sup>	.14 (.13)	2.4 (2.6)
3D69-1	Small Void	Pyrolyzed	4635	.12	3.9
2			4320	.12	3.6
3			3815 (4260)	.11 (.12)	3.5 (3.6)
3D61-1	Lack of Wetting	Pyrolyzed	5035	.22	2.3
2			5455	.22	2.5
3			4810 (5100)	.16 (.20)	3.0 (2.3)
3D64-1	Weave	Pyrolyzed	4825	.16	3.0
2			3815	.13	2.9
3			4670 (4440)	.16 (.15)	2.9 (2.9)
3D75-1	No-Intentional	Graphitized	5720	.19	3.0
2			4360	.14	3.1
3			3920	.13	3.0
4			3120	.15	2.1
5			2680 (3960)	.14 (.15)	1.9 (2.6)

UNIAXIAL COMPRESSION TEST RESULTS FOR PYROLYZED AND GRAPHITIZED  
DACLOCK 120 MULTIDIRECTIONAL COMPOSITES

Specimen	Defect	Condition	Ultimate Compressive Strength, (psi)	Strain to Failure, (%)	Secant <sup>(1)</sup> Modulus, (10 <sup>6</sup> psi)	Initial Modulus, (10 <sup>6</sup> psi)	Middle Modulus, (10 <sup>6</sup> psi)	Final Modulus, (10 <sup>6</sup> psi)
3D74 1	No-Intentional	Pyrolyzed	14.6	1.27	1.2	2.3	1.3	.67
2			15.0	1.14	1.3	2.2	1.2	1.05
3D71 3			17.5	1.60	1.1	2.1	1.1	0.90
4			16.7	1.43	1.2	1.9	1.2	0.70
5			17.6 (16.3) <sup>(2)</sup>	1.46 (1.40)	1.2 (1.2)	2.0 (2.1)	1.3 (1.2)	0.95 (.86)
3D68 1	Small Void	Pyrolyzed	5.7	.55	1.0	1.6	1.0	0.8
2			6.2	.59	1.1	1.8	1.0	0.7
3			6.5	.82	0.8	1.3	0.8	0.6
6			6.4 (6.2)	.74 (.68)	0.9 (1.0)	1.7 (1.6)	0.9 (0.9)	0.7 (0.7)
3D61 1	Lack of Wetting	Pyrolyzed	8.7	.96	0.9	1.4	0.8	0.7
2			10.0	.89	1.1	1.5	1.2	1.3
3			8.4	.86	1.0	1.4	1.0	0.7
4			9.3 (9.1)	.87 (.90)	1.1 (1.0)	1.5 (1.5)	1.0 (1.0)	1.1 (1.0)
3D64 1	Weave	Pyrolyzed	10.7	.91	1.2	1.8	1.2	0.9
2			10.7	.93	1.2	2.0	1.2	1.0
3			10.1	.86	1.2	2.2	1.2	1.1
3D66 4			9.4 (10.2)	.84 (.90)	1.2 (1.2)	1.8 (2.0)	1.2 (1.2)	0.9 (1.0)
3D75 1	No-Intentional	Graphitized	8.8	1.45	0.6	1.2	0.6	0.5
2			9.3	1.07	0.9	1.1	0.8	0.7
3			7.9	.92	0.9	1.1	0.8	0.6
3D72 4			10.7	1.44	0.7	1.2	0.8	0.5
5			10.2 (9.4)	1.18 (1.21)	0.9 (0.8)	1.3 (1.2)	0.8 (0.8)	0.7 (0.6)

(1) Calculated from strain to failure.

(2) Average value.

APPENDIX III

NONDESTRUCTIVE TEST DATA ON UNIDIRECTIONAL  
MECHANICAL TEST SPECIMENS

NONDESTRUCTIVE TEST MEASUREMENTS ON PYROLIZED VYB 70 1/2 - SC1008  
TENSILE SPECIMENS AT 1.6 MHZ

Specimen	Defect Group	Ultrasonic Longitudinal Velocity, (10 <sup>5</sup> in/sec)	Bulk <sup>(1)</sup> Density, (g/cc)
14D 1	No-Intentional- Defects	.97	--
2		--	--
3		--	1.32
14D 4		.97	1.31
5		.96(.96)	1.32(1.32)
18D 1	Crack	.96	1.32
31A 2		.91	1.34
3		.89(.92)	1.32(1.34)
17A 1	Delamination	1.19	1.28
2		1.18	1.29
3		1.15(1.17)	1.28(1.29)
15D 1	Weave Irregularity	.70	1.27
2		.65	1.26
3		.63(.66)	1.27(1.27)
20B 1	Noncarbonaceous Impurities	.54	1.14
2		.52	1.18
3		.44(.50)	1.17(1.16)
22A 1	Lack of Wetting	.45	1.19
2		.49	1.20
3		.52(.49)	1.19(1.19)
25B 1	Small Voids	.44	1.19
2		.51	1.20
3		.46(.47)	1.18(1.19)
27A 1	Large Voids	.82	1.23
2		.91	1.26
3		.94(.89)	1.27(1.25)
29C	Poor Fiber Bundle Penetration	.45	1.13
29D		.45	1.12
30C		.43(.44)	1.16(1.14)

(1) Weight-scalar measurements.

(2) Average value in parentheses.

NONDESTRUCTIVE TEST MEASUREMENTS ON PYROLIZED VYB 70 1/2 - SC1008  
SHEAR TEST SPECIMENS AT 1.6 MHz

Specimen	Defect Group	Ultrasonic Longitudinal Velocity, (10 <sup>3</sup> in/sec)	Bulk <sup>(1)</sup> Density, (g/cc)
14B 1	No-Intentional- Defects	.89	1.29
2		.86	1.31
3		.87	1.28
4		.85	1.31
31C 5		.87(.87) <sup>(2)</sup>	1.32(1.30)
18C 1	Crack	1.08	1.32
2		1.14	1.32
3		1.14	1.32
4		1.05(1.10)	1.30(1.32)
19B 1	Delamination	.92	1.35
2		.85	1.34
3		.93	1.35
4		.97(.92)	1.37(1.35)
16C 1	Weave Irregularity	.68	1.19
2		.65	1.20
3		.87	1.17
4		.78(.74)	1.16(1.18)
21A 2	Noncarbonaceous Impurities	.45	--
3		.81	--
4		.41(.56)	1.20
22D 1	Lack of Wetting	.49	1.20
2		.48	1.22
3		.51	1.21
4		.58(.51)	1.18(1.20)
26D 1	Small Voids	.87	1.21
2		--	--
26A 3		.90	1.22
4		.93(.90)	1.24(1.22)
27C 1	Large Voids	.65	1.09
2		.79	1.13
3		.81	1.13
4		.79(.81)	1.14(1.12)
29B 1	Poor Fiber Bundle Penetration	.49	--
2		--	--
3		--	--
4		--	--

(1) Weight-scalar measurements

(2) Average value in parentheses



NONDESTRUCTIVE TEST MEASUREMENTS ON GRAPHITIZED VYB 70 1/2 - SC1008  
TENSILE TEST SPECIMENS AT 0.8 MHz

Specimen	Defect Group	Ultrasonic Longitudinal Velocity, (10 <sup>5</sup> in/sec)	Bulk <sup>(1)</sup> Density, (g/cc)
18A 1	No-Intentional	.75	1.23
2		.64	1.23
14A 3		.72	1.20
4		.69	1.21
14A 5		.70	1.17
6		.73(.71) <sup>(2)</sup>	1.23(1.21)
24A 3	Small Voids	.42	1.13
25C 1		.38	1.06
2		.41(.40)	1.12(1.10)
22B 1	Lack of Wetting	.34	1.13
2		.37	1.16
C 3		.40	1.26
23B 4		.36(.37)	1.13(1.17)
16D 1	Weave	.65	1.25
2		.56	1.16
3		.76(.66)	1.05(1.15)
18B 1	Cracks	.71	1.23
2		.69	1.22
3		.68(.69)	1.23(1.23)

(1) Weight-scalar measurements

(2) Average value

NONDESTRUCTIVE TEST MEASUREMENTS ON GRAPHITIZED VYB 70 1/2 - SC1008  
SHEAR TEST SPECIMENS AT 0.8 MHz

Specimen	Defect Group	Ultrasonic Longitudinal Velocity, (10 <sup>3</sup> in/sec)	Bulk <sup>(1)</sup> Density, (g/cc)
18A 1	No-Intentional	.65	1.23
2		.65	1.23
3		.69	1.23
4		.70	1.22
5		.68	1.23
6		.67	1.21
7		.68(.68) <sup>(2)</sup>	1.24(1.23)
26C 4	Small Void	.52	1.21
B 1		.55	1.22
2		.52	1.19
3		.57(.54)	1.21(1.21)
23D 1	Lack of Wetting	.45	1.21
2		.46	1.21
3		.47	1.19
4		.49(.47)	1.17(1.20)
16B 1	Weave	.55	--
2		.54	1.10
3		.61	1.08
4		.60(.57)	1.07(1.08)
15B 1	Large Void	.33	1.03
2		.41	1.05
3		.32	1.05
4		.35(.35)	1.05(1.05)

- (1) Weight-scalar measurements  
(2) Average value

NONDESTRUCTIVE TEST MEASUREMENTS ON PYROLYZED  
VYB 70 1/2 - PITCH COMPOSITE TENSILE AND SHEAR SPECIMENS

Specimen <sup>(1)</sup>	Defect	Ultrasonic Longitudinal Velocity at 1.6 MHz, (10 <sup>5</sup> in/sec	Bulk <sup>(2)</sup> Density, (g/cc)
13D T1	No-Intentional	1.11	1.55
T2		1.13	1.54
T3		1.13 (1.12) <sup>(3)</sup>	1.52 (1.54)
21A T4	Small Void	1.06	1.34
T5		0.97	1.43
21B T1		1.01	1.44
T2		0.98	1.45
T3		0.93 (0.99)	1.45 (1.42)
24A T1	Weave	0.90	1.43
T2		0.90	1.43
T3		0.92	1.43 (1.43)
6B T1	Lack of Wetting	0.96	1.38
2		0.91	1.39
3		0.93 (0.93)	1.41 (1.39)
13B S1	No-Intentional	1.20	1.52
S2		1.20	1.51
S4		1.02 (1.14)	1.44 (1.49)
21C S1	Small Void	1.02	1.44
S2		1.09	1.43
S3		1.00	1.43
S4		0.95	1.44
S5		1.01 (1.01)	1.45 (1.44)
24D S1	Weave	0.96	1.38
S2		0.88	1.39
S3		0.96 (0.93)	1.42 (1.40)
6A S1	Lack of Wetting	0.98	1.38
2		0.99	1.36
3		1.00	1.38
4		1.03 (1.00)	1.38 (1.38)

(1) T - Tension

S - Shear

(2) Weight-scalar measurements

(3) Average value

NONDESTRUCTIVE TEST MEASUREMENTS ON GRAPHITIZED  
VYB 70 1/2 - PITCH COMPOSITE TENSILE AND SHEAR SPECIMENS

Specimen <sup>(1)</sup>	Defect	Ultrasonic Longitudinal Velocity at 0.8 MHz, (10 <sup>5</sup> in/sec)	Bulk <sup>(2)</sup> Density, (g/cc)
12C T1	No-Intentional	0.87	1.47
T2		0.85	1.45
T3		0.83	1.44
13C T1		0.84 (0.85) <sup>(3)</sup>	1.44 (1.45)
22C T1	Small Void	0.81	1.43
T2		0.81	1.42
T3		0.80 (0.81)	1.43 (1.43)
24B T1	Weave	0.78	1.41
T2		0.81	1.41
T3		0.73 (0.77)	1.42 (1.41)
5A T1	Lack of Wetting	0.70	1.38
T2		0.72	1.38
T3		0.69 (0.70)	1.39 (1.38)
13A S1	No-Intentional	0.91	1.46
S2		0.94	1.46
S3		0.94	1.47
S4		0.94	1.47
S5		0.92 (0.93)	1.51 (1.47)
22D S1	Small Void	0.89	1.43
S2		0.85	1.44
S3		0.87	1.43
S4		0.83 (0.88)	1.42 (1.43)
24C S1	Weave	0.80	1.42
S2		0.77	1.42
S3		0.74	1.43
S4		0.74 (0.78)	1.42 (1.42)
5B S1	Lack of Wetting	0.70	1.38
S2		0.69	1.35
S3		0.69	1.38
S4		0.69 (0.69)	1.38 (1.38)

(1) T - Tension

S - Shear

(2) Weight-scalar measurements

(3) Average value

NONDESTRUCTIVE TEST MEASUREMENTS ON PYROLYZED  
MODMOR II - PITCH COMPOSITE TENSILE AND SHEAR SPECIMENS

Specimen <sup>(1)</sup>	Defect	Ultrasonic Longitudinal Velocity at 1.6 MHz, (10 <sup>5</sup> in/sec)	Bulk <sup>(2)</sup> Density, (g/cc)
M1-6T	No-Intentional	.89	1.73
-7T		.89	1.73
-10T		.90	1.74
M2-6T		.87	1.75
M3-7T		.65 (.84) <sup>(3)</sup>	1.75 (1.74)
M3-1 S1	No-Intentional	.67	1.76
S2		.67	1.76
S3		.67	1.76
S4		.67	1.76
S5		.67	1.76
M3-6 S6		.61	1.75
S7		.62	1.75
S8		.62 (.65)	1.75 (1.76)
M56-3T	Weave	.65	1.75
M56-7T1		.59	1.75
9T2		.61 (.61)	1.75 (1.75)
M56-1S1	Weave	.62	1.74
S2		.58	1.74
S3		.60	1.74
S4		.58	1.74
S5		.61 (.60)	1.74 (1.74)
M13D T1	Lack of Wetting	.99	1.58
C T2		.99	1.55
T3		.98 (.98)	1.51 (1.55)
M13D S1	Lack of Wetting	1.08	1.51
S2		1.06	1.54
S3		1.03 (1.04)	1.53 (1.53)
M14A T1	Small Void	1.10	1.53
T2		0.98	1.50
T3		1.01 (1.03)	1.52 (1.51)
M14D S1	Small Void	1.07	1.52
S2		1.00	1.51
S3		0.98	1.49
S4		1.03 (1.02)	1.52 (1.51)

(1) T - Tension

S - Shear

(2) Weight-scalar measurements

(3) Average value

NONDESTRUCTIVE TEST MEASUREMENTS ON GRAPHITIZED  
MODMOR II - PITCH COMPOSITE TENSILE AND SHEAR SPECIMEN

Specimen <sup>(1)</sup>	Defect	Ultrasonic Longitudinal Velocity at 0.8 MHz, (10 <sup>5</sup> in/sec)	Bulk <sup>(2)</sup> Density, (g/cc)
2-1 T	No-Intentional	.61	1.92
2-4 T		.62	1.91
2-9 T		.61	1.89
2-11 T		.60 (.61)(3)	1.89 (1.90)
2-2 S1	No-Intentional	.60	1.73
S2		.61	1.73
S3		.62	1.73
S4		.62	1.73
S5		.61	1.73
S6		.61 (.61)	1.73 (1.73)
M56-4T1	Weave	.66	1.82
T2		.64	1.82
M56-5T3		.73 (.68)	1.76 (1.80)
M56-9S1	Weave	.65	1.97
S2		.64 (.65)	1.97
S3		(4)	1.97
S4		(4)	1.97 (1.97)
13 T1	Small Void	.70	1.63
T2		.64	1.63
T3		.67 (.67)	1.63 (1.63)
13 S1	Small Void	.73	1.60
S2		.72	1.60
S3		.72	1.61
S4		.74 (.73)	1.62 (1.61)
14 T1	Lack of Wetting	.71	1.58
T2		.61 (.66)	1.55 (1.57)
14 S1	Lack of Wetting	.77	1.55
S2		.77	1.55
S3		.79 (.78)	1.57 (1.56)

(1) T - Tension

S - Shear

(2) Weight-scalar measurements

(3) Average value

(4) Material attenuation prohibited measurement

## REFERENCES

1. Evangelides, J. S. and Meyer, R. A., "Investigation of the Properties of Carbon-Carbon Composites and Their Relationship to Nondestructive Test Measurements," AFML-TR-70-213, Contract F33615-69-C-1640, June 1970.
2. Ritter, H. L. and Drake, N. J., "Pore Size Distribution in Porous Materials", Industrial and Engineering Chemistry, Vol. 17, December 1945, p. 782-786.
3. Kratsch, K. M. and Meyer, R. A., "Final Report Erosion Mechanics and Improvement of Graphitic Materials", Vol. I, Microstructure Characterization, AFML F33615-69-C-1631.
4. Serabian, S., "Implications of the Attenuation Produced Pulse Distortion Upon the Ultrasonic Method of Nondestructive Testing", Materials Evaluation, September 1968.
5. McMaster, R. C., Nondestructive Testing Handbook, 1959.
6. Hashin, Zvi, "The Elastic Moduli of Heterogeneous Materials", Journal of Applied Mechanics, March 1962, pp 143-150.
7. Berger, H., "Neutron Radiography", Elsevier Publishing Company, 1965.
8. Cook, J. L., "Development of Nondestructive Test Techniques for Multidirectional Fiber-Reinforced Resin Matrix Composites", AFML-TR-70-239, Contract F33615-69-C-1624, December 1970.
9. Blome, J., "Development of A Thermal Protection System for the Wing of a Space Shuttle Vehicle", Report MSC 02562, February 1971.
10. Fitzer, E. and Terwiesch, B. "Carbon-Carbon Composites Fabricated by Wet Winding Endless Carbon Fibers with Pitch", Tenth Biennial Conference on Carbon, June 1971.
11. Communications with W. L. Shelton, Air Force Materials Laboratory.
12. Stineberg, R. C., Schultz, A. W. and Orner, J. W., "Investigation of Nondestructive Methods for the Evaluation of Graphite Materials", AFML-TR-67-128, February 1969.
13. Zimmer, J. E. and Cost, J. R., "Determination of the Elastic Constants of a Unidirectional Fiber Composite Using Ultrasonic Velocity Measurements," J. Acoustical Society of America, Vol. 47, No.3, March 1970, pp. 795-803.

Unclassified

Security Classification

## DOCUMENT CONTROL DATA - R &amp; D

(Security classification of title, body of abstract and indexing annotation must be entered when the overall report is classified)

1. ORIGINATING ACTIVITY (Corporate author) McDonnell Douglas Astronautics Company Santa Monica, California 90406		2a. REPORT SECURITY CLASSIFICATION <b>Unclassified</b>	
		2b. GROUP	
3. REPORT TITLE  Investigation of the Properties of Carbon-Carbon Composites and Their Relationship to Nondestructive Test Measurements			
4. DESCRIPTIVE NOTES (Type of report and inclusive dates) Final Report June 1969 - June 1971			
5. AUTHOR(S) (First name, middle initial, last name) John S. Evangelides Robert A. Meyer James E. Zimmer			
6. REPORT DATE September 1970		7a. TOTAL NO. OF PAGES	7b. NO. OF REFS 13
8a. CONTRACT OR GRANT NO. F33615-69-C-1640		9a. ORIGINATOR'S REPORT NUMBER(S) AFML-TR-70-213, Pt. II	
b. PROJECT NO. 9M-676			
c.		9b. OTHER REPORT NO(S) (Any other numbers that may be assigned this report) MDC G1004	
d.			
10. DISTRIBUTION STATEMENT  Approved for public release; distribution unlimited.			
11. SUPPLEMENTARY NOTES		12. SPONSORING MILITARY ACTIVITY Metals and Ceramics Division Air Force Materials Laboratory Wright Patterson AFB, Ohio 45433	
13. ABSTRACT Material variations and discrete discontinuities can be encountered in carbon-carbon composites. The object of this program was to identify and evaluate those factors that affect the quality and performance of carbon-carbon composites by nondestructive and destructive test methods. In addition, it was to be determined what correlations existed between the nondestructive test response data and the physical and mechanical property measurements. The general approach was to characterize the precursor materials, apply the nondestructive test techniques to the composites on an in-process basis, determine mechanical and physical properties and determine what relationships may exist between the NDT and property measurements. A number of different types of defects were intentionally introduced during the processing steps to aid in this evaluation.  The characterization of the VYB 70 1/2 yarn has indicated that considerable weight losses and shrinkages occur upon heating. The Thornel 50 and Modmor II graphite fibers did not undergo any significant weight loss under similar conditions. By selected binder pretreatments, coke values of some coal tar pitch components were increased.  The combination of the X-ray radiography and attenuation and velocity techniques detected the intentional defects introduced into the unidirectional and multidirectional composites. The use of an X-ray absorbing doping agent provided additional defect information on Thornel 50-pitch unidirectional composites. The pulse echo technique was only useful in evaluating fine weave-high density composites. The ultrasonic			

DD FORM 1473  
1 NOV 65

Unclassified

Security Classification



DOCUMENT CONTROL DATA R&D (Cont'd)

attenuation increased while the longitudinal velocity decreased with increasing porosity of the composites.

Different mechanical properties were obtained depending on the type of yarn and binder used, the material condition and the type of intentional defect present. The porosity present in the composites had a significant and different effect on each of the mechanical properties. An optimum porosity level appears to exist for the tensile properties of the composites, implying that the highest density does not always result in the highest tensile strength. The nondestructive test measurements were correlated to the porosity and mechanical properties of the carbon-carbon composites. The test data suggested that in-process prediction of final composite properties is possible.

It was concluded that monitoring material nonuniformities, detecting discrete discontinuities and predicting material properties in unidirectional and multidirectional carbon-carbon composites on an in-process basis can be successfully accomplished.

---

Unclassified

Security Classification

14. KEY WORDS	LINK A		LINK B		LINK C	
	ROLE	WT	ROLE	WT	ROLE	WT
Nondestructive Testing Carbon-Carbon Composites Unidirectional Multidirectional X-ray Radiography Ultrasonic Attenuation Ultrasonic Velocity Ultrasonic Pulse Echo Neutron Radiography Mechanical Properties Carbon Yarn Characterization Coal Tar Pitch Characterization						

Unclassified

Security Classification